Development of Novel Methodologies to Analyze the Adsorption Kinetics of Nonionic Surfactants

by

Srinivas Nageswaran Moorkanikkara

Submitted to the Department of Chemical Engineering
in partial fulfillment of the requirements for the degree of

Doctor of Philosophy in Chemical Engineering

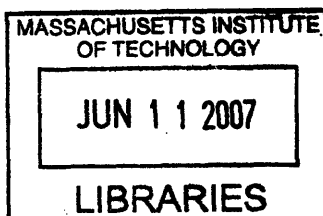at the

MASSACHUSETTS INSTITUTE OF TECHNOLOGY

May 2007
(September 2007)

Author..
Department of Chemical Engineering
May 25, 2007

Certified by..
Daniel Blankschtein
Professor of Chemical Engineering
Thesis Supervisor

Accepted by..
William Deen
Professor of Chemical Engineering
Chairman, Committee for Graduate Students

Development of Novel Methodologies to Analyze the Adsorption Kinetics of Nonionic Surfactants

by

Srinivas Nageswaran Moorkanikkara

Abstract

When an aqueous surfactant solution is exposed to a clean water/air surface, it takes a finite time for the surfactant molecules to physically transport from the bulk aqueous solution to the surface in order to adsorb and reduce the surface tension. The time scales associated with the reduction in surface tension can vary between milliseconds to hours depending on the surfactant type and its concentration. Accordingly, development of a fundamental understanding of the underlying physical phenomena involved in the kinetics of surfactant adsorption will help to: (i) understand the observed Dynamic Surface Tension (DST) behavior of surfactants, and (ii) design optimal surfactant formulations for applications in which the surfactant adsorption kinetics plays a significant role in determining the effectiveness of the formulation.

This thesis deals with modeling the adsorption kinetics of *nonionic* surfactants at *premicellar* surfactant concentrations. Traditionally, the adsorption kinetics of nonionic surfactants at premicellar surfactant concentrations has been understood in the context of two models: (1) the diffusion-controlled model, which assumes that diffusion of surfactant molecules from the bulk solution to the surface is the rate-limiting step, and (2) the mixed diffusion-barrier controlled model, which hypothesizes the existence of an energy barrier for surfactant adsorption from the bulk solution to the surface, and assumes that both diffusion and the energy barrier determine the overall rate of surfactant adsorption. Although the existence of the energy barrier was hypothesized more than 50 years ago, the physical basis underlying the existence of the energy barrier has not yet been elucidated.

The first major contribution of this thesis was demonstrating that the energy barrier is associated with the adsorption of a *single* surfactant molecule onto a *clean* surface, contrary to the broadly-held view that the energy barrier is associated with collective interactions between the adsorbed surfactant molecules. This was demonstrated by developing a generalized mixed diffusion-barrier controlled model and deriving a short-time adsorption kinetics formalism for this generalized model. The short-time formalism revealed that, when adsorption takes place onto an initially clean surface, the adsorption kinetics is independent of the specific interactions between the adsorbed surfactant molecules, and is solely controlled by the energy barrier at asymptotic short times. This observation led to the important conclusion that the energy barrier is related to the adsorption of a *single* surfactant molecule onto a *clean* surface.

One of the major drawbacks with the traditional procedure to determine the adsorption kinetics rate-limiting mechanism (diffusion-controlled vs. mixed diffusion-barrier controlled), including the

values of the relevant adsorption kinetics parameters, from experimental DST data is that it requires a specific model for the *equilibrium* adsorption behavior of the surfactant, where the deduced results were found to be extremely sensitive to the accuracy of the specific equilibrium model used. As a result, it has not been possible to elucidate the underlying physical basis of the energy barrier by analyzing the experimental DST data of nonionic surfactants. With this limitation in mind, the second major contribution of this thesis was the development of a new methodology to determine the adsorption kinetics rate-limiting mechanism, including the values of the relevant adsorption kinetics parameters, from the experimental DST data without using any model for the equilibrium surfactant adsorption behavior. The new methodology was implemented to analyze the experimental DST behavior of several alkyl poly(ethylene) oxide, C_iE_j, nonionic surfactants, and revealed that the energy barrier may be related to the hydrophobic effect.

The third major contribution of this thesis was the development of a novel approach to determine the *equilibrium* adsorption properties of nonionic surfactants from experimental *dynamic* surface tension data, a novel concept which has never been explored in the surface tension literature. Motivated by the observed high sensitivity of the predicted DST profiles to the accuracy of the model used to describe the equilibrium surfactant adsorption behavior, a new methodology was developed to determine the Equilibrium Surface Tension versus surfactant bulk solution Concentration (ESTC) behavior of nonionic surfactants from experimental DST data when the adsorption kinetics rate-limiting mechanism is diffusion-controlled. The new methodology requires: (1) experimental DST data measured at a *single* surfactant bulk solution concentration, C_b, (2) the diffusion coefficient of the surfactant molecule, and (3) one equilibrium surface tension value measured at a *single* surfactant bulk solution concentration, to determine the *entire ESTC curve* corresponding to surfactant bulk solution concentrations which are less than, or equal to, C_b. The new methodology was implemented to analyze the experimental pendant-bubble DST data of $C_{12}E_4$ and $C_{12}E_6$. For this purpose, the time scale associated with the validity of the assumption involving diffusive transport of surfactant molecules in the bulk solution in a pendant-bubble DST measurement was first determined, and the experimental DST data at those time scales was analyzed using the new methodology to predict the ESTC curves of $C_{12}E_4$ and $C_{12}E_6$. In both cases, the predicted ESTC behavior compared very well with the appropriate experimental DST results reported in the literature.

The final major contribution of this thesis was the development of a novel theoretical framework to design optimal surfactant formulations that meet specific adsorption kinetics requirements, which circumvents the more widely used and time consuming experimental trail-and-error surfactant selection approach. Specifically, the new theoretical framework involves using predictive DST models in conjunction with optimization techniques to identify the most efficient surfactant formulation that meets a specific surfactant adsorption kinetics requirement. The technical feasibility of the new theoretical framework and its effectiveness was demonstrated in the context of the adsorption kinetics of nonionic surfactants.

Overall, the results obtained in this thesis contribute to: (1) the development of a fundamental physical understanding of the energy barrier, (2) the development of efficient and reliable methodologies to more accurately analyze experimental DST data, and (3) the design of optimal surfactant formulations in industrial applications.

Thesis Supervisor: Daniel Blankschtein
Title: Professor of Chemical Engineering

Acknowledgments

I would like to thank my advisor, Professor Daniel Blankschtein, for his kind mentoring throughout the duration of my Ph.D. in his laboratory. I am grateful for the intellectual flexibility he offered me in exploring different areas, and for constantly guiding me in the development and consolidation of the solution approaches, including tackling the conceptual challenges in the course. I am also grateful for his patient nurturing of research and related skills, including making presentations and writing reports, with his detailed and prompt feedback. Overall, in his inimitable teaching style, he has been instrumental in the development of every aspect of my personality during my Ph.D. I cherish my learning experience and the affection I enjoyed with Professor Blankschtein. I believe this learning will stand me in good stead in my future endeavors. I would like to thank my thesis committee members: Professors Barton, Deen, and Doyle for their support and cooperation throughout the duration of my Ph.D.

I would like to specially thank Professor Shi-Yow Lin of National Taiwan University of Science and Technology for kindly sharing with me his actual experimental dynamic surface tension data measured using the pendant-bubble apparatus for several nonionic surfactants. The availability of this data was extremely helpful in testing the validity and effectiveness of the different novel methodologies developed in this thesis. I would like to thank Professor Charles Maldarelli of City College of New York for helpful and insightful discussions on the pendant-bubble apparatus, in particular, and on dynamic surface tension in general.

I would like to thank all the past and present members of the Blankschtein research group for making this place feel like home! Interacting with Isaac was loads of fun, and I enjoyed the several scientific and philosophical discussions that I have had with him. I also enjoyed trying to learn Spanish from Arthur and teaching him Tamil (my native language), in return. I enjoyed the interactions with Carlota, Paulo and Priscilla (the Brazilian visitors), Dick (the Dutch visitor), Leo (the visitor from UK), and Hitoshi (the Japanese visitor). I carry fond memories of my interaction with past members: Vibha, Brian, Henry, and Joe. I wish all the present group members: Jonathan, Baris, Amanda, Jennifer, and Shang Chao all the very best in their research pursuits, and wish them grand successes in their endeavors.

My family and friends have helped me immensely at a personal and emotional level towards

I dedicate this thesis to my father

Sathyaméva Jayathé
(Truth alone triumphs)

Contents

List of Figures

16

17

18

List of Tables

Chapter 1

Introduction

1.1 Motivation

Surfactants are specialty chemicals composed of a hydrophilic group (referred to as the head) and a hydrophobic group (referred to as the tail). When surfactants are added to water (even in very small quantities), they produce a significant reduction of the surface tension of the water/fluid(air or oil) interface. This behavior has been attributed to the preferential adsorption of the surfactant molecules at the interface driven by the hydrophobic effect [1], where the hydrophilic heads remain in the aqueous phase and the hydrophobic tails are removed into the adjacent fluid phase. Therefore, these molecules are also referred to as 'surface-active' chemicals. This behavior is depicted schematically in Figure 1-1 for the case of a water/air interface.

Note that when surfactant molecules in aqueous solution are exposed to an initially clean water/fluid (air or oil) interface, surfactant adsorption does not take place instantaneously. Instead, it takes a finite time for the surfactant molecules to physically transport from the bulk solution to the interface in order to adsorb and reduce the surface tension. The time scales associated with the reduction in surface tension, for different surfactant types and at different surfactant concentrations, can vary between milliseconds to hours [2]. Various applications, in which the time required for the surfactant molecules to reduce the surface tension is of great practical importance, include the development of therapeutic lung surfactants to treat the respiratory distress syndrome [3],[1] ink-jet

---

[1]The respiratory distress syndrome is among the top five diseases leading to infant mortality in the US [4].
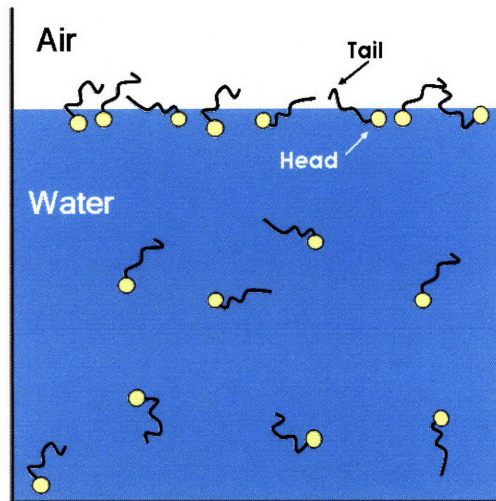
Figure 1-1: Surfactant molecules adsorbed at a water/air interface, with their hydrophilic heads in the water phase and their hydrophobic tails in the air phase.

printing [5], air-assist atomization [6], pesticide sprays [7], film coatings [8], and the generation of foams [9] and emulsions [10]. For example, the respiratory distress syndrome in new born babies results when the lungs fail to inflate due to a slower reduction of the surface tension induced by the surfactants present in the alveoli (the air sacs of the lungs) [3]. In processes like foam generation and emulsion formation, where very large surface areas are created within a short period of time, the surfactant molecules must quickly adsorb at the newly created fluid/fluid interfaces in order to stabilize the newly formed foam surfaces and emulsion droplets. In all the applications listed above, in order to attain a desired rate of surfactant adsorption at the interface, a careful choice of the surfactants used and of their concentrations must be made. The dynamic aspects of surface tension are also important in phenomena like interfacial turbulence [11], the Marangoni effect [12], thin-film stability [11], surface rheology [11], drop impact [13–15], and the spreading of drops on surfaces [16, 17]. Use of the dynamic surface tension of biological fluids as a diagnostic tool in medicine is also being explored [18, 19].

The area of *kinetics of surfactant adsorption* seeks to develop a fundamental understanding of the underlying physical phenomena involved in the dynamics of surfactant adsorption. Based on the chemical structure of the surfactant molecule and the solution conditions (including the surfactant concentration and the temperature), different fundamental phenomena are involved in affecting the kinetics of the surfactant adsorption process. In Table 1.1, I give an idea of the breadth of this

Table 1.1: Various characteristics that affect the kinetics of surfactant adsorption.

Characteristic	Comment
Interactions between the adsorbed surfactant molecules	The adsorbed surfactant molecules interact through a combination of attractive and repulsive forces. Depending on the nature of these interactions and on their relative magnitudes, the adsorbed surfactant molecules may exhibit long-range surface orientational ordering[21], or undergo surface phase transitions [22].
Ionic/nonionic nature	The kinetics associated with the adsorption of ionic surfactants is different from that of nonionic surfactants because, as the adsorption process progresses, the surface acquires charge, and the resulting electric field slows down any further adsorption of the ionic surfactant molecules [23].
Bulk solution concentration	Surfactant molecules form aggregates called *micelles* in the bulk solution when the surfactant bulk solution concentration is greater than a threshold concentration known as the critical micelle concentration (CMC). When the surfactant concentration exceeds the CMC, the presence of micelles in the bulk solution affects the kinetics of surfactant adsorption [24, 25].

research area by identifying *independent characteristics* that affect the kinetics of the adsorption process. Note that the characteristics listed in Table 1.1 are associated with the adsorption of *single* surfactants. The presence of other surfactants induces competitive or synergistic adsorption depending on the nature of the surfactants and the solution conditions (including total surfactant concentration, surfactant composition, and temperature), and results in a rich variety of adsorption kinetics phenomena [20].

In terms of the three characteristics listed in Table 1.1, in this thesis, I investigate the adsorption

kinetics of *simple nonionic surfactants*[2] *at premicellar bulk solution concentrations*. The remainder of this Chapter is organized as follows. In Section 1.2, I present relevant background on the adsorption kinetics of nonionic surfactants, and in Section 1.3, I discuss specific thesis objectives.

1.2 Background on the Adsorption Kinetics of Nonionic Surfactants

1.2.1 Modeling the Adsorption Kinetics

Traditionally, the adsorption process has been viewed as consisting of the following three steps[26]:

Step 1: Transport of the surfactant molecules from the bulk solution to the sub-surface[3].

Step 2: Adsorption of the surfactant molecules from the sub-surface onto the surface.

Step 3: Possible reorganization of the surfactant molecules at the surface.

Macroscopically, the kinetics of the surfactant adsorption process results in a time-dependent surface tension behavior, which is referred to as the Dynamic Surface Tension (DST). Accordingly, the experimentally observed DST behavior represents the net effect of the three steps listed above.

Based on this understanding, two classes of kinetics models have been advanced, each defined by a set of suitable assumptions[28].

Diffusion-Controlled Model

Assumption 1: Transport of the surfactant molecules in the bulk solution is governed by Fickian diffusion.

Assumption 2: Adsorption of the surfactant molecules from the sub-surface onto the surface is instantaneous. In other words, the sub-surface and the surface reach equilibrium instantaneously.

Assumption 3: The adsorbed surfactant molecules either do not undergo any reorganization at the surface or the reorganization is instantaneous.

---

[2]The term *simple surfactants*, as used in this thesis, refers to surfactants that do not exhibit phase transitions or any form of aggregation at the surface.
[3]The sub-surface is the zone of a few angstroms thickness adjacent to the surface, according to Ward and Tordai [27].

Mixed Diffusion-Barrier-Controlled Model[4]

Assumption 1: Transport of the surfactant molecules in the bulk solution is governed by Fickian diffusion.

Assumption 2: Adsorption and desorption of the surfactant molecules between the sub-surface and the surface takes place at a finite rate. Specifically, the surfactant molecules at the sub-surface need to overcome an energy barrier, E_a, in order to adsorb onto the surface.

Assumption 3: The adsorbed surfactant molecules either do not undergo any reorganization at the surface or the reorganization is instantaneous.

The specific form of the kinetics model depends on the equilibrium adsorption isotherm model of the surfactant, since the kinetics model should reduce to the equilibrium adsorption isotherm model at equilibrium conditions. While the diffusion-controlled adsorption model contains *one* kinetics parameter: D – the bulk solution diffusion coefficient of the surfactant molecule, the mixed-controlled adsorption model contains *two* kinetics parameters: D and β, where β is the energy-barrier parameter representing the rate constant for the adsorption of surfactant molecules from the sub-surface onto the surface. Although the effect of the energy barrier on surfactant adsorption at the surface has been accounted for in the mixed-controlled model in terms of the model parameter β, the physical basis underlying the existence of the energy barrier is still unclear [28].

1.2.2 Experimental Investigation of the Kinetics of Surfactant Adsorption

Experimental investigation of the kinetics of surfactant adsorption is typically carried out to identify the applicability of the two classes of models described above. These investigations typically involve measuring the DST of surfactant solutions at different initial surfactant bulk solution concentrations [29]. Measurement of dynamic surfactant surface concentrations has also become possible recently due to advances in the ability to carry out ellipsometry measurements in a dynamic system [30]. Recall that the time scales associated with the kinetics of surfactant adsorption, using different surfactant types and at different surfactant concentrations, can vary between milliseconds to hours [29]. Different experimental techniques are employed to measure DST's depending on the time scales associated with the adsorption kinetics process. In Figure 1-2, I reproduce a chart

---

[4]I shall refer hereafter to the mixed diffusion-barrier-controlled model as the mixed-controlled model.

published in Ref.[2] that specifies the time windows for DST measurements using various existing experimental techniques.
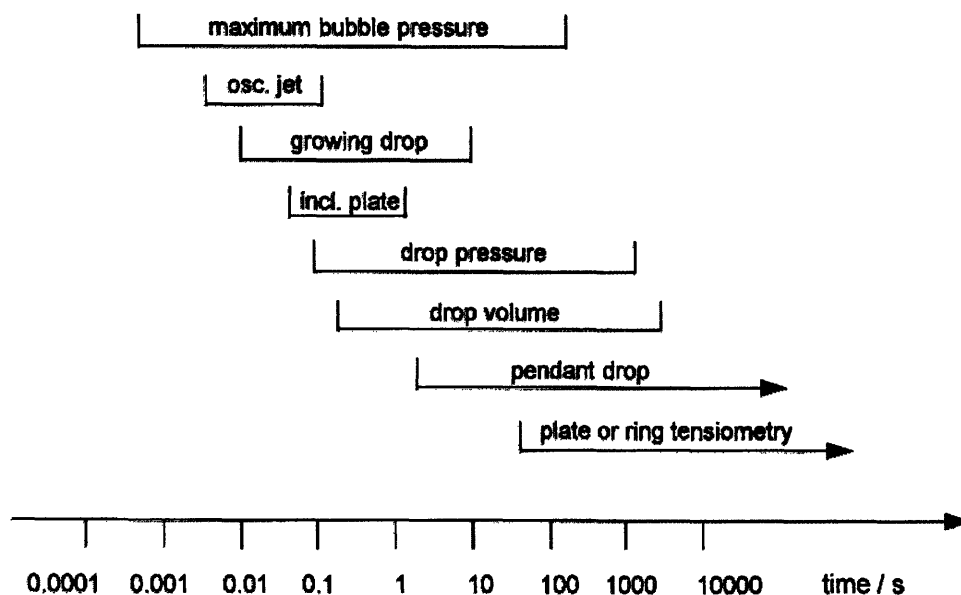
Figure 1-2: Various existing experimental techniques to measure DST and their respective time ranges for measurement (from Ref.[2]).

1.3 Specific Thesis Objectives

With the background provided in Section 1.2 in mind, the central goal of my thesis involves:

The development of novel methodologies to analyze the adsorption kinetics of nonionic surfactants

The specific research objectives of my Ph.D. include:

1. Resolution of a long-standing conceptual contradiction between existing adsorption kinetics models: the diffusion-controlled model and the mixed-controlled model.

2. Development of a new methodology to determine the rate-limiting adsorption kinetics mechanism from experimental DST data.

3. Development of a novel approach to determine surfactant *equilibrium* properties from experimental DST data.

30

4. Exploration of a new theoretical framework to design optimal nonionic surfactant formulations that exhibit a desired adsorption kinetics behavior.

Below, I provide a brief overview of the key results obtained in each of the specific objectives listed above.

1.3.1 Specific Thesis Objective 1: Resolution of Conceptual Contradiction

The experimental DST behavior of several nonionic surfactants exhibits a $\sqrt{t}$ variation at short-times. Traditionally, the observed $\sqrt{t}$ behavior has been interpreted using the asymptotic short-time analysis of the diffusion-controlled model. As a result of this interpretation, the fundamental physical nature of the energy barrier associated with the adsorption of surfactant molecules from the sub-surface onto the surface has been proposed to be related to high surfactant surface concentrations.

In addressing specific thesis objective 1, I will: (i) point out that the asymptotic short-time analysis of the diffusion-controlled model leads to inconsistent predictions, and conclude that this analysis cannot be used to describe the short-time adsorption kinetics behavior, (ii) demonstrate that the observed short-time $\sqrt{t}$ DST behavior can be interpreted using a nonasymptotic short-time formalism of the mixed-controlled model, and (iii) analyze the consequence of the new interpretation and conclude that the energy barrier is associated with the adsorption of a *single* surfactant molecule onto a *clean* surface. A detailed account of the resolution of the conceptual contradiction as well as the analysis of the consequence are presented in Chapter 2. A schematic representation of the key contribution made in addressing specific thesis objective 1 is shown in Figure 1-3.
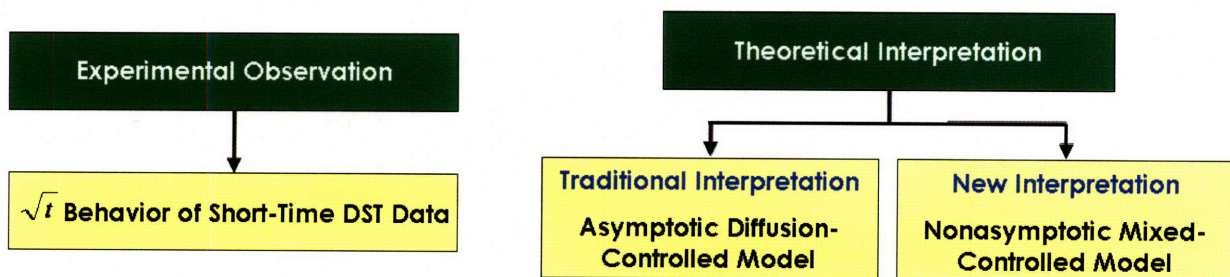
Figure 1-3: Specific Thesis Objective 1 - Interpretation of the $\sqrt{t}$ behavior of the short-time DST data - A comparison of the existing interpretation and the new interpretation.

1.3.2 Specific Thesis Objective 2: Development of a New Methodology to Determine the Rate-Limiting Adsorption Kinetics Mechanism from Experimental DST Data

The traditional procedure to determine the rate-limiting adsorption kinetics mechanism (diffusion-controlled vs. mixed-controlled), and the values of the kinetics parameters (D and β) uses[31]: (i) experimental DST data measured at several surfactant bulk solution concentrations, and (ii) a known model for the equilibrium adsorption isotherm of the surfactant. It has been observed that the deduced results are highly sensitive to the choice of the equilibrium adsorption isotherm model of the surfactant[32]. Note that the equilibrium adsorption isotherm models differ in the manner in which they account for the interactions between the adsorbed surfactant molecules[33], and as such, they should not affect the value of D, the *bulk solution* diffusion coefficient of the surfactant molecule, and β, which as I will show as part of specific thesis objective 1, is related to the adsorption of a *single* surfactant molecule onto a *clean* surface.

In addressing specific thesis objective 2, I will develop a new methodology to determine the rate-limiting adsorption kinetics mechanism (diffusion-controlled vs. mixed-controlled), including deducing the kinetics parameters (D and β) from experimental DST data. The new methodology has the following advantages over the existing procedure used to analyze the experimental DST data: (a) it does not require using a model for the equilibrium adsorption isotherm, and (b) it only requires using the experimental short-time DST data measured at two initial surfactant bulk solution concentrations. A schematic representation of the new methodology developed is shown in Figure 1-4.
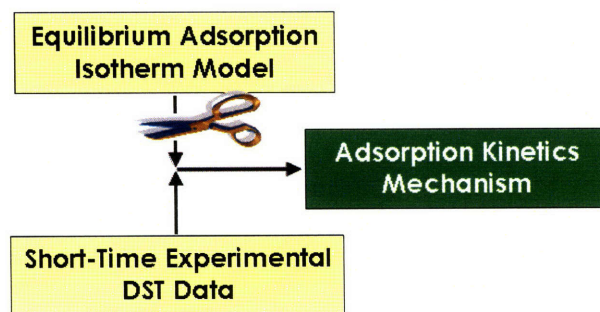
Figure 1-4: Specific Thesis Objective 2 - New methodology to determine the adsorption kinetics rate-limiting mechanism from experimental DST data.

The development and implementation of the new methodology to determine the adsorption kinetics rate-limiting mechanism of several poly(ethylene) oxide, C_iE_j, nonionic surfactants are discussed in Chapter 3.

1.3.3 Specific Thesis Objective 3: Development of a Novel Approach to Determine Equilibrium Adsorption Properties from Experimental DST data

In addressing specific thesis objective 3, I will explore a novel approach to determine *equilibrium* adsorption properties from experimental *dynamic* surface tension data and the known rate-limiting adsorption kinetics mechanism. Specifically, I will develop a new methodology to determine the Equilibrium Surface Tension vs. bulk solution Concentration (ESTC) behavior of nonionic surfactants using experimental pendant-bubble DST data when the adsorption kinetics is diffusion-controlled.

First, I will analyze the experimental pendant-bubble DST data of two nonionic surfactants, $C_{12}E_4$ and $C_{12}E_6$, and will show that the assumption of diffusive transport of the surfactant molecules in the bulk solution is likely valid only for time $t <\approx 100 - 200$ s, since for $t >\approx 100 - 200$ s, the experimental DST data exhibit a 'super-adsorption' behavior. I will then hypothesize the onset of natural convection in the pendant-bubble experimental setup for these nonionic surfactants when $t >\approx 100 - 200$. The analysis of the experimental pendant-bubble DST data and the discussion leading to the hypothesis of the onset of natural convection are presented in Chapter 4. Following this, in Chapter 5, I will develop the new framework to determine the ESTC behavior of nonionic surfactants using experimental pendant-bubble DST data when the adsorption kinetics is diffusion-controlled, and will demonstrate the applicability of the new framework by determining the ESTC behaviors of $C_{12}E_4$ and $C_{12}E_6$. A schematic representation of the novel approach is shown in Figure 1-5.
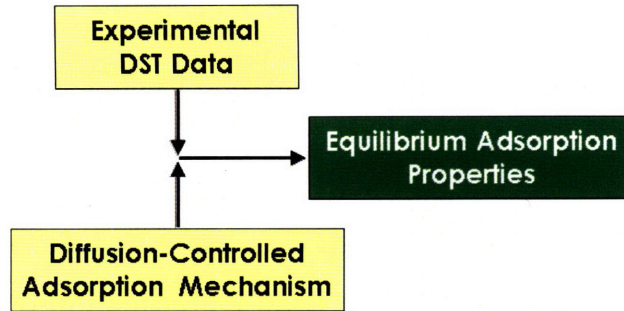
Figure 1-5: Specific Thesis Objective 3: New Approach to determine equilibrium adsorption properties of nonionic surfactants.

1.3.4 Specific Thesis Objective 4: Development of a New Theoretical Framework to Design Optimal Nonionic Surfactant Formulations that Exhibit a Desired Adsorption Kinetics Behavior

In addressing specific thesis objective 4, I will propose a new theoretical framework to identify the optimal nonionic surfactant formulation that most closely meets a desired adsorption kinetics behavior. Specifically, the new theoretical framework poses the design of the surfactant formulation as an *optimization problem* using predictive adsorption kinetics models, and finds the solution of the formulated optimization problem using numerical algorithms implemented in commercial optimization packages. As proof of technical feasibility of the proposed new theoretical framework, I will: (a) consider the problem of identifying the *nonionic* surfactant formulation that optimally satisfies a desired adsorption kinetics behavior specified in terms of a desired *dynamic surface tension profile*, (b) formulate the problem defined in (a) as an optimization problem using the Mulqueen-Stebe-Blankschtein (MSB) adsorption kinetics model[20], and (c) develop a framework to find the solution of the optimization problem formulated in (b) using the Sequential Nonlinear OPTimization (SNOPT) package [34]. Finally. I will demonstrate the effectiveness of the new theoretical framework by analyzing a representative case study. The development of the new theoretical framework and the demonstration of its utility to design optimal nonionic surfactant formulations are discussed in Chapter 6. A schematic representation of the new theoretical framework is shown in Figure 1-6.

In summary, the remainder of my thesis is organized as follows. In Chapter 2, I discuss the resolution of the conceptual contradiction. In Chapter 3, I discuss the development of a new

34
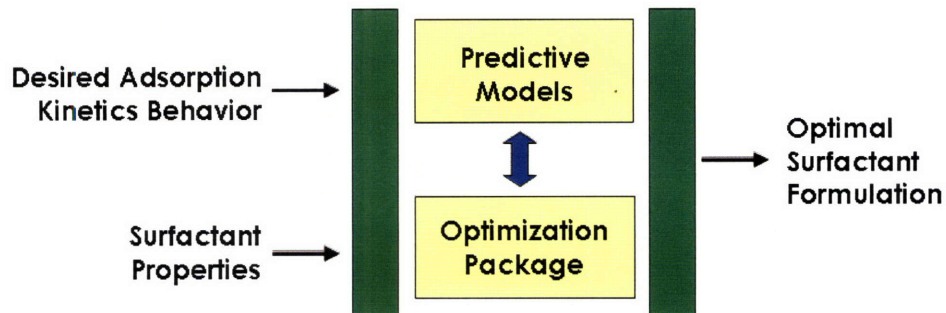
Figure 1-6: Specific Thesis Objective 4 - New theoretical framework to identify the optimal nonionic surfactant formulation that most closely meets a desired adsorption kinetics behavior.

methodology to determine the adsorption kinetics rate-limiting mechanism. In Chapter 4, I present an analysis of the pendant-bubble experimental DST data. In Chapter 5, I discuss the development of a new approach to determine equilibrium adsorption properties from experimental DST data. In Chapter 6, I discuss the development of a new theoretical framework to design optimal nonionic surfactant formulations. Finally, in Chapter 7, I summarize the key conclusions of this thesis and discuss possible future research directions.

Bibliography

[1] C. Tanford. *The Hydrophobic Effect: Formation of Micelles and Biological membranes*. Wiley-Interscience, second edition, 1980.

[2] J. Eastoe and J. S. Dalton. Dynamic surface tension and adsorption mechanisms of surfactants at the air-water interface. *Advances in Colloid and Interface Science*, 85:103–144, 2000.

[3] R. H. Notter and J. N. Finkelstein. Pulmonary surfactant: an interdisciplinary approach. *Journal of Applied Physiology*, 57(6):1613–1624, 1984.

[4] T. J. Mathews, P. H. Fay Menacker, and M. F. MacDorman. Infant mortality statistics from the 2001 period linked birth/infant death data set. *National Vital Statistics Reports*, 52(2):1–28, 2003.

[5] Andrew M. Howe. Some aspects of colloids in photography. *Current Opinion in Colloid and Interface Science*, pages 288–300, 2000.

[6] U. Shavit and N. Chigier. The role of dynamic surface tension in air-assist atomization. *Physics of Fluids*, 7(1):24–33, 1995.

[7] C-H. Chang and Elias I. Franses. Adsorption dynamics of surfactants at the air/water interface: a critical review of mathematical models, data, and mechanisms. *Colloids and Surfaces A: Physicochemical and Engineering Aspects*, 100:1–45, 1995.

[8] J. E. Valentini, W. R. Thomas, P. Sevenhuysen, T. S. Jiang, Y. Liu, H. O. Lee, and S-C. Yen. Role of dynamic surface tension in slide coating. *Ind. Eng. Chem. Res.*, 30:453–461, 1991.

[9] P. R. Garrett and P. L. Gratton. Dynamic surface tensions, foam and the transition from micellar solution to lamellar phase dispersion. *Colloids and Surfaces A: Physicochemical and Engineering Aspects*, 103:127–145, 1995.

[10] V. Schröder, O. Behrend, and H. Schubert. Effect of dynamic interfacial tension on the emulsification process using microporous, ceramic membranes. *Journal of Colloid and Interface Science*, 202:334–340, 1998.

[11] D. A. Edwards, H. Brenner, and D. T. Wasan. *Interfacial Transport Processes and Rheology*. Butterworth-Heinemann, 1991.

[12] A. D. Nikolov, D. T. Wasan, A. Chengara, K. Koczo, G. A. Policello, and I. Kolossvary. Superspreading driven by marangoni flow. *Advances in Colloid and Interface Science*, 96:325–338, 2002.

[13] X. Zhang and O. A. Basaran. Dynamic surface tension effects in impact of a drop with solid surface. *Journal of Colloid and Interface Science*, 187:166–178, 1997.

[14] R. Crooks, J. C-Whitez, and D. V. Boger. The role of dynamic surface tension and elasticity on the dynamics of drop impact. *Chemical Engineering Science*, 56:5575–5592, 2001.

[15] N. M-Candoni, B. P-Foch, F. Legay, M. V-Adler, and K. Wong. Influence of dynamic surface tension on the spreading of surfactant solution droplets impacting onto a low-surface-energy solid substrate. *Journal of Colloid and Interface Science*, 192:129–141, 1997.

[16] M. von Bahr, F. Tiberg, and B. V. Zhmud. Spreading dynamics of surfactant solutions. *Langmuir*, 15:7069–7075, 1999.

[17] M. J. Rosen and L. D. Song. Superspreading, skein wetting, and dynamic surface tension. *Langmuir*, 12:4945–4949, 1996.

[18] V. N. Kazakov, A. F. Vozianov, O. V. Sinyachenko, D. V. Trukhin, V. I. Kovalchuk, and U. Pison. Studies on the application of dynamic surface tensiometry of serum and cerebrospinal liquid for diagnostics and monitoring of treatment in patients who have rheumatic, neurological or oncological diseases. *Advances in Colloid and Interface Science*, 86:1–38, 2000.

[19] D.V. Trukhin, O.V. Sinyachenko, V.N. Kazakov, S.V. Lylyk, A.M. Belokon, and U. Pison. Dynamic surface tension and surface rheology of biological liquids. *Colloids and Surfaces B: Biointerfaces*, 21:231–238, 2001.

[20] M. Mulqueen, K. J. Stebe, and D. Blankschtein. Dynamic interfacial adsorption in aqueous surfactant mixtures: Theoretical study. *Langmuir*, 17:5196–5207, 2001.

[21] J. Y. Shin and N. L. Abbott. Using light to control dynamic surface tensions of aqueous solutions of water soluble surfactants. *Langmuir*, 15:4404 – 4410, 1999.

[22] R. Subramanyam and C. Maldarelli. Fluorescence evidence that a phase transition causes the induction time in the reduction in dynamic tension during surfactant adsorption to a clean air/water interface and a kinetic-diffusive transport model for the phase-induced induction. *Journal of Colloid and Interface Science*, 253:377–392, 2002.

[23] C. A. MacLeod and C.J. Radke. Charge effects in the transient adsorption of ionic surfactants at fluid interfaces. *Langmuir*, 10:3555–3566, 1994.

[24] C. D. Dushkin, I. B. Ivanov, and P. A. Kralchevsky. The kinetics of the surface tension of micellar surfactant solutions. *Colloids and Surfaces*, 60:235 – 261, 1991.

[25] R. Miller. Adsorption kinetics of surfactants from micellar solutions. *Colloid and Polymer Science*, 259:1124 – 1128, 1981.

[26] S. S. Dukhin, G. Kretzschmar, and R. Miller, editors. *Dynamics of adsorption of liquid interfaces: theory, experiment, applications*. Elsevier, 1995.

[27] A. F. H. Ward and L.Tordai. Diffusion controlled adsorption. *Journal of Chemical Physics*, 14:453, 1946.

[28] R. Pan, J. Green, and C. Maldarelli. Theory and experiment on the measurement of kinetic rate constants for surfactant exchange at an air/water interface. *Journal of Colloid and Interface Science*, 205:213–230, 1998.

[29] J.Eastoe, A.Rankin, R.Wat, and C. D. Bain. Surfactant adsorption dynamics. *International Reviews in Physical Chemistry*, 20(3):357–386, 2001.

[30] B. P. Binks, P. D. I. Fletcher, V. N. Paunov, and D. Segal. Equilibrium and dynamic adsorption of $C_{12}E_5$ at the air-water surface investigated usin ellipsometry and tensiometry. *Langmuir*, 16:8926–8931, 2000.

[31] S-Y. Lin, K. McKeigue, and C. Maldarelli. Diffusion-controlled surfactant adsorption studied by pendant drop digitization. *AIChE Journal*, 36:1785 – 1795, 1990.

[32] C-T. Hsu, C-H. Chang, and S-Y. Lin. Comments on the adsorption isotherm and determination of adsorption kinetics. *Langmuir*, 13:6204–6210, 1997.

[33] S. N. Moorkanikkara and D. Blankschtein. Short time behavior of mixed barrier-diffusion controlled adsorption. *Journal of Colloid and Interface Science*, 296:442–457, 2006.

[34] P. E. Gill, W. Murray, and M. A. Saunders. SNOPT: An SQP algorithm for large-scale constrained optimization. *SIAM Review*, 47:99–131, 2005.

Chapter 2

New Short-Time Formalism for the Mixed Diffusion-Barrier Controlled Adsorption Model

2.1 Introduction

Recall that, traditionally, the surfactant adsorption process is envisioned to consist of the following three steps [1–11](see Section 1.2.1): Step 1: Diffusion of the surfactant molecules from the bulk solution to the sub-surface [1], Step 2: Adsorption from the sub-surface onto the surface, and Step 3: Reorientation of the surfactant molecules at the surface leading to a further reduction of the surface tension.

The popular diffusion-controlled adsorption model assumes that the rate-limiting step for adsorption is the diffusive transport of the surfactant molecules from the bulk solution to the sub-surface. Although the diffusion-controlled adsorption model predicts the experimental Dynamic Surface Tension (DST) data reasonably well for many nonionic surfactants at *low* premicellar surfactant concentrations, systematic deviations are observed at higher premicellar surfactant concentrations [13–16]. The observed deviations were attributed to the existence of an *energy barrier* for adsorption from the sub-surface onto the surface [13, 17–23]. The mixed diffusion-barrier con-

---

[1]The sub-surface is the zone of a few angstroms thickness adjacent to the surface, according to Ward and Tordai [12].

trolled model [2] takes into account the existence of an energy barrier for the adsorption of surfactant molecules at the surface, in addition to the diffusive transport of the surfactant molecules from the bulk solution to the sub-surface.

A short-time asymptotic analysis of the mixed-controlled model predicts pure barrier-controlled adsorption (as opposed to diffusion-controlled adsorption) [18, 24–28]. Specifically, at asymptotic short-times, the mixed-controlled model predicts barrier-controlled adsorption, where the DST varies linearly with time t [18, 24–28] . This contrasts with the asymptotic short-time behavior of the diffusion-controlled adsorption model, which predicts a $\sqrt{t}$ variation of the DST [18, 24–27, 29]. It is noteworthy, that the diffusion-controlled adsorption model *is not valid at asymptotic short times*, since it predicts an unphysical infinite flux at $t = 0$ (see Section 2.3.1 and [21, 24, 30, 31]).

Interestingly, the experimental DST behavior of many nonionic surfactant systems appears to contradict the theoretical predictions summarized above: the experimental DST behavior of these nonionic surfactant systems exhibits a $\sqrt{t}$ variation at short times, and this behavior is considered as a fingerprint for the existence of diffusion-controlled adsorption at short times based on the short-time asymptotic prediction of the diffusion-controlled model [8, 9, 26, 32–37]. Furthermore, based on this interpretation of the experimental observations, it has been proposed that the fundamental physical basis underlying the existence of the energy barrier is associated with high surfactant surface concentrations [8, 20, 33, 34].

With the background provided above in mind, the central objective of this chapter is to reconcile the apparent contradiction between the theoretical prediction of barrier-controlled adsorption at asymptotic short times and the experimental observations which appear to imply the existence of diffusion-controlled adsorption at asymptotic short times. I address this objective by deriving an analytical solution of the *non-asymptotic* short-time behavior of the mixed-controlled model describing surfactant adsorption onto a spherical pendant-bubble surface, including determining the ranges of time and surfactant surface concentration values where the short-time formalism is applicable. I find that, when $t >\approx 50\tau_s$, the mixed-controlled model results in an apparent $\sqrt{t}$ behavior of the DST, where τ_s is a time scale associated with the mixed-controlled adsorption at

---

[2]We shall refer hereafter to the mixed diffusion-barrier controlled model as the mixed-controlled model.

short times. This behavior is consistent with the experimental observations of a $\sqrt{t}$ behavior of the DST at short-times. I analyze the consequence of this finding in the context of the physical nature of the energy barrier. I conclude that the energy barrier is related to the adsorption of a *single* surfactant molecule onto a *clean* surface.

The remainder of the chapter is organized as follows. In Section 2.2, (i) I develop a generalized mixed-controlled model for surfactant adsorption at a spherical surface valid for any model for the equilibrium adsorption isotherm (see Section 2.2.1), and (ii) I derive a new non-asymptotic short-time formalism of the generalized mixed-controlled model (see Section 2.2.2). In Section 2.3, (i) I use the short-time formalism to address the apparent contradiction between theory and experiment regarding the surfactant adsorption mechanism at short-times (see Section 2.3.1), and (ii) I discuss how my analysis affects the interpretation of the physical basis underlying the existence of the energy barrier (see Section 2.3.2). Finally, in Section 2.4, I summarize the main results of the chapter. In addition, in Appendix 2.A, I derive the solution of the partial differential equation corresponding to the mixed-controlled model. In Appendix 2.B and Appendix 2.C, I determine the range of time and the range of surfactant surface concentation, respectively, in which the new short-time formalism is valid. In Appendix 2.D, I state and prove a proposition.

2.2 Theory

2.2.1 The Generalized Mixed-Controlled Model

In the literature, mixed-controlled models are typically presented in the context of a *specific model* for the equilibrium adsorption isotherm. In this section, I first develop a generalized mixed-controlled model which is applicable for *any model* for the equilibrium adsorption isotherm, and then derive the short-time formalism for this generalized mixed-controlled model.

Traditionally, in order to understand the physics associated with the adsorption of nonionic surfactants, their adsorption onto a freshly formed surface has been studied. In a typical pendant-bubble experiment to measure the dynamic surface tension, a bubble possessing a clean surface (containing a negligible number of surfactant molecules) is exposed to an aqueous solution containing surfactant at a bulk concentration C_b. Subsequently, the change in the surface tension due

to the adsorption of the surfactant molecules at the water/air bubble surface is measured as a function of time, t, until the surface tension reaches its equilibrium value corresponding to the surfactant concentration C_b. During a pendant-bubble experiment, as soon as the clean bubble surface is exposed to the bulk surfactant solution, the surfactant molecules closest to the surface (that is, those in the sub-surface) adsorb. This adsorption results in the reduction of the surfactant concentration at the sub-surface. The resulting surfactant concentration gradient between the sub-surface and the bulk solution drives a diffusive flux of surfactant molecules from the bulk solution towards the surface.

Assuming negligible convection effects associated with the formation of the bubble, the transport of the nonionic surfactant molecules in the bulk solution can be modeled as Brownian-diffusion obeying Fick's law. Assuming spherical symmetry of the pendant-bubble, the surfactant diffusive transport along the radial direction, r, towards the spherical surface is given by:

$$\frac{\partial C}{\partial t} = \frac{D}{r^2}\frac{\partial}{\partial r}(r^2\frac{\partial C}{\partial r}), \qquad r \geq r_0, \qquad t \geq 0 \tag{2.1}$$

where C is the surfactant concentration, D is the surfactant diffusion coefficient, and r_0 is the radius of the pendant bubble.

Assuming no evaporation of the adsorbed surfactant molecules into the air phase inside the bubble, the rate of surfactant adsorption at the surface is equal to the net flux of surfactant molecules leaving the sub-surface towards the surface, that is:

$$D\left.\frac{\partial C}{\partial r}\right|_{r=r_0} = \frac{d\Gamma}{dt} \tag{2.2}$$

where Γ is the surfactant surface concentration. Note that, if the internal phase was oil instead of air, or if the adsorbing chemical was volatile, the concentration of the surfactant molecules in the internal phase must be considered in formulating the mass balanc·· equation at the surface.

The model for the energy barrier for adsorption of the surfactan molecules from the sub-surface to the surface in the mixed-controlled model was inspired by mode.s proposed in the field of *Chemical Reaction Kinetics*. In such a model, the surfactant molecules in the sub-surface are considered as 'reactants', while the adsorbed surfactant molecules are considered as 'products'. Accordingly,

the adsorption of the surfactant molecules from the sub-surface onto the surface is considered as a 'forward reaction' while the desorption of the adsorbed surfactant molecules is considered as a 'reverse reaction'. At equilibrium, when the forward reaction rate is equal to the reverse reaction rate, the adsorption and desorption rate equations should reduce to the model for the equilibrium adsorption isotherm of the surfactant. The form of the mixed-controlled model, therefore, depends on the model used for the equilibrium adsorption isotherm of the surfactant. Available models for the equilibrium adsorption isotherm differ in the manner in which they treat the interactions between the surfactant molecules at the surface. A generalized form of the equilibrium adsorption isotherm can be written as follows:

$$C_b(1 - \frac{\Gamma}{\Gamma_\infty}) = a_G e^{\Phi(\Gamma)} \Gamma \tag{2.3}$$

where Γ_∞ is the maximum surfactant surface concentration, $\Phi(\Gamma)$ models the energy associated with the interactions between the surfactant molecules at the surface, and a_G is a model parameter that accounts for the hydrophobicity of the surfactant molecules. It is customary to write the equilibrium adsorption isotherm in terms of Γ/Γ_∞ instead of Γ. With this in mind, Eq.(2.3) can be written as follows:

$$C_b(1 - \frac{\Gamma}{\Gamma_\infty}) = a e^{\Phi(\Gamma)} \frac{\Gamma}{\Gamma_\infty} \tag{2.4}$$

where $a = a_G \Gamma_\infty$. When no interactions between the adsorbed surfactant molecules are accounted for, $\Phi(\Gamma) = 0$, and Eq. (2.4) reduces to the well-known Langmuir adsorption isotherm [38]. When the interactions are modeled as $\Phi(\Gamma) = K \left(\frac{\Gamma}{\Gamma_\infty}\right)^n$, where K and n are model parameters, Eq. (2.4) reduces to the generalized Frumkin adsorption isotherm [39]. The values of the parameters K and n are determined by regressing the predictions of the generalized Frumkin model with experimental equilibrium adsorption data. A positive value of K corresponds to a net repulsion between the adsorbed surfactant molecules (referred to as 'anti-cooperative' adsorption), and a negative value of K corresponds to a net attraction between the adsorbed surfactant molecules (referred to as 'cooperative' adsorption). When the interactions are modeled as $\Phi(\Gamma) = A(\Gamma) + B(\Gamma)$, where $A(\Gamma)$ models the surfactant head interactions at the surface in terms of hard-sphere repulsions, and $B(\Gamma)$ models the van der Waals attractions between the surfactant tails at the surface, Eq. (2.4)

corresponds to the molecular adsorption isotherm developed by Nikas *et al.* [40]. The functions, $A(\Gamma)$ and $B(\Gamma)$, depend only on the molecular structure of the surfactant molecule, and contain no adjustable parameters that require experimental fitting.

It is important to note that $\Phi(\Gamma)$ in Eq.(2.4) models the interactions between the *adsorbed* surfactant molecules (that is, between the 'products'), and therefore, it should only affect the reverse reaction, that is, the *desorption* of the surfactant molecules from the surface into the bulk solution. With this in mind, one can write the generalized adsorption and desorption rate equations in the mixed-controlled model as follows:

$$\frac{d\Gamma}{dt} = \beta C_{r_0}(1 - \frac{\Gamma}{\Gamma_\infty}) - \alpha e^{\Phi(\Gamma)}\Gamma, \qquad t \geq 0 \tag{2.5}$$

where C_{r_0} is the instantaneous surfactant sub-surface concentration ($C|_{r=r_0}$). The first term on the right-hand side of Eq.(2.5) models the rate of adsorption of the surfactant molecules at the surface, and the second term models the rate of desorption from the surface. In Eq.(2.5), the adsorption is considered as an elementary *reaction* between the surfactant molecules at the sub-surface (C_{r_0}) and the free-sites for adsorption at the surface ($1 - \frac{\Gamma}{\Gamma_\infty}$), whereas the desorption is considered as a first-order reaction of the surfactant molecules at the surface (Γ). In Eq.(2.5), β and α are the rate constants for adsorption and for desorption, respectively, and are related to each other by the equilibrium adsorption isotherm. Specifically, at equilibrium, when $d\Gamma/dt = 0$ and $C_{r_0} = C_b$, Eq.(2.5) reduces to the generalized form of the equilibrium adsorption isotherm (see Eq. (2.4)), where

$$a = \frac{\alpha \Gamma_\infty}{\beta} \tag{2.6}$$

Note that: (i) when $\Phi(\Gamma) = 0$, Eq.(2.5) reduces to the kinetics model corresponding to the Langmuir adsorption isotherm, which has been used to model the adsorption kinetics behavior of alcohols [22, 23], (ii) when $\Phi(\Gamma) = K\left(\frac{\Gamma}{\Gamma_\infty}\right)^n$, Eq.(2.5) reduces to the kinetics model corresponding to the Generalized Frumkin adsorption isotherm, which has been used to model the adsorption kinetics behavior of various $C_i E_j$ nonionic surfactants [13, 41–43].

For the case of diffusion-controlled adsorption, the diffusive transport of the surfactant molecules from the bulk solution to the surface constitutes the rate-limiting step, and the adsorption-desorption

of the surfactant molecules at the surface is assumed to reach equilibrium instantaneously (corresponding to α and $\beta \to \infty$). Consequently, Eq. (2.4) becomes the boundary condition instead of the kinetics description given in Eq. (2.5).

Assuming that the far field ($r \to \infty$) surfactant concentration is uniform at a value C_b, the boundary condition for Eq. (2.1) is given by:

$$C(t \geq 0, r \to \infty) = C_b \qquad (2.7)$$

Assuming a clean surface and a homogeneous bulk solution at the beginning of the adsorption process, the initial conditions associated with the governing equations (Eqs. (2.1) and (2.5)) can be expressed as follows:

$$\Gamma(t = 0) = 0 \qquad \text{and} \qquad C(t = 0, r > r_0) = C_b \qquad (2.8)$$

The governing model equations, Eqs. (2.1) and (2.5), along with the initial and boundary conditions in Eqs. (2.7), (2.8), and (2.2), define completely the time evolution of the surfactant surface concentration, $\Gamma(t)$. The equation of state (EOS), which relates Γ to the resulting reduction in the surface tension (or surface pressure), Π, corresponding to the generalized equilibrium adsorption isotherm in Eq. (2.4), can be derived using the Gibbs adsorption isotherm [38]. Recall that the Gibbs adsorption isotherm relates the change in the equilibrium value of Π with changes in C_b, at constant temperature, to the equilibrium value of Γ as follows:

$$\Gamma = \frac{1}{RT} \left(\frac{\partial \Pi}{\partial \ln C_b} \right)_T \qquad (2.9)$$

where R is the gas constant and T is the absolute temperature. Substituting C_b as a function of Γ from Eq.(2.4) in Eq.(2.9) and rearranging, one obtains:

$$\Gamma \left\{ d \left[\ln \left(\frac{\frac{\Gamma}{\Gamma_\infty}}{1 - \frac{\Gamma}{\Gamma_\infty}} \right) \right] + \frac{d\Phi(\Gamma)}{d\Gamma} d\Gamma \right\} = \frac{1}{RT} d\Pi \qquad (2.10)$$

47

Integrating the two sides of Eq.(2.10) from $(\Gamma = 0, \Pi = 0)$ to (Γ, Π), one obtains the EOS corresponding to the generalized equilibrium adsorption isotherm in Eq.(2.4). Specifically,

$$\Pi(\Gamma) = -\Gamma_\infty RT \left[\ln(1 - \frac{\Gamma}{\Gamma_\infty}) - \frac{1}{\Gamma_\infty} \int_0^\Gamma \left(\frac{d\Phi(\Gamma)}{d\Gamma} \right) \Gamma d\Gamma \right] \qquad (2.11)$$

Note that: (i) when $\Phi(\Gamma) = 0$, Eq. (2.11) reduces to the Langmuir EOS, (ii) when $\Phi(\Gamma) = K \left(\frac{\Gamma}{\Gamma_\infty} \right)^n$, it reduces to the generalized Frumkin EOS [39], and (iii) when $\Phi(\Gamma) = A(\Gamma) + B(\Gamma)$, it reduces to the molecular EOS developed by Nikas et al. [40].

The solution of the mixed-controlled model described by Eqs. (2.1) and (2.5), along with the EOS in Eq. (2.11), enables the prediction of the dynamic surface tension at any given premicellar bulk solution concentration C_b, of the nonionic surfactant. Note that the EOS in Eq.(2.11) can be used to obtain $\Pi(t)$ from $\Gamma(t)$, since after the surfactant molecules adsorb at the surface, they require negligible time to reduce the surface tension as compared to the time scale associated with the adsorption process itself. Indeed, molecular dynamics simulations of surfactant molecules at air/water surfaces are performed for a duration of about 4 ns in order to study *equilibrium* surface properties [44–49]. On the other hand, typical time scales associated with surfactant adsorption kinetics vary from milliseconds to tens of hours depending on the surfactant and its initial bulk solution concentration [8]. Accordingly, it is appropriate to use the dynamic surface concentration, $\Gamma(t)$, to determine the dynamic surface pressure, $\Pi(t)$, using the equilibrium surface pressure (EOS) expression given in Eq.(2.11). Specifically,

$$\Pi(t) = \Pi(\Gamma(t)) = -\Gamma_\infty RT \left[\ln(1 - \frac{\Gamma(t)}{\Gamma_\infty}) - \frac{1}{\Gamma_\infty} \int_0^{\Gamma(t)} \left(\frac{d\Phi(\Gamma)}{d\Gamma} \right) \Gamma d\Gamma \right] \qquad (2.12)$$

In Section 2.2.2, I develop a short-time formalism for the generalized mixed-controlled model presented here.

2.2.2 The New Short-Time Formalism

The new short-time formalism is defined by the range of time, t, and the range of dynamic surfactant surface concentrations, $\Gamma(t)$, for which the formalism is applicable. Assumptions (i) and (ii) below define qualitatively these ranges for t and $\Gamma(t)$, respectively.

48

Assumption (i): According to the model developed in Section 2.2.1, the initial state of the surface corresponds to a clean surface ($\Gamma(t = 0) = 0$). Since the desorption flux is proportional to the surfactant surface concentration, Γ, *we will assume that, at short-times, the desorption flux is negligible relative to the adsorption flux.* Let $t \leq t^*$ define the time range for which this assumption is applicable.

Implementing assumption (i) in Eq.(2.5) yields the *desorption-free mixed-controlled model*:

$$\frac{d\Gamma}{dt} = \beta C_{r0}(1 - \frac{\Gamma}{\Gamma_\infty}), \qquad 0 \leq t \leq t^* \tag{2.13}$$

Neglecting the effect of desorption, my analysis then considers the combined action of adsorption and diffusion on the adsorption kinetics.

Equation (2.13) clearly shows that, at short times, the non-ideal interactions between the surfactant molecules at the surface (reflected in $\Phi(\Gamma)$) *do not affect the kinetics* of accumulation of the surfactant molecules at the surface.

Assumption (ii): *The restriction imposed by the finiteness in the number of free-sites at the surface on adsorption is negligible at short times for adsorption onto a clean surface.* Mathematically, this assumption can be stated as: $\Gamma \ll \Gamma_\infty$. In fact, one can better quantify the inequality between Γ and Γ_∞. For example, in Ref. [24], Adamczyk and Petlicki performed numerical integration of the governing equations of the mixed-controlled adsorption model onto a flat surface, using the Henry and the Langmuir adsorption isotherms, and observed that the effect of the reduction in the number of free sites at the surface on the adsorption of the surfactant molecules can be neglected at short times until a surface coverage of approximately 25% of the maximum coverage is reached (that is, for $\frac{\Gamma}{\Gamma_\infty} < 0.25$). However, their study focussed on a specific surfactant system, and therefore, cannot be generalized to all surfactants. For the moment, let us assume that there exist a value Γ^*, such that, for $\Gamma(t) \leq \Gamma^*$, the restriction imposed by the finiteness in the number of free-sites at the surface on adsorption is negligible. I will determine Γ^* more rigorously in Appendix 2.C by comparing the result of the short-time analysis presented here with the exact numerical solution of the desorption-free mixed-controlled model given in Eq.(2.13).

49

Implementing assumption (ii), Eq. (2.13) yields:

$$\frac{d\Gamma}{dt} = \beta C_{r0}, \qquad 0 \le t \le t^*, \qquad \Gamma \le \Gamma^* \tag{2.14}$$

Using Eq. (2.14) in Eq. (2.2), the boundary condition becomes:

$$D \left. \frac{\partial C}{\partial r} \right|_{r=r_0} = \beta C_{r0} \tag{2.15}$$

Interestingly, Eq.(2.1), along with the boundary and initial conditions in Eqs. (2.15), (2.7), and (2.8), is similar to the partial differential equation (PDE) describing the diffusion in the exterior of a spherical cavity with a convection boundary condition at the surface of the cavity [50]. I used the method of Laplace Transforms to solve this PDE, and the complete derivation is presented in Appendix 2.A. The solution of this PDE can be expressed as follows (see Eqs.(2.A.1), (2.A.2), (2.A.15)- (2.A.17)):

$$\frac{\Gamma(\tau)}{C_b} = m(\tau, \ell_s, \lambda) \tag{2.16}$$

where

$$m(\tau, \ell_s, \lambda) = \frac{\ell_s}{\lambda^3} \left\{ \lambda^2 \tau (\lambda - 1) + 2\lambda\sqrt{\frac{\tau}{\pi}} + \mathrm{erfc}\left(\lambda\sqrt{\tau}\right) \exp\left(\lambda^2 \tau\right) - 1 \right\} \tag{2.17}$$

and

$$\lambda = 1 + \frac{\ell_s}{r_0}, \qquad \tau = \frac{t}{\tau_s}, \qquad \tau_s = \frac{\ell_s^2}{D}, \qquad \text{and} \qquad \ell_s = \frac{D}{\beta} \tag{2.18}$$

In Eq. (2.18), the non-dimensional λ reflects the effect of the surface curvature (r_0) on the adsorption kinetics, τ is the non-dimensional time, τ_s is the time scale associated with the mixed-controlled adsorption process at short (s) times, and ℓ_s is the corresponding length scale. It is noteworthy, that $m(\tau, \ell_s, \lambda)$ in Eq. (2.16): (i) is *independent* of the *surfactant bulk solution concentration* C_b, (ii) is independent of the model used to describe the equilibrium surfactant adsorption behavior, and (iii) *depends only on the kinetics parameters,* D and β, of the surfactant molecule for a specified value of the pendant-bubble radius, r_0 (see Eq. (2.18)).

Note that in implementing assumptions (i) and (ii), I have considered a range of t and Γ values where non-ideal interactions *do not affect the kinetics* of surfactant adsorption. However, once the surfactant molecules adsorb at the surface, non-ideal interactions *can* play a role in determining the

resulting reduction in the surface tension given by Eq.(2.11). Again, this is because, as discussed earlier, after the surfactant molecules reach the surface, they require negligible time to reduce the surface tension as compared to the time scale associated with the adsorption process itself.

Validation of the New Short-Time Formalism (Eq.(2.16))

I validate the new short-time formalism in Eq.(2.16) by comparing its prediction at different conditions to the theoretical results reported in the literature.

Case 1: For the special case of a flat surface ($r_0 \to \infty$), $\lambda = 1$ in Eq.(2.18), and Eqs. (2.16) and (2.17) yield:

$$\frac{\Gamma(\tau)}{\ell_s C_b} = 2\sqrt{\frac{\tau}{\pi}} + \text{erfc}(\sqrt{\tau})\exp(\tau) - 1 \tag{2.19}$$

Note that Sutherland solved the mixed-controlled model exactly for adsorption onto a flat interface, with the desorption term included, for the special case of an *ideal adsorption isotherm*, where $\Gamma = MC_b$ and M is a constant. Specifically, Sutherland's solution is given by [17]:

$$\frac{\Gamma}{MC_b} = 1 - \frac{y}{y-x}\exp(Dtx^2)\text{erfc}(x\sqrt{Dt}) + \frac{x}{y-x}\exp(Dty^2)\text{erfc}(y\sqrt{Dt}) \tag{2.20}$$

where

$$x = \frac{1}{2\ell_s} - \sqrt{\frac{1}{4\ell_s^2} - \frac{1}{M\ell_s}} \quad \text{and} \quad y = \frac{1}{2\ell_s} + \sqrt{\frac{1}{4\ell_s^2} - \frac{1}{M\ell_s}} \tag{2.21}$$

Since Eq.(2.19) is independent of the model used to describe the equilibrium surfactant adsorption behavior, Sutherland's solution in Eq.(2.20) should reduce to Eq.(2.19) when the desorption is assumed to be negligible, that is, when $M \to \infty$. Using the series expansion for $\sqrt{1-z} \approx 1 - \frac{z}{2}$ to approximate the expressions for x and y in Eq.(2.21) at conditions where $M \to \infty$, I obtain:

$$x \approx \frac{1}{M} \quad \text{and} \quad y \approx \frac{1}{\ell_s} - \frac{1}{M} \tag{2.22}$$

Note that

$$\text{erfc}(\sqrt{z})\exp(z) = 1 - 2\sqrt{\frac{z}{\pi}} + z + \mathcal{O}(z^{3/2}), \qquad \text{for small } z \tag{2.23}$$

Substituting x and y from Eq.(2.22) in Eq.(2.20) , using Eq.(2.23) to simplify the term $\exp(Dtx^2)\text{erfc}(x\sqrt{Dt})$, and then letting $M \to \infty$, I find that Eq.(2.20) reduces to Eq.(2.19), as expected.

Case 2: Using Eq.(2.23) in the asymptotic limit $\tau \to 0$, along with the definition of τ, τ_s, and ℓ_s in Eq.(2.18), Eq.(2.19) reduces to the asymptotic short-time limit derived by Hansen for mixed-controlled (mc) adsorption onto a flat ($flat$) surface [18]:

$$\Gamma_{mc}^{flat}(t) = \beta C_b t, \qquad t \to 0 \tag{2.24}$$

Case 3: In the case of diffusion-controlled (dc) adsorption, the adsorption of the surfactant molecules from the sub-surface to the surface is extremely fast, the adsorption rate constant $\beta \to \infty$, which according to Eq.(2.18) leads to $\ell_s \to 0$ and $\tau_s \to 0$, and hence, to $\lambda \to 1$. In this case, Eqs.(2.16) - (2.18) simplify to the following expression derived by Makievski *et al.* in Ref.[51]:

$$\frac{\Gamma_{dc}(t)}{C_b} = 2\sqrt{\frac{Dt}{\pi}} + \frac{Dt}{r_0} \tag{2.25}$$

Equation (2.25) clearly shows that the smaller the radius (r_0) of the pendant bubble, the greater is the adsorption at short-times, consistent with the results presented in Ref. [29]. Equation (2.25) has been used previously in order to study protein and surfactant adsorption onto drops and bubbles [51–53].

Case 4: For the case of a flat surface, $r_0 \to \infty$, and Eq.(2.25) reduces to the well-known short-time asymptotic prediction of the diffusion-controlled adsorption model [18]:

$$\frac{\Gamma_{dc}}{C_b} = 2\sqrt{\frac{Dt}{\pi}} \tag{2.26}$$

Determination of the Limits of Applicability of the New Short-Time Formalism

Note that assumptions (i) and (ii) only specify *qualitatively* the ranges of t and Γ values where the new short-time formalism is applicable. In order to determine *quantitatively* the ranges of t and Γ values where the new short-time formalism is applicable, I compare the adsorption kinetics behaviors that are predicted by making and not making these two assumptions. Developing a quantitative understanding of these limits can be useful when utilizing the new short-time formalism to analyze experimental DST data.

Recall that assumption (i) specifies that the short-time t is sufficiently small ($t \leq t^*$) for the

desorption flux to be negligible as compared to the adsorption flux. In addition, recall that the surface is initially clean (see Eq.(2.8)) and that the desorption flux, which is proportional to the surfactant surface concentration (see Eq.(2.5)), is therefore equal to zero at $t = 0$. In other words, at $t = 0$, there is only adsorption onto the surface, and no desorption takes place. As t increases, the surfactant surface concentration increases, and consequently, the desorption flux begins to be comparable to the adsorption flux. Accordingly, the error associated with neglecting the desorption flux as compared to the adsorption flux increases with time. Note that the sub-surface and the surface are in local equilibrium when the desorption flux is equal to the adsorption flux. Now, consider the following two adsorption cases: (i) β is finite (corresponding to mixed-controlled adsorption), and (ii) β is infinite (corresponding to diffusion-controlled adsorption). When β is finite, α is also finite according to Eq.(2.6), and consequently, adsorption and desorption take place at finite rates, and it takes a finite time for the sub-surface and the surface to reach local equilibrium. On the other hand, when β is infinite, α is also infinite according to Eq.(2.6), and as a result, adsorption and desorption take place at infinite rates, such that the sub-surface and the surface reach instantaneous equilibrium (corresponding to diffusion-controlled adsorption). Considering these two cases, one can expect that the assumption involving a negligible desorption flux as compared to the adsorption flux is least valid for the case of a diffusion-controlled adsorption process. Accordingly, the error associated with assuming a negligible desorption flux for the case of a diffusion-controlled adsorption process can be expected to provide an upper bound to the error corresponding to cases when β is finite (mixed-controlled adsorption). Consequently, the time below which the negligible desorption flux assumption can be considered valid for the diffusion-controlled adsorption case (t_D^*) should provide a lower limit for t^* [3].In view of this, in Appendix 2.B, I determine the time below which the assumption of negligible desorption flux can be considered valid, as well as the associated error, for the case of a diffusion-controlled adsorption process. Based on the results presented in Appendix 2.B, I conclude that assumption (i) is valid to at most 2% error when $t \leq 4.0 \times 10^{-4} \left(\frac{h^2}{D} \right)$, where $h = \left(\frac{\Gamma}{C_b} \right)_e$, with Γ given in Eq.(2.4), and e denoting equilibrium, that is, $t^* = 4.0 \times 10^{-4} \left(\frac{h^2}{D} \right)$.

Recall that I have defined Γ^* based on assumption (ii), such that, for $\Gamma \leq \Gamma^*$, one can neglect

---

[3]A detailed mathematical proof of this proposition is presented in Appendix 2.D.

the restriction imposed by the finiteness in the number of free-sites at the surface on adsorption. I then implemented this assumption in the desorption-free mixed-controlled model (Eq.(2.13)) to obtain Eq.(2.14). In Appendix 2.C, I determine Γ^* by comparing the short-time behavior derived in Eq.(2.16) with the exact numerical solution of the desorption-free mixed-controlled model using Eq.(2.13). Specifically, I compare the dynamic surfactant surface concentrations predicted by the short-time formalism (Γ_{st}) and by the exact numerical solution of the desorption-free mixed-controlled adsorption model (Γ_{exact}). I find that the maximum error between the new formalism and the exact solution, $\Delta\Gamma^*$, in the region $\Gamma(t) \leq \Gamma^* = 0.25\Gamma_\infty$, is given by:

$$\Delta\Gamma^* = \max\ (\Gamma_{st} - \Gamma_{exact}) = 0.02\Gamma_\infty \qquad (2.27)$$

It is noteworthy, that the value of $\Gamma^* = 0.25\Gamma_\infty$ is consistent with the results of Adamczyk and Petlicki [24], who concluded that one can neglect the restriction imposed by the finiteness in the number of free-sites at the surface on adsorption for $\Gamma \leq 0.25\Gamma_\infty$.

Combining the results in Appendices B and C, I conclude that the new short-time formalism provides a suitable description of the short-time behavior of mixed-controlled adsorption when: (a) $t \leq 4.0 \times 10^{-4} \left(\frac{h^2}{D}\right)$, and (b) $\Gamma(t) \leq 0.25\Gamma_\infty$.

Note that both conditions (a) and (b) above, which define the applicability of assumptions (i) and (ii), respectively, need to be satisfied for the new short-time formalism to be valid. Therefore, the assumption that breaks down first should limit the applicability of the new formalism to approximate the short-time adsorption behavior. Which of the two assumptions ((i) or (ii)) limits the applicability of the new formalism depends on the initial surfactant bulk solution concentration C_b. At low C_b values, the driving force for adsorption from the bulk solution to the surface is relatively small, and as a result, it takes a longer time for the surfactant molecules to adsorb at the surface. Over longer times, the desorption of the surfactant molecules from the surface is no longer negligible, and therefore, assumption (i) breaks down before assumption (ii) does. On the other hand, at higher C_b values, the driving force for surfactant adsorption is larger, and as a result, it takes less time for surfactant adsorption to take place. Therefore, the surfactant surface concentration increases faster, and the limitation on the available number of free-sites at the surface on adsorption begins to play an important role in determining the rate of surfactant adsorption.

2.3 Discussion

This section is organized as follows. In Section 2.3.1, I use the new short-time formalism to reconcile the apparent contradiction between theory and experiment regarding the rate-controlling surfactant adsorption kinetics mechanism at short-times. In Section 2.3.2, I discuss how the results of the chapter affect the interpretation of the physical basis underlying the existence of the energy barrier.

2.3.1 Mechanism of Short-Time Surfactant Adsorption

First,I provide some background on the apparent contradiction by reviewing the theoretical prediction and experimental observations with respect to the short-time behavior of DST, and subsequently, I analyze the prediction of the short-time formalism derived in Section 2.2 to reconcile the apparent contradiction.

The Contradiction: Is the Adsorption at Short Times Barrier-Controlled or Diffusion-Controlled?

At asymptotic short times, the diffusion-controlled (*dc*) adsorption model predicts the following change in the surfactant surface concentration with time [18, 24–27] (see also Eq.(2.26)):

$$\Gamma_{dc}(t) = 2C_b\sqrt{\frac{Dt}{\pi}}, \qquad \text{short } t \qquad (2.28)$$

Using Eq.(2.28), along with the ideal surface EOS ($\Pi(\Gamma) = RT\Gamma$), the diffusion-controlled adsorption model predicts a $\sqrt{t}$ variation of the DST at asymptotic short times [18, 24–27]:

$$\Pi_{dc}(t) = 2RTC_b\sqrt{\frac{Dt}{\pi}}, \qquad \text{short } t \qquad (2.29)$$

However, the diffusion-controlled adsorption model is not valid at asymptotic short times, since the model predicts an *unphysical infinite surfactant flux at the surface as* $t \to 0$ [21, 24, 30, 31]. Indeed, differentiating Eq. (2.28) with respect to t, one obtains the following expression for the surfactant adsorption flux at the surface at short times:

$$\frac{d\Gamma_{dc}(t)}{dt} = C_b\sqrt{\frac{D}{\pi}}\frac{1}{\sqrt{t}}, \qquad \text{short } t \qquad (2.30)$$

Equation (2.30) clearly shows that the surfactant adsorption flux at the surface tends to infinity as $t \to 0$.

An asymptotic short-time analysis of the more general mixed-controlled (*mc*) adsorption model predicts that the adsorption is *purely barrier-controlled at asymptotic short times*, and that the surfactant surface concentration varies with time as follows [18, 24–27] (see also Eq.(2.24)):

$$\Gamma_{mc}(t) = \beta C_b t, \qquad \text{short } t \tag{2.31}$$

Using Eq.(2.31), along with the ideal surface EOS, the mixed-controlled adsorption model predicts a linear t variation of the DST at asymptotic short times:

$$\Pi_{mc}(t) = RT \beta C_b t, \qquad \text{short } t \tag{2.32}$$

The prediction of the short-time surfactant adsorption flux by the mixed-controlled adsorption model is obtained by differentiating Eq.(2.31) with respect to t. This yields:

$$\frac{d\Gamma_{mc}(t)}{dt} = \beta C_b, \qquad \text{short } t \tag{2.33}$$

Equation (2.33) shows that the mixed-controlled adsorption model predicts a more realistic *finite value for the short-time adsorption flux at the surface.*

Interestingly, experimental DST data for many nonionic surfactants show a $\sqrt{t}$ behavior at short times [8, 9, 26, 32–37]. The linear t variation of $\Pi(t)$ predicted by the mixed-controlled adsorption model in Eq.(2.32) contrasts with the $\sqrt{t}$ variation of $\Pi(t)$ predicted by the diffusion-controlled adsorption model in Eq.(2.29) to such an extent that a $\sqrt{t}$ behavior of the experimental $\Pi(t)$ at short times is considered as a fingerprint for the existence of diffusion-controlled adsorption. As a result, in spite of the unphysical behavior of the surfactant adsorption flux at the surface as $t \to 0$ predicted by the short-time asymptotic behavior of the diffusion-controlled adsorption model (see Eq.(2.30)), short-time experimental DST data for these surfactant systems have been interpreted in the context of Eq.(2.29) [8, 9, 26, 32–37]. Indeed, it is typical to plot the short-time experimental DST as a function of $\sqrt{t}$, and to extract D values from the resulting *slope* using Eq.(2.29). However, as stressed above, the asymptotic short-time behavior of DST in Eq.(2.29) cannot possibly be valid

56

in view of the unphysical behavior predicted by Eq.(2.30) as $t \rightarrow 0$.

Reconciliation of the Apparent Contradiction

The new short-time formalism sheds light on the existence of a length scale (ℓ_s) and of a time scale (τ_s), associated with ℓ_s, that govern the short-time adsorption kinetics in the context of the mixed-controlled model (see Eq.(2.18)). The development of a physical understanding of the length scale, as well as of the associated time scale, provides insight into the relative significance of diffusion and the energy barrier in governing the overall rate of surfactant adsorption at the surface at short-times. In order to understand the existence of the length scale, let us compare mixed barrier-diffusion controlled adsorption with diffusion-controlled adsorption: the presence of an energy barrier for adsorption at the surface slows down the overall rate of surfactant adsorption as compared to purely diffusion-driven adsorption. Since diffusion and barrier adsorption take place *sequentially*, I compare the *additional time* required for the surfactant molecules to adsorb at the surface, due to the presence of the energy barrier after reaching the sub-surface, to a situation where the surfactant molecules diffuse through an *additional liquid layer* of thickness ℓ_a before *instantaneously* adsorbing at the surface. Note that considering the effect of the energy barrier as being equivalent to diffusion over an additional length ℓ_a provides a convenient strategy to compare the relative magnitudes of the two steps (diffusion-driven and barrier-driven adsorptions) in determining the overall rate of surfactant adsorption at the surface. I calculate ℓ_a by equating the flux due to diffusion through a layer of thickness ℓ_a to the flux due to barrier adsorption. The flux of surfactant molecules at the surface in the presence of the energy barrier ($\dot{q}_e$), at short times, is given by (see Eq. (2.33)):

$$\dot{q}_e = \beta C_b \tag{2.34}$$

The scale value for the surfactant flux associated with diffusion of the surfactant molecules through a layer of thickness ℓ_a ($\dot{q}_d$) is given by Fick's Law as:

$$\dot{q}_d = D \frac{C_b}{\ell_a} \tag{2.35}$$

When the diffusive flux through ℓ_a equals the rate of surfactant adsorption at the surface in the presence of the energy barrier, that is, when $\dot{q}_d = \dot{q}_e$, one can use Eqs. (2.34) and (2.35) to

estimate ℓ_a. Specifically, recalling that $\ell_s = D/\beta$ (see Eq.(2.18)), one obtains:

$$\ell_a = \frac{D}{\beta} = \ell_s \qquad (2.36)$$

Equation (2.36) reveals that the length scale, ℓ_s, can be interpreted as the *additional distance* that the surfactant molecules have to diffuse across before reaching the surface. Consequently, $\tau_s = \frac{\ell_s^2}{D}$ in Eq.(2.18) can be interpreted as the characteristic time associated with the diffusion of the surfactant molecules across this additional layer of thickness ℓ_s. When the adsorption is diffusion controlled, $\beta \to \infty$, and the surfactant molecules adsorb instantaneously at the surface as soon as they reach the sub-surface. In this case, $\ell_s \to 0$, implying that the surfactant molecules do not have to diffuse any additional distance from the sub-surface in order to reach the surface. Also, note that when the length scale associated with diffusion in the bulk solution is much greater than ℓ_s, then the effect of the energy barrier in determining the overall rate of surfactant adsorption at the surface can be neglected. In that case, the adsorption process becomes diffusion controlled.

In the short-time limit, specifically, in the desorption-free adsorption regime, the length scale over which diffusion takes place (ℓ_D) varies with time. Using the diffusion scaling of the length and time scales, ℓ_D can be expressed as follows [54]:

$$\ell_D \sim \sqrt{Dt} \qquad (2.37)$$

Therefore, as adsorption takes place, ℓ_D increases progressively from zero. At asymptotic short-time limits, $t \to 0$ and $\ell_D \ll \ell_s$, indicating that the adsorption kinetics is barrier controlled, a prediction which is consistent with the short-time asymptotic analysis of the mixed-controlled adsorption model (see Eq.(2.31)). As t increases, ℓ_D increases according to Eq.(2.37), and one can expect that diffusion in the bulk solution becomes as significant as the energy barrier in controlling the overall rate of surfactant adsorption. As t increases further, ℓ_D becomes much greater than ℓ_s, and therefore, one can expect that the adsorption kinetics becomes diffusion controlled. From the length scale analysis presented here, I see that *mixed-controlled adsorption behaves like diffusion-limited adsorption as t increases*! While this observation is interesting, some questions still remain: With time, as diffusion becomes more important in controlling the rate of surfactant adsorption,

what is the resulting adsorption behavior? How would this behavior compare with the short-time asymptotic $\sqrt{t}$ behavior predicted by the diffusion-controlled adsorption model? I address these questions by performing a quantitative analysis of the new short-time formalism.

In Figure 2-1, I compare the short-time mixed-controlled adsorption behavior onto a *flat surface* (see Eq. (2.19)) with the short-time asymptotic behavior predicted by the diffusion-controlled adsorption model (see Eq. (2.28)) in terms of non-dimensional variables. Specifically, the non-dimensional surfactant surface concentration, $\bar{\Gamma} = \Gamma/(\ell_s C_b)$, is plotted as a function of the square root of the non-dimensional time, $\sqrt{\tau} = \sqrt{t/\tau_s}$ (see Eq.(2.18)). One can see that $\bar{\Gamma}$ corresponding
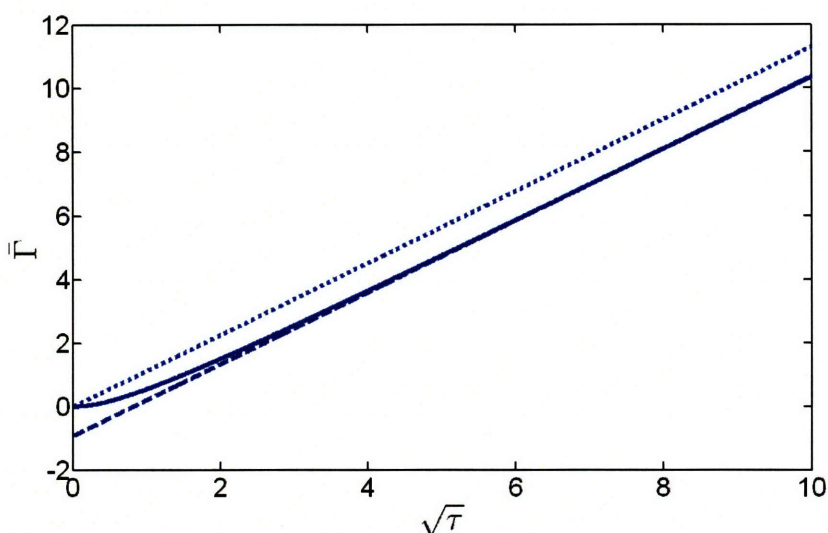
Figure 2-1: Comparison of the prediction of the short-time mixed-controlled model (solid line) with the prediction of the short-time diffusion-controlled model (dotted line), where the non-dimensional surfactant surface concentration, $\bar{\Gamma}$, is plotted as a function of the square root of the non-dimensional time, $\sqrt{\tau}$. The dashed line indicates the approach of the mixed-controlled model to a $\sqrt{\tau}$ behavior.

to diffusion-controlled adsorption (the dotted line in Figure 2-1) is higher than $\bar{\Gamma}$ corresponding to mixed-controlled adsorption (the solid line in Figure 2-1) at all $\tau > 0$, indicating greater adsorption in the diffusion-controlled case relative to the mixed-controlled case. In Figure 2-2, I plot the slopes of $\bar{\Gamma}$ with respect to $\sqrt{\tau}$ ($d\bar{\Gamma}/d\sqrt{\tau}$) as a function of $\sqrt{\tau}$ predicted by the mixed-controlled adsorption model using Eq.(2.19) (solid line) and by the diffusion-controlled adsorption model using Eq.(2.28) (dashed line). I find that when $\sqrt{\tau} > \approx 7$, there is less than 1% difference between the slopes predicted by the mixed-controlled and the diffusion-controlled models: that is, *the mixed-controlled*
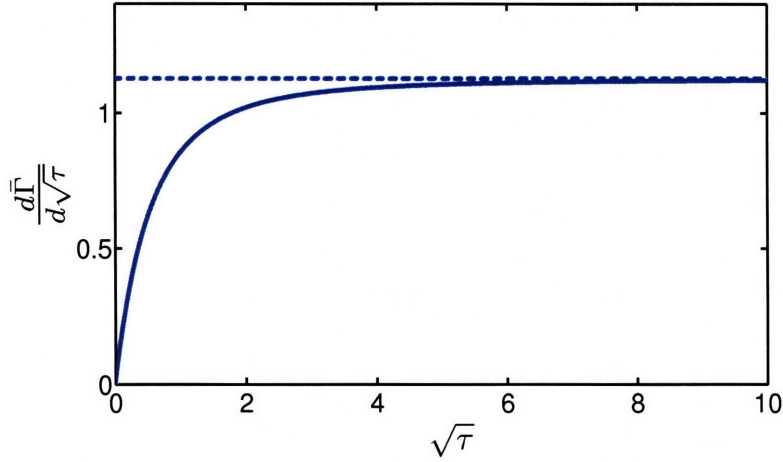
Figure 2-2: Comparison of the prediction of the short-time mixed-controlled model (solid line) with the asymptotic prediction of the diffusion-controlled model (dashed line), where the differential of the non-dimensional surfactant surface concentration with respect to $\sqrt{\tau}$, $\frac{d\bar{\Gamma}}{d\sqrt{\tau}}$, is plotted as a function of the square root of the non-dimensional time, $\sqrt{\tau}$.

adsorption model predicts a $\sqrt{\tau}$ variation for $\sqrt{\tau} > \approx 7$.

In other words, for $\tau > \approx 50$, the slope of Eq. (2.19), for all practical purposes, is equal to $2/\sqrt{\pi}$, the slope predicted by the short-time asymptotic diffusion-controlled adsorption behavior. Note that this result is in agreement with the results of the length-scale analysis discussed above. If t^* denotes the time until which the short-time formalism is valid, then, Figure 2-1 reveals that in order to observe an overall $\sqrt{t}$ dependence of $\Gamma(t)$, t^* should be greater than about $100\tau_s$. Using the definition of τ_s in Eq.(2.18), this condition translates into:

$$\beta \geq 10\sqrt{\frac{D}{t^*}} = \beta_{min} \tag{2.38}$$

Similarly, if Γ^* denotes the maximum dynamic surfactant surface concentration until which the short-time formalism is valid, then, Figure 2-1 reveals that in order to observe an overall $\sqrt{t}$ dependence of $\Gamma(t)$, Γ^* should be greater than about $10\ell_s C_b$. Using the definition of ℓ_s in Eq.(2.18), this condition translates into:

$$C_b \leq \frac{\Gamma^*\beta}{10D} = C_{b,max} \tag{2.39}$$

60

Combining the conditions in Eqs.(2.38) and (2.39) , I conclude that an overall $\sqrt{t}$ dependence of $\Gamma(t)$ can be observed even for a mixed-controlled adsorption process whenever (a) $\beta \geq \beta_{min}$, and (b) $C_b \leq C_{b,max}$.

The region where $\bar{\Gamma}$, given by Eq. (2.19), approaches a $\sqrt{\tau}$ behavior (that is, the region $\sqrt{\tau} \geq 7$) can be approximated by a linear fit, as shown by the dashed line in Figure 2-1, given by:

$$\Gamma_{mc}(t) \approx 2C_b\sqrt{\frac{Dt}{\pi}} - \frac{0.92C_bD}{\beta} \qquad (2.40)$$

In Ref.[26], Fainerman $et\ al.$ derived the following approximate short-time mixed-controlled adsorption behavior for cases where the effect of the barrier is significant as compared to that of diffusion::

$$\Gamma = \frac{2C_b\sqrt{\frac{Dt}{\pi}}}{1 + \frac{2}{\beta}\sqrt{\frac{D}{\pi t}}}, \qquad \text{for} \qquad \beta \ll \sqrt{\frac{D}{\pi t}} \qquad (2.41)$$

Although Eq.(2.41) is not valid whenever $\beta \geq 10\sqrt{\frac{D}{t^*}}$ (see Eq.(2.38)) , it is interesting to note that Eq.(2.41) also reduces to a form similar to Eq.(2.40) when a series expansion for $(1+z)^{-1} \approx 1-z$ is used to approximate the denominator of Eq.(2.41):

$$\Gamma = 2C_b\sqrt{\frac{Dt}{\pi}} - \frac{4C_bD}{\pi\beta} \qquad (2.42)$$

Note that Eqs.(2.40) and (2.42) differ by a constant factor in the second term (0.92 in Eq.(2.40) vs. $\frac{4}{\pi}$ in Eq.(2.42)). This is probably because Eq.(2.41) was derived specifically for conditions when $\beta \ll \sqrt{\frac{D}{\pi t}}$, and here it is used to approximate the adsorption behavior in the range when $\beta \geq 10\sqrt{\frac{D}{t^*}}$.

Combining Eq.(2.40) with the Ideal surface EOS, which is expected to be valid for small values of Π, one obtains:

$$\Pi_{mc}(t) \approx 2RTC_b\sqrt{\frac{Dt}{\pi}} - \frac{0.92C_bDRT}{\beta} \qquad (2.43)$$

An important implication of Eq.(2.43) is that $one\ can\ expect\ to\ observe\ a\ \sqrt{t}\ variation\ of\ the\ DST$ $at\ short\ times\ even\ in\ the\ case\ of\ mixed-controlled\ adsorption.$ From the above analysis, it follows that an apparent $\sqrt{t}$ variation of the DST at short times does not necessarily imply the applicability

61

of Eq.(2.29), or the conclusion that adsorption is diffusion-controlled at asymptotic short times. As stressed earlier, the diffusion-controlled adsorption model predicts an unphysical infinite flux at $t = 0$, and the mixed-controlled adsorption model is expected to be closer to reality at short times. Therefore, the observed $\sqrt{t}$ behavior of the experimental DST should be interpreted in the context of the mixed-controlled model in Eq.(2.43) rather than in the context of the diffusion-controlled adsorption model in Eq.(2.29). For many surfactant systems, the τ_s values can be extremely small, and as a result, the DST behavior of the mixed-controlled adsorption model may result in a $\sqrt{t}$ behavior at the time scales where experimental DST measurements are possible.

Interestingly, the slope of the DST corresponding to the $\sqrt{t}$ behavior predicted by the mixed-controlled adsorption model (see Eq.(2.43)) is the same as the slope of the DST corresponding to the $\sqrt{t}$ behavior predicted by the diffusion-controlled adsorption model (see Eq.(2.29)). This observation implies that, although the applicability of Eq.(2.29) to analyze the short-time experimental DST is questionable, the D values obtained using Eq.(2.29) can be expected to be reasonable. Consequently, my analysis does not affect the D values obtained in the past using Eq.(2.29). Moreover, Eq.(2.43) reveals that while D values can be obtained from the *slope* (S) of the $\sqrt{t}$ behavior of the experimental DST data, β values can be estimated from the *intercept* ($\Delta\Pi_0$) of the linear $\sqrt{t}$ fit at short times. In other words, if $\Pi(t) = S\sqrt{t} - \Delta\Pi_0$ is the best fit equation obtained from the experimental DST data at short times, then D and β values can be obtained using Eq. (2.43) as follows:

$$D = \pi \left(\frac{S}{2RTC_b} \right)^2 \quad \text{and} \quad \beta = \left(\frac{0.92RTC_bD}{\Delta\Pi_0} \right) \tag{2.44}$$

The ability to extract β values from the short-time experimental DST data using Eqs. (2.43) and Eqs.(2.44) can be very useful from a practical viewpoint.

2.3.2 On the Nature of the Energy Barrier

Although the effect of the energy barrier on surfactant adsorption at the surface has been accounted for in the mixed-controlled model in terms of the model parameter β, the physical basis underlying the existence of the energy barrier is still unclear [2, 3, 8, 55, 56].

Some of the current notions for the existence of the energy barrier associate its physical basis to *high* surfactant surface concentrations [8, 20, 33, 34]. This conclusion is based primarily on the

interpretation that the observed $\sqrt{t}$ behavior of the *short-time* DST of many nonionic surfactants corresponds to a diffusion-controlled adsorption at asymptotic short-times (see Eq.(2.29)). This, in turn, has been interpreted as implying that adsorption onto a *clean surface* corresponds to *diffusion-controlled adsorption*. Combining this interpretation, along with the fact that the effect of the energy barrier is more pronounced at higher initial surfactant bulk solution concentrations C_b [13, 16] , the origin of the energy barrier has been associated with the high surfactant concentrations that exist at the surface at high values of C_b. In fact, energy barrier values have been estimated by analyzing the *long-time* experimental DST behavior, where the surfactant surface concentrations are expected to be high [33–35, 57, 58]. However, in Section 2.3.1, I demonstrated that mixed-controlled adsorption also results in an apparent $\sqrt{t}$ behavior of the DST at short times for $\sqrt{\tau} > \approx 7$ (or $t > \approx 50\tau_s$). Therefore, an apparent $\sqrt{t}$ variation of the experimental DST at short times does not necessarily imply that the adsorption is purely diffusion controlled at asymptotic short-times. In view of these important new findings, it appears necessary to re-evaluate the physical basis underlying the existence of the energy barrier.

It is noteworthy, that the mixed-controlled model predicts that at asymptotic short-times, when a clean surface is exposed to a bulk surfactant solution, the adsorption is *barrier-controlled* [18, 24–27]. At short-times, when the surface is clean and when the surfactant concentration in the bulk solution is uniform, the surfactant molecules near the surface adsorb. Therefore, it is reasonable that, at short-times, surfactant adsorption at the surface constitutes the rate-limiting step. Note that at asymptotic short-times, the surface is relatively clean and the interactions between the adsorbed surfactant molecules are expected to be negligible. Moreover, the mixed-controlled model predicts that at *asymptotic long-times*, the adsorption is *diffusion-controlled* for any C_b value [18, 25–27, 59]). At long-times, as the system nears equilibrium, the surfactant concentration in the sub-surface approaches the surfactant concentration in the bulk solution interior. Since the diffusive flux is proportional to the *gradient* of the surfactant concentration, the driving force for diffusion decreases progressively to zero as the system approaches equilibrium. It is important to note that, while the driving force for diffusion is proportional to the *gradient* of the surfactant concentration, the driving force responsible for the kinetic process of adsorption is proportional to the *absolute value* of the surfactant concentration (see Eq.(2.5)). Therefore, it is reasonable that this asymptotic

63

decrease in the driving force associated with the diffusive flux makes diffusion the rate-limiting step for adsorption at long-times, and that the kinetic process of adsorption at the surface is not rate limiting at long-times. Accordingly, the long-time asymptotic prediction of the mixed-controlled model implies that the energy barrier for adsorption has no effect on the long-time DST behavior, irrespective of how high is the surfactant surface concentration.

Based on the prediction of the mixed-controlled model that adsorption is always *barrier-controlled* at *asymptotic short-times,* one may conclude that the energy barrier for adsorption corresponding to the energy barrier associated with the adsorption of a *single* surfactant molecule onto a *clean surface.* The prediction of the mixed-controlled model that the energy barrier is associated with a single surfactant molecule adsorbing onto a clean surface is consistent with the reported observation of an energy barrier in several molecular dynamics simulation studies. Indeed, in these simulation studies, the adsorption of various *single* nonionic solute molecule onto a *clean* water-vapor surface were investigated. Specifically, potential of mean force (PMF) calculations modeling the adsorption of: (i) a n-decanol molecule at a water-air surface [55], (ii) a phenol molecule at a water-vapor surface [60], (iii) a p-n-pentylphenol molecule at a water-vapor surface [61] , (iv) an ethanol molecule at a water-vapor surface [62], and (v) a methanol molecule at a water-vapor surface [63], all predict the existence of an energy barrier close to the interfacial region.

2.4 Conclusions

In this chapter, I have reconciled the apparent contradiction between theoretical prediction and experimental observations on the nature of the adsorption kinetics mechanism at short-times: while the more general mixed-controlled adsorption model predicts a purely barrier-controlled adsorption process at asymptotic short times, experimental DST data for many nonionic surfactants have been interpreted in the context of a purely diffusion-controlled adsorption process at asymptotic short times. This is because, at asymptotic short times, the mixed-controlled adsorption model predicts a linear variation of Π with time t, the diffusion-controlled adsorption model predicts a $\sqrt{t}$ variation of Π with t, and the experimental DST of many nonionic surfactants display a $\sqrt{t}$ behavior. I resolved this apparent contradiction by deriving a new *non-asymptotic* short-time formalism for the mixed-controlled adsorption model, including determining the ranges of time t values and

of dynamic surfactant surface concentration $\Gamma(t)$ values for which the formalism is applicable. I find that the mixed-controlled adsorption model, while predicting barrier-controlled adsorption at asymptotic short-times, also predicts a $\sqrt{t}$ behavior of Π when $t >\approx 50\tau_s$, where τ_s is the time scale associated with mixed-controlled adsorption at short times. Accordingly, the experimentally observed $\sqrt{t}$ behavior of the DST does not necessarily imply the existence of purely diffusion-controlled adsorption at asymptotic short times. I have also discussed how this finding affects some of the current notions of the physical basis underlying the existence of the energy barrier. I concluded that the energy barrier is associated with the adsorption of a *single* surfactant molecule onto a *clean* surface, and is not related to high surfactant surface concentrations.

Recall that the new short-time formalism introduced here was found to be applicable over a range of t and Γ values where reliable experimental DST measurements can be carried out. In Chapter 3, I develop a new methodology where the new formalism is used to estimate the kinetics parameters, D and β, from short-time experimental DST data measured using a pendant-bubble apparatus.

Appendix 2.A: Solution of the Partial Differential Equation (PDE) Using Laplace Transforms

In this Appendix, I derive the solution of the governing PDE corresponding to the mixed-controlled model where assumptions (i) and (ii) are applicable (Eqs.(2.1) and (2.14)) using the method of Laplace Transforms.

Before the Laplace Transformation was applied to the governing PDE, the equations were written in terms of the following non-dimensional variables:

$$\bar{C} = \frac{C}{C_b}, \qquad \bar{\Gamma} = \frac{\Gamma}{C_b \ell_s}, \qquad x = \frac{r - r_0}{\ell_s}, \qquad \text{and} \qquad \tau = \frac{t}{\tau_s} \tag{2.A.1}$$

where τ_s and ℓ_s are the time and length scales associated with the kinetics of adsorption at short-times. For the case of mixed-controlled adsorption at short-times at conditions where assumptions (i) and (ii) are valid, τ_s and ℓ_s can be determined from a scaling analysis of Eqs.(2.1) and (2.14) as follows:

$$\tau_s = \frac{\ell_s^2}{D} \qquad \text{and} \qquad \ell_s = \frac{D}{\beta} \tag{2.A.2}$$

The mixed-controlled model equations after implementing assumptions (i) and (ii) (Eqs.(2.1) and (2.14)) , as well as the boundary and initial conditions in Eqs. (2.2), (2.7), and (2.8), can be written in terms of the non-dimensional variables in Eq.(2.A.1) as follows:

$$\frac{\partial \bar{C}}{\partial \tau} = \frac{1}{(Ax+1)^2} \frac{\partial}{\partial x} \left[(Ax+1)^2 \frac{\partial \bar{C}}{\partial x} \right], \qquad x \geq 0, \qquad \tau \geq 0 \tag{2.A.3}$$

$$\frac{d\bar{\Gamma}}{d\tau} = \bar{C}|_{x=0} \tag{2.A.4}$$

$$\left(\frac{\partial \bar{C}}{\partial x} \right)_{x=0} = \frac{d\bar{\Gamma}}{d\tau} \tag{2.A.5}$$

$$\bar{C}(\tau \geq 0, x \to \infty) = 1 \tag{2.A.6}$$

66

$$\bar{\Gamma}(\tau = 0) = 0, \qquad \bar{C}(\tau = 0, x \geq 0) = 1 \tag{2.A.7}$$

where $A = \ell_s/r_0$.

Laplace Transforms of the governing equations, Eqs. (2.A.3) and (2.A.4), using the initial condition in Eq.(2.A.7), yields:

$$s\bar{C}_s - 1 = \frac{2A}{(Ax+1)}\frac{d\bar{C}_s}{dx} + \frac{d^2\bar{C}_s}{dx^2} \tag{2.A.8}$$

and

$$s\bar{\Gamma}_s = \bar{C}_s|_{x=0} \tag{2.A.9}$$

where $\bar{C}_s$ and $\bar{\Gamma}_s$ are the Laplace variables of $\bar{C}$ and $\bar{\Gamma}$, respectively, and s is the Laplace domain variable.

Laplace Transforms of the boundary conditions, Eqs. (2.A.5) and (2.A.6), yields:

$$\frac{d\bar{C}_s}{dx}\bigg|_{x=0} = s\bar{\Gamma}_s \tag{2.A.10}$$

and

$$\bar{C}_s|_{x=\infty} = \frac{1}{s} \tag{2.A.11}$$

The second-order ODE (Eq.(2.A.8)) can be solved for $\bar{C}_s$ using the boundary conditions given in Eqs.(2.A.11) and (2.A.10). This yields:

$$\bar{C}_s(x) = \frac{e^{-\sqrt{s}x}}{Ax+1}\left(-\frac{s\bar{\Gamma}_s}{\sqrt{s}+A}\right) + \frac{1}{s} \tag{2.A.12}$$

From Eq.(2.A.12) with $x = 0$, if follows that the Laplace Transform of the non-dimensional surfactant sub-surface concentration is given by:

$$\bar{C}_s^0 = \bar{C}_s(x = 0) = \frac{1}{s} - \frac{s\bar{\Gamma}_s}{\sqrt{s}+A} \tag{2.A.13}$$

Solving for $\bar{C}_s^0$ (or for $\bar{\Gamma}_s$) by taking an inverse Laplace Transform of Eq.(2.A.13) requires an additional relation between $\bar{C}_s^0$ and $\bar{\Gamma}_s$. In the case of diffusion-limited adsorption, $\bar{\Gamma}_s$ and $\bar{C}_s^0$ are related by the Laplace Transform of the equilibrium adsorption isotherm. In the case of mixed-

controlled adsorption, $\bar{\Gamma}_s$ and $\bar{C}_s^0$ are related by the Laplace Transform of the mixed-controlled model (Eq.(2.5)). Specifically, for the case of mixed-controlled adsorption at short-times where assumptions (i) and (ii) are valid, Eq.(2.A.9) can be used with Eq.(2.A.13) to obtain:

$$\bar{\Gamma}_s = \frac{1}{s^2 \left[1 + \frac{1}{\sqrt{s}+A}\right]} \tag{2.A.14}$$

Taking the inverse Laplace Transform of Eq.(2.A.14), and then substituting the expressions for $\bar{\Gamma}$ and $\bar{C}$ in Eq.(2.A.1), yields:

$$\frac{\Gamma(\tau)}{C_b} = m(\tau, \ell_s, \lambda) \tag{2.A.15}$$

where

$$m(\tau, \ell_s, \lambda) = \frac{\ell_s}{\lambda^3} \left\{ \lambda^2 \tau(\lambda - 1) + 2\lambda\sqrt{\frac{\tau}{\pi}} + \mathrm{erfc}\left(\lambda\sqrt{\tau}\right) \exp\left(\lambda^2 \tau\right) - 1 \right\} \tag{2.A.16}$$

and

$$\lambda = 1 + A = 1 + \frac{\ell_s}{r_0} \tag{2.A.17}$$

Equation (2.A.15) describes the variation of Γ as a function of non-dimensional time, τ, for given values of C_b, r_0, D, and β (see Eqs.(2.A.2) and (2.A.17)).

Appendix 2.B: Determination of t_D^*

In this Appendix, I determine t_D^*, defined as the time until which the assumption of negligible desorption is applicable for the case of diffusion-controlled adsorption, by comparing the exact solution of the diffusion-controlled adsorption model to the case where desorption is considered negligible.

Recall that Eq.(2.A.13) relates the Laplace image of the non-dimensional surfactant sub-surface concentration ($\bar{C}_s^0$) to the Laplace image of the instantaneous non-dimensional surfactant surface concentration ($\bar{\Gamma}_s$). In the case of the diffusion-controlled adsorption model, $\bar{\Gamma}_s$ and $\bar{C}_s^0$ are related by the Laplace Transform of the equilibrium adsorption isotherm, after the equilibrium adsorption isotherm is expressed in terms of the non-dimensional surfactant surface concentration, $\bar{\Gamma}$, and, the non-dimensional surfactant sub-surface concentration, $\bar{C}^0$. Therefore, given an equilibrium adsorption isotherm, $\bar{\Gamma}_s$ can be determined using Eq.(2.A.13) , and subsequently, taking the inverse Laplace Transform yields the time evolution of $\bar{\Gamma}$. Note that an exact solution of $\bar{\Gamma}$ using Eq.(2.A.13) requires knowledge of an equilibrium adsorption isotherm. Since one is interested in the short-time adsorption behavior where C^0 is small, I will assume a linear Henry's Law relation between Γ and C^0, that is,

$$\Gamma = hC^0 \tag{2.B.1}$$

where h is a measure of the surface activity of the nonionic surfactant. Note that for a real system, h may not be constant, and may change as a function of C^0. Using the definitions of the non-dimensional variables in Eq.(2.A.1), Eq.(2.B.1) can be written as follows:

$$\bar{\Gamma} = h_n \bar{C}^0 \qquad \text{where} \qquad h_n = \frac{h}{\ell_s} \tag{2.B.2}$$

Taking a Laplace Transform of Eq.(2.B.2) yields:

$$\bar{\Gamma}_s = h_n \bar{C}_s^0 \tag{2.B.3}$$

Using Eq.(2.B.3) in Eq.(2.A.13) and rearranging yields:

$$\bar{\Gamma}_s = h_n \frac{\sqrt{s} + A}{(sh_n + \sqrt{s} + A)s} \tag{2.B.4}$$

The inverse Laplace Transform of Eq.(2.B.4) gives the time evolution of the non-dimensional surfactant surface concentration in the case of diffusion-controlled adsorption:

$$\frac{\bar{\Gamma}(\tau)}{h_n} = 1 + \frac{-\sqrt{s_1}\exp(s_1\tau)\text{erfc}(-\sqrt{s_1\tau}) + \sqrt{s_2}\exp(s_2\tau)\text{erfc}(-\sqrt{s_2\tau})}{-\sqrt{s_2} + \sqrt{s_1}} \tag{2.B.5}$$

where $\sqrt{s_1}$ and $\sqrt{s_2}$ are the roots of the following quadratic equation:

$$sh_n + \sqrt{s} + A = 0 \tag{2.B.6}$$

Using the definitions of the non-dimensional variables in Eq.(2.A.1), Eq.(2.B.5) can be written as follows:

$$\frac{\Gamma(\tau_D)}{hC_b} = 1 + \frac{-r_1\exp(r_1^2\tau_D)\text{erfc}(-r_1\tau_D^{1/2}) + r_2\exp(r_2^2\tau_D)\text{erfc}(-r_2\tau_D^{1/2})}{-r_2 + r_1} \tag{2.B.7}$$

where:

$$r_1 = \frac{-1 + \sqrt{1 - 4h_r}}{2}, \qquad r_2 = \frac{-1 - \sqrt{1 - 4h_r}}{2}, \qquad \tau_D = \frac{tD}{h^2}, \qquad \text{and} \qquad h_r = \frac{h}{r_0}$$

$$\tag{2.B.8}$$

Equation (2.B.7) represents the dynamic surfactant surface concentration (Γ) for the case of a diffusion-controlled adsorption process. The predicted dynamic surfactant surface concentration (Γ^p), assuming a negligible desorption flux, for the case when $\beta \to \infty$ is given by Eq.(2.25) . In order to facilitate the comparison between Γ and Γ^p, Eq.(2.25) is first written in terms of the nondimensional variables defined in Eq.(2.B.8):

$$\frac{\Gamma^p}{hC_b} = 2\sqrt{\frac{\tau_D}{\pi}} + \tau_D h_r \tag{2.B.9}$$

The percentage error (ϵ) associated with assuming a negligible desorption flux can be defined as follows:

$$\epsilon = \left(\frac{\Gamma^p - \Gamma}{\Gamma}\right) 100 \tag{2.B.10}$$

where Γ^p is given in Eq.(2.B.9) and Γ is given in Eq.(2.B.7).

Equations (2.B.10) and (2.B.8) show that the percentage error associated with assuming negligible desorption is a function of the non-dimensional diffusion time-scale, τ_D, and of the non-dimensional curvature, h_r. In Figure 2-3, I plot $\epsilon(\tau_D)$ in Eq.(2.B.10) for three values of h_r : the solid line corresponds to $h_r = 0$, the dashed line corresponds to $h_r = 5$, and the dotted line corresponds to $h_r = 10$. Figure 2-3 shows that for the values of h_r considered, $\epsilon = 2$ when τ_D is about $1 \times 10^{-3.4}$. This implies that the error associated with assuming negligible desorption in the case of diffusion-controlled adsorption is at most 2% when $\tau_D \leq \tau_D^* = 4.0 \times 10^{-4}$, or using Eq.(2.B.8), when $t \leq t_D^* = 4.0 \times 10^{-4} \left(\frac{h^2}{D} \right)$. The maximum nondimensional surface concentration for $t \leq t_D^*$ can be estimated using Eq.(2.B.7) to be about $0.02hC_b$. Or equivalently, using the existence of equilibrium between the sub-surface and the surface (see Eq.(2.B.1)) , the surfactant sub-surface concentration C^0 changes from 0 to $0.02C_b$.
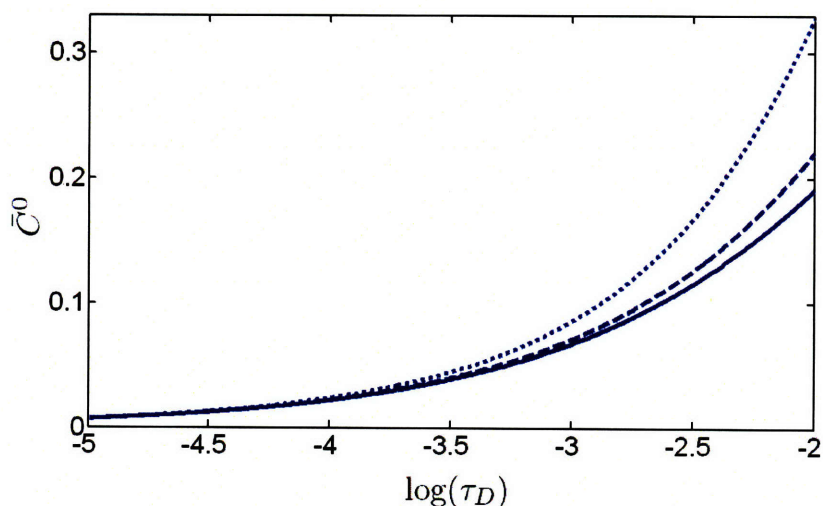
Figure 2-3: Time evolution of the percentage error associated with assuming a negligible desorption, ϵ , for the diffusion-controlled adsorption model, plotted as a function of the non-dimensional time, $\log(\tau_D)$, for three values of the non-dimensional curvature, $h_r = 0$ (solid line), $h_r = 5$ (dashed line), and $h_r = 10$ (dotted line).

For the purpose of estimating t_D^* for a typical nonionic surfactant, consider the adsorption kinetics of the alkyl ethoxylate nonionic surfactant $C_{12}E_4$ having an initial surfactant bulk solution concentration C_b. The equilibrium adsorption isotherm for the $C_{12}E_4$ surfactant was found to be

described well by the Generalized Frumkin (GF) adsorption isotherm [64], which is given by:

$$\frac{\Gamma}{\Gamma_\infty} = \frac{C_b}{C_b + a \exp\left(K[\frac{\Gamma}{\Gamma_\infty}]^n\right)} \qquad (2.B.11)$$

The GF parameter values for $C_{12}E_4$ have been reported in Ref. [64] to be: $\Gamma_\infty = 6.585$ x 10^{-10} mol/cm^2, $a = 2.942$ x 10^{-10} mol/cm^3, $K = 4.105$, and $n = 0.717$. The variation of $h = \frac{\Gamma}{C_b}$ as a function of C_b corresponding to Eq.(2.B.11) is plotted in Figure 2-4, which shows that h decreases as C_b increases. Recall that I had assumed a constant value for h in the derivation of Eq.(2.B.7),
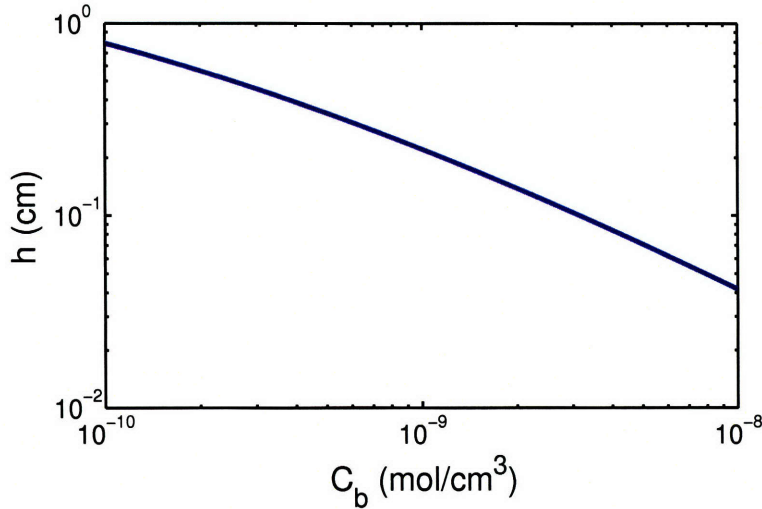
Figure 2-4: Plot of $h = \left(\frac{\Gamma}{C_b}\right)_e$ as a function of the initial surfactant bulk solution concentration C_b, for the nonionic surfactant $C_{12}E_4$ using the Generalized Frumkin equilibrium adsorption isotherm (see Eq.(2.B.11)).

and that the maximum surfactant surface concentration for $t \leq t_D^* = 4.0$ x $10^{-4} \left(\frac{h^2}{D}\right)$ was given by $C^0 = 0.02C_b$. Therefore, as the surfactant sub-surface concentration increases from $C^0 = 0$ to $C^0 = 0.02C_b$, h decreases from h_1 to h_2, where: (i) $h_1 = (\Gamma/C^0)_e$ is evaluated at $C^0 = 0$, (ii) $h_2 = (\Gamma/C^0)_e$ is evaluated at $C^0 = 0.02C_b$, and (iii) $h_2 < h_1$. Note that for a case where h remains constant at a value of h_1, the formalism will be valid until $t \leq t_{D,1}^* = 4.0$ x $10^{-4} \left(\frac{h_1^2}{D}\right)$, and for a case where h remains constant at a value of h_2, the formalism will be valid until $t \leq t_{D,2}^* = 4.0$ x $10^{-4} \left(\frac{h_2^2}{D}\right)$. Note that, since $h_2 < h_1$, it follows that $t_{D,2}^* < t_{D,1}^*$. Accordingly, when h changes from h_1 to h_2 for a real surfactant system, one can expect the formalism to be valid until at least

$t \leq t^*_{D,2}$. In other words, a *lower limit* for t^*_D corresponding to an actual surfactant is given by $t^*_{D,2} = 4.0 \times 10^{-4} \left(\frac{h_2}{D}\right)$.

The estimated value of the lower limit for t^*_D is plotted as a function of C_b in Figure 2-5, where a diffusivity value of $D = 6.4 \times 10^{-6}$ cm^2/s [64] was used in the estimation. Considering that DST measurements corresponding to $C_{12}E_4$ have been carried out for time values as small as a fraction of a second [65], Figure 2-5 shows that t^*_D spans a sufficiently broad time range where reliable DST measurements may actually be carried out.
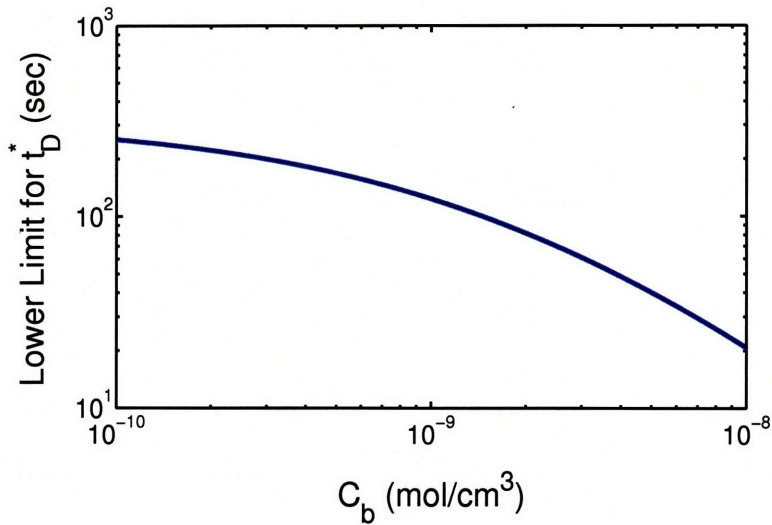
Figure 2-5: Plot of the lower limit of the time until which assumption (i) can be considered valid, denoted as Lower Limit for t^*_D, as a function of the initial surfactant bulk solution concentration C_b, for the nonionic surfactant $C_{12}E_4$ using the Generalized Frumkin equilibrium adsorption isotherm(see Eq.(2.B.11))

Appendix 2.C: Determination of Γ^*

In this Appendix, I determine Γ^*, the range of surfactant surface concentrations for which the effect of the restriction imposed by the fact that there is a finite number of sites for adsorption at the surface can be neglected (see assumption (ii) in Section 2.2.2). Keeping in mind that I implemented assumption (ii) in the desorption-free mixed-controlled model in Eq.(2.13) to derive the new short-time formalism, I will determine Γ^* by comparing the short-time behavior derived in Eq.(2.16) with the exact numerical solution of the desorption-free mixed-controlled model using Eq.(2.13).

First, I summarize all the governing equations for the desorption-free mixed-controlled model:

$$\frac{\partial C}{\partial t} = \frac{D}{r^2}\frac{\partial}{\partial r}(r^2\frac{\partial C}{\partial r}), \qquad r \geq r_0, \qquad t \geq 0 \tag{2.C.1}$$

$$C(t \geq 0, r \to \infty) = C_b \tag{2.C.2}$$

$$\frac{d\Gamma}{dt} = \beta C_{r0}(1 - \frac{\Gamma}{\Gamma_\infty}) \tag{2.C.3}$$

$$\Gamma(t = 0) = 0 \quad \text{and} \quad C(t = 0, r > r_0) = C_b \tag{2.C.4}$$

$$D\left.\frac{\partial C}{\partial r}\right|_{r=r_0} = \frac{d\Gamma}{dt} \tag{2.C.5}$$

Second, I rewrite Eqs. (2.C.1)-(2.C.5) in terms of the non-dimensional variables defined as follows:

$$\bar{C} = \frac{C}{C_n}, \qquad \bar{\Gamma} = \frac{\Gamma}{\Gamma_n}, \qquad x = \frac{r - r_0}{\ell_n}, \qquad \text{and} \qquad \tau = \frac{t}{\tau_n} \tag{2.C.6}$$

where C_n, Γ_n, ℓ_n, and τ_n are the normalizing scale values for the surfactant bulk solution concentration, the surfactant surface concentration, the length, and the time, respectively. In order to facilitate comparison of the predictions of the desorption-free mixed controlled model and the predictions of the short-time formalism (Eq.(2.16)), I choose the normalizing scale values for time

(τ_n) and for length (ℓ_n) to be the same as the time (τ_s) and length (ℓ_s) scale values of the short-time formalism (Eq.(2.18)). Specifically, I choose:

$$\tau_n = \tau_s = \frac{\ell_s^2}{D}, \quad \text{and} \quad \ell_n = \ell_s = \frac{D}{\beta} \tag{2.C.7}$$

Recall that the assumption of neglecting the finiteness in the number of free-sites for adsorption leads to the assumption that the term $(1 - \frac{\Gamma}{\Gamma_\infty})$ in the desorption-free mixed-controlled model (see (Eq.(2.13))) is approximately equal to 1 (see Eq.(2.14)). Therefore, it is appropriate to choose the normalizing scale value for Γ as Γ_∞. That is, I choose:

$$\Gamma_n = \Gamma_\infty \tag{2.C.8}$$

Considering that the initial surfactant bulk solution concentration is C_b (see Eq.(2.C.4)), I choose the normalizing scale value for the surfactant bulk solution concentration, C_n, to be equal to C_b, that is, I choose:

$$C_n = C_b \tag{2.C.9}$$

The desorption-free mixed-controlled model equations (Eqs. (2.C.1) - (2.C.5)) can be written in terms of the non-dimensional variables in Eq.(2.C.6), with the normalizing scale values defined in Eqs.(2.C.7) - (2.C.9), as follows:

$$\frac{\partial \bar{C}}{\partial \tau} = \frac{1}{(Ax+1)^2} \frac{\partial}{\partial x} \left[(Ax+1)^2 \frac{\partial \bar{C}}{\partial x} \right], \quad x \geq 0, \quad \tau \geq 0 \tag{2.C.10}$$

$$\bar{C}(\tau \geq 0, x \to \infty) = 1 \tag{2.C.11}$$

$$\frac{d\bar{\Gamma}}{d\tau} = k\bar{C}_{x=0}(1 - \bar{\Gamma}) \tag{2.C.12}$$

$$\bar{\Gamma}(\tau = 0) = 0, \quad \bar{C}(\tau = 0, x \geq 0) = 1 \tag{2.C.13}$$

$$k \left(\frac{\partial \bar{C}}{\partial x} \right)_{x=0} = \frac{d\bar{\Gamma}}{d\tau} \qquad (2.C.14)$$

where

$$A = \frac{\ell_s}{r_0}, \qquad k = \frac{C_b}{C_e}, \qquad \text{and} \qquad C_e = \frac{\Gamma_\infty \beta}{D} \qquad (2.C.15)$$

I find that the non-dimensionalization of the desorption-free mixed-controlled model presented above identifies two independent non-dimensional quantities, A and k, that affect the short-time surfactant adsorption kinetics. The quantities A - the non-dimensional curvature of the pendant drop and k - the non-dimensional initial surfactant bulk solution concentration, reflect the importance of the pendant-bubble curvature and of the initial surfactant bulk solution concentration, respectively, on the short-time adsorption kinetics. Below, I will find that the concentration scale C_e in Eq.(2.C.15) indicates the initial surfactant bulk solution concentration at which the effect of the energy (e) barrier in controlling the adsorption kinetics becomes significant. For typical values of $\beta \approx 0.004$ cm/s [41], $D \approx 7$ x 10^{-6} cm^2/s [64], and $\Gamma_\infty \approx 5$ x 10^{-10} mol/cm^2 for C_iE_j surfactants [64], C_e has a value of the order of 1 x 10^{-7} mol/cm^3 (see Eq.(2.C.15)), and ℓ_s has a value of the order of 0.001 cm (see Eq.(2.C.7)). For typical values of the critical micelle concentration of C_iE_j surfactants (of the order of 1 x 10^{-7} mol/cm^3 [38]), the *maximum* value of k is of the order of 1. For typical values of the radius of the pendant bubble ($r_0 \approx 0.1$ cm [64]), the quantity A has a value of the order of 0.01.

In Figure 2-6, for the case of a flat surface ($r_0 \to \infty$, $A \to 0$), I compare the exact numerical solution of the desorption-free mixed-controlled model (solid lines) with the predictions of the short-time formalism using Eq.(2.16) (dashed lines) for $k = 0.01$, 0.1, and 1. In Figure 2-6, I also compare the predictions of the short-time diffusion-controlled adsorption model in Eq.(2.26) (dotted lines) for $k = 0.01$, 0.1, and 1 to the short-time formalism in Eq.(2.16) and to the exact numerical solution.

The following observations follow from Figure 2-6:

1. The short-time formalism provides a good approximation of the short-time behavior of the desorption-free mixed-controlled model for $\bar{\Gamma} = \Gamma/\Gamma_\infty \leq 0.25$, and a better approximation as compared to the short-time diffusion-controlled adsorption model.
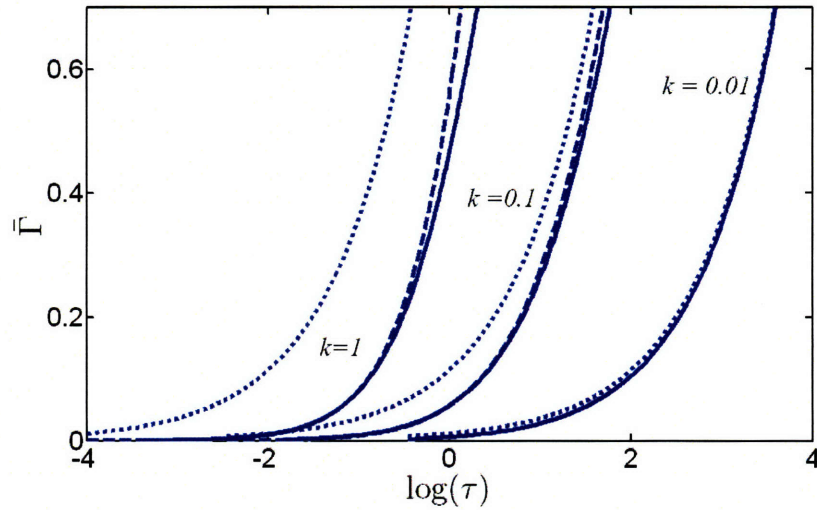
Figure 2-6: Comparison of the predictions ($\bar{\Gamma}$ vs. $\log(\tau)$) of the short-time formalism for the mixed-controlled model (dashed lines) and for the diffusion-controlled model (dotted lines) with the exact numerical solution of the desorption-free mixed-controlled model (solid lines) for three values of the non-dimensional initial surfactant bulk solution concentration, $k = 0.01$, $k = 0.1$, and $k = 1$, in the case of adsorption onto a *flat* surface ($A = 0$).

2. The diffusion-controlled adsorption model provides a better approximation of the desorption-free mixed-controlled adsorption model at smaller surfactant bulk solution concentrations ($k = 0.01$) than at higher surfactant bulk solution concentrations ($k = 0.1$ and 1). This is in agreement with the known observations [13–16] that: (i) the diffusion-controlled adsorption model describes well the kinetics of surfactant adsorption at lower surfactant bulk solution concentrations, and (ii) the effect of the energy barrier is more pronounced at higher surfactant bulk solution concentrations. This implies *that an analysis of short-time DST measurements conducted at lower surfactant bulk solution concentrations is not suitable for the accurate determination of the barrier parameter β.* This finding is also consistent with the conclusions of Ref. [21].

3. The non-dimensional concentration, k, serves as a good indicator of the initial surfactant bulk solution concentration for which the effect of the energy barrier on the kinetics of surfactant adsorption at short times becomes significant. Specifically, for $k = 0.01$, Figure 2-6 shows that the overall adsorption behavior corresponds essentially to diffusion-controlled adsorption, and that the effect of the energy barrier is not significant. On the other hand, for $k = 0.1$

77

and 1, significant deviations are observed between the predictions of the diffusion-controlled adsorption model and the desorption-free mixed-controlled adsorption model. Accordingly, when $C_b \ll C_e$, diffusion controls the overall rate of surfactant adsorption, when $C_b \sim C_e$, the energy barrier controls the overall rate of surfactant adsorption, and at intermediate values of C_b, the adsorption is mixed-controlled.

In Figure 2-7, I compare the exact numerical solution of the desorption-free mixed controlled model (solid lines) with the short-time formalism (dashed lines), and with the short-time diffusion-controlled formalism in Eq.(2.25) (dotted lines) for a curved surface ($A = 0.01$) for $k = 0.01$, 0.1, and 1. Again, I find that the short-time formalism provides a good approximation of the desorption-free mixed controlled model for $\Gamma \leq 0.25\Gamma_\infty$.
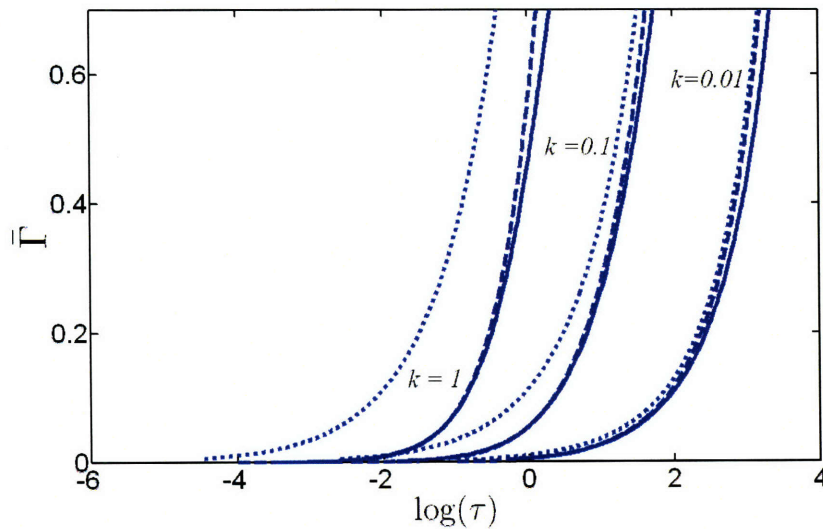
Figure 2-7: Comparison of the predictions ($\bar{\Gamma}$ vs. $\log(\tau)$) of the short-time formalism for the mixed-controlled model (dashed lines) and for the diffusion-controlled model (dotted lines) with the exact numerical solution of the desorption-free mixed-controlled model (solid lines) for three values of the non-dimensional initial surfactant bulk solution concentration, $k = 0.01$, $k = 0.1$, and $k = 1$, in the case of adsorption onto a *spherical* surface ($A = 0.01$).

Comparing the dynamic surfactant surface concentrations predicted by the new short-time formalism (Γ_{st}) and by the exact numerical solution of the desorption-free mixed-controlled adsorption model (Γ_{exact}), one finds that the maximum error between the new formalism and the exact solution, $\Delta\Gamma^*$, in the region $\Gamma(t) \leq 0.25\Gamma_\infty$ occurs for $k = 0.01$, $A = 0.01$, and $\Gamma(t) = 0.25\Gamma_\infty$, and

is given by:

$$\Delta\Gamma^* = \max\left(\Gamma_{st} - \Gamma_{exact}\right) = 0.02\Gamma_\infty \tag{2.C.16}$$

Overall, Figures 2-6 and 2-7 indicate that, the new short-time formalism provides a good approximation to the exact numerical solution of the desorption-free mixed-controlled model until a surface coverage of about $\Gamma^* = 0.25\Gamma_\infty$ is reached.

One can also express the limit of applicability of assumption (ii) in terms of the measured surface pressure, $\Pi(t)$, rather than in terms of $\Gamma(t)$, since $\Gamma(t)$ is typically not measured experimentally. The Π limit of applicability of the new short-time formalism, referred to as Π^*, can be obtained by substituting $\Gamma = \Gamma^* = 0.25\Gamma_\infty$ in Eq.(2.11). This yields:

$$\Pi^* = \Pi(\Gamma^*) = \Gamma_\infty RT \left[0.2877 + \frac{1}{\Gamma_\infty}\int_0^{\Gamma^*}\left(\frac{d\Phi(\Gamma)}{d\Gamma}\right)\Gamma d\Gamma\right] \tag{2.C.17}$$

For the special case of the Generalized Frumkin adsorption isotherm, for which $\Phi(\Gamma) = K\left(\frac{\Gamma}{\Gamma_\infty}\right)^n$, Eq.(2.C.17) reduces to:

$$\Pi^* = \Gamma_\infty RT \left[0.2877 + Kn\frac{(0.25)^{n+1}}{n+1}\right] \tag{2.C.18}$$

For example, consider again the case of the $C_{12}E_4$ nonionic surfactant. The Π^* value for which the new short-time formalism is valid was estimated using Eq.(2.C.18) and the GF parameters appearing in Eq.(2.B.11) to be 7.3 mN/m. Recalling that reliable DST measurements can be carried out to measure changes in surface tension as small as 0.2 mN/m [66], one finds that the Π^* value spans a range of experimentally relevant DST values.

Appendix 2.D: Proof of the Proposition

In this Appendix, I state and prove the proposition that the error associated with assuming a negligible desorption flux is maximum when the adsorption kinetics is diffusion-controlled.

Proposition

If $\Gamma^a(t; \beta, D)$ denotes the actual (a) dynamic surfactant surface concentration for a process involving adsorption-desorption and diffusion , and $\Gamma^p(t; \beta, D)$ denotes the predicted (p) dynamic surfactant surface concentration for a process involving only adsorption and diffusion (that is, desorption is assumed to be negligible), then, the error associated with this assumption can be defined as follows:

$$\Delta\Gamma(t; \beta, D) = \Gamma^p(t; \beta, D) - \Gamma^a(t; \beta, D) \tag{2.D.1}$$

Equation (2.D.1) indicates that the time evolutions of $\Delta\Gamma$, Γ^p, and Γ^a depend on the parameters β and D. Note that the error in Eq.(2.D.1) is defined after recognizing that $\Gamma^p(t; \beta, D)$ is expected to be larger than $\Gamma^a(t; \beta, D)$.

The proposition that the error associated with assuming a negligible desorption flux is maximum when the adsorption kinetics is diffusion-controlled (corresponding to $\beta \rightarrow \infty$) takes on the following mathematical form:

$$\max_{\beta}[\Delta\Gamma(t; \beta, D)] = \Delta\Gamma(t; D)_{\beta \rightarrow \infty} \tag{2.D.2}$$

Proof

To prove the proposition, I will first demonstrate that the error $\Delta\Gamma$ is a non-decreasing function of β, that is, that

$$\frac{d\Delta\Gamma}{d\beta} \geq 0 \tag{2.D.3}$$

where the inequality holds for any finite value of β, and the equality is satisfied only when $\beta \rightarrow \infty$. While the inequality for finite values of β ensures that the error is larger for a higher value of β, the equality at $\beta \rightarrow \infty$ ensures that the error saturates at a finite value. From Eq.(2.D.3), I will show that the error is maximum in the case of a diffusion-controlled adsorption process.

Consider the following form for the change of Γ^a with time based on the generalized mixed-

80

controlled model (see Eq.(2.5)):

$$\frac{d\Gamma^a}{dt} = \beta C_{r0}^a - \alpha e^{\Phi(\Gamma^a)}\Gamma^a \qquad (2.D.4)$$

where C_{r0}^a denotes the sub-surface surfactant concentration for the case where *adsorption-desorption and diffusion* take place. Note that the factor $(1 - \frac{\Gamma}{\Gamma_\infty})$ has not been included in the adsorption term in Eq.(2.D.4). Considering that one is interested in the short-time behavior where the effect of the term $(1 - \frac{\Gamma}{\Gamma_\infty})$ will be neglected in view of assumption (ii) in Section 2.2.2, I will assume the validity of Eq.(2.D.4) in the remainder of the proof. This form of Eq.(2.D.4) is also convenient, because if this term were included, the algebra associated with the proof becomes intractable.

Recall that α and β are not independent, but instead, are related by the equilibrium adsorption isotherm (see Eq.(2.6)). With this in mind, using Eq.(2.6) and the definition $a = a_G \Gamma_\infty$, yields:

$$\alpha = \beta a_G \qquad (2.D.5)$$

Using Eq.(2.D.5) in Eq.(2.D.4), I obtain:

$$\frac{d\Gamma^a}{dt} = \beta[C_{r0}^a - a_G e^{\Phi(\Gamma^a)}\Gamma^a] \qquad (2.D.6)$$

Using the definition of Γ^p, the change of Γ^p with time can be written based on the mixed-controlled model as follows:

$$\frac{d\Gamma^p}{dt} = \beta C_{r0}^p \qquad (2.D.7)$$

where C_{r0}^p denotes the sub-surface surfactant concentration for the case where *only adsorption and diffusion take place*. The flux balances at the interface for the two cases (adsorption-desorption-diffusion and adsorption-diffusion) are given by:

$$D \left.\frac{\partial C^a}{\partial r}\right|_{r=r_0} = \frac{d\Gamma^a}{dt} \qquad (2.D.8)$$

$$D \left.\frac{\partial C^p}{\partial r}\right|_{r=r_0} = \frac{d\Gamma^p}{dt} \qquad (2.D.9)$$

81

While the adsorption process at the interface reduces the surfactant sub-surface concentration C_{r0}, the resulting diffusive flux from the bulk solution tends to increase C_{r0}. Consequently, determining the exact behavior of C_{r0} will involve solving diffusion partial differential equations. In the analysis here, I will use the concept of a *diffusion penetration depth* [4] to approximate the solution of the diffusion equation, due to its analytical simplicity, in order to obtain expressions for C_{r0}^a and C_{r0}^p. According to this concept, the depth of penetration of *any* disturbance at the boundary of a semi infinite *flat* surface into the bulk is given by $\delta_D(t) = \sqrt{\pi D t}$, and the flux at the surface (s) can be approximated as follows [4]:

$$\left.\frac{\partial C}{\partial z}\right|_s \approx \frac{C_b - C_s}{\delta_D(t)} \tag{2.D.10}$$

where z denotes the direction normal to the flat surface and C_s is the sub-surface surfactant concentration. Note that $\delta_D(t) = \sqrt{\pi D t}$ is applicable only for a *flat* surface [4]. The existence of curvature at the surface could possibly influence $\delta_D(t)$. Considering this possibility, let $\delta_{D,r_0}(t)$ be the diffusion penetration depth for the case of a curved surface, where r_0 is the radius of the surface. Using the diffusion penetration depth formulation in Eqs.(2.D.8) and (2.D.9), and substituting the resulting equations in Eqs.(2.D.6) and (2.D.7), I obtain:

$$D\frac{C_b - C_{r0}^a}{\delta_{D,r_0}(t)} = \beta[C_{r0}^a - a_G e^{\Phi(\Gamma^a)}\Gamma^a] \tag{2.D.11}$$

$$D\frac{C_b - C_{r0}^p}{\delta_{D,r_0}(t)} = \beta C_{r0}^p \tag{2.D.12}$$

Solving for C_{r0}^a and C_{r0}^p in Eqs.(2.D.11) and (2.D.12) yields:

$$C_{r0}^a = \frac{DC_b + \beta a_G \delta_{D,r_0}(t) e^{\Phi(\Gamma^a)}\Gamma^a}{D + \beta\delta_{D,r_0}(t)} \tag{2.D.13}$$

$$C_{r0}^p = \frac{DC_b}{D + \beta\delta_{D,r_0}(t)} \tag{2.D.14}$$

Using Eqs.(2.D.13) and (2.D.14) in Eqs.(2.D.6) and (2.D.7), I obtain:

$$\frac{d\Gamma^a}{dt} = \frac{D\beta}{D + \beta\delta_{D,r_0}(t)}\left(C_b - a_G e^{\Phi(\Gamma^a)}\Gamma^a\right) \tag{2.D.15}$$

82

$$\frac{d\Gamma^p}{dt} = \frac{D\beta}{D + \beta\delta_{D,r_0}(t)}C_b \tag{2.D.16}$$

One should note that use of the concept of *diffusion penetration depth* has reduced the problem to solving two Ordinary Differential Equations (ODEs) in Eqs.(2.D.15) and (2.D.16).

Next, I subtract Eq.(2.D.15) from Eq.(2.D.16) in order to obtain a single ODE which governs the propagation of the error $\Delta\Gamma$ with time. Specifically:

$$\frac{d\Delta\Gamma}{dt} = \frac{D\beta}{D + \beta\delta_{D,r_0}(t)}a_G e^{\Phi(\Gamma^a)}\Gamma^a \tag{2.D.17}$$

Since $\Gamma^a(t = 0) = 0$ and $\Gamma^p(t = 0) = 0$, it follows that $\Delta\Gamma(t = 0) = 0$. Note that surfactant molecules adsorb at the surface as t increases, and therefore, $\Gamma^a > 0$ for all $t > 0$. Equation (2.D.17) indicates that *the error $\Delta\Gamma$ increases with time*.

Since one is interested in $\frac{d\Delta\Gamma}{d\beta}$ (see Eq.(2.D.2)), I next differentiate both sides of Eq.(2.D.17) with respect of β. This yields:

$$\frac{d}{d\beta}\left(\frac{d\Delta\Gamma}{dt}\right) = \frac{D^2}{(D + \beta\delta_{D,r_0}(t))^2}a_G e^{\Phi(\Gamma^a)}\Gamma^a + \frac{D\beta}{D + \beta\delta_{D,r_0}(t)}a_G\left(\frac{d[e^{\Phi(\Gamma^a)}\Gamma^a]}{d\Gamma^a}\right)\frac{d\Gamma^a}{d\beta}$$

$$\tag{2.D.18}$$

Using the commutative property of mixed second-order derivatives, I can write the left-hand side of Eq.(2.D.18) as follows:

$$\frac{d}{d\beta}\left(\frac{d\Delta\Gamma}{dt}\right) = \frac{d}{dt}\left(\frac{d\Delta\Gamma}{d\beta}\right) \tag{2.D.19}$$

Combining Eqs.(2.D.19) and (2.D.18), I obtain the following ODE that governs how $\frac{d\Delta\Gamma}{d\beta}$ varies with time:

$$\frac{d}{dt}\left(\frac{d\Delta\Gamma}{d\beta}\right) = \frac{D^2}{(D + \beta\delta_{D,r_0}(t))^2}a_G e^{\Phi(\Gamma^a)}\Gamma^a + \frac{D\beta}{D + \beta\delta_{D,r_0}(t)}a_G\left(\frac{d[e^{\Phi(\Gamma^a)}\Gamma^a]}{d\Gamma^a}\right)\frac{d\Gamma^a}{d\beta}$$

$$\tag{2.D.20}$$

Next, I make the following three important observations about Eq.(2.D.20):

(i) When β is finite and $\Gamma^a > 0$, the first term on the RHS is greater than 0. When β is infinite, this term is equal to 0.

(ii) The derivative $\frac{d\Gamma^a}{d\beta}$ indicates how the actual surfactant surface concentration changes as β changes. Recalling that β represents the rate constant for the adsorption of the surfactant molecules from the sub-surface onto the surface, with a *higher* value of β indicating a *weaker* effect of the energy barrier in controlling the rate of adsorption, one can anticipate that Γ^a increases as β increases. In the limiting condition, when β is infinity, Γ^a should correspond to the value resulting from a diffusion-controlled adsorption process. Consequently,

$$\frac{d\Gamma^a}{d\beta} > 0, \quad \text{if } \beta \text{ is finite}$$

$$\frac{d\Gamma^a}{d\beta} = 0, \quad \text{if } \beta \text{ is infinite}$$

(iii) I will assume that the interaction term $\Phi(\Gamma^a)$ is such that it satisfies the following condition:

$$1 + \Gamma^a \left(\frac{d\Phi(\Gamma^a)}{d\Gamma^a} \right) > 0 \tag{2.D.21}$$

The condition in Eq.(2.D.21) ensures that:

$$\frac{d[e^{\Phi(\Gamma^a)}\Gamma^a]}{d\Gamma^a} > 0 \tag{2.D.22}$$

Note that the condition in Eq.(2.D.21) can be expected to be valid for most nonionic surfactants. In the case of surfactants that experience a net repulsive interaction at the interface, like the C_iE_j nonionic surfactants, $\Phi(\Gamma^a)$ is positive, and an increasing function of Γ^a [64]. Consequently, these surfactants satisfy Eq.(2.D.21). For surfactants that involve a net attractive interaction at the interface, like $C_{10}OH$ and C_9OH [64], Eq.(2.D.21) was found to be satisfied for $\Gamma \leq \Gamma^* = 0.25\Gamma_\infty$.

84

Combining (i)-(iii) above, I conclude that:

$$\frac{d}{dt}\left(\frac{d\Delta\Gamma}{d\beta}\right) > 0, \quad \text{if } \beta \text{ is finite} \qquad (2.D.23)$$

$$\frac{d}{dt}\left(\frac{d\Delta\Gamma}{d\beta}\right) = 0, \quad \text{if } \beta \text{ is infinite}$$

Equation (2.D.23) indicates that $\frac{d\Delta\Gamma}{d\beta}$ is an *increasing* function of t for any *finite value of* β. Note that the initial condition that $\Delta\Gamma(t = 0) = 0$ is *independent* of β. Therefore,

$$\left.\frac{d\Delta\Gamma}{d\beta}\right|_{t=0} = 0 \qquad (2.D.24)$$

Combining Eqs.(2.D.23) and (2.D.24) one may conclude that:

(i) When β is finite and $t > 0$, $\frac{d\Delta\Gamma}{d\beta}$ is *greater than zero*, and it increases with time.

(ii) When β is infinite, $\frac{d\Delta\Gamma}{d\beta}$ is equal to zero.

Statements (i) and (ii) above indicate that $\Delta\Gamma$ is maximum when β is infinite, which in turn, corresponds to the diffusion-controlled process. Therefore, the proposition in Eq.(2.D.2) has been proven.

Bibliography

[1] G. Kretzschmar and R. Miller. Dynamic properties of adsorption layers of amphiphilic substances at fluid interfaces. *Advances in Colloid and Interface Science*, 36:65–124, 1991.

[2] B. A. Noskov. Fast adsorption at the liquid-gas interface. *Advances in Colloid and Interface Science*, 69:63–129, 1996.

[3] F. Ravera, M. Ferrari, and L. Liggieri. Adsorption and partitioning of surfactants in liquid-liquid systems. *Advances in Colloid and Interface Science*, 88:129–177, 2000.

[4] P. Joos. *Dynamic Surface Phenomena*. VSP, The Netherlands, 1999.

[5] R. Defay and G. Petre. Dynamic surface tension. In E. Matijevic, editor, *Surface and Colloid Science*, volume 3, pages 27–81. Wiley, 1971.

[6] S. S. Dukhin, G. Kretzschmar, and R. Miller, editors. *Dynamics of adsorption of liquid interfaces: theory, experiment, applications*. Elsevier, 1995.

[7] C-H. Chang and Elias I. Franses. Adsorption dynamics of surfactants at the air/water interface: a critical review of mathematical models, data, and mechanisms. *Colloids and Surfaces A: Physicochemical and Engineering Aspects*, 100:1–45, 1995.

[8] J. Eastoe and J. S. Dalton. Dynamic surface tension and adsorption mechanisms of surfactants at the air-water interface. *Advances in Colloid and Interface Science*, 85:103–144, 2000.

[9] R. Miller, P. Joos, and V. B. Fainerman. Dynamic surface and interfacial tensions of surfactant and polymer solutions. *Advances in Colloid and Interface Science*, 49:249–302, 1994.

[10] V. Pillai and D. O. Shah, editors. *Dynamic Properties of Interfaces and Association Structures*. AOCS Press, 1996.

[11] F. Ravera, L. Liggieri, and R. Miller. Molecular orientation as a controlling process in adsorption dynamics. *Colloids and Surfaces A: Physicochemical and Engineering Aspects*, 175:51–60, 2000.

[12] A. F. H. Ward and L.Tordai. Diffusion controlled adsorption. *Journal of Chemical Physics*, 14:453, 1946.

[13] R. Pan, J. Green, and C. Maldarelli. Theory and experiment on the measurement of kinetic rate constants for surfactant exchange at an air/water interface. *Journal of Colloid and Interface Science*, 205:213–230, 1998.

[14] H-C. Chang, C-T. Hsu, and S-Y. Lin. Adsorption kinetics of $C_{10}E_8$ at the air-water interface. *Langmuir*, 14:2476–2484, 1998.

[15] S-Y. Lin, R-Y. Tsay, L-W. Lin, and S-I. Chen. Adsorption kinetics of $C_{12}E_8$ at the air-water interface: Adsorption onto a clean interface. *Langmuir*, 12:6530–6536, 1996.

[16] C. Dong, C-T. Hsu, C-Y. Chiu, and S-Y. Lin. A study on surfactant adsorption kinetics: Effect of bulk concentration on the limiting adsorption rate constant. *Langmuir*, 16:4573–4580, 2000.

[17] K. L. Sutherland. The kinetics of adsorption at liquid surfaces. *Australian Journal of Scientific Research*, A5:683–696, 1952.

[18] R. S. Hansen. Diffusion and the kinetics of adsorption of aliphatic acids and alcohols at the water-air interface. *Journal of Colloid Science*, 16:549–560, 1961.

[19] J. F. Baret. Theoretical model for an interface allowing a kinetic study of adsorption. *Journal of Colloid and Interface Science*, 30:1–12, 1969.

[20] J. F. Baret. Kinetics of adsorption from a solution. Role of the diffusion and of the adsorption-desorption antagonism. *The Journal of Physical Chemistry*, 72:2755–2758, 1968.

[21] R. P. Borwankar and D. T. Wasan. The kinetics of adsorption of surface active agents at gas-liquid surfaces. *Chemical Engineering Science*, 38(10):1637 – 1649, 1983.

[22] R. Bleys and P. Joos. Adsorption kinetics of bolaform surfactants at the air/water interface. *Journal of Physical Chemistry*, 89:1027–1032, 1985.

[23] P. Joos and G. Serrien. Adsorption kinetics of lower alkanols at the air/water interface: Effect of structure makers and structure breakers. *Journal of Colloid and Interface Science*, 127(1):97–103, 1989.

[24] Z. Adamczyk and J. Petlicki. Adsorption and desorption kinetics of molecules and colloidal particles. *Journal of Colloid and Interface Science*, 118(1):20–49, 1987.

[25] K. D. Danov, D. S. Valkovska, and P. A. Kralchevsky. Adsorption relaxation for nonionic surfactants under mixed barrier-diffusion and micellization-diffusion control. *Journal of Colloid and Interface Science*, 251:18–25, 2002.

[26] V. B. Fainerman, A. V. Makievski, and R. Miller. The analysis of dynamic surface tension of sodium alkyl sulphate solutions, based on asymptotic equations of adsorption kinetic theory. *Colloids and Surfaces A: Physicochemical and Engineering Aspects*, 87:61 – 75, 1994.

[27] L. K. Filippov. Dynamic surface tension of aqueous surfactant solutions. *Journal of Colloid and Interface Science*, 164:471–482, 1994.

[28] L.K. Filippov. Dynamic surface tension of aqueous surfactant solutions: 1. Diffusion-convective controlled adsorption. *Journal of Colloid and Interface Science*, 163:49–60, 1994.

[29] J. K. Ferri, S. Y. Lin, and K. J. Stebe. Curvature effects in the analysis of Pendant bubble data: Comparison of numerical solutions, asymptotic arguments, and data. *Journal of Colloid and Interface Science*, 241:154–168, 2001.

[30] E. Yariv and I. Frankel. The diffusion-controlled limit revisited. *Physical Review Letters*, 89(26):266107, 2002.

[31] R. S. Hansen. The theory of diffusion controlled absorption kinetics with accompanying evaporation. *AIChE*, 64:637–641, 1960.

[32] Q. Jiang and Y. C.Chiew. A simple test for diffusion-controlled adsorption at an air/water interface. *Langmuir*, 9:273–277, 1993.

[33] J. Eastoe, J. S. Dalton, P. G. A. Rogueda, E. R. Crooks, A. R. Pitt, and E. A. Simister. Dynamic surface tensions of nonionic surfactant solutions. *Journal of Colloid and Interface Science*, 188:423–430, 1997.

[34] J.Eastoe, A.Rankin, R.Wat, and C. D. Bain. Surfactant adsorption dynamics. *International Reviews in Physical Chemistry*, 20(3):357–386, 2001.

[35] J-B. Jeong, J-Y. Kim, H-C. Kim, and J-D. Kim. Dynamic surface tension and its diffusional decay of dodecyl ethoxylates with different homologue distribution. *Journal of Colloid and Interface Science*, 250:496–502, 2002.

[36] J. Liu and U. Messow. Diffusion-controlled adsorption kinetics at the air/solution interface. *Colloid and Polymer Science*, 278:124–129, 2000.

[37] E. V. Aksenenko, A. V. Makievski, R. Miller, and V. B. Fainerman. Dynamic surface tension of aqueous alkyl dimethyl phosphine oxide solutions. Effect of the alkyl chain length. *Colloids and Surfaces A: Physicochemical and Engineering Aspects*, 143:311–321, 1998.

[38] M. J. Rosen. *Surfactants and Interfacial Phenomena*. Wiley Interscience, 1989.

[39] V. B. Fainerman, R. Miller, and E. V. Aksenenko. Simple model for predictions of surface tension of mixed surfactant solutions. *Advances in Colloid and Interface Science*, 96:339–359, 2002.

[40] Y. J. Nikas, S. Puvvada, and D. Blankschtein. Surface tensions of aqueous nonionic surfactant mixtures. *Langmuir*, 8:2680–2689, 1992.

[41] Y-C. Lee, K. J. Stebe, H-S. Liu, and S-Y. Lin. Adsorption and desorption kinetics of C_mE_8 on impulsively expanded or compressed air-water interfaces. *Colloids and Surfaces A: Physicochemical and Engineering Aspects*, 220:139–150, 2003.

[42] Y-C. Lee, S-Y. Lin, and M-J. Shao. Adsorption kinetics of $C_{12}E_6$ at the air-water interface. *Journal of Chinese Institute of Chemical Engineers*, 33(6):631–643, 2002.

[43] Y-C. Lee, H-S. Liu, and S-Y. Lin. Adsorption kinetics of $C_{10}E_4$ at the air/water interface: consider molecular interaction or reorientation. *Colloids and Surfaces A: Physicochemical and Engineering Aspects*, 212:123–134, 2003.

[44] J. Chanda, S. Chakraborty, and S. Bandyopadhyay. Monolayer of Aerosol-OT surfactants adsorbed at the air/water interface: An atomistic computer simulation study. *Journal of Physical Chemistry B*, 109:471 – 479, 2005.

[45] M. Tarek, D. J. Tobias, and M. L. Klein. Molecular dynamics simulation of tetradecyltrimethy-lammonium bromide monolayers at the air/water interface. *Journal of Physical Chemistry*, 99:1393–1402, 1995.

[46] H. Kuhn and H. Rehage. Molecular orientation of monododecyl pentaethylene glycol at water/air and water/oil interfaces. A molecular dynamics computer simulation study. *Colloid and Polymer Science*, 278:114–118, 2000.

[47] H. Kuhn and H. Rehage. Molecular orientation of monododecyl pentaethylene glycol ($C_{12}E_5$) surfactants at infinite dilution at the air/water interface. a molecular dynamics computer simulation study. *Physical Chemistry Chemical Physics*, 2:1023–1028, 2000.

[48] H. Kuhn and H. Rehage. Molecular dynamics computer simulations of surfactant monolayers: Monododecyl pentaethylene glycol at the surface between air and water. *Journal of Physical Chemistry B*, 103:8493–8501, 1999.

[49] S. Bandyopadhyay and J. Chanda. Monolayer of monododecyl diethylene glycol surfactants adsorbed at the air/water interface: A molecular dynamics study. *Langmuir*, 19:10443–10448, 2003.

[50] H. S. Carslaw. *Introduction to the mathematical theory of the conduction of heat in solids.* Macmillan and Company (London), 1954.

[51] A. V. Makievski, G. Loglio, J. Kragel, R. Miller, V. B. Fainerman, and A. W. Neumann. Adsorption of protein layers at the water/air interface as studied by axisymmetric drop and bubble shape analysis. *Journal of Physical Chemistry B*, 103:9557–9561, 1999.

[52] R. Miller, V. B. Fainerman, A. V. Makievski, J. Kragel, D. O. Grigoriev, V. N. Kazakov, and O. V. Sinyachenko. Dynamics of protein and mixed protein/surfactant adsorption layers at the water/fluid interface. *Advances in Colloid and Interface Science*, 86:39–82, 2000.

[53] R. Miller, V. B. Fainerman, E. V. Aksenenko, M. E. Leser, and M. Michel. Dynamic surface tension and adsorption kinetics of beta-casein at the solution air interface. *Langmuir*, 3:771–777, 2004.

[54] W. M. Deen. *Analysis of Transport Phenomena*. Oxford University Press, 1998.

[55] J. Y. Shin and N. L. Abbott. Combining molecular dynamic simulations and transition state theory to evaluate the sorption rate constants for decanol at the surface of water. *Langmuir*, 17:8434–8443, 2001.

[56] R. Miller, E. V. Aksenenko, L. Liggieri, F. Ravera, M. Ferrari, and V. B. Fainerman. Effect of reorientation of oxyethylated alcohol molecules within the surface layer on equilibrium and dynamic surface pressure. *Langmuir*, 15:1328–1336, 1999.

[57] J. Eastoe, J. S. Dalton, and P. G. A. Rogueda. Evidence for activation-diffusion controlled dynamic surface tension with a nonionic surfactant. *Langmuir*, 14:979–981, 1998.

[58] J. Eastoe, J.S. Dalton, and R.K. Heenan. Dynamic surface tension and micelle structures of dichained phosphatidylcholine surfactant solutions. *Langmuir*, 14:5719–5724, 1998.

[59] A. V. Makievski, V. B. Fainerman, R. Miller, M. Bree, L. Liggieri, and F. Ravera. Determination of equilibrium surface tension values by extrapolation via long time approximations. *Colloids and Surfaces A: Physicochemical and Engineering Aspects*, 122:269–273, 1997.

[60] A. Pohorille and I. Benjamin. Molecular dynamics of phenol at the liquid-vapor interface of water. *Journal of Chemical Physics*, 94:5599 – 5605, 1991.

[61] A. Pohorille and I. Benjamin. Structure and energetics of model amphiphilic molecules at the water liquid-vapor interface. A molecular dynamics study. *Journal of Physical Chemistry*, 97:2664 – 2670, 1993.

[62] R. S. Taylor, D. Ray, and B. C. Garrett. Understanding the mechanism for the mass acco-modation of ethanol by a water droplet. *Journal of Physical Chemistry B*, 101:5473–5476, 1997.

[63] L. X. Dang. Computational study of ion binding to the liquid interface of water. *Journal of Physical Chemistry B*, 106:10388–10394, 2002.

[64] S-Y. Lin, Y-C. Lee, M-W Yang, and H-S Liu. Surface equation of state of nonionic $C_m E_n$ surfac-tants. *Langmuir*, 19:3164 – 3171, 2003.

[65] C-T. Hsu, M-J. Shao, and S-Y. Lin. Adsorption kinetics of $C_{12}E_4$ at the air-water interface: Adsorption onto a fresh interface. *Langmuir*, 16:3187–3194, 2000.

[66] S-Y. Lin, K. McKeigue, and C. Maldarelli. Diffusion-controlled surfactant adsorption studied by pendant drop digitization. *AIChE Journal*, 36:1785 – 1795, 1990.

Chapter 3

New Methodology to Determine the Rate-Limiting Adsorption Kinetics Mechanism from Experimental Dynamic Surface Tension Data

3.1 Introduction

In order to develop a mechanistic understanding of the various factors that affect the kinetics of nonionic surfactant adsorption, recall that, traditionally, the adsorption process has been viewed as consisting of the following three steps [1–11](see Section 1.2.1): Step 1: Diffusion of the surfactant molecules from the bulk solution to the sub-surface[1], Step 2: Adsorption of the surfactant molecules from the sub-surface onto the surface, and Step 3: Reorientation of the surfactant molecules at the surface leading to a further reduction of the surface tension. In order to physically understand the effect of Step 2 on the adsorption kinetics, it has been hypothesized that Step 2 involves adsorption across an *energy barrier* [13–20], whose fundamental origin has not been explained to date. Based on this understanding, two different classes of kinetics models have been advanced: (i) Diffusion-controlled adsorption models, which assume that Step 1 controls the overall rate of

---

[1]The sub-surface is the zone of a few angstroms thickness adjacent to the surface, according to Ward and Tordai [12].

surfactant adsorption, and (ii) mixed diffusion-barrier controlled adsorption models[2], which assume that Steps 1 and 2 control the overall rate of surfactant adsorption. The specific form of the kinetics model depends on the equilibrium adsorption isotherm model of the surfactant, since the kinetics model should reduce to the equilibrium adsorption isotherm model at equilibrium conditions. While a diffusion-controlled adsorption model contains *one* kinetics parameter: D, the bulk solution diffusion coefficient of the surfactant molecule, a mixed-controlled adsorption model contains *two* kinetics parameters: D and β, where β is the energy-barrier parameter representing the rate constant for the adsorption of surfactant molecules from the sub-surface onto the surface. As I have shown in Section 2.3.2, β is related to the adsorption of a *single* surfactant molecule onto a *clean* surface.

The existing procedure used to determine the rate-limiting adsorption kinetics mechanism (diffusion-controlled vs. mixed-controlled), as well as to determine the values of the kinetics parameters, D and β, involves the following three steps [20–30]:

Step 1: Choosing a model for the equilibrium adsorption isotherm.

Step 2: Assuming a diffusion-controlled adsorption mechanism, and using the experimental Dynamic Surface Tension (DST) data corresponding to the entire surface tension relaxation profile, measured at a single initial surfactant bulk solution concentration, C_b, to regress for the value of D. This step is then repeated for experimental DST data measured at different C_b values. If the regressed value of D is found to decrease as C_b increases, then this trend is interpreted as indicating the existence of a mixed-controlled adsorption mechanism.

Step 3: If there are indications of the existence of mixed-controlled adsorption, the regressed value of D obtained by analyzing the experimental DST data measured at lower C_b values is considered as the actual diffusion coefficient of the surfactant molecules, and the entire experimental DST data measured at the higher C_b values is used to regress for β.

After implementing this three-step procedure, one can determine: (a) if the adsorption is diffusion-controlled or mixed-controlled, and (b) the values of β (if the adsorption is mixed-controlled) and D. Note that this procedure involves choosing a specific model for the equilibrium adsorption isotherm (Step 1 above). Consequently, *the accuracy of the equilibrium adsorption*

---

[2]I shall refer hereafter to the mixed diffusion-barrier controlled model as the mixed-controlled model.

isotherm model affects the regressed values of the kinetics parameters, D and β [31, 32]. In fact, the regressed values of D and β are found to be quite sensitive to the choice of the equilibrium adsorption isotherm model [31–34]. For example, consider the adsorption kinetics of the nonionic surfactant $C_{12}E_8$ [26]. While three different equilibrium adsorption isotherm models, namely, the Langmuir, the Frumkin, and the Generalized Frumkin adsorption isotherms, all appear to describe the experimental equilibrium adsorption behavior (that is, the equilibrium surface tension vs. surfactant bulk solution concentration data) reasonably well, they result in very different values of the regressed kinetics parameters when analyzing the experimental DST behavior. Specifically, the Langmuir model results in a D value of 21×10^{-6} cm^2/s, the Frumkin model results in a D value of 11×10^{-6} cm^2/s, and the Generalized Frumkin model results in a D value of 8.0×10^{-6} cm^2/s. In view of the observed high sensitivity of the regressed values of the kinetics parameters to the chosen equilibrium adsorption isotherm model, Lin et al. [25] and Pan et al. [20] proposed carrying out surface expansion measurements, in addition to performing equilibrium surface tension measurements, to further validate the equilibrium adsorption isotherm model chosen to analyze the experimental DST data. These authors concluded that surface expansion measurements can be useful in testing various equilibrium adsorption isotherm models, and hence, in obtaining more reliable estimates of the kinetics parameters, D and β.

Note that the equilibrium adsorption isotherm models differ in the manner in which they account for the interactions between the adsorbed surfactant molecules (see Section 2.2.1), and as such, they *should not* affect the value of D, the *bulk solution* diffusion coefficient of a surfactant molecule, and β, which as I have shown in Section 2.3.2, is related to the adsorption of a *single* surfactant molecule onto a *clean* surface [35]. Moreover, note that the existing procedure uses the entire experimental DST data measured at all values of C_b to regress for the values of D and β, and therefore, it does not allow for an *independent testing* of its predictive capabilities. Recognizing that a fundamental physical understanding of the energy barrier is still lacking, a reliable determination of the rate-limiting adsorption kinetics mechanism, including extracting reliable values of the kinetics parameters, D and β, for various nonionic surfactant systems, is of great fundamental and practical value.

With the background provided above in mind, in this chapter, I develop a new methodology,

which does not make use of a model for the equilibrium adsorption isotherm, and can be utilized to determine the rate-limiting adsorption kinetics mechanism and to obtain reliable values of the kinetics parameters, D and β, from experimental DST data. Specifically, the new methodology is based on the short-time analysis of the mixed-controlled model that I derived in Chapter 2, an analysis which requires *only* the experimental *short-time* DST data measured at *two* initial surfactant bulk solution concentrations. The new methodology involves extracting adsorption kinetics-specific information from the experimental DST data, and then regressing for the values of the kinetics parameters, D and β. I utilize the new methodology presented here to determine the rate-limiting adsorption kinetics mechanisms, and to obtain the kinetics parameters, D and β, for various alkyl poly(ethylene oxide), C_iE_j, nonionic surfactants, namely, $C_{12}E_4$, $C_{12}E_6$, $C_{12}E_8$, and $C_{10}E_8$. Since the new methodology requires only the short-time DST data measured at two initial surfactant bulk solution concentrations, I *test* the results by predicting the short-time DST behavior at other initial surfactant bulk solution concentrations, and subsequently, by comparing these predictions with the corresponding experimentally measured DST data. I also compare the results obtained utilizing the new methodology with those obtained utilizing the existing procedure, and find that assuming the applicability of an equilibrium adsorption isotherm model may affect not only the deduced values of the kinetics parameters, D and β, but also the determination of the underlying rate-limiting adsorption kinetics mechanism (diffusion-controlled vs. mixed-controlled).

The remainder of the chapter is organized as follows. In Section 3.2, I present the new methodology to extract purely adsorption kinetics-specific information from the experimental DST data, and to regress for the D and β values. In Section 3.3, I: (i) utilize the new methodology to determine the rate-limiting adsorption kinetics mechanism (diffusion-controlled vs. mixed-controlled), to deduce the values of the corresponding kinetics parameters, D and β, and to test the results against experiments, for various C_iE_j nonionic surfactants (Section 3.3.1), and (ii) compare the results obtained utilizing the new methodology with those obtained utilizing the existing procedure (Section 3.3.2). Finally, in Section 3.4, I summarize the main results of the chapter. In addition, in Appendix 3.A, I demonstrate the reliability of the new methodology, and in Appendix 3.B, I validate the range of experimental short-time DST data used in the new methodology.

3.2 The New Methodology

The experimentally measured DST data contains information about both the adsorption kinetics and the equilibrium adsorption isotherm. Specifically, while the rate of surfactant adsorption at the surface is governed by various factors affecting the kinetics, the resulting reduction in the surface tension depends on the equation of state, which in turn, depends on the equilibrium adsorption isotherm through the Gibbs adsorption equation [36]. As discussed in Section 3.1, traditionally, one assumes the applicability of a model for the equilibrium adsorption isotherm, and then extracts the adsorption kinetics information from the experimental DST data. In this section, I develop a new methodology to regress reliable values of the kinetics parameters, D and β, which *does not make use of a model for the equilibrium adsorption isotherm*. The methodology involves transforming the mixed-controlled model and the experimental DST data into a form that is purely adsorption kinetics-specific, and then performing a suitable regression to determine the values of D and β.

Transforming the Mixed-Controlled Model

Recall that in Section 2.2.2, I derived a non-asymptotic short-time formalism for a *generalized* mixed-controlled adsorption model, involving the adsorption of nonionic surfactant molecules onto a spherical surface. According to this formalism, at short-times, the Dynamic Surface Coverage (DSC), $\Gamma(t)$, is given by the following expression (Eqs.(2.16)-(2.18)):

$$\frac{\Gamma(t, C_b)}{C_b} = m(t) \tag{3.1}$$

where

$$m(t) = \frac{\ell_s}{\lambda^3} \left\{ \lambda^2(\lambda - 1)\frac{t}{\tau_s} + 2\lambda\sqrt{\frac{t}{\pi\tau_s}} + \text{erfc}\left(\lambda\sqrt{\frac{t}{\tau_s}}\right) \exp\left(\lambda^2\frac{t}{\tau_s}\right) - 1 \right\} \tag{3.2}$$

and

$$\lambda = 1 + \frac{\ell_s}{r_0}, \qquad \tau = \frac{t}{\tau_s}, \qquad \tau_s = \frac{\ell_s^2}{D}, \qquad \text{and} \qquad \ell_s = \frac{D}{\beta} \tag{3.3}$$

In Eq.(3.1), C_b is the initial surfactant bulk solution concentration at which the DST measurement is conducted. In Eq. (3.3), the non-dimensional λ reflects the effect of the surface curvature, r_0, on the adsorption kinetics, τ is the non-dimensional time, τ_s is the time scale associated with the mixed-controlled adsorption process at short (s) times, and ℓ_s is the corresponding length scale.

Recall that Eq.(3.1) was shown to provide an acceptable description of the short-time adsorption kinetics behavior over the following range of t and $\Gamma(t)$ values (see Section 2.2.2):

$$t \text{ range}: \quad t \leq t^* = 4 \text{ x } 10^{-4} \left(\frac{h^2}{D}\right)$$

$$\Gamma(t) \text{ range}: \quad \Gamma(t) \leq \Gamma^* = 0.25\Gamma_\infty \tag{3.4}$$

where $h = \left(\frac{\Gamma}{C_b}\right)_e$, with e denoting the equilibrium conditions, and Γ_∞ is the maximum surface coverage of the surfactant molecules.

It is noteworthy that $m(t)$ in Eq. (3.2): (i) *is independent of the surfactant bulk solution concentration C_b*, (ii) *is independent of the model used to describe the equilibrium adsorption behavior*, and (iii) *depends only on the kinetics parameters, D and β, of the surfactant molecule for a specified value of the pendant-bubble radius, r_0 (see Eq. (3.3))*. In other words, Eq.(3.2) reveals the existence of a function $m(t)$, which is specific to every individual surfactant and which directly reflects the kinetics aspect of its adsorption, and which is independent of the surfactant bulk solution concentration or its surface properties.

Theoretically, Eqs.(3.1) - (3.3) can used to estimate the values of D and β from adsorption kinetics measurements carried out at a *single* surfactant bulk solution concentration, C_b, in the two cases discussed below:

Case 1: If the DSC, $\Gamma(t)$, were measured experimentally instead of the DST, then, Eq.(3.1) shows that $m(t)$ can be extracted simply by dividing the experimental $\Gamma(t)$ by C_b. Once $m(t)$ is determined experimentally in this manner, the kinetics parameters, D and β, can be regressed using Eq.(3.2). In that case, one would only require the short-time DSC measured at a *single* initial surfactant bulk solution concentration to estimate the values of D and β. However, unfortunately, $\Gamma(t)$ is not typically measured experimentally.

Case 2: If the 'real' equilibrium adsorption isotherm (referred to hereafter as the 'real' isotherm) was known, then, Eq.(3.1) could be used along with the 'real' isotherm to predict the short-time DST, which would be a function of the two kinetics parameters, D and β. In that case, the predicted short-time DST expression, parameterized in terms of D and β, could be used along

100

with the experimentally measured DST to regress for the values of D and β. Again, in this case, one would, theoretically, require only the experimental short-time DST data measured at a *single* initial surfactant bulk solution concentration to estimate the values of D and β. However, as already stated, this requires knowledge of the 'real' isotherm, and obtaining a reliable approximation of the 'real' isotherm to describe changes in surface tension of about a few mN/m is extremely difficult [37].

Keeping cases 1 and 2 above in mind, I transform Eqs.(3.1) - (3.3) to a form which will enable us to extract the values of D and β from experimental short-time *DST* data measured at *two* initial surfactant bulk solution concentrations. The specific transformation is discussed below.

First, I assume the existence of an (unknown) equation of state relating the reduction in surface tension, or the surface pressure, Π, to the surfactant surface concentration, Γ, given by:

$$\Pi = f(\Gamma) \tag{3.5}$$

where $f(\Gamma)$ is an unknown function. The existence of an equation of state implies that there is a unique value of the surface pressure for a specific value of the surfactant surface concentration. Next, I assume that the function $f(\Gamma)$ is one-to-one, that is, that for any given value of the surface pressure, Π, there exists a unique value of the surfactant surface concentration, Γ. This assumption implies that the function $f(\Gamma)$ is invertible, that is, that:

$$\Gamma = f^{-1}(\Pi) \tag{3.6}$$

Note that the assumption embodied in Eq.(3.6) may not be valid for surfactants that undergo a phase change at the surface. This is because, when a phase change takes place at the surface, Π has the same value for two different values of Γ. In that case, it is not possible to assign a unique value of Γ for a given value of Π. For example, the assumption underlying Eq.(3.6) is not applicable for surfactants [29, 38–43] and proteins [44–49] that have been shown to undergo a Gas(G)-Liquid Expanded(LE) surface phase transition at small values of $\Pi < 1$ mN/m.

Let C_1 and C_2 be the two initial surfactant bulk solution concentrations at which the DST experiments are conducted. Using Eqs.(3.1) and (3.2), the short-time DSC, $\Gamma(t)$, at these two

conditions are given by:

$$\Gamma(t, C_1) = \frac{\ell_s}{\lambda^3} \left\{ \lambda^2(\lambda - 1)\frac{t}{\tau_s} + 2\lambda\sqrt{\frac{t}{\pi\tau_s}} + \text{erfc}\left(\lambda\sqrt{\frac{t}{\tau_s}}\right)\exp\left(\lambda^2\frac{t}{\tau_s}\right) - 1 \right\} C_1 \qquad (3.7)$$

and

$$\Gamma(t, C_2) = \frac{\ell_s}{\lambda^3} \left\{ \lambda^2(\lambda - 1)\frac{t}{\tau_s} + 2\lambda\sqrt{\frac{t}{\pi\tau_s}} + \text{erfc}\left(\lambda\sqrt{\frac{t}{\tau_s}}\right)\exp\left(\lambda^2\frac{t}{\tau_s}\right) - 1 \right\} C_2 \qquad (3.8)$$

Using Eq.(3.6) along with Eqs.(3.7) and (3.8), the short-time Dynamic Surface Pressure (DSP), $\Pi(t)$, at the two conditions can be written as follows:

$$f^{-1}(\Pi(t, C_1)) = \frac{\ell_s}{\lambda^3} \left\{ \lambda^2(\lambda - 1)\frac{t}{\tau_s} + 2\lambda\sqrt{\frac{t}{\pi\tau_s}} + \text{erfc}\left(\lambda\sqrt{\frac{t}{\tau_s}}\right)\exp\left(\lambda^2\frac{t}{\tau_s}\right) - 1 \right\} C_1 \qquad (3.9)$$

and

$$f^{-1}(\Pi(t, C_2)) = \frac{\ell_s}{\lambda^3} \left\{ \lambda^2(\lambda - 1)\frac{t}{\tau_s} + 2\lambda\sqrt{\frac{t}{\pi\tau_s}} + \text{erfc}\left(\lambda\sqrt{\frac{t}{\tau_s}}\right)\exp\left(\lambda^2\frac{t}{\tau_s}\right) - 1 \right\} C_2 \qquad (3.10)$$

Note that the EOS in Eq.(3.6) can be used to relate $\Pi(t)$ and $\Gamma(t)$ (in Eqs.(3.7) - (3.10)), since after the surfactant molecules adsorb at the surface, they require negligible time to reduce the surface tension as compared to the time scale associated with the adsorption process itself. Indeed, molecular dynamics simulations of surfactant molecules adsorbed at air/water surfaces are performed for a duration of about 4 ns in order to study *equilibrium* surface properties [50–55]. On the other hand, typical time scales associated with the surfactant adsorption kinetics vary from milliseconds to tens of hours depending on the surfactant and its initial bulk solution concentration [8]. Accordingly, it is appropriate to relate the DSC, $\Gamma(t)$, and the DSP, $\Pi(t)$, using Eq.(3.6).

Consider next an arbitrary (*a*) DSP value of $\Pi = \Pi_a$. If t_1 and t_2 are the times at which the DSP reaches the value of Π_a at conditions where $C_b = C_1$ and $C_b = C_2$, respectively, then:

$$\Pi(t_1, C_1) = \Pi_a \qquad (3.11)$$

and

$$\Pi(t_2, C_2) = \Pi_a \qquad (3.12)$$

102

Using Eqs.(3.9) and (3.10), along with Eqs.(3.11) and (3.12), yields the following relationship between t_1 and t_2, such that the reductions in the surface tension attained at these two conditions are the same:

$$\frac{\ell_s}{\lambda^3}\left\{\lambda^2(\lambda-1)\frac{t_1}{\tau_s}+2\lambda\sqrt{\frac{t_1}{\pi\tau_s}}+\operatorname{erfc}\left(\lambda\sqrt{\frac{t_1}{\tau_s}}\right)\exp\left(\lambda^2\frac{t_1}{\tau_s}\right)-1\right\}C_1=$$
$$\frac{\ell_s}{\lambda^3}\left\{\lambda^2(\lambda-1)\frac{t_2}{\tau_s}+2\lambda\sqrt{\frac{t_2}{\pi\tau_s}}+\operatorname{erfc}\left(\lambda\sqrt{\frac{t_2}{\tau_s}}\right)\exp\left(\lambda^2\frac{t_2}{\tau_s}\right)-1\right\}C_2 \qquad (3.13)$$

Note that Eq.(3.13) corresponds to the theoretical prediction of the relationship between t_1 and t_2 such that the surface pressure at $t = t_1$ measured when $C_b = C_1$ is the same as the surface pressure at $t = t_2$ measured when $C_b = C_2$. Moreover, using the definitions of λ and τ_s in Eq.(3.3), it follows that Eq.(3.13) depends only on the two kinetics parameters, D and β, and on the radius of the spherical surface, r_0, and is *independent of the equilibrium adsorption isotherm model*. In other words, by transforming the short-time behavior in Eq.(3.1) into the predicted relationship between t_1 and t_2 given in Eq.(3.13), I am essentially filtering out information which is specific only to the adsorption kinetics mechanism.

Transforming the Experimental DST Data

The experimentally observed relationship between t_1 and t_2 can be obtained by: (i) plotting t as a function of the measured DSP, $\Pi(t)$, at the two conditions, $C_b = C_1$ and $C_b = C_2$ (instead of utilizing the traditional way of plotting the measured DST as a function of t), (ii) choosing arbitrary values of Π_a, and (iii) finding the corresponding times at the two conditions of measurement. As an illustration, in Figure 3-1, the short-time DSP data (t vs. $\Pi(t)$), calculated from the experimental short-time DST data measured at two C_b values, are represented by the solid and the dotted lines, where the solid line corresponds to $C_b = C_1$ and the dotted line corresponds to $C_b = C_2$. Figure 3-1 shows that it takes a longer time for the surface pressure to reach a specific value on the solid line as compared to the time that it takes for the surface pressure to reach the same specific value on the dotted line. In other words, the dotted line exhibits a higher rate of surfactant adsorption as compared to the solid line. Considering that the driving force for adsorption increases as C_b increases, the solid line corresponds to experimental DST data measured at a lower surfactant bulk solution concentration, that is, $C_1 < C_2$. The resulting t_1 vs. t_2 relationship for the illustrative

experimental DST data shown in Figure 3-1 is presented in Figure 3-2 as the solid line. A 45 degree dotted straight line is drawn in Figure 3-2 to indicate that t_1 is always greater than t_2, since $C_1 < C_2$.
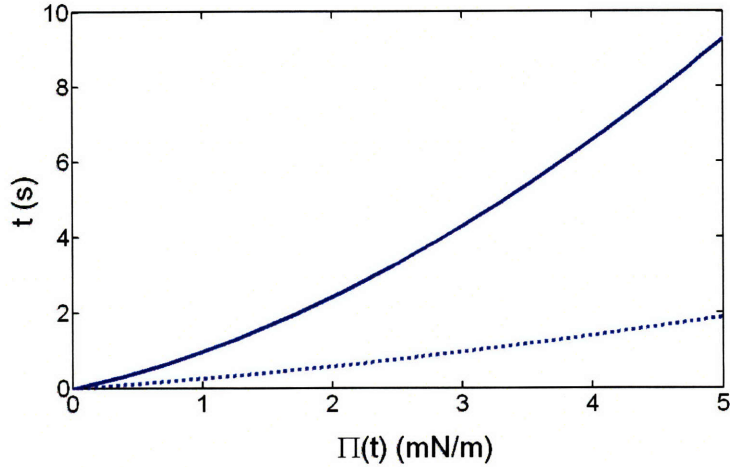
Figure 3-1: Illustration of the short-time DSP data measured at two surfactant bulk solution concentrations: $C_b = C_1$ (solid line) and $C_b = C_2$ (dotted line).
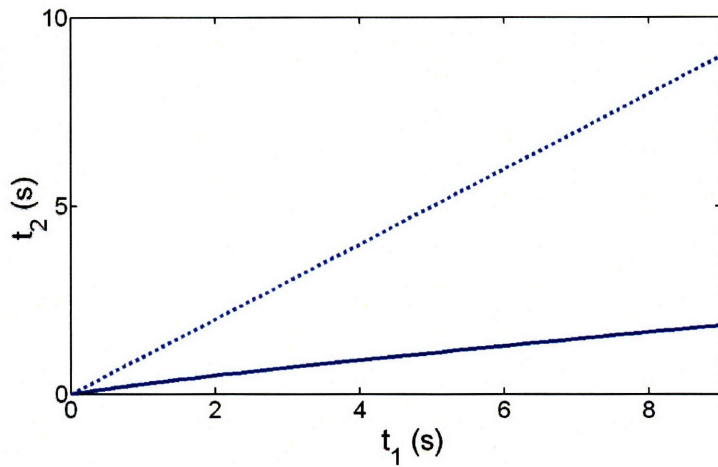
Figure 3-2: The solid line is the t_1 vs. t_2 variation corresponding to the DST lines shown in Figure 3-1. The 45 degree dotted straight line indicates that t_1 is always greater than t_2, since $C_1 < C_2$ in Figure 3-1.

Performing the t_1 vs. t_2 Regression

The parameters D and β can now be obtained by regressing the predicted relationship between t_1 and t_2 given in Eq.(3.13) with the illustrative experimentally observed t_1 vs. t_2 relation-

ship shown in Figure 3-2. This involves performing non-linear regression of an implicit equation (Eq.(3.13)) in the two-parameter (D, β) space. Due to the scatter in the DST measurements (typically ~ 0.2 mN/m), it is likely that this regression could result in a large confidence region in the (D, β) parameter space. In such cases, in order to obtain a tighter estimate of the D and β parameter values, 'trimming' of the confidence region obtained at the end of the t_1 vs. t_2 regression needs to be performed as described next.

Trimming of the Confidence Region

Note that the parameters D and β completely define the kinetics aspect of the adsorption process. From the known values of D and β, the experimental DST data can, in fact, be used to obtain equilibrium adsorption isotherm information, specifically, the surface Equation Of State (EOS) of the surfactant. For any given combination of D and β values, Eq.(3.1) can be used to separately predict the time variation of the surface surfactant concentration, $\Gamma(t)$, at the two conditions, $C_b = C_1$ and $C_b = C_2$. Keeping in mind that, at any given time, Γ is related to Π by a unique surface EOS, one can use $\Gamma(t)$ obtained from the theory, along with $\Pi(t)$ obtained from the experimentally measured DST, to find the EOS: $\Pi = f(\Gamma)$. Note that, in this manner, it is possible to obtain the EOS separately by analyzing the DST data measured at C_1 and C_2, for *every* combination of D and β values in the confidence region of the t_1 vs. t_2 regression. Recalling that any valid EOS should reduce to the Ideal EOS ($\Pi = RT\Gamma$) at small values of Π, trimming of the (D, β) confidence region can be achieved by imposing the condition that the resulting EOS should tend to the Ideal EOS (with a slope value equal to RT) at small values of Π. The combination of D and β values that results in a slope value that is closest to RT is then considered as the *best-fit* combination of D and β values of the regression analysis.

Overall, the t_1 vs. t_2 regression, together with the EOS-based trimming of the confidence region, should identify the combinations of D and β values that: (a) best fit the observed experimental short-time DST behavior, and (b) result in an EOS which behaves ideally at small values of Π. I next analyze the regression results to determine the rate-limiting adsorption kinetics mechanism (diffusion-controlled vs. mixed-controlled) and its dependence on the surfactant bulk solution concentration.

Analyzing the Regression Results

Theoretically, the adsorption kinetics of nonionic surfactants is purely diffusion-controlled only when $\beta = \infty$. Note that β is related to the velocity with which the surfactant molecules strike the surface [15]. Consequently, in practice, β should have a *finite* value for *any* nonionic surfactant molecule. With this in mind, the *adsorption of any nonionic surfactant at any of its premicellar surfactant bulk solution concentrations*[3] *should be mixed diffusion-barrier controlled*. However, the *relative* effect of the energy barrier vs. diffusion on the *overall* rate of surfactant adsorption does depend on the surfactant bulk solution concentration[4] [20]. Specifically, the effect of the energy barrier on the overall rate of surfactant adsorption becomes increasingly important as the surfactant bulk solution concentration, C_b, increases . At lower C_b values, characterized by negligible effect of the energy barrier on the overall rate of surfactant adsorption, the *rate-limiting* adsorption kinetics mechanism is diffusion-controlled. In such cases, the relevant kinetics parameter is the surfactant bulk solution diffusion coefficient, D. At higher C_b values, characterized by a significant effect of the energy barrier on the overall rate of surfactant adsorption, the *rate-limiting* adsorption kinetics mechanism is mixed-controlled. In such cases, both D and β need to be specified to completely characterize the kinetics aspect of the surfactant adsorption. Therefore, whenever the diffusion-controlled adsorption model is found to satisfactorily explain the experimentally observed adsorption kinetics behavior, it effectively implies that the C_b values probed experimentally are not sufficiently high to observe any significant effect of the energy barrier on the overall rate of surfactant adsorption [20]. According to the results presented in Refs.[20] and [35], the effect of the energy barrier (e) on the overall rate of surfactant adsorption can be neglected when:

$$C_b \ll C_e = \frac{\beta \Gamma_\infty}{D} \tag{3.14}$$

Specifically, the numerical solution of the mixed-controlled adsorption model presented in Refs.

---

[3]Note that I focus only on C_b values below the Critical Micelle Concentration (CMC), since, when $C_b > CMC$, the surfactant molecules kinetically self-assemble in the aqueous bulk solution to form micelles, whose existence significantly affects the dynamic adsorption behavior of the surfactant molecules [56–60]. Since the mixed-controlled model does not account for the effect of the kinetics of micelle formation on the kinetics of surfactant adsorption, it is not applicable when $C_b > CMC$.

[4]Recently, Jin et al. [61] demonstrated theoretically that when r_0 is of the order of micrometers, then, the adsorption process is mixed-controlled at all surfactant bulk solution concentrations. Since DST measurements typically involve r_0 values which are of the order of millimeters or higher [62], the results of Ref.[61] are not applicable in the analysis of typical experimental DST measurements.

[20] and [35] indicates that the effect of the energy barrier can be neglected when $C_b \leq 0.01 C_e$. Accordingly, the maximum (max) surfactant bulk solution concentration below which the rate-controlling adsorption kinetics mechanism can be considered to be diffusion (d) controlled, C_d^{max}, is given by:

$$C_d^{max} = \frac{0.01 \beta \Gamma_\infty}{D} \tag{3.15}$$

With the observations above in mind, and considering that the Critical Micelle Concentration (CMC) is the highest premicellar surfactant bulk solution concentration, I analyze the regression results to determine *if the CMC of the surfactant studied is sufficiently high to observe a significant effect of the energy barrier.* I accomplish this by first estimating C_d^{max}, using the β and D values deduced by the regression analysis, and subsequently, by comparing the estimated C_d^{max} value with the known CMC of the surfactant studied. Note that estimating C_d^{max} using Eq.(3.15) requires knowledge of Γ_∞, which can be estimated from the known surfactant molecular structure following the method described in Ref. [63]. Specifically, if a is the cross-sectional area of the surfactant molecule, then Γ_∞ can be estimated as $1/(aN_A)$, where N_A is Avogadro's number. If a_h is the surfactant polar head cross-sectional area, and a_t is the surfactant hydrocarbon tail cross sectional area, then $a = a_h$ when $a_h \geq a_t$, and $a = a_t$ when $a_h < a_t$ [63]. Use of this molecular framework to estimate Γ_∞ is convenient, since it requires *only* knowledge of the surfactant molecular structure, and does not make use of any experimentally measured inputs.

If the estimated value of $C_d^{max} \geq CMC$, then I conclude that the rate-limiting adsorption kinetics mechanism is diffusion-controlled *at any premicellar C_b value* of the surfactant studied. On the other hand, if the estimated value of $C_d^{max} \leq CMC$, then, I conclude that the rate-limiting adsorption kinetics mechanism is diffusion-controlled for $C_b < C_d^{max}$, and that it is mixed-controlled for $CMC \geq C_b > C_d^{max}$.

Testing the Regression Results

Since the new methodology uses only the experimental short-time DST data measured at two C_b values, the regression results can be tested for internal consistency using the experimentally observed DST data at other C_b values. Specifically, short-time DST can be predicted at other C_b values using the regressed values of D and β and the EOS, and these predictions can be compared with the experimentally observed DST behavior at these C_b values.

Demonstrating the Reliability of the New Methodology

I demonstrate the reliability of the new methodology by: (i) artificially generating experimental short-time DST data corresponding to specific values of D and β and a specific EOS, (ii) applying the new methodology to the generated experimental DST data, including determining the D and β values and the EOS, and (iii) comparing the D and β values and the EOS, determined using the new methodology in (ii), with those that were used to generate the DST data in (i). A detailed description of: (a) the artificial generation of the experimental short-time DST data, and (b) the various steps associated with implementing the new methodology to analyze the DST data, including a description of the regression procedure used, are provided in Appendix 3.A. Based on the results presented in Appendix 3.A, I find that the new methodology is able to reliably determine the values of D and β, as well as the EOS, using the short-time DST data measured at two surfactant bulk solution concentrations as the only inputs.

3.3 Discussion

I utilize the new methodology presented in Section 3.2 to analyze the experimental DST data of the following C_iE_j nonionic surfactants: $C_{12}E_4$, $C_{12}E_6$, $C_{12}E_8$, and $C_{10}E_8$. Lin and co-workers have conducted extensive DST measurements for these four surfactants using the pendant-bubble apparatus at $T = 298$ K and have published their data, including an analysis using the existing procedure, in the following references: (i) for $C_{12}E_4$ in Ref. [21], (ii) for $C_{12}E_6$ in Ref. [23], (iii) for $C_{12}E_8$ in Ref. [26], and (iv) for $C_{10}E_8$ in Ref. [24]. The new methodology presented in Section 3.2 is used below to analyze the DST data published in the above references.

Recall that the effect of the energy barrier has been shown to be more pronounced at higher C_b values [17, 20, 24, 26, 35, 64]. However, at extremely high C_b values, the DST may vary very fast, which could limit the availability of reliable DST data at small Π values. This is important to recognize, since the new methodology uses only the experimental short-time DST data *corresponding to small Π values*. With these observations in mind, the DST measured at sufficiently high surfactant bulk solution concentrations, C_1 and C_2, where reliable short-time DST measurements were possible, were chosen for the regression analysis. Figures 3-3(a - d) show the experimental short-time DSP, $\Pi(t)$, as a function of the square root of time, t, corresponding to the experimental DST
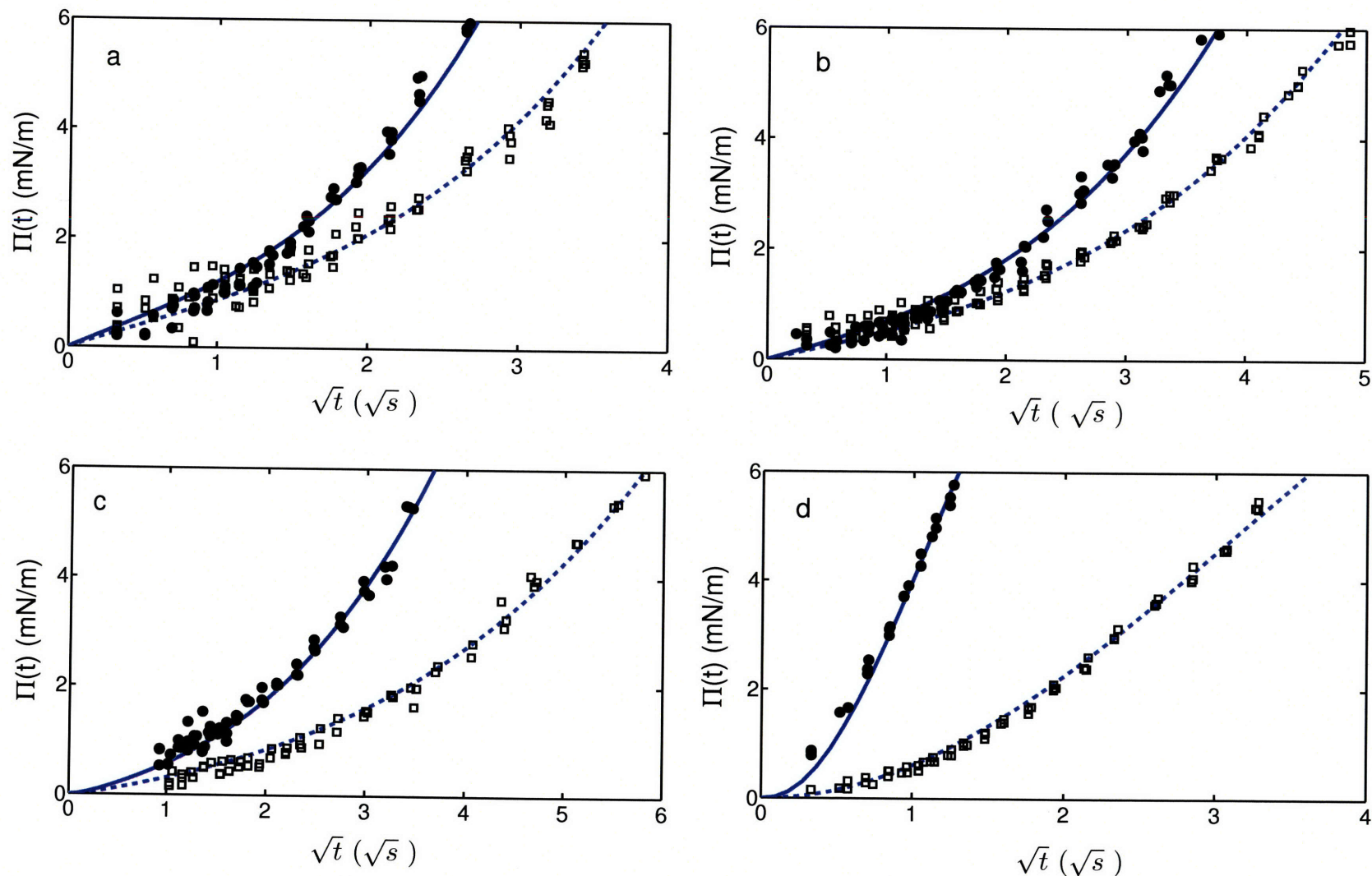
Figure 3-3: Regression of the experimental short-time dynamic surface pressure, $\Pi(t)$, as a function of the square root of time, t, data using the new methodology for: (a) $C_{12}E_4$, (b) $C_{12}E_6$, (c) $C_{12}E_8$, and (d) $C_{10}E_8$. In these figures, the dashed lines regress the experimental data corresponding to the open squares, and the solid lines regress the experimental data corresponding to the filled circles. The surfactant bulk solution concentrations corresponding to the open squares and the filled circles, respectively, are: (a) 1.5×10^{-8} mol/cm^3 and 2.0×10^{-8} mol/cm^3, (b) 1.0×10^{-8} mol/cm^3 and 1.3×10^{-8} mol/cm^3, (c) 0.6×10^{-8} mol/cm^3 and 1.0×10^{-8} mol/cm^3, and (d) 1.0×10^{-8} mol/cm^3 and 3.0×10^{-8} mol/cm^3.

data, for $C_{12}E_4$, $C_{12}E_6$, $C_{12}E_8$, and $C_{10}E_8$, respectively, used for the regression analysis. The open squares and the filled circles in Figures 3-3(a - d) correspond, respectively, to the experimental DST data measured at: (a) 1.5 x 10^{-8} mol/cm^3 and 2.0 x 10^{-8} mol/cm^3, (b) 1.0 x 10^{-8} mol/cm^3 and 1.3 x 10^{-8} mol/cm^3, (c) 0.6 x 10^{-8} mol/cm^3 and 1.0 x 10^{-8} mol/cm^3, and (d) 1.0 x 10^{-8} mol/cm^3 and 3.0 x 10^{-8} mol/cm^3. A r_0 value of 0.1 cm [62] was used in the regression analysis. A detailed account of the various steps associated with implementing the new methodology to analyze the experimental DST data, including a description of the regression procedure used, is provided in Appendix 3.A (Section 3.A.2). In Figures 3-3(a - d), the dashed lines regress the experimental data corresponding to the open squares, and the solid lines regress the experimental data corresponding to the filled circles. The R^2 values for all the regressed lines were found to between 0.95 and 0.99, indicating good fits.

Note that the short-time DST data used for the regression needs to satisfy the conditions set by Eq.(3.4), since the ranges of t and Γ values specified by Eq.(3.4) defines the range of applicability of Eq.(3.13). In Eq.(3.4), since the evaluation of t^* requires knowledge of h, which depends on the equilibrium adsorption isotherm, it is not possible to estimate t^* accurately for these surfactants. Nevertheless, it is possible to estimate *lower bound* values for t^* *without* using any equilibrium adsorption isotherm model. On the other hand, Eq.(3.4) also shows that Γ^* depends on Γ_∞, which can be estimated from the known molecular structure of the surfactant [63]. Appendix 3.B discusses the evaluation of Γ^* and of the lower bound values of t^* for the four C_iE_j nonionic surfactants considered. Results presented in Appendix 3.B indicate that the DST data used for the regression satisfy the conditions specified in Eq.(3.4).

In the remainder of this section, I present the results of the regression analysis (Section 3.3.1), and compare my results with the results obtained using the existing procedure (Section 3.3.2).

3.3.1 Results of the Regression Analysis

The best-fit combinations of D and β values, as well as the 90% confidence regions obtained at the end of the EOS-based trimming, for $C_{12}E_4$, $C_{12}E_6$, $C_{12}E_8$, and $C_{10}E_8$, are shown in Figures 3-4(a - d), respectively. In the case of $C_{12}E_4$ and $C_{12}E_6$ shown in Figures 3-4(a) and 3-4(b), respectively, all the points on the dark horizontal lines correspond to the best-fit combinations of
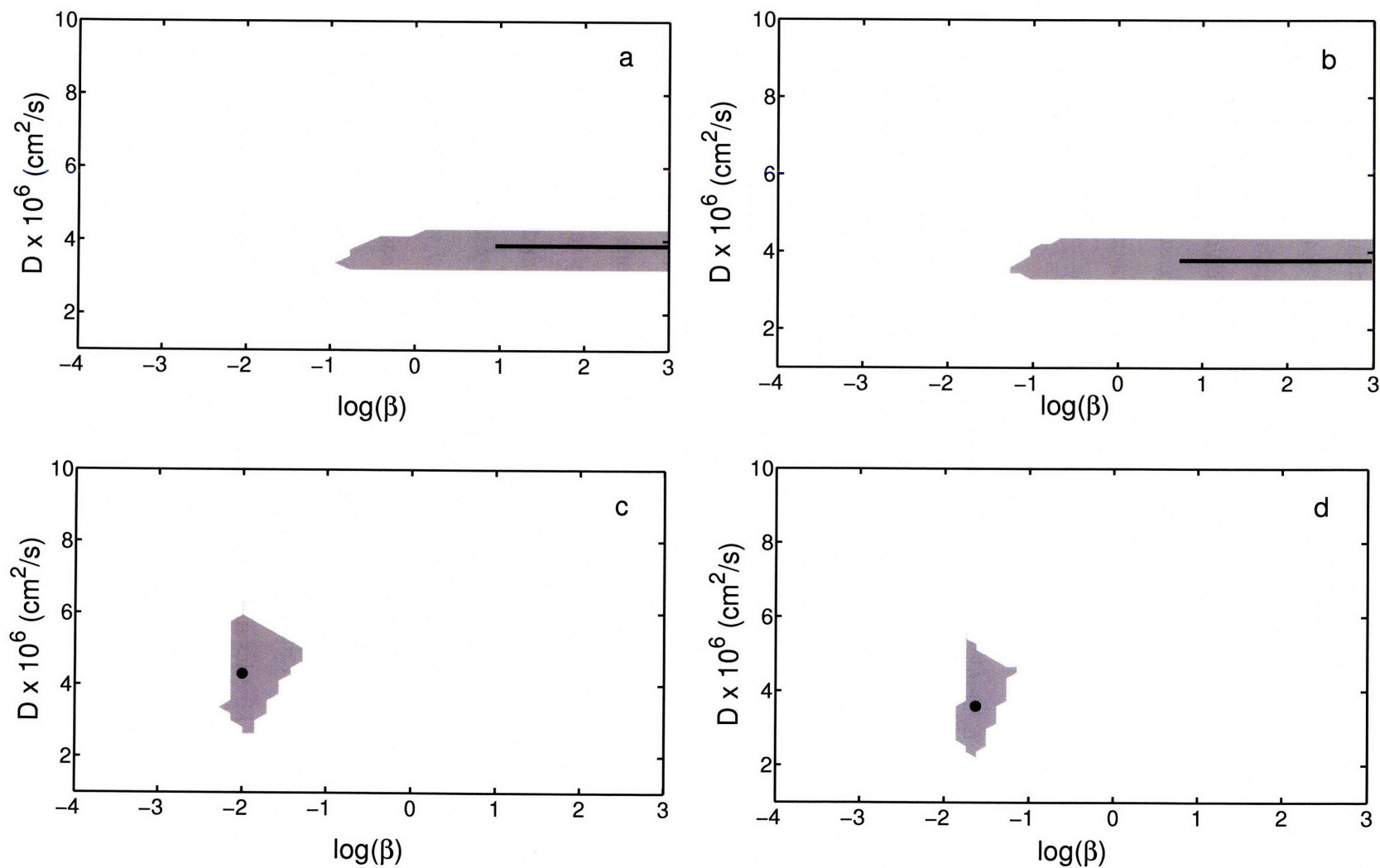
Figure 3-4: Regression results for: (a) $C_{12}E_4$, (b) $C_{12}E_6$, (c) $C_{12}E_8$, and (d) $C_{10}E_8$. The best-fit combinations of D and β values are indicated by the dark horizontal lines in Figures 3-4(a) and 3-4(b), and by the filled circles in Figures 3-4(c) and 3-4(d). The grey regions in the four figures indicate the 90% confidence regions. The units of β are cm/s.

D and β values. On the other hand, in the case of $C_{12}E_8$ and $C_{10}E_8$, unique best-fit combinations of D and β values were identified, and are shown in Figures 3-4(c) and 3-4(d) as the filled circles. In the four figures, the grey regions indicate the 90% confidence regions obtained at the end of the EOS-based trimming. Figures 3-5(a) and 3-5(b) show the surface equation of state obtained for the four nonionic surfactants. In this section, I discuss the results of the regression analysis in terms of: (i) the rate-limiting adsorption kinetics mechanism, (ii) the regressed values of D and β, and (iii) the surface EOS. Following this, I test the results for internal consistency.

Rate-Limiting Adsorption Kinetics Mechanism

For each of the four C_iE_j nonionic surfactants studied, I first determine the rate-limiting adsorption kinetics mechanism at the surfactant bulk solution concentrations used in the regression analysis, and then predict the mechanism at other premicellar surfactant bulk solution concentrations.

Results for $C_{12}E_4$ and $C_{12}E_6$

Note that the regression results for $C_{12}E_4$ and $C_{12}E_6$, shown in Figures 3-4(a) and 3-4(b), respectively, while indicating a very narrow range for the D values, allow orders of magnitude variability in the β values. Specifically, note that the best-fit combinations (indicated by the dark horizontal lines), as well as the confidence regions (indicated by the grey regions), both allow β to vary by orders of magnitude. The confidence regions in Figures 3-4(a) and 3-4(b) also reveal the existence of a lower (l) bound for the value of β (denoted by β_l). For example, in Figure 3-4(b), $\beta_l \approx 10^{-1.3}$ cm/s = 0.05 cm/s for $C_{12}E_6$. The large variability in the β values in both the best-fit combinations, as well as in the confidence regions, observed in the case of $C_{12}E_4$ and $C_{12}E_6$, indicates that β is not as critical as D in determining the short-time DST behavior of these two surfactants over the range of C_b values used in the regression analysis. This finding indicates that the rate-limiting adsorption kinetics mechanism is *diffusion-controlled* for $C_{12}E_4$ and $C_{12}E_6$ at the C_b values used in the regression analysis.

Results for $C_{12}E_8$ and $C_{10}E_8$

In contrast to $C_{12}E_4$ and $C_{12}E_6$, Figures 3-4(c) and 3-4(d) show that for $C_{12}E_8$ and $C_{10}E_8$, the regression identifies unique combinations of best-fit D and β values (indicated by the filled circles), and specifies associated confidence regions that are bounded in *both* the D and the β

values (indicated by the grey regions). This implies that the regression, and therefore, the short-time DST behavior, are sensitive to the specific values of both D and β for these two surfactants. This indicates that the adsorption of $C_{12}E_8$ and $C_{10}E_8$ is *mixed-controlled* at the C_b values used in the regression analysis.

Rate-Limiting Adsorption Kinetics Mechanism at Other C_b Values

In order to determine the rate-limiting adsorption kinetics mechanism at *other* surfactant bulk solution concentrations of interest, I first estimate the maximum surfactant bulk solution concentration below which the rate-limiting adsorption kinetics mechanism can be considered to be diffusion-controlled, C_d^{max}, using Eq.(3.15), for each of the four C_iE_j nonionic surfactants studied, and then compare the estimated C_d^{max} values with the respective CMC values of these surfactants.

Note that the estimation of the C_d^{max} values using Eq.(3.15) requires estimating Γ_∞, D, and β, for each of the four C_iE_j nonionic surfactants studied. Regarding Γ_∞, following the procedure described in Ref.[63], $\Gamma_\infty = 1/(a_h N_A)$, since, for C_iE_j nonionic surfactant molecules, the polar (E_j) groups are typically bulkier as compared to the hydrocarbon (C_i) tails (that is, $a_h \geq a_t$) [63]. For the C_iE_j nonionic surfactant polar (E_j) heads considered here, the following correlation has been developed [63]:

$$a_h(n_j) = a_{h0} \left(\frac{n_j}{6} \right)^z \tag{3.16}$$

where a_h is the head cross-sectional area in $\mathring{A}^2$, n_j denotes the number of ethylene oxide units in the E_j head, $a_{h0} = 36.3 \ \mathring{A}^2$ denotes the cross-sectional area of a hexa(ethylene oxide) head $(n_j = 6)$, and $z = 0.5$ [63, 65–67] models the scaling of the head cross-sectional area with n_j. Regarding D, the best-fit D values identified by the regression analysis are used as estimates for the four nonionic surfactants studied. Regarding β, considering that the confidence regions of $C_{12}E_4$ and $C_{12}E_6$ specify only the lower bounds for β, for consistency, I use the *lower bound* β_l values identified by the regression analysis as estimates for the β values for all the four nonionic surfactants studied. Using the estimated values of Γ_∞ and D, along with the *lower bound* β_l values in Eq.(3.15), one can estimate the *lower bound* for the C_d^{max} values for the four C_iE_j nonionic surfactants studied.

Table 3.1 summarizes the results of the estimations in terms of: (i) the values of Γ_∞ estimated using Eq.(3.16), (ii) the values of D and β_l obtained from Figures 3-4(a-d), (iii) the lower bound values of C_d^{max} estimated using Eq.(3.15), and (iv) the experimentally reported CMC values from

Table 3.1: For the four C_iE_j nonionic surfactants studied, the table lists: (i) the values of Γ_∞ estimated using Eq.(3.16), (ii) the values of D and β_l obtained from Figures 3-4(a-d), (iii) the lower bound values of C_d^{max} estimated using Eq.(3.15), and (iv) the reported experimental CMC values from Ref.[36].

C_iE_j Nonionic Surfactant	Γ_∞ x 10^{10} (mol/cm^2)	D x 10^6 (cm^2/s)	β x 10^2 (cm/s)	Lower Bound of C_d^{max} (mol/cm^3)	CMC (mol/cm^3)
$C_{12}E_4$	5.60	3.9	11.2	1.6 x 10^{-7}	6.4 x 10^{-8}
$C_{12}E_6$	4.57	3.8	5.6	6.8 x 10^{-8}	8.9 x 10^{-8}
$C_{12}E_8$	3.96	4.3	0.5	4.8 x 10^{-9}	1.0 x 10^{-7}
$C_{10}E_8$	3.96	3.6	1.4	1.5 x 10^{-8}	1.0 x 10^{-6}

Ref.[36]. Comparing the estimated lower bound values of C_d^{max} with the corresponding CMC values, I have reached the following conclusions regarding the rate-limiting adsorption kinetics mechanism of the four C_iE_j nonionic surfactants studied:

For $C_{12}E_4$: Since the estimated lower bound of $C_d^{max} > CMC$, it follows that the rate-limiting adsorption kinetics mechanism of $C_{12}E_4$ is *diffusion-controlled* at all premicellar C_b values.

For $C_{12}E_6$: Note that while the estimated lower bound of $C_d^{max} < CMC$, it is of the same order of magnitude as the CMC. Based on the estimated lower bound of C_d^{max}, it follows that the rate-limiting adsorption kinetics mechanism of $C_{12}E_6$ is *diffusion-controlled* when $C_b \leq 6.8$ x 10^{-8} mol/cm^3. In the remaining very narrow range of relevant C_b values, 8.9 x 10^{-8} mol/cm$^3 \geq C_b > 6.8$ x 10^{-8} mol/cm^3, it is possible that the energy barrier may begin to affect the overall rate of $C_{12}E_6$ adsorption. However, because 6.8 x 10^{-8} mol/cm^3 corresponds to the estimated *lower bound* of C_d^{max}, and because this estimate is of the same order of magnitude as the CMC, I speculate that it is reasonable to consider the rate-limiting adsorption kinetics mechanism of $C_{12}E_6$ to be diffusion-controlled even when 8.9 x 10^{-8} mol/cm$^3 \geq C_b > 6.8$ x 10^{-8} mol/cm^3. With this in mind, I conclude that the rate-limiting adsorption kinetics mechanism of $C_{12}E_6$ is *diffusion-controlled* at all premicellar C_b values.

For $C_{12}E_8$: Since the estimated lower bound of C_d^{max} is about two orders of magnitude lower

than the CMC, I conclude that the rate-limiting adsorption kinetics mechanism of $C_{12}E_8$ is *diffusion-controlled* when $C_b \leq 4.8$ x 10^{-9} mol/cm^3, and that it is *mixed-controlled* when 1.0 x 10^{-7} mol/cm$^3 \geq C_b > 4.8$ x 10^{-9} mol/cm^3. Note that the above conclusion is consistent with the observed unique best-fit combination of D and β values when the DST data measured at the C_b values of 1 x 10^{-8} mol/cm^3 and 0.6 x 10^{-8} mol/cm^3 was used in the regression analysis. Since the two C_b values used in the regression analysis are greater than the estimated lower bound value of $C_d^{max} = 4.8$ x 10^{-9} mol/cm^3, it is reasonable that the regression analysis detected the existence of the effect of the energy barrier, and identified a unique best-fit β value.

For $C_{10}E_8$: Since the estimated lower bound of C_d^{max} is about two orders of magnitude lower than the CMC, I conclude that the rate-limiting adsorption kinetics mechanism of $C_{10}E_8$ is *diffusion-controlled* when $C_b \leq 1.5$ x 10^{-8} mol/cm^3, and that it is *mixed-controlled* when 1.0 x 10^{-6} mol/cm$^3 \geq C_b > 1.5$ x 10^{-8} mol/cm^3. Note that the above conclusion is consistent with the observed unique best-fit combination of D and β values when the DST data measured at the C_b values of 1 x 10^{-8} mol/cm^3 and 3.0 x 10^{-8} mol/cm^3 was used in the regression analysis. Since at least one of the two C_b values used in the regression analysis (3.0 x 10^{-8} mol/cm^3) was greater than the estimated lower bound value of $C_d^{max} = 1.5$ x 10^{-8} mol/cm^3, it is reasonable that the regression analysis detected the existence of the effect of the energy barrier, and identified a unique best-fit β value.

The Regressed D and β Values

(i) *D Values:* The regressed diffusion coefficient values for the four C_iE_j nonionic surfactants studied, along with their 90% confidence intervals which were calculated based on the confidence regions in Figures 3-4(a-d), are summarized in Table 3.2. Note that in Table 3.2, the uncertainties in the regressed D values are between 0.6 x 10^{-6} cm^2/s and 1.6 x 10^{-6} cm^2/s. Considering that an accuracy in the diffusion coefficient to within ± 1 x 10^{-6} cm^2/s has been sufficient to predict the adsorption kinetics behavior of nonionic surfactants [21, 22, 25, 68, 69], it follows that the new methodology is able to determine the best-fit D values within an acceptable degree of accuracy. Note that the diffusion coefficient of $C_{12}E_8$ reported in Table 3.2 (about 4.3 x 10^{-6} cm^2/s) is consistent with the value of about 5 x 10^{-6} cm^2/s at 306 K reported in Ref.[70]. The D values

Table 3.2: Regressed values of the kinetics parameters, D and β, obtained using the new methodology to study the experimental DST behavior of the four C_iE_j nonionic surfactants studied, and comparison with the values obtained using the existing procedure. D_{WC} denotes the diffusion coefficient predicted using the Wilke-Chang correlation. Superscripts in the results using the existing procedure refer to the following references: a. Ref.[21], b. Ref. [23], c. Ref. [26], and d. Ref. [68].

C_iE_j Nonionic Surfactant	Results using the New Methodology		Correlation Results	Results using the Exiting Procedure	
	D x 10^6 (cm^2/s)	$\log(\beta)$ β in (cm/s)	D_{WC} x 10^6 (cm^2/s)	D x 10^6 (cm^2/s)	$\log(\beta)$ β in (cm/s)
$C_{12}E_4$	3.9 ± 0.6	> -0.95	3.77	6.4[a]	NA
$C_{12}E_6$	3.8 ± 0.6	> -1.25	3.37	7.3[b]	-2.7[b]
$C_{12}E_8$	4.3 ± 1.6	-2±0.50	3.07	7.3[c]	-2.7[c]
$C_{10}E_8$	3.6 ± 1.5	-1.63±0.35	3.18	6.5[d]	-2.6[d]

corresponding to the other three C_iE_j nonionic surfactants have not been measured experimentally, and therefore, a direct validation of the regressed D values is not possible. In view of this, I compare the regressed D values with D values obtained using correlations, as well as with D values measured for related solutes. Diffusion coefficient values can be estimated using the Wilke-Chang (WC) Correlation given below [71]:

$$D_{WC} = 7.4 \text{ x } 10^{-8} \frac{T\sqrt{\phi M_B}}{\eta_B V_A^{0.6}} \qquad (3.17)$$

where D_{WC} is the predicted diffusion coefficient in cm^2/s, M_B is the molecular weight of solvent B (water, in this case) in g/mol, T is the absolute temperature in K, η_B is the viscosity of solvent B in cP, V_A is the solute molal volume at the normal boiling temperature in cm^3/g-mol, and ϕ is the dimensionless association factor of solvent B. For water, $\phi = 2.6$. For the four C_iE_j nonionic surfactants studied, the V_A values were estimated using the La Bas's group-contribution method, which has been demonstrated to predict V_A for different solutes with an accuracy of 3% [72], and are equal to: $V_A(C_{12}E_4) = 528.6$, $V_A(C_{12}E_6) = 639.4$, $V_A(C_{12}E_8) = 750.2$, and $V_A(C_{10}E_8) = 705.8$ (all in units of cm^3/g-mol). Using $M_B = 18$ g/mol for the molecular weight of water,

$T = 298$ K, and $\eta_B = 0.89$ cP, Eq.(3.17) was used to predict the diffusion coefficient values for the four C_iE_j nonionic surfactants studied, and the predicted D_{WC} values are reported in Table 3.2. Considering that the Wilke-Chang correlation has been shown to be accurate to within about 10 to 15% [72], the regressed D values obtained using the new methodology are in good agreement with the correlation results. Moreover, Schonhoff and Sodermann have measured the diffusion coefficient of $C_{12}E_5$ using NMR, and obtained a value of $D = 3.9$ x 10^{-6} cm^2/s [73], which is again in close agreement with the D values regressed for the four C_iE_j nonionic surfactants studied.

(ii) β *Values:* Since the regression analysis of $C_{12}E_4$ and $C_{12}E_6$ did not result in a unique best-fit value of β, shown by the dark horizontal lines in Figures 3-4(a-b), respectively, I am not able to assign specific values of β to these two surfactants. I could only estimate the lower bound β_l values for these surfactants based on the confidence regions in Figures 3-4(a-b), and these values are listed in Table 3.2. Fortunately, this does not limit the utility of the new methodology, since, based on the regression results, I concluded that: (i) the rate-limiting adsorption kinetics mechanism of $C_{12}E_4$ is diffusion-controlled at all its premicellar surfactant bulk solution concentrations, and (ii) the rate-limiting adsorption kinetics mechanism of $C_{12}E_6$ is diffusion-controlled until a C_b value close to its CMC. These conclusions imply that β is not a relevant kinetics parameter for $C_{12}E_4$, and that the relevance of β is less important for $C_{12}E_6$. In the cases of $C_{12}E_8$ and $C_{10}E_8$, the regression analysis identified unique best-fit values of β, as shown by the filled circles in Figures 3-4(c-d), and these values are listed in Table 3.2. The uncertainties in the β values for $C_{12}E_8$ and $C_{10}E_8$ reported in Table 3.2, are calculated based on the 90% confidence regions in Figures 3-4(c-d), respectively. Specifically, Figure 3-4(c) identifies that the β value of $C_{12}E_8$ is in the range of $10^{-2.28}$ cm/s = 0.5 x 10^{-2} cm/s and $10^{-1.29}$ cm/s = 5.1 x 10^{-2} cm/s, and Figure 3-4(d) identifies that the β value of $C_{10}E_8$ is in the range of $10^{-1.86}$ cm/s = 1.4 x 10^{-2} cm/s and $10^{-1.16}$ cm/s = 6.9 x 10^{-2} cm/s.

Note that the lower bound β_l value of $C_{12}E_4 = 10^{-0.95}$ cm/s = 11.2 x 10^{-2} cm/s is higher than the upper bound β value of $C_{12}E_8 = 5.1$ x 10^{-2} cm/s. Accordingly, it follows that β *decreases as the size of the surfactant E_j head group increases* for the same C_{12} hydrocarbon tail. On the other hand, since the 90% confidence regions of $C_{12}E_8$ and $C_{10}E_8$ overlap, it is not possible to determine how β varies with the length of the C_i hydrocarbon tail for the same surfactant E_8 head group.

The Equation of State

In Figure 3-5(a), I plot the surface Equation Of State (EOS) (Π vs. Γ), determined using the new methodology, for $C_{12}E_4$, $C_{12}E_6$, and $C_{12}E_8$. Note that these three nonionic surfactants have the same hydrocarbon tail (C_{12}), but have different poly (ethylene oxide) heads (E_4, E_6, and E_8). In Figure 3-5(b), I plot the EOS, determined using the new methodology, for $C_{10}E_8$ and $C_{12}E_8$. Note that these two nonionic surfactants have the same poly (ethylene oxide) head (E_8), but have different hydrocarbon tails (C_{10} and C_{12}). The ideal EOS is also plotted in Figures 3-5(a) and 3-5(b) as the dotted lines. Obtaining reliable experimental EOS data for small values of Π has been difficult due to the presence of trace impurities, and due to the long equilibration times associated with the measurements, as well as due to significant surfactant depletion effects involving the reduction of the surfactant bulk solution concentrations due to the adsorption process[37]. Surface expansion measurements have been used in Refs. [21, 23, 24, 26] to obtain EOS data for several C_iE_j nonionic surfactants. These measurements relate Π to Γ/Γ_{ref}, where Γ_{ref} is an unknown constant value. In Ref. [62], Lin et al. suggested applying the Gibbs adsorption equation to the experimental equilibrium surface tension vs. C_b data to evaluate Γ_{ref}, and reported the resulting EOS (Π vs. Γ) for several C_iE_j nonionic surfactants. In Figures 3-5(a) and 3-5(b), I also compare the reported EOS for $C_{12}E_4$ and $C_{10}E_8$ [62] with the EOS determined using the new methodology. The open squares in Figure 3-5(a) correspond to the experimental EOS data for $C_{12}E_4$ [62], and the open circles in Figure 3-5(b) correspond to the experimental EOS data for $C_{10}E_8$ [62]. A comparison of the predicted EOS profiles for $C_{12}E_6$ and $C_{12}E_8$ was not possible due to the absence of reliable EOS data for the small Π values involved. Figures 3-5(a) and 3-5(b) show that the equations of state of $C_{12}E_4$ and $C_{10}E_8$ obtained using the new methodology are both consistent with the results of the surface expansion measurements reported in Ref.[62]. In addition, I carried out additional qualitative validation of the EOS predicted using the new methodology. Specifically,

(i) As shown in Figures 3-5(a) and 3-5(b), the predicted EOS of the four C_iE_j nonionic surfactants studied exhibit *positive deviations from the ideal behavior*. This indicates that *net repulsive* interactions operate between the adsorbed C_iE_j surfactant molecules. This finding is consistent with those reported in Refs.[62, 63].

(ii) Figure 3-5(a) reveals that $C_{12}E_8$ exhibits the strongest nonideal behavior, followed by $C_{12}E_6$,
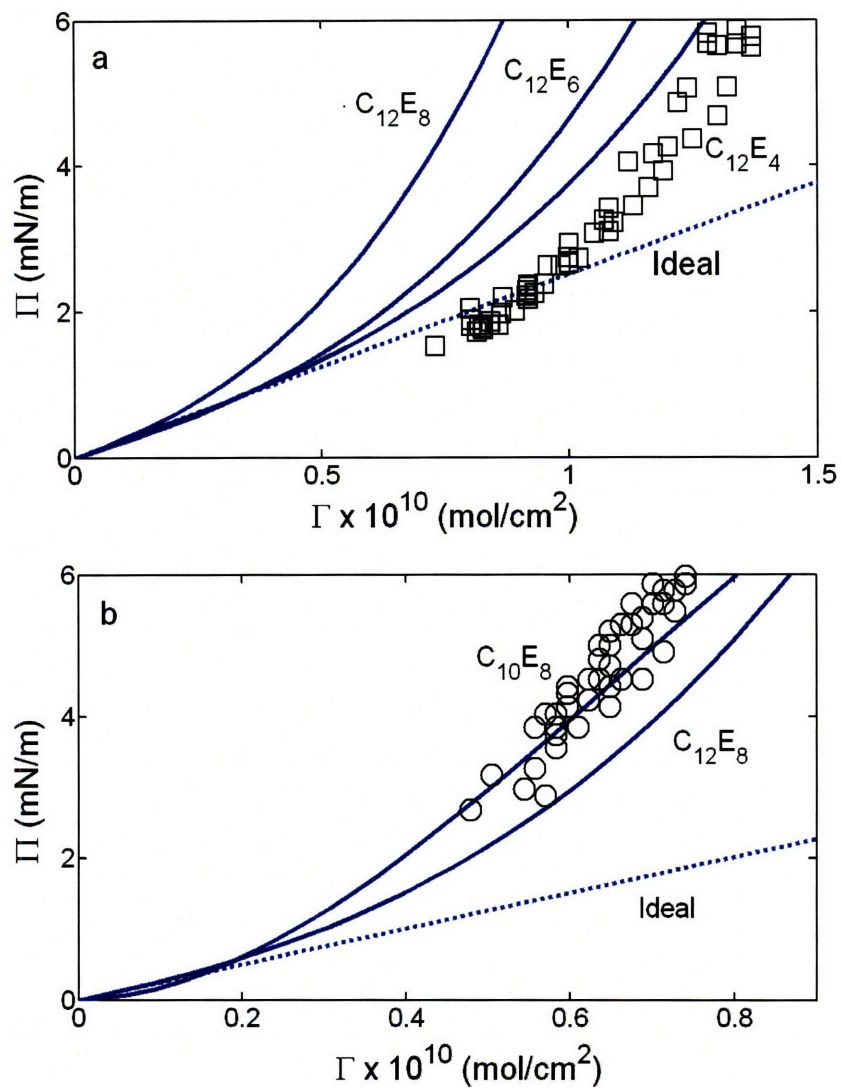
Figure 3-5: Comparison of the surface equation of state (EOS) obtained for $C_{12}E_4$, $C_{12}E_6$, $C_{12}E_8$, and $C_{10}E_8$ using the new methodology with the experimental data obtained from surface expansion measurements for $C_{12}E_4$ and $C_{10}E_8$. Figure 3-5(a) compares the EOS of the three surfactants having the same tail (C_{12}) and shows the experimental EOS data for $C_{12}E_4$ as the open squares. Figure 3-5(b) compares the EOS of the two surfactants having the same poly (ethylene oxide) heads (E_8), and shows the experimental EOS data for $C_{10}E_8$ as the open circles. The dotted lines in both figures correspond to the ideal EOS.

and then by $C_{12}E_4$. In addition, Figure 3-5(b) reveals that $C_{10}E_8$ exhibits a stronger non-ideal behavior than $C_{12}E_8$. The findings in Figures 3-5(a) and 3-5(b) are consistent with the expected trends based on the nature of the interactions between the adsorbed C_iE_j non-ionic surfactant molecules. Specifically, consider the molecular-based framework to model the equilibrium adsorption isotherm behavior of the adsorbed C_iEj nonionic surfactant molecules presented in Ref. [63] . According to this theoretical framework, the interactions between the surfactant C_i hydrocarbon tails are modeled in terms of attractive van der Waals interactions, and the interactions between the surfactant E_j heads are modeled in terms of repulsive hard-disc interactions. In this description, as the size of the E_j head increases, for a given C_i tail, the repulsive interactions between the C_iE_j surfactant molecules become stronger. As a result, this leads to larger deviations from the ideal behavior, consistent with the results in Figure 3-5(a). On the other hand, as the length (i) of the C_i tail increases, for a given E_j head, the attractive interactions between the C_iE_j surfactant molecules become stronger. As a result, this leads to smaller deviations from the ideal behavior, consistent with the results in Figure 3-5(b).

Testing the Validity of the New Methodology

Since the new methodology requires only experimental short-time DST data measured at two initial surfactant bulk solution concentrations, one can test its validity by predicting the DST at other initial surfactant bulk solution concentrations, and subsequently, by comparing these predictions with the corresponding experimentally measured DST data. For each C_iE_j nonionic surfactant studied, Eq.(3.1) was used to predict $\Gamma(t)$ at different C_b values using the regressed best-fit D and β values reported in Table 3.2. Since I concluded that the rate-limiting adsorption kinetics mechanisms for $C_{12}E_4$ and $C_{12}E_6$ are diffusion-controlled, th β values for these surfactants were set to ∞. Subsequently, the DST was predicted using the predicted $\Gamma(t)$ in conjunction with the predicted EOS (Π vs. Γ) shown in Figures 3-5(a) and 3-5(b). In Figures 3-6(a-d), I compare the predicted $\Pi(t)$ vs. $\sqrt{t}$ with the experimentally observed DST behavior for: (a) $C_{12}E_4$, (b) $C_{12}E_6$, (c) $C_{12}E_8$, and (d) $C_{10}E_8$. In these figures, the dashed lines are the predicted behaviors corresponding to the experimental data represented by the open squares, and the solid lines are the predicted behaviors corresponding to the experimental data represented by the filled circles. The surfactant bulk solu-
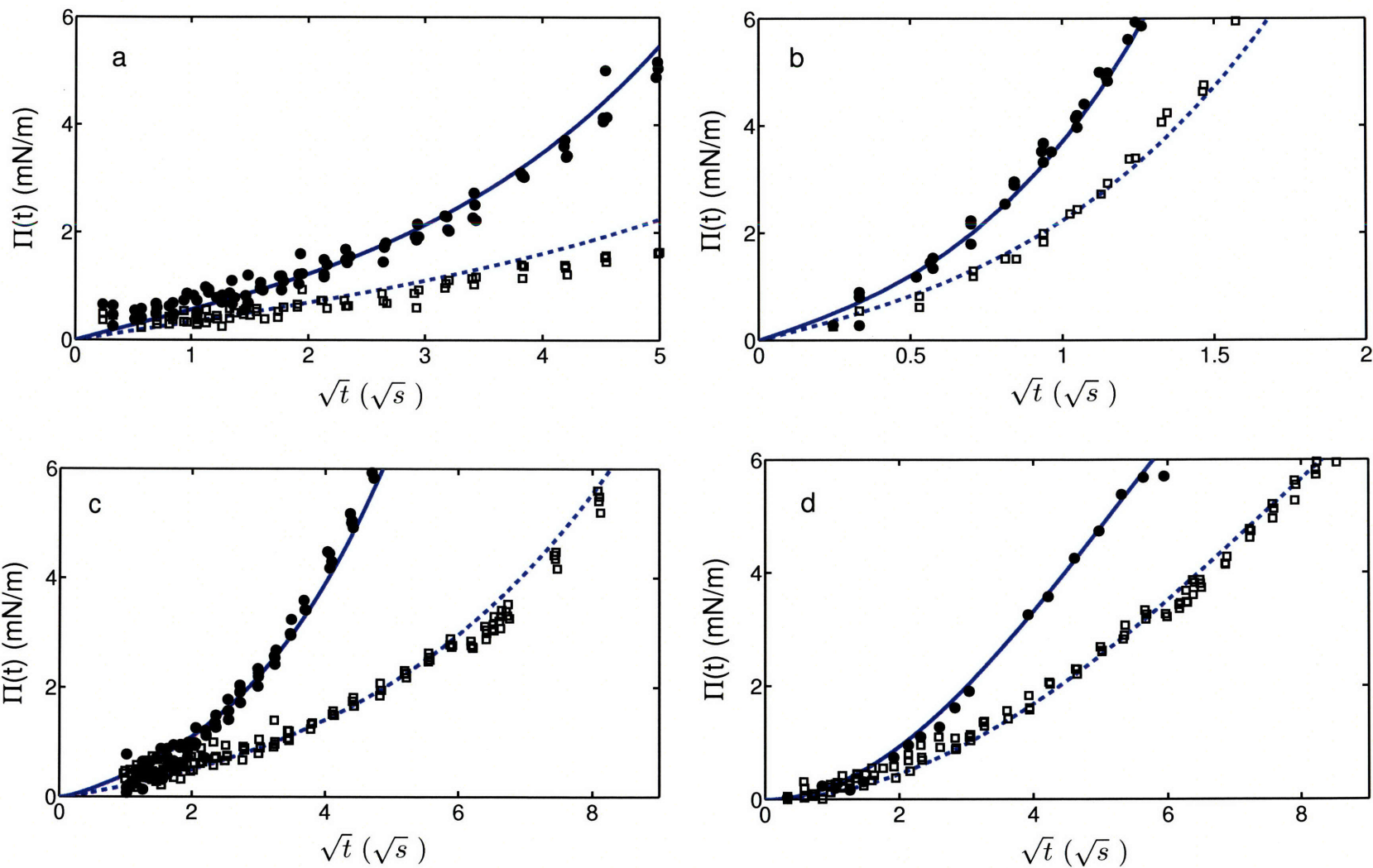
Figure 3-6: Comparison of the predicted dynamic surface pressure, $\Pi(t)$, as a function of the square root of time, t, using the new methodology with the experimentally observed DST behavior for: (a) $C_{12}E_4$, (b) $C_{12}E_6$, (c) $C_{12}E_8$, and (d) $C_{10}E_8$. In these figures, the dashed lines show the predicted behaviors corresponding to the experimental data represented by the open squares, and the solid lines show the predicted behaviors corresponding to the experimental data represented by the filled circles. The surfactant bulk solution concentrations corresponding to the open squares and the filled circles, respectively, are: (a) 0.6×10^{-8} mol/cm^3 and 1.0×10^{-8} mol/cm^3, (b) 3.0×10^{-8} mol/cm^3 and 4.0×10^{-8} mol/cm^3, (c) 0.4×10^{-8} mol/cm^3 and 0.73×10^{-8} mol/cm^3, and (d) 0.4×10^{-8} mol/cm^3 and 0.6×10^{-8} mol/cm^3.

tion concentrations corresponding to the open squares and the filled circles, respectively, are: (a) 0.6 x 10^{-8} mol/cm^3 and 1.0 x 10^{-8} mol/cm^3, (b) 3.0 x 10^{-8} mol/cm^3 and 4.0 x 10^{-8} mol/cm^3, (c) 0.4 x 10^{-8} mol/cm^3 and 0.73 x 10^{-8} mol/cm^3, and (d) 0.4 x 10^{-8} mol/cm^3 and 0.6 x 10^{-8} mol/cm^3. Figures 3-6(a-d) show that the predictions agree well with the experimentally observed DST behaviors for the four C_iE_j surfactants studied at the concentrations studied. Accordingly, Figures 3-6(a-d) serve to validate the results of the new methodology.

3.3.2 Comparison of the New Methodology with the Existing Procedure

In Table 3.2, I summarize the values of D and β, obtained using the existing procedure to analyze the *same* set of experimental DST data used in this chapter for the four C_iE_j nonionic surfactants studied. Note that the results obtained by implementing the existing procedure reported in Table 3.2 correspond to the Generalized Frumkin adsorption isotherm model for the four C_iE_j nonionic surfactants studied.

Several differences can be observed between the results obtained using the new methodology and those obtained using the existing procedure. The D values regressed using the existing procedure are *consistently higher* than the D values regressed using the new methodology for the four C_iE_j surfactants studied. Also, the β values of $C_{12}E_8$ and $C_{10}E_8$ regressed using the existing procedure are about an order of magnitude lower than the β values regressed using the new methodology.

The differences in the D values obtained using the two methods may be associated with the use of a specific model for the equilibrium adsorption isotherm by the existing procedure. Consider, for example, the case of $C_{12}E_8$ [26]. Use of the Langmuir adsorption isotherm predicts a D value of 21 x 10^{-6} cm^2/s, use of the Frumkin adsorption isotherm predicts a D value of 11 x 10^{-6} cm^2/s, and use of the Generalized Frumkin adsorption isotherm predicts a D value of 8 x 10^{-6} cm^2/s. The observed trend of obtaining a reduced value of D as the equilibrium adsorption isotherm model becomes increasingly refined has been observed for almost all the C_iE_j surfactants studied [62]. Therefore, the higher values of D obtained using the existing procedure may be related to the use of a specific model for the equilibrium adsorption isotherm in the existing procedure.

The differences in the β values obtained using the two methods may be associated with the

higher estimates of D obtained using the existing procedure. Note that a higher value of D implies a faster adsorption. Therefore, in order to fit the predicted DST with the experimentally observed DST, the regression algorithm may have reduced the values of β in order to *slow down* the overall rate of surfactant adsorption to compensate for the higher values of D used.

In order to *quantitatively* assess the reliability of the two methods, I next compare the two methods with respect to their *predictive* capabilities. For this purpose, consider, the case of $C_{12}E_6$: the new methodology predicts that the rate-limiting adsorption kinetics mechanism of $C_{12}E_6$ is diffusion-controlled until a C_b value of at least 5.2×10^{-8} mol/cm^3 (close to its CMC), and does not provide a specific value for β, while the existing procedure predicts that the effect of the energy barrier is significant for $C_b > 3 \times 10^{-9}$ mol/cm^3 [23], and provides a specific value for β shown in Table 3.2. In Figures 3-7(a-c), I compare the predictions of the two methods with the experimental short-time DST data measured at three C_b values: (a) $C_b = 1.3 \times 10^{-8}$ mol/cm^3, (b) $C_b = 3.0 \times 10^{-8}$ mol/cm^3, and (c) $C_b = 4.0 \times 10^{-8}$ mol/cm^3. In these figures, the predictions based on the new methodology correspond to the solid lines, the predictions based on the existing procedure correspond to the dashed lines, and the filled circles correspond to the experimental data points. Note that all the three C_b values considered are less than 5.2×10^{-8} mol/cm^3. Figures 3-7(a-c) clearly show that at the three C_b values studied, the predictions based on the new methodology compare much more favorably with the experimental short-time DST data than those based on the existing procedure. In other words, the observed experimental short-time DST behavior can be explained more adequately based on a diffusion-controlled adsorption model, as predicted by the new methodology, than based on the reported mixed-controlled adsorption model, as predicted by the existing procedure. This example clearly shows that assuming a specific model for the equilibrium adsorption isotherm can lead not only to different values of the kinetics parameters, D and β, but that it can also result in a completely different determination of the underlying rate-limiting adsorption kinetics mechanism. Note that this finding is also in agreement with the observed high sensitivity of the regression analysis results to the specific model used to describe the equilibrium adsorption isotherm in the existing procedure [31, 32]. Since the new methodology does not use a model for the equilibrium adsorption isotherm, it should provide a more reliable computational framework to determine the rate-limiting adsorption kinetics mechanism, and the associated kinetics parameters, D and β.
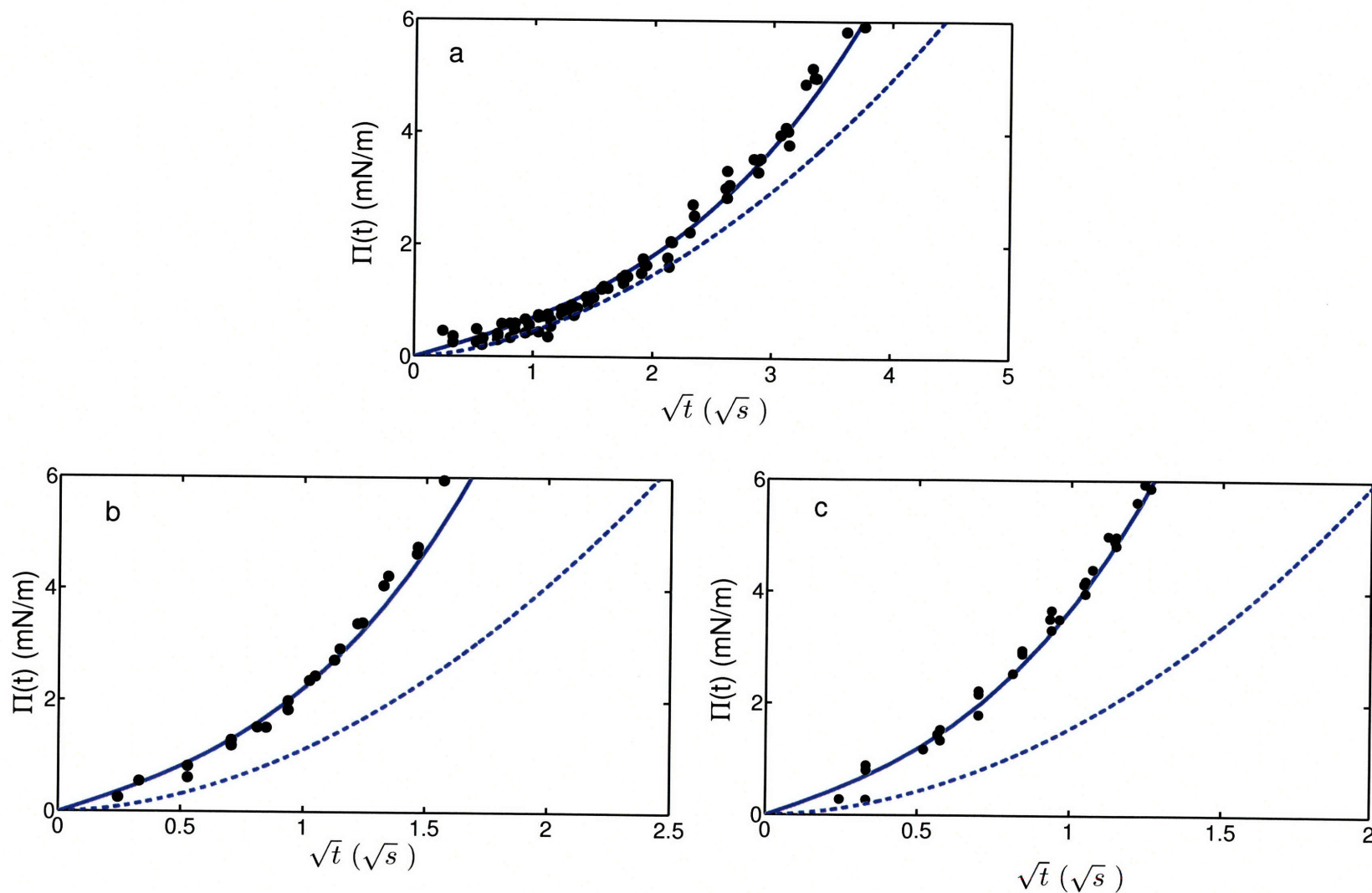
Figure 3-7: Comparison of the results obtained using the new methodology and those obtained using the existing procedure with the dynamic surface pressure, $\Pi(t)$, of $C_{12}E_6$ as a function of the square root of time, t, measured at three conditions: (a) $C_b = 1.3 \times 10^{-8}$ mol/cm^3, (b) $C_b = 3.0 \times 10^{-8}$ mol/cm^3, and (c) $C_b = 4.0 \times 10^{-8}$ mol/cm^3. In these figures, the solid lines correspond to predictions based on the new methodology, the dashed lines correspond to predictions based on the existing procedure, and the filled circles correspond to the experimental data points.

3.4 Conclusions

In the absence of a fundamental physical understanding of the energy barrier for the adsorption of surfactant molecules from the sub-surface onto the surface, reliable determination of the rate-limiting adsorption kinetics mechanism (diffusion-controlled vs. mixed diffusion-barrier controlled), including extracting reliable values of the kinetics parameters (namely, D, the diffusion coefficient of the surfactant molecule, and β, the energy barrier parameter), for various surfactant systems, is of great fundamental and practical value. Although the rate-limiting adsorption kinetics mechanism, and the values of the kinetics parameters, D and β, should not depend on the equilibrium adsorption isotherm behavior of the surfactant, the existing procedure of extracting this information from the experimentally measured DST data uses a model for the equilibrium adsorption isotherm, and it has been shown that the results obtained are quite sensitive to the specific choice of the model for the equilibrium adsorption isotherm[31–34].

In this chapter, I presented a new methodology to determine the rate-limiting adsorption kinetics mechanism, including determining the values of the kinetics parameters, D and β, from the experimental DST data, that *does not* use a model for the equilibrium adsorption isotherm. In addition, the new methodology has the following advantages over the existing procedure used to analyze the experimental DST data: (i) it requires as input only the experimental *short-time* DST data measured at *two* initial surfactant bulk solution concentrations, and (ii) the results of applying the new methodology can be *tested independently* for internal consistency. I applied the new methodology to analyze the experimental short-time DST data of the following C_iE_j nonionic surfactants: $C_{12}E_4$, $C_{12}E_6$, $C_{12}E_8$, and $C_{10}E_8$. I found that the rate-limiting adsorption kinetics mechanism of $C_{12}E_4$ and $C_{12}E_6$ is diffusion-controlled at any of their respective premicellar surfactant bulk solution concentrations. On the other hand, for $C_{12}E_8$ and $C_{10}E_8$, I found that their respective CMC values are large enough to begin to observe a significant effect of the energy barrier on the overall rate of surfactant adsorption. Accordingly, I concluded that, for $C_{12}E_8$ and $C_{10}E_8$, the rate-limiting adsorption kinetics mechanism shifts from diffusion-controlled to mixed-controlled as the premicellar surfactant bulk solution concentration increases.

I determined the relevant kinetics parameter values for the four C_iE_j nonionic surfactants studied. Results of applying the new methodology for $C_{12}E_j$ ($j = 4, 6$, and 8) nonionic surfactants

indicated that the β value decreases as the size of the surfactant polar head group (E_j) increases. On the other hand, based on the results of applying the new methodology for $C_{10}E_8$ and $C_{12}E_8$, no conclusion could be reached on the specific dependence of β on the length of the surfactant hydrocarbon tail (C_i). Note that the observed dependence of β on the size of the surfactant polar head group (E_j) is based on analyzing the behavior of a few C_iE_j nonionic surfactants. Therefore, in order to develop a complete understanding of the dependence of β on the surfactant polar head groups and on the hydrocarbon tail groups, β values need to be determined for different classes of nonionic surfactants, including n-alcohols and n-phosphine oxide surfactants. A fundamental understanding of the dependence of β on the nonionic surfactant head and tail groups could provide valuable insights on the nature of the energy barrier. In this regard, the new methodology presented in this chapter can be useful for extracting reliable β values for various nonionic surfactant systems from the experimental DST data.

I tested the new methodology by predicting the short-time DST profiles at other initial surfactant bulk solution concentrations, and subsequently, by comparing the predicted DST profiles with those measured experimentally using the pendant-bubble apparatus. Very good agreement was obtained for the four C_iE_j nonionic surfactants studied. I also compared the results of implementing the new methodology with those of implementing the existing procedure, and concluded that using a model for the equilibrium adsorption isotherm can lead not only to different values of D and β, but it can also lead to a completely different determination of the rate-limiting adsorption kinetics mechanism. Since the new methodology proposed here does not require using a model for the equilibrium adsorption isotherm, I concluded that it should provide a more reliable determination of the rate-limiting adsorption kinetics mechanism, including the deduced kinetics parameters, D and β.

In Chapter 4, I analyze the experimental pendant-bubble DST data of $C_{12}E_4$ and $C_{12}E_6$ corresponding to the *entire relaxation process*, and demonstrate that these nonionic surfactants appear to adsorb at a rate which is faster than that predicted by the diffusion-controlled model, specifically when $t > 100 - 200$ s. I hypothesize the onset of natural convection in order to rationalize the apparent faster rate of adsorption.

Appendix 3.A: Reliability of the New Methodology

In this Appendix, I demonstrate the reliability of the new methodology by: (i) artificially generating experimental short-time DST data corresponding to specific values of D and β and to a specific EOS (Section 3.A.1), (ii) applying the new methodology to the artificially generated data (Section 3.A.2), and (iii) comparing the results (the D and β values and the EOS) obtained using the new methodology with those that were used to artificially generate the DST data (Section 3.A.2).

3.A.1 Generation of the Artificial Experimental Short-Time DST Data

To artificially generate the experimental short-time DST data, consider the mixed-controlled adsorption of a nonionic surfactant characterized by 'representative' values of $D = 4 \times 10^{-6}$ cm^2/s and $\beta = 1 \times 10^{-2}$ cm/s. Let the surface EOS of the nonionic surfactant satisfy the Generalized Frumkin EOS:

$$\Pi(\Gamma) = -\Gamma_\infty RT \left[\log(1 - x) - \frac{Knx^{n+1}}{1 + n} \right], \qquad x = \frac{\Gamma}{\Gamma_\infty} \tag{3.A.1}$$

where $K = 3.0$, $n = 1.0$, and $\Gamma_\infty = 6.0 \times 10^{-10}$ mol/cm^2. Note that these EOS parameter values are chosen such that the resulting EOS displays nonideal behavior for small values of Π (~ 6 mN/m). For the chosen values of β, D, and Γ_∞, the maximum surfactant concentration below which the overall adsorption kinetics can be considered to be diffusion-controlled, $C_d^{\max}$, can be evaluated using Eq.(3.15) to be 1.5×10^{-8} mol/cm^3. With this value of $C_d^{\max}$ in mind, I choose the two surfactant bulk solution concentrations at which the DST data is generated artificially to be $C_1 = 1 \times 10^{-8}$ mol/cm^3 and $C_2 = 3 \times 10^{-8}$ mol/cm^3, such that : (a) one of the surfactant bulk solution concentration values ($C_b = C_1$) is smaller than $C_{\max}^d$, while the other ($C_b = C_2$) is larger than $C_{\max}^d$, and (b) the surfactant bulk solution concentration that is larger than $C_{\max}^d$ ($C_b = C_2$) is not much larger than $C_{\max}^d$. These two considerations ensure that there is a non-negligible effect of the energy barrier in at least one of the C_b values chosen in the regression analysis, but that this effect is not pronounced. These conditions were chosen to test if the new methodology can detect the effect of the energy barrier, and if it can provide a reasonable estimate of the β value, *even when the effect of the energy barrier is not as pronounced.*

First, with the D and β values selected above, and with $r_0 = 0.1$ cm, short-time dynamic surfactant surface concentrations profiles, $\Gamma(t)$'s, are generated at the chosen values of C_1 and C_2 using Eq.(3.1). Subsequently, the generated $\Gamma(t)$ profiles are used in conjunction with Eq.(3.A.1) to generate the short-time DST profiles at C_1 and C_2. Since the measurement of DST typically involves measuring the surface tension at specific time t values, short-time DST values are obtained for specific t values from the generated short-time DST profiles. The values of t used to generate the experimental DST data are obtained by generating random numbers satisfying a uniform distribution in the range 0 - 40 s. This range of t values is chosen such that the DST decreases to about at least 6 mN/m at the surfactant bulk solution concentrations considered. In order to generate a realistic representation of the actual experimental DST data, random errors were introduced in the generated DST values. For this purpose, random numbers were generated that satisfy a normal distribution with a mean value of 0, and a standard deviation value of 0.1. A value of 0.1 was chosen since the typical error associated with the DST measurements using the pendant-bubble apparatus has been reported to be about 0.1 mN/m [74]. The artificially generated experimental short-time DST data is shown in Figure 3-8, where the short-time dynamic surface pressure, $\Pi(t)$, is plotted in the x-axis and time t is plotted in the y-axis. The open squares correspond to $C_1 = 1 \times 10^{-8}$ mol/cm^3, and the filled circles correspond to $C_2 = 3 \times 10^{-8}$ mol/cm^3. For a discussion of the various lines in Figure 3-8, see Section 3.A.2.

3.A.2 Regression Methodology

The following steps are involved in implementing the new methodology to analyze the artificially generated experimental DST data:

Step 1: Approximating the Experimental DST Data

Recall that, by definition, t_1 and t_2 correspond to the two times at which the dynamic surface pressure, Π, attains the *same* value. Also, recall that in a typical pendant-bubble experiment, the surface tension is measured at specific time values. Therefore, it is rare to find exactly the same value of the surface pressure reported at different times for experiments conducted at two different surfactant bulk solution concentrations. Accordingly, I first approximate the artificially generated experimental data points (t vs. $\Pi(t)$) in Figure 3-8 with polynomial best-fit curves, and
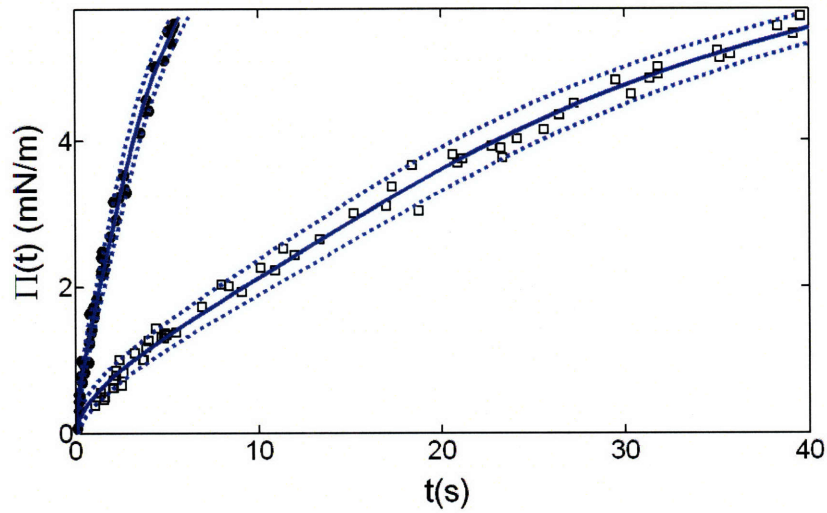
Figure 3-8: Artificially generated experimental short-time DST data at two surfactant bulk solution concentration values, $C_1 = 1 \times 10^{-8}$ mol/cm^3 and $C_2 = 3 \times 10^{-8}$ mol/cm^3, and the polynomial approximations for the experimental data points at these two conditions. The open squares correspond to C_1 and the filled circles correspond to C_2. The polynomial approximations correspond to the solid lines. The dotted lines on either side of the solid lines represent the 90% prediction bands for the polynomial approximations.

their associated 90% prediction bands. Note that the prediction bands reflect the scatter in the experimental DST data. Approximating the experimental DST data with a polynomial best-fit curve enables us to obtain t_1 and t_2 for any arbitrary value of the surface pressure, and the prediction bands enable us to estimate the errors in the values of t_1 and t_2 (see Step 2 below). For the artificially generated experimental DST data points in Figure 3-8, the polynomial best-fit curves are shown as the solid black lines that pass through the data points. The 90% prediction bands associated with the polynomial approximations are also shown in Figure 3-8 as the dotted lines on either side of each approximation.

Step 2: Obtaining t_1 and t_2

Having represented the artificially generated experimental data points measured at two surfactant bulk solution concentrations, C_1 and C_2, in the form of polynomial best-fit lines (t vs. $\Pi(t)$) with the associated 90% prediction bands, I then plot t_1 vs. t_2 by identifying the two times at which Π has the same value at these two conditions. The resulting t_2 vs. t_1 relationship corresponding to the artificially generated data shown in Figure 3-8 is plotted as the solid line in Figure 3-9. Note
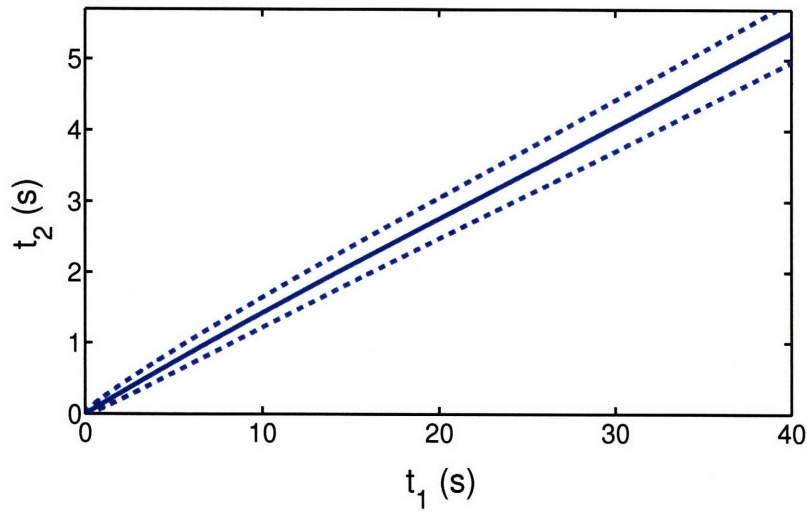
Figure 3-9: The observed relationship between t_1 and t_2 for the artificially generated experimental short-time DST data shown in Figure 3-8 is represented as the solid line. The x-axis error is determined by the error in the estimation of t_1, and the y-axis error is determined by the error in the estimation of t_2. Together, these error bars represent the 90% confidence interval envelope, which in the figure, is bounded by the two dashed lines.

that the error associated with t_1 in Figure 3-8 becomes the x-axis error in Figure 3-9, and the error associated with t_2 in Figure 3-8 becomes the y-axis error in Figure 3-9. Together, the two errors generate the 90% confidence interval envelope in t_2 vs. t_1, shown in Figure 3-9 as being bounded by the two dashed lines. Accordingly, the confidence interval envelope reflects the scatter in the experimental DST data.

Step 3: Regressing for D and β

Having represented the artificially generated experimental DST data in the form of t_2 vs. t_1 with the associated confidence interval envelope, I then regress Eq.(3.13) for D and β. The regression is carried out by generating the sum of squared errors surface over a 2-d (D, β) parameter space. The combinations of D and β values, which result in a t_2 vs. t_1 line that falls within the 90% confidence interval envelope, are then determined. Accordingly, these combinations of D and β values form the 90% confidence region of the regression in the (D, β) parameter space. The 90% confidence region, corresponding to the t_2 vs. t_1 relationship in Figure 3-9, is shown in Figure 3-10 as the light grey region. One can clearly see that the 90% confidence region, while significantly reducing the possible combinations of D and β parameter values in the (D, β) parameter space, does not yield

130
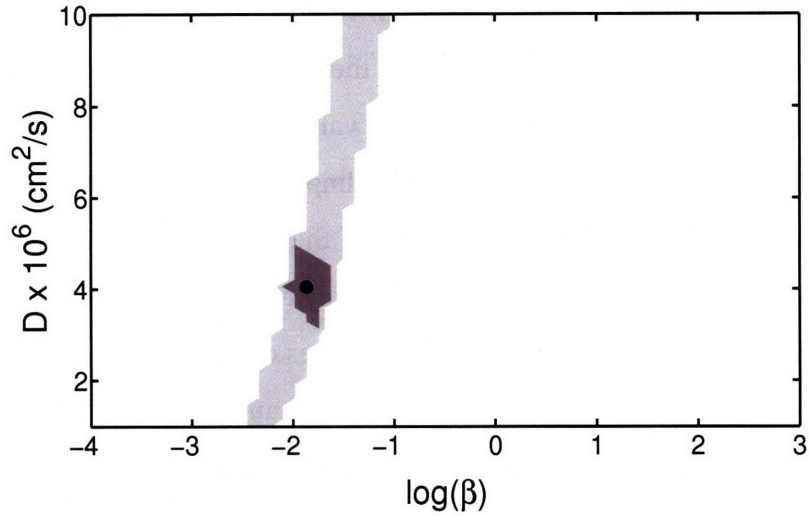
Figure 3-10: The confidence region in the D - β parameter space corresponding to the artificially generated experimental short-time DST data shown in Figure 3-8. The units of β are cm/s. The light grey region corresponds to the 90% confidence region at the end of the t_1 vs. t_2 regression, and the dark grey region corresponds to the confidence region obtained after the EOS-based filtering of the D and β values. The filled circle indicates the best-fit combination of the D and β values.

the parameter values with the desired level of accuracy. For example, in Figure 3-10, the light grey region indicates an uncertainty in the D value between 1 x 10^{-6} cm^2/s and 10 x 10^{-6} cm^2/s, which is very high when compared to the acceptable error of about $\pm$ 1 x 10^{-6} cm^2/s. In order to obtain a tighter estimate of the D and β parameter values, trimming of the confidence region is carried out, as described in Step 4 below.

Step 4: Using the EOS to Filter the D and β Values

In Section 3.2, I stressed that for any combination of D and β values, it is possible to determine the EOS using the experimental DST data in conjunction with Eq.(3.1). Accordingly, EOS curves were generated for each of the combinations of D and β values identified at the end of Step 3. Trimming of the (D, β) region is then carried out using the fact that the resulting EOS should approach the Ideal EOS at very small values of the surface pressure. In other words, for $\Pi \rightarrow 0$, the EOS should reduce to:

$$\Pi = RT\Gamma \qquad (3.A.2)$$

Accordingly, for each combination of the D and β values in the light grey region in Figure 3-10, we

131

estimate: (i) the slope of the EOS at small values of Π, and (ii) the 90% confidence bands for the estimated slope values. Subsequently, trimming of the light grey region in Figure 3-10 is carried out by imposing the requirement that the ideal slope value of RT needs to lie within the estimated 90% confidence bands of the estimated slope values. Imposing this constraint on the combinations of D and β values results in a significant reduction of the confidence region identified at the end of Step 3, which is shown in Figure 3-10 as the dark grey region. The combination of the D and β values that resulted in an EOS whose slope at small values of Π was closest to the ideal EOS slope value of RT is considered as the *best-fit* combination of D and β values. The best-fit combination corresponding to the artificially generated experimental data, indicated by the filled circle in Figure 3-10, is found to be: $D^* = 4.1 \times 10^{-6}$ cm^2/s and $\beta^* = 10^{-1.86}$ cm/s $= 1.4 \times 10^{-2}$ cm/s.

At the end of the EOS-based filtering of the D and β parameter values, considering the best-fit combination of D and β values and the associated 90% confidence region (see the dark grey region in Figure 3-10), the regressed values of the kinetics parameters are reported as: $D^* = 4.1 \pm 0.9 \times 10^{-6}$ cm^2/s, and $\log(\beta^*) = -1.86 \pm 0.24$ (β in cm/s). In other words, β^* is regressed to be between $10^{-2.10} = 0.8 \times 10^{-2}$ cm/s and $10^{-1.63} = 2.3 \times 10^{-2}$ cm/s. Note that these D^* and β^* values are consistent with the D and β values that were used to artificially generate the experimental short-time DST data, that is, $D = 4 \times 10^{-6}$ cm^2/s, and $\beta = 1 \times 10^{-2}$ cm/s. The EOS corresponding to D^* and β^* was determined by separately using the generated DST data at the two concentrations, C_1 and C_2. The EOS obtained by this procedure is compared with the EOS used to artificially generate the DST data in Figure 3-11. In Figure 3-11, the open squares are the EOS data points obtained using the short-time DST data corresponding to C_1, the filled circles are the EOS data points obtained using the short-time DST data corresponding to C_2, the solid line is the EOS that was used to artificially generate the experimental short-time DST data in Eq.(3.A.1), and the dotted line is the ideal EOS. Figure 3-11 clearly shows that the EOS determined using the new methodology is consistent with the EOS used to artificially generate the short-time DST data.

Based on the results of the analysis presented in this Appendix, I conclude that the new methodology can be used to reliably determine the values of D and β, and of the EOS, using the experimental short-time DST data measured at two surfactant bulk solution concentrations as the only inputs.
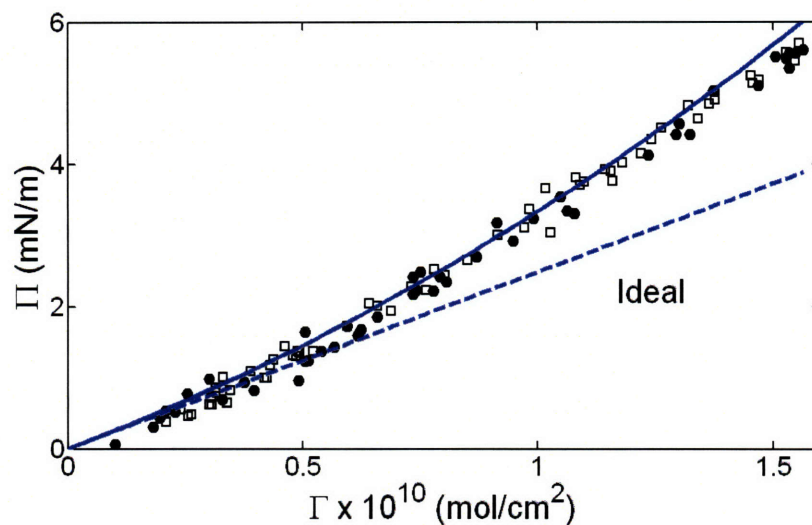
Figure 3-11: Comparison of the EOS obtained using the new methodology to analyze the artificially generated experimental short-time DST data shown in Figure 3-8, with the actual EOS that was used to generate the data. The open squares are the EOS data points obtained using the experimental short-time DST data corresponding to C_1, the filled circles are the EOS data points obtained using the experimental short-time DST data corresponding to C_2, and the solid line is the EOS that was used to artificially generate the experimental short-time DST data in Eq.(3.A.1). The dashed straight line denotes the ideal EOS.

Appendix 3.B: Validating the Range of Experimental Short-Time DST Data Used in the New Methodology

The conditions set by Eq.(3.4) define the ranges of t values ($t \leq t^*$) and of $\Gamma(t)$ values ($\Gamma(t) \leq \Gamma^*$) over which the new methodology can be applied. In this Appendix, I confirm that the experimental short-time DST data used to perform the regression for the four C_iE_j nonionic surfactants considered do satisfy the conditions set by Eq.(3.4).

Equation(3.4) shows that the evaluation of t^* involves evaluating $h = (\Gamma/C_b)_e$, which depends on the equilibrium adsorption isotherm. Considering that the *maximum* surfactant sub-surface concentration for $t \leq t^*$ is about $0.02C_b$ [35], I estimate *lower bound* values for h by dividing the Γ obtained using the EOS by $0.02C_b$. Using this estimated lower bound values for h, along with the regressed estimates for D, I estimate *lower bound* values for t^* (see Eq.(3.4)) for the four C_iE_j nonionic surfactants considered at the two C_b values used in the regression. Note that the evaluation of Γ^* requires knowledge of Γ_∞, which can be estimated using the known molecular structure information of the surfactants utilizing the method described in Ref.[63].

For the four C_iE_j nonionic surfactants considered, in Table 3.3, I have listed: (i) the maximum value of $\Gamma(t)$ involved in the regression analysis, Γ_{max}^{exp}, determined using the EOS in Figures 3-5(a) and 3-5(b), (ii) Γ^* estimated using the method described in Ref.[63], (iii) the values of the two surfactant bulk solution concentrations, C_b, used in the regression analysis, (iv) the maximum value of t used in the regression analysis, t_{max}^{exp}, corresponding to each of the two C_b values, and (v) the estimated lower limit of t^* at the two C_b values. We find that for all the cases considered, $t_{max}^{exp} <$ lower limit values of t^* and $\Gamma_{max}^{exp} < \Gamma^*$.

Based on the results presented in this appendix, I conclude that the experimental short-time DST data used in the new methodology do satisfy the requirements specified by Eq.(3.4).

134

Table 3.3: For the four C_iE_j nonionic surfactants considered, the table lists: (i) the maximum value of $\Gamma(t)$ involved in the regression analysis, Γ_{max}^{exp}, determined using the EOS in Figures 3-5(a) and 3-5(b), (ii) Γ^* estimated using the method described in Ref.[63], (iii) the values of the two surfactant bulk solution concentrations, C_b, used in the regression analysis, (iv) the maximum value of t used in the regression analysis, t_{max}^{exp}, corresponding to each of the two C_b values, and (v) the estimated lower limit of t^* at the two C_b values.

C_iE_j Surfactant	$\Gamma_{max}^{exp} \times 10^{10}$ (mol/cm^2)	$\Gamma^* \times 10^{10}$ (mol/cm^2)	$C_b \times 10^8$ (mol/cm^3)	t_{max}^{exp} (s)	Lower Bound of t^* (s)
$C_{12}E_4$	1.28	1.40	2.0	7.4	10.4
			1.5	12.7	18.5
$C_{12}E_6$	1.13	1.14	1.3	14.1	20.1
			1.0	23.0	34.0
$C_{12}E_8$	0.87	0.99	1.0	13.5	17.6
			0.6	33.6	48.8
$C_{10}E_8$	0.80	0.99	3.0	1.7	2.0
			1.0	13.1	17.8

Bibliography

[1] G. Kretzschmar and R. Miller. Dynamic properties of adsorption layers of amphiphilic substances at fluid interfaces. *Advances in Colloid and Interface Science*, 36:65–124, 1991.

[2] B. A. Noskov. Fast adsorption at the liquid-gas interface. *Advances in Colloid and Interface Science*, 69:63–129, 1996.

[3] F. Ravera, M. Ferrari, and L. Liggieri. Adsorption and partitioning of surfactants in liquid-liquid systems. *Advances in Colloid and Interface Science*, 88:129–177, 2000.

[4] P. Joos. *Dynamic Surface Phenomena*. VSP, The Netherlands, 1999.

[5] R. Defay and G. Petre. Dynamic surface tension. In E. Matijevic, editor, *Surface and Colloid Science*, volume 3, pages 27–81. Wiley, 1971.

[6] S. S. Dukhin, G. Kretzschmar, and R. Miller, editors. *Dynamics of adsorption of liquid interfaces: theory, experiment, applications*. Elsevier, 1995.

[7] C-H. Chang and Elias I. Franses. Adsorption dynamics of surfactants at the air/water interface: a critical review of mathematical models, data, and mechanisms. *Colloids and Surfaces A: Physicochemical and Engineering Aspects*, 100:1–45, 1995.

[8] J. Eastoe and J. S. Dalton. Dynamic surface tension and adsorption mechanisms of surfactants at the air-water interface. *Advances in Colloid and Interface Science*, 85:103–144, 2000.

[9] R. Miller, P. Joos, and V. B. Fainerman. Dynamic surface and interfacial tensions of surfactant and polymer solutions. *Advances in Colloid and Interface Science*, 49:249–302, 1994.

[10] V. Pillai and D. O. Shah, editors. *Dynamic Properties of Interfaces and Association Structures*. AOCS Press, 1996.

[11] F. Ravera, L. Liggieri, and R. Miller. Molecular orientation as a controlling process in adsorption dynamics. *Colloids and Surfaces A: Physicochemical and Engineering Aspects*, 175:51–60, 2000.

[12] A. F. H. Ward and L.Tordai. Diffusion controlled adsorption. *Journal of Chemical Physics*, 14:453, 1946.

[13] K. L. Sutherland. The kinetics of adsorption at liquid surfaces. *Australian Journal of Scientific Research*, A5:683–696, 1952.

[14] R. S. Hansen. Diffusion and the kinetics of adsorption of aliphatic acids and alcohols at the water-air interface. *Journal of Colloid Science*, 16:549–560, 1961.

[15] J. F. Baret. Theoretical model for an interface allowing a kinetic study of adsorption. *Journal of Colloid and Interface Science*, 30:1–12, 1969.

[16] J. F. Baret. Kinetics of adsorption from a solution. Role of the diffusion and of the adsorption-desorption antagonism. *The Journal of Physical Chemistry*, 72:2755–2758, 1968.

[17] R. P. Borwankar and D. T. Wasan. The kinetics of adsorption of surface active agents at gas-liquid surfaces. *Chemical Engineering Science*, 38(10):1637 – 1649, 1983.

[18] R. Bleys and P. Joos. Adsorption kinetics of bolaform surfactants at the air/water interface. *Journal of Physical Chemistry*, 89:1027–1032, 1985.

[19] P. Joos and G. Serrien. Adsorption kinetics of lower alkanols at the air/water interface: Effect of structure makers and structure breakers. *Journal of Colloid and Interface Science*, 127(1):97–103, 1989.

[20] R. Pan, J. Green, and C. Maldarelli. Theory and experiment on the measurement of kinetic rate constants for surfactant exchange at an air/water interface. *Journal of Colloid and Interface Science*, 205:213–230, 1998.

[21] C-T. Hsu, M-J. Shao, and S-Y. Lin. Adsorption kinetics of $C_{12}E_4$ at the air-water interface: Adsorption onto a fresh interface. *Langmuir*, 16:3187–3194, 2000.

[22] Y-C. Lee, H-S. Liu, and S-Y. Lin. Adsorption kinetics of $C_{10}E_4$ at the air/water interface: consider molecular interaction or reorientation. *Colloids and Surfaces A: Physicochemical and Engineering Aspects*, 212:123–134, 2003.

[23] Y-C. Lee, S-Y. Lin, and M-J. Shao. Adsorption kinetics of $C_{12}E_6$ at the air-water interface. *Journal of Chinese Institute of Chemical Engineers*, 33(6):631–643, 2002.

[24] H-C. Chang, C-T. Hsu, and S-Y. Lin. Adsorption kinetics of $C_{10}E_8$ at the air-water interface. *Langmuir*, 14:2476–2484, 1998.

[25] S-Y. Lin, Y-C. Lee, M-J. Shao, and C-T. Hsu. A study on surfactant adsorption kinetics: The role of the data of equation of state for $C_{14}E_8$. *Journal of Colloid and Interface Science*, 244:372–376, 2001.

[26] S-Y. Lin, R-Y. Tsay, L-W. Lin, and S-I. Chen. Adsorption kinetics of $C_{12}E_8$ at the air-water interface: Adsorption onto a clean interface. *Langmuir*, 12:6530–6536, 1996.

[27] S-Y. Lin, T-L. Lu, and W-B. Hwang. Adsorption kinetics of decanol at the air-water interface. *Langmuir*, 11:555–562, 1995.

[28] Y-C. Lee, Y-B. Liou, R. Miller, H-S. Liu, and S-Y. Lin. Adsorption kinetics of nonanol at the air-water interface: Considering molecular interaction or aggregation within surface layer. *Langmuir*, 18:2686–2692, 2002.

[29] S-Y.Lin, K. McKeigue, and C. Maldarelli. Diffusion-limited interpretation of the induction period in the relaxation in surface tension due to the adsorption of straight chain, small polar group surfactants: Theory and experiment. *Langmuir*, 7:1055–1066, 1991.

[30] S-Y. Lin, W-J. Wang, and C-T. Hsu. Adsorption kinetics of 1-octanol at the air-water interface. *Langmuir*, 13:6211 – 6218, 1997.

[31] C-T. Hsu, C-H. Chang, and S-Y. Lin. Comments on the adsorption isotherm and determination of adsorption kinetics. *Langmuir*, 13:6204–6210, 1997.

[32] Y.-C. Lee, S.-Y. Lin, and H.-S. Liu. Role of equation of state on studying surfactant adsorption kinetics. *Langmuir*, 17:6196–6202, 2001.

[33] C.-T. Hsu, C.-H. Chang, and S.-Y. Lin. A study of surfactant adsorption kinetics: Effects of interfacial curvature and molecular interaction. *Langmuir*, 16:1211–1215, 2000.

[34] C.-T. Hsu, C.-H. Chang, and S.-Y. Lin. A study of surfactant adsorption kinetics: Effect of intermolecular interaction between adsorbed molecules. *Langmuir*, 15:1952–1959, 1999.

[35] S. N. Moorkanikkara and D. Blankschtein. Short time behavior of mixed barrier-diffusion controlled adsorption. *Journal of Colloid and Interface Science*, 296:442–457, 2006.

[36] M. J. Rosen. *Surfactants and Interfacial Phenomena*. Wiley Interscience, 1989.

[37] C. D. Taylor, D. S. Valkovska, and C. D. Bain. A simple and rapid method for the determination of the surface equations of state and adsorption isotherms for efficient surfactants. *Physical Chemistry Chemical Physics*, 5:4885–4891, 2003.

[38] J. K. Ferri and K. J. Stebe. Soluble surfactants undergoing surface phase transitions: A Maxwell construction and the dynamic surface tension. *Journal of Colloid and Interface Science*, 209:1–9, 1999.

[39] Md. M. Hossain, T. Suzuki, and T. Kato. Phases and phase transition in Gibbs monolayers of an alkyl phosphate surfactant. *Journal of Colloid and Interface Science*, 288:342–349, 2005.

[40] Md. M. Hossain, T. Suzuki, and T. Kato. Phase diagram of n-tetradecyl phosphate in Gibbs monolayers. *Colloids and Surfaces A: Physicochemical and Engineering Aspects*, 284-285:234–238, 2006.

[41] M. L. Pollard, R. Pan, C. Steiner, and C. Maldarelli. Phase behavior of sparingly soluble polyethoxylate monolayers at the air-water surface and its effect on dynamic tension. *Langmuir*, 14:7222–7234, 1998.

[42] R. Subramanyam and C. Maldarelli. Fluorescence evidence that a phase transition causes the induction time in the reduction in dynamic tension during surfactant adsorption to a clean

air/water interface and a kinetic-diffusive transport model for the phase-induced induction. *Journal of Colloid and Interface Science*, 253:377–392, 2002.

[43] R-Y. Tsay, T-F. Wu, and S-Y. Lin. Observation of G-LE and LE-LC phase transitions of adsorbed 1-dodecanol monolayer from dynamic surface tension profiles. *Journal of Physical Chemistry B*, 108:18623–18629, 2004.

[44] S. Sundaram, J. K. Ferri, D. Vollhardt, and K. J. Stebe. Surface phase behavior and surface tension evolution for lysozyme adsorption onto clean interfaces and into DPPC monolayers: Theory and experiment. *Langmuir*, 14:1208–1218, 1998.

[45] J. S. Erickson, S. Sundaram, and K. J. Stebe. Evidence that the induction time in the surface pressure evolution of lysozyme solutions is caused by a surface phase transition. *Langmuir*, 16:5072–5078, 2000.

[46] Md. M. Hossain, T. Suzuki, K. Iimura, and T. Kato. Kinetic appearance of first-order gas-liquid expanded and liquid-expanded-liquid condensed phase transitions below the triple point. *Langmuir*, 22:1074–1078, 2006.

[47] Md. M. Hossain, T. Suzuki, and T. Kato. Interaction of an organic cation with Gibbs monolayers of *n*-hexadecyl phosphate. *Journal of Colloid and Interface Science*, 292:186–194, 2005.

[48] Md. M. Hossain, T. Suzuki, and T. Kato. Effect of an amino acid on the surface phase behavior of n-hexadecyl phosphate in Gibbs adsorption layers. *Colloids and Surfaces A: Physicochemical and Engineering Aspects*, 284 285:119–124, 2006.

[49] Md. M. Hossain, T. Suzuki, and T. Kato. Unusual transition in a two-dimensional condensed phase to a mosaic texture. *Langmuir*, 16:9109–9112, 2000.

[50] J. Chanda, S. Chakraborty, and S. Bandyopadhyay. Monolayer of Aerosol-OT surfactants adsorbed at the air/water interface: An atomistic computer simulation study. *Journal of Physical Chemistry B*, 109:471 – 479, 2005.

[51] M. Tarek, D. J. Tobias, and M. L. Klein. Molecular dynamics simulation of tetradecyltrimethy-

lammonium bromide monolayers at the air/water interface. *Journal of Physical Chemistry*, 99:1393–1402, 1995.

[52] H. Kuhn and H. Rehage. Molecular orientation of monododecyl pentaethylene glycol at water/air and water/oil interfaces. A molecular dynamics computer simulation study. *Colloid and Polymer Science*, 278:114–118, 2000.

[53] H. Kuhn and H. Rehage. Molecular orientation of monododecyl pentaethylene glycol ($C_{12}E_5$) surfactants at infinite dilution at the air/water interface. a molecular dynamics computer simulation study. *Physical Chemistry Chemical Physics*, 2:1023–1028, 2000.

[54] H. Kuhn and H. Rehage. Molecular dynamics computer simulations of surfactant monolayers: Monododecyl pentaethylene glycol at the surface between air and water. *Journal of Physical Chemistry B*, 103:8493–8501, 1999.

[55] S. Bandyopadhyay and J. Chanda. Monolayer of monododecyl diethylene glycol surfactants adsorbed at the air/water interface: A molecular dynamics study. *Langmuir*, 19:10443–10448, 2003.

[56] B. A. Noskov. Kinetics of adsorption from micellar solutions. *Advances in Colloid and Interface Science*, 95:237 – 293, 2002.

[57] R. Miller. Adsorption kinetics of surfactants from micellar solutions. *Colloid and Polymer Science*, 259:1124 – 1128, 1981.

[58] J. V. Mitrancheva, C. D. Dushkin, and P. Joos. Kinetics of the surface tension of micellar solutions: Comparison of different experimental techniques. *Colloid and Polymer Science*, 274:356 – 367, 1996.

[59] C. D. Dushkin, I. B. Ivanov, and P. A. Kralchevsky. The kinetics of the surface tension of micellar surfactant solutions. *Colloids and Surfaces*, 60:235 – 261, 1991.

[60] L. K. Filippov and N. L. Filippova. Dynamic surface tension and adsorption kinetics from micellar solutions on planar surfaces. *Journal of Colloid and Interface Science*, 187:304 – 312, 1997.

[61] F. Jin, R. Balasubramaniam, and K. J. Stebe. Surfactant adsorption to spherical particles: The intrinsic length scale governing the shift from diffusion to kinetic controlled mass transfer. *Journal of Adhesion*, 90:773 – 796, 2004.

[62] S-Y. Lin, Y-C. Lee, M-W Yang, and H-S Liu. Surface equation of state of nonionic $C_m E_n$ surfactants. *Langmuir*, 19:3164 – 3171, 2003.

[63] Y. J. Nikas, S. Puvvada, and D. Blankschtein. Surface tensions of aqueous nonionic surfactant mixtures. *Langmuir*, 8:2680–2689, 1992.

[64] C. Dong, C-T. Hsu, C-Y. Chiu, and S-Y. Lin. A study on surfactant adsorption kinetics: Effect of bulk concentration on the limiting adsorption rate constant. *Langmuir*, 16:4573–4580, 2000.

[65] R. Sedev. Limiting area per molecule of nonionic surfactants at the water/air interface. *Langmuir*, 17:562 – 564, 2001.

[66] Nitin Kumar and Robert D. Tilton. Unified model to predict self-assembly of nonionic surfactants in solution and adsorption on solid or fluid hydrophobic surfaces: Effect of molecular structure. *Langmuir*, 20:4452–4464, 2004.

[67] Nitin Kumar, Stephen Garoff, and Robert D. Tilton. Experimental observations on the scaling of adsorption isotherms for nonionic surfactants at a hydrophobic solid-water interface. *Langmuir*, 20:4446 – 4451, 2004.

[68] Y-C. Lee, K. J. Stebe, H-S. Liu, and S-Y. Lin. Adsorption and desorption kinetics of $C_m E_8$ on impulsively expanded or compressed air-water interfaces. *Colloids and Surfaces A: Physicochemical and Engineering Aspects*, 220:139–150, 2003.

[69] M. Mulqueen, S. S. Datwani, K. J. Stebe, and D. Blankschtein. Dynamic surface tension of aqueous surfactant mixtures: Experimental investigation. *Langmuir*, 17:5801–5812, 2001.

[70] N. Kamenka, M. Puyal, B. Brun, G. Haouche, and B. Lindman. Tracer self-diffusion studies of surfactant association. In K. L. Mittal and B. Lindman, editors, *Surfactants in Solution*, volume 1, pages 359–372. Plenum Press, New York, 1984.

[71] C. R. Wilke and P. Chang. Correlation of diffusion coefficients in dilute solutions. *AIChE Journal*, 1:264–270, 1955.

[72] R. C. Reid, J. M. Prausnitz, and T. K. Sherwood. *The properties of gases and liquids*. McGraw-Hill Book Company, 3 edition, 1977.

[73] W. S. Schonhoff and O. Soderman. Self-diffusion coefficients of some hydrocarbons in water: Measurements and scaling relations. *J. Phys. Chem. A*, 104:5892 – 5894, 2000.

[74] S-Y. Lin, K. McKeigue, and C. Maldarelli. Diffusion-controlled surfactant adsorption studied by pendant drop digitization. *AIChE Journal*, 36:1785 – 1795, 1990.

Chapter 4

'Super Diffusive' Adsorption Kinetics Behavior in Pendant-Bubble Experimental Dynamic Surface Tension Data

4.1 Introduction

An important experimental method to study the adsorption kinetics behavior of surfactants involves conducting Dynamic Surface Tension (DST) measurements of surfactant solutions using the pendant-bubble apparatus [1]. In a typical pendant-bubble experiment, an air bubble is created at the tip of an inverted needle that is immersed in a quartz cell filled with the surfactant solution. As surfactant molecules adsorb from the bulk solution onto the freshly formed bubble surface, the surface tension of the bubble decreases as a function of time. Digital images of the bubble profile are taken at regular time intervals, and the instantaneous surface tension is calculated by numerically matching the solution of the Young-Laplace equation to the measured bubble profile. A detailed description of the manner in which DST measurements are conducted using the pendant-bubble apparatus can be found in Ref.[2].

Experimental pendant-bubble DST data has been used to investigate the adsorption kinetics

behavior of several alkyl poly(ethylene) oxide, C_iE_j, nonionic surfactants in the context of both the diffusion-controlled model and the mixed-controlled model[3–8]. In addition to determining the rate-limiting adsorption kinetics mechanism (diffusion-controlled vs. mixed-controlled), experimental DST data has been used to determine the values of the kinetics parameters, D, the diffusion-coefficient of the surfactant molecule, and β, the energy barrier parameter. Specifically, the existing procedure to analyze the experimental pendant-bubble DST data involves the following three steps [3–13]:

Step 1: Choosing a model for the Equilibrium Surface Tension vs. bulk solution Concentration (*referred to hereafter as ESTC*) behavior.

Step 2: Assuming a diffusion-controlled adsorption mechanism, and using the experimental DST data measured at a single initial surfactant bulk solution concentration, C_b, to regress for the value of D. This step is then repeated for experimental DST data measured at different C_b values. If the regressed value of D is found to decrease as C_b increases, then this trend is interpreted as indicating the existence of a mixed-controlled adsorption mechanism.

Step 3: If there are indications of the existence of mixed-controlled adsorption, the regressed value of D obtained by analyzing the experimental DST data measured at lower C_b values is considered as the actual diffusion coefficient of the surfactant molecules, and the entire experimental DST data measured at the higher C_b values is used to regress for the value of β.

In Refs.[14, 15], it was pointed out that the accuracy of the chosen ESTC model significantly affects the deduced adsorption kinetics rate-limiting mechanism, including the regressed values of the kinetics parameters, D and β. In view of the observed high sensitivity of the regressed values of the kinetics parameters to the accuracy of the chosen ESTC model, Lin et al. [9] and Pan et al. [6] proposed conducting surface-expansion measurements, in addition to conducting equilibrium surface tension measurements, to further validate the ESTC model chosen to analyze the experimental DST data. These authors concluded that surface-expansion measurements can be extremely useful in testing various ESTC models, and hence, in obtaining more reliable estimates of the kinetics parameters, D and β.

It is noteworthy that one of the key assumptions made in the existing procedure to analyze experimental pendant-bubble DST data is that the transport of surfactant molecules in the bulk so-

lution occurs purely by diffusion. In this chapter, I present an analysis of the experimental pendant-bubble DST data of $C_{12}E_4$ and $C_{12}E_6$, originally published in Refs.[3] and [5], respectively, which indicates an apparent 'super-diffusion' kinetics adsorption behavior of these two nonionic surfactants. Specifically, the analysis presented here involves the following steps:

1. Identifying an ESTC model that fits *both* the equilibrium surface tension measurements and the surface-expansion measurements.

2. Choosing a D value that best estimates the diffusion coefficient of the surfactant molecule based on the D values measured for structurally similar solutes.

3. Predicting the DST behavior at several C_b values corresponding to the diffusion-controlled adsorption model using the ESTC model identified in Step 1 and the D value chosen in Step 2. Note that I have chosen the diffusion-controlled adsorption model since it leads to the fastest decrease of the DST with time when surfactant molecules adsorb from a quiescent fluid onto a stagnant surface[1].

4. Comparing the predicted DST profiles with the corresponding experimental pendant-bubble DST data measured at these C_b values.

A comparison of the DST profiles predicted following steps 1-4 above with the experimental pendant-bubble DST data reveals *systematic deviations*, where the experimental DST values decrease faster with time than the predicted DST values over the time range, $t > \approx 100$ - 200 s, for both $C_{12}E_4$ and $C_{12}E_6$ at all the C_b values considered. With this apparent 'super diffusion' kinetics adsorption behavior in mind, I investigate possible causes for the observed systematic deviations, including analyzing possible inaccuracies in the model input specifications, and the breakdown of key assumptions underlying the diffusion-controlled model. The analysis presented here reveals that a breakdown of the assumption of diffusive transport of the surfactant molecules in the bulk solution may explain the observed systematic deviations. Specifically, I hypothesize the onset of natural convection in the bulk solution, resulting from the evaporative cooling of water at the pendant bubble surface, and demonstrate that this hypothesis can be used to rationalize the observed systematic deviations.

The remainder of the chapter is organized as follows. In Section 4,2, I: (i) review the diffusion-controlled model, including emphasizing the key underlying modeling assumptions, (ii) predict

147

DST profiles corresponding to the diffusion-controlled model for $C_{12}E_4$ and $C_{12}E_6$ at several C_b values, and (iii) compare the predicted DST profiles with the experimental pendant-bubble DST data of these two nonionic surfactants published in Refs.[3] and [5]. In Section 4.3, I investigate possible causes for the observed *systematic deviations* between the DST profiles predicted in Section 4.2 and the experimentally observed DST behavior, hypothesize the onset of natural convection in the bulk solution, and show that this hypothesis can be used to rationalize the observed systematic deviations. In Section 4.4, I summarize the main results of this chapter. Finally, in Appendix 4.A, I estimate the time for the onset of natural convection when a spherical air bubble is introduced into an aqueous solution.

4.2 Predictions of the Diffusion-Controlled Model

In this section, I: (i) review the diffusion-controlled model (Section 4.2.1), (ii) identify an input ESTC model for $C_{12}E_4$ and an input ESTC model for $C_{12}E_6$ that fit their respective equilibrium surface tension measurements and surface-expansion measurements (Section 4.2.2), (iii) choose input D values for $C_{12}E_4$ and $C_{12}E_6$ that best estimate the respective diffusion-coefficient values (Section 4.2.3), (iv) choose an input value for the radius of the pendant-bubble, r_0, and (v) predict the DST behavior corresponding to the diffusion-controlled model for the chosen value of r_0 using the ESTC models identified and the chosen D values for $C_{12}E_4$ and $C_{12}E_6$ at several C_b values (Section 4.2.4).

4.2.1 Diffusion-Controlled Adsorption Onto the Pendant-Bubble Surface

Recall that, traditionally, the surfactant adsorption process is viewed as consisting of the following three steps (see Section 1.2.1):

Step 1: Transport of the surfactant molecules from the bulk solution to the sub-surface.

Step 2: Adsorption of the surfactant molecules from the sub-surface onto the surface.

Step 3: Possible reorganization of the surfactant molecules at the surface.

Macroscopically, the kinetics associated with the surfactant adsorption process results in a time-dependent surface tension behavior, which is referred to as the Dynamic Surface Tension (DST).

148

Accordingly, the experimentally observed DST behavior represents the net effect of the three steps listed above.

In the context of the above mechanistic understanding of the surfactant adsorption process, the classical diffusion-controlled model involves the following *key assumptions*[1]:

Assumption 1: Transport of the surfactant molecules in the bulk solution is governed by Fickian diffusion.

Assumption 2: Adsorption of surfactant molecules from the sub-surface onto the surface is instantaneous. In other words, the sub-surface and the surface reach equilibrium instantaneously.

Assumption 3: The adsorbed surfactant molecules either do not undergo any reorganization at the surface or the reorganization is instantaneous.

In addition to these three key modeling assumptions, the following fourth assumption is typically made in the analysis of the pendant-bubble DST data [2]:

Assumption 4: Adsorption of the surfactant molecules onto the pendant-bubble surface can be modeled as adsorption onto a spherical surface.

A detailed analysis of the diffusion-controlled model describing the dynamics of surfactant adsorption onto a spherical surface can be found in Ref.[16]. Below, I summarize the key governing equations and the associated boundary and initial conditions:

- The surfactant diffusive transport along the radial direction, r, towards the spherical surface is given by:

$$\frac{\partial C}{\partial t} = \frac{D}{r^2}\frac{\partial}{\partial r}\left(r^2\frac{\partial C}{\partial r}\right), \qquad r \geq r_0,\ t \geq 0 \tag{4.1}$$

where C is the surfactant concentration, and r_0 is the radius of the pendant bubble.

- The rate of surfactant adsorption at the surface is equal to the net flux of surfactant molecules leaving the sub-surface towards the surface, that is,

$$\frac{d\Gamma}{dt} = D\left.\frac{\partial C}{\partial r}\right|_{r=r_0} \tag{4.2}$$

where Γ is the surfactant surface concentration.

- With the far field ($r \to \infty$) surfactant concentration being uniform at a value C_b, the boundary condition for Eq.(4.1) is given by

$$C(t, r \to \infty) = C_b, \qquad t \geq 0 \tag{4.3}$$

- For a surfactant surface concentration, Γ_0, and a homogeneous bulk solution at the beginning of the adsorption process, the initial conditions associated with the governing equations (Eqs.(4.1) and (4.2)) can be expressed as follows:

$$\Gamma(t = 0) = \Gamma_0 \qquad \text{and} \qquad C(t = 0, r) = C_b, \qquad r \geq r_0 \tag{4.4}$$

Equations (4.1) - (4.4) can be solved using the method of Laplace Transforms to yield [16]:

$$\Gamma(t) = \Gamma_0 + \frac{D}{r_0}\left[C_b t - \int_0^t C_s(t)dt\right] + 2\sqrt{\frac{D}{\pi}}\left[C_b\sqrt{t} - \int_0^{\sqrt{t}} C_s(t-\eta)d\sqrt{\eta}\right] \tag{4.5}$$

where $C_s(t)$ is the instantaneous surfactant sub-surface concentration ($C(t, r = r_0)$) and is related to the instantaneous surfactant surface concentration, $\Gamma(t)$, through the Equilibrium Adsorption Isotherm (EAI):

$$\Gamma_e = g(C_b^e) \tag{4.6}$$

where Γ_e is the equilibrium surfactant surface concentration and C_b^e is the equilibrium surfactant bulk solution concentration. Specifically, since the diffusion-controlled model assumes that the sub-surface and the surface reach equilibrium instantaneously (see Assumption 2 above), $C_s(t)$ is related to $\Gamma(t)$ through the EAI in Eq.(4.6), that is,

$$\Gamma(t) = g(C_s(t)) \tag{4.7}$$

Solution of the diffusion-controlled model involves solving Eqs.(4.5) and (4.7) simultaneously to predict $\Gamma(t)$. Once $\Gamma(t)$ is known, the following equilibrium Equation Of State (EOS) is used to predict the DST, $\gamma(t)$:

$$\gamma_{w/a} - \gamma_e = f(\Gamma_e) \tag{4.8}$$

150

where $\gamma_{w/a}$ is the pure water/air surface tension, γ_e is the equilibrium surface tension, and the function $f(\Gamma_e)$ is the EOS. Specifically, since the diffusion-controlled model assumes that any reorientation of the adsorbed surfactant molecules at the surface occurs instantaneously (see Assumption 3 above), $\Gamma(t)$ is also related to $\gamma(t)$ through the equilibrium EOS in Eq.(4.8), that is,

$$\gamma_{w/a} - \gamma(t) = f(\Gamma(t)) \tag{4.9}$$

Note that the EAI, Eq.(4.6), is related to the equilibrium EOS, Eq.(4.8), through the Gibbs adsorption equation [17]:

$$\Gamma_e = -\frac{1}{RT}\frac{d\gamma_e}{d\ln C_b^e} \tag{4.10}$$

Typically, the equilibrium adsorption behavior of the surfactant is obtained by relating the Equilibrium Surface Tension, γ_e, to the equilibrium surfactant bulk solution Concentration, C_b^e (ESTC). One then uses the obtained ESTC relation in conjunction with the Gibbs adsorption equation, Eq.(4.10), to determine the EOS of the surfactant. The EAI, Eq.(4.6), is then determined by eliminating γ_e between the specified ESTC behavior and the EOS determined through the application of Eq.(4.10).

Accordingly, the diffusion-controlled model implemented to model the kinetics of surfactant adsorption onto a pendant-bubble surface involves the following *three specifications*:

1. The surfactant ESTC model.
2. The diffusion coefficient of the surfactant molecule, D.
3. The radius of the spherical bubble, r_0.

With the three specifications listed above, the diffusion-controlled model can predict the DST behavior at a given initial surfactant bulk solution concentration, C_b, and at an initial surfactant surface concentration, Γ_0.

4.2.2 Input Equilibrium Surface Tension vs. Bulk Solution Concentration (ESTC) Model

Recall that in the diffusion-controlled adsorption model, the input ESTC model serves two purposes: (a) it relates the instantaneous surfactant sub-surface concentration, $C_s(t)$, to the instantaneous

surfactant surface concentration, $\Gamma(t)$, through the equilibrium adsorption isotherm (Eq.(4.6)), and (b) it relates the instantaneous surfactant surface concentration, $\Gamma(t)$, to the instantaneous surface tension, $\gamma(t)$, through the corresponding equation of state (Eq.(4.8)). The existing methods to test the accuracy of the input ESTC model involve [18]: (a) comparing the ESTC model predictions with the equilibrium surface tension measurements, and (b) comparing the predictions of the EOS corresponding to the ESTC model to surface expansion measurements. Note that the equilibrium surface tension measurements relate γ_e to C_b^e, and the surface expansion measurements relate γ_e to the normalized equilibrium surfactant surface concentration, Γ_e/Γ_{ref}, where Γ_{ref} is a reference value of the surfactant surface concentration. Note that, typically, the *equilibrium surface tension measurements are used to fit* the ESTC model, and the *surface-expansion measurements are used to test* the fitted ESTC model. In Ref.[14, 15, 18], it was demonstrated that: (i) using only the equilibrium surface tension measurements to fit the ESTC model can lead to significantly different predictions of the equation of state, and (ii) the surface-expansion measurements can be extremely useful to validate the accuracy of the fitted ESTC model.

Keeping all of the above in mind, I use *both the equilibrium surface tension measurements and the surface-expansion measurements in order to identify the ESTC models* for $C_{12}E_4$ and $C_{12}E_6$. The steps followed to identify the ESTC models for $C_{12}E_4$ and $C_{12}E_6$ involve:

1. Use the surface-expansion measurements to fit a polynomial relating Γ_e/Γ_{ref} to γ_e:

$$\Gamma_e/\Gamma_{ref} = p(\gamma_e) \qquad (4.11)$$

such that the resulting polynomial passes through the point ($\Gamma = 0, \gamma_e = \gamma_{w/a} = 72.0$ mN/m), corresponding to $T = 298$ K[3, 5].

2. Use the Gibbs adsorption equation (Eq.(4.10)) to determine the corresponding ESTC model. Specifically, applying the Gibbs Adsorption equation to the polynomial EOS in Eq.(4.11) yields:

$$p(\gamma_e)\Gamma_{ref} = -\frac{1}{RT}\frac{d\gamma_e}{d\ln C_b^e} \qquad (4.12)$$

152

Rearranging Eq.(4.12) then yields:

$$d \ln C_b^e = -\frac{1}{RT\Gamma_{\text{ref}}} \left[\frac{d\gamma_e}{p(\gamma_e)} \right] \tag{4.13}$$

Integrating Eq.(4.13) between the limits: (C_b^r, γ_r) and (C_b^e, γ_e) yields:

$$\ln C_b^e = \ln C_b^r - \frac{1}{RT\Gamma_{\text{ref}}} \int_{\gamma_r}^{\gamma_e} \frac{d\gamma_e}{p(\gamma_e)} \tag{4.14}$$

where γ_r is an arbitrary reference (r) value for γ_e, and C_b^r is the surfactant bulk solution concentration corresponding to $\gamma_e = \gamma_r$. Note that: (i) the ESTC behavior in Eq.(4.14) needs to approach the Henry's Law region as $C_b^e \to 0$, and (ii) γ_r cannot be chosen to be equal to $\gamma_{w/a}$ since in that case, $C_b^r = 0$ (corresponding to the pure water solution), and the value of $\ln C_b^r$ diverges. Note that choosing $\gamma_r <\approx \gamma_{w/a}$ eliminates the divergence problem in item (ii) above, and enables the application of the Henry's equation between C_b^e and γ_e when $C_b^e \leq C_b^r$ [17]:

$$C_b^e = \left(\frac{\gamma_{w/a} - \gamma_e}{\gamma_{w/a} - \gamma_r} \right) C_b^r, \quad \text{for} \quad C_b^e \leq C_b^r \tag{4.15}$$

In the analysis presented in this chapter, a γ_r value[1] of 71.5 mN/m is used for both $C_{12}E_4$ and $C_{12}E_6$.

Note that equation (4.14) contains two unknown parameters, Γ_{ref} and C_b^r. The values of these parameters are fit using the known polynomial $p(\gamma_e)$ and the experimental equilibrium surface tension data.

With the specifications of $p(\gamma_e)$, Γ_{ref}, and C_b^r, Eq.(4.14) corresponds to the surfactant ESTC model, and with the specifications of $p(\gamma_e)$ and Γ_{ref}, Eq.(4.11) corresponds to the surfactant EOS.

I implemented the approach described above to identify ESTC and EOS models for $C_{12}E_4$ and $C_{12}E_6$ using the equilibrium surface tension measurements and surface-expansion measurements reported in Refs.[3] and [5], respectively. Figure 4-1(a) shows the polynomial EOS fit obtained with Eq.(4.11) using the surface-expansion measurements for $C_{12}E_4$, and Figure 4-1(b) shows the ESTC fit obtained with Eq.(4.14) using the equilibrium surface tension measurements for $C_{12}E_4$.

---

[1] I have carried out the analysis presented in this chapter for several values of γ_r between 71.9 to 71.0 and observed that the resulting equilibrium relation between C_b^e and γ_e is independent of the specific γ_r value chosen.
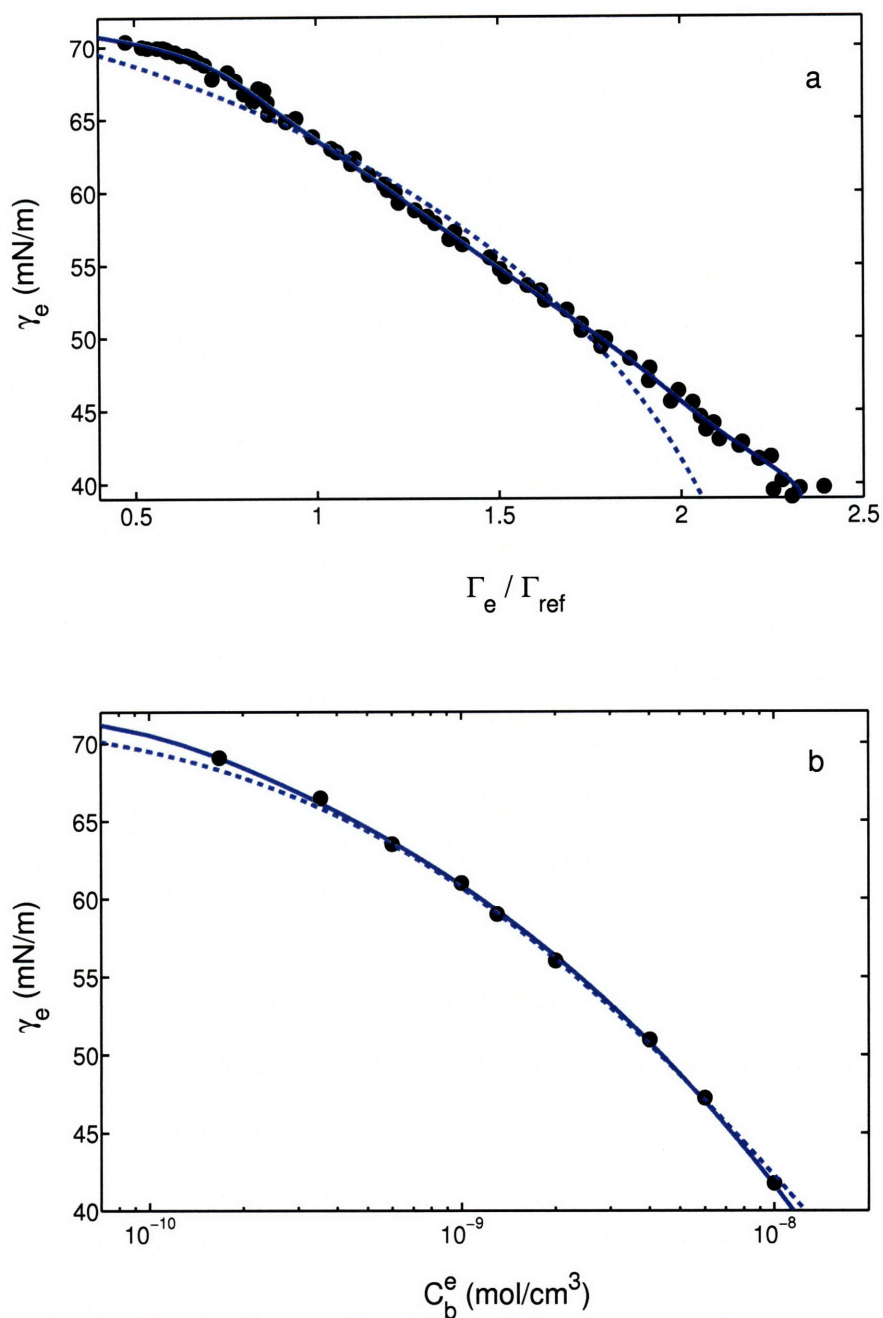
Figure 4-1: Comparison of: (a) the polynomial EOS fit obtained with Eq.(4.11) using the surface-expansion measurements for $C_{12}E_4$, and (b) the ESTC fit obtained with Eq.(4.14) using the equilibrium surface tension measurements for $C_{12}E_4$. In these figures, the solid lines correspond to the fits obtained following the approach described in Section 4.2.2, the dashed lines correspond to the predictions of the best-fit Frumkin ESTC model reported in Ref.[3], the filled circles in (a) correspond to the experimental surface-expansion measurements, and the filled circles in (b) correspond to the experimental equilibrium surface tension measurements.

154

Similarly, Figures 4-2(a) and 4-2(b) show the fitted EOS and ESTC for $C_{12}E_6$. For comparison, in Figures 4-1 and 4-2, I also show the predictions corresponding to the Frumkin ESTC model that was originally designed to fit only the equilibrium surface tension measurements [3, 5]. In Figures 4-1 and 4-2, the filled circles represent experimental data points, the solid lines correspond to the best-fit obtained using the procedure described above, and the dashed lines correspond to the predictions of the best-fit Frumkin ESTC model. Figures 4-1 and 4-2 show that the agreement between the ESTC and the EOS model fits using the procedure described above and the experimental data is better than the agreement with the fit corresponding to the Frumkin adsorption isotherm model.

4.2.3 Input Diffusion Coefficient Value, D

The D values corresponding to $C_{12}E_4$ and $C_{12}E_6$ have not been measured experimentally, and therefore, a direct validation of the D values is not possible. Nevertheless, one can estimate the D values using correlations as well as using the D values measured experimentally for structurally similar solutes. Specifically, recall that applying the Wilke-Chang correlation [19] to $C_{12}E_4$ and $C_{12}E_6$ estimated their respective D values to be 3.77 x 10^{-6} cm^2/s and 3.37 x 10^{-6} cm^2/s (see Table 3.2 in Chapter 3). In addition, recall that, in Chapter 3, the new methodology developed to determine the rate-limiting adsorption kinetics mechanism [20] was used to analyze the DST data of $C_{12}E_4$ and $C_{12}E_6$, and the D values of these surfactants were determined to be 3.9 ± 0.6 x 10^{-6} cm^2/s and 3.8 ± 0.6 x 10^{-6} cm^2/s, respectively (see Table 3.2). Moreover, Schonhoff and Sodermann have measured the diffusion coefficient of the structurally similar nonionic surfactant $C_{12}E_5$ using NMR, and obtained a value of $D = 3.9$ x 10^{-6} cm^2/s [21], which is in close agreement with the estimates of the Wilke-Chang correlation and with the values obtained using the new methodology [20].

Keeping the above findings in mind, the D values of the two nonionic surfactants considered were assumed to span the range: $D = 3.9 \pm 0.6$ x 10^{-6} cm^2/s for $C_{12}E_4$, and $D = 3.8 \pm 0.6$ x 10^{-6} cm^2/s for $C_{12}E_6$. Accordingly, diffusion-controlled model predictions were made separately for the nominal, upper, and lower bound D values of $C_{12}E_4$ and $C_{12}E_6$.
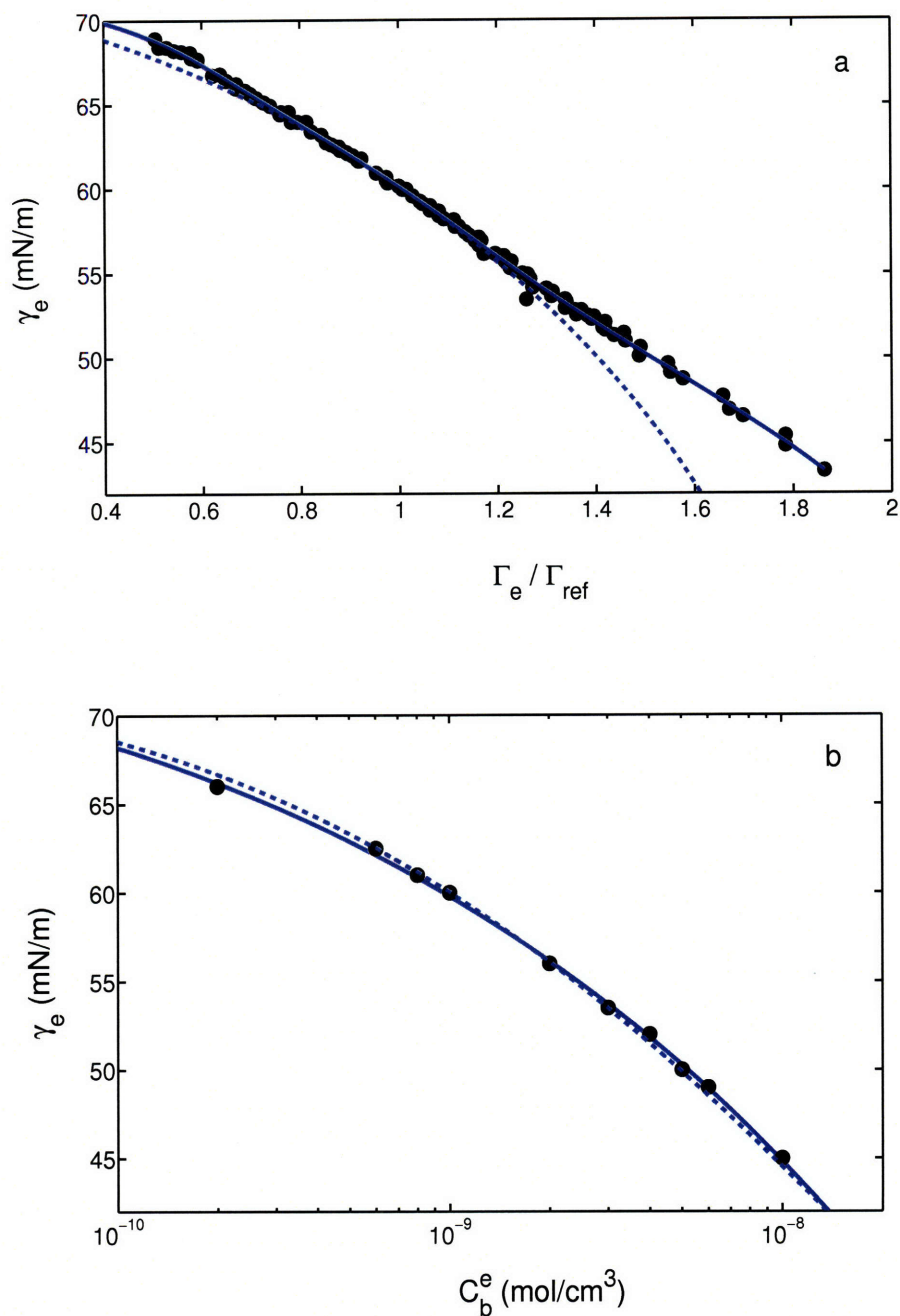
Figure 4-2: Comparison of: (a) the polynomial EOS fit obtained with Eq.(4.11) using the surface-expansion measurements for $C_{12}E_6$, and (b) the ESTC fit obtained with Eq.(4.14) using the equilibrium surface tension measurements for $C_{12}E_6$. In these figures, the solid lines correspond to the fits obtained following the approach described in Section 4.2.2, the dashed lines correspond to the predictions of the best-fit Frumkin ESTC model reported in Ref.[5], the filled circles in (a) correspond to the experimental surface-expansion measurements, and the filled circles in (b) correspond to the experimental equilibrium surface tension measurements.

4.2.4 Input Radius of the Spherical Bubble, r_0

The radius, r_0, of the spherical bubble corresponding to the pendant-bubble surface was taken as the radius of curvature of the pendant-bubble measured at its apex [2]. In the pendant-bubble experiments conducted for $C_{12}E_4$ [3], the initial value of r_0 was varied between 0.10 cm to 0.15 cm as C_b changed from 2 x 10^{-8} mol/cm^3 to 0.4 x 10^{-8} mol/cm^3. Similarly, in the pendant-bubble experiments conducted for $C_{12}E_6$[5], the initial value of r_0 varied between 0.10 cm to 0.15 cm as C_b changed from 2 x 10^{-8} mol/cm^3 to 0.2 x 10^{-8} mol/cm^3. Note that the DST measurements at the higher C_b values were conducted at lower initial r_0 values to ensure that the bubbles remained stable as the DST values decreased[22]. A constant value of r_0 = 0.10 cm, corresponding to the lower limit of the experimental r_0 value, was used in the analysis reported here. Note that the rate of surfactant adsorption increases as the value of r_0 decreases [16] (see Eq.(4.5)). Therefore, choosing the lower limit value of r_0 = 0.10 cm corresponds to a case of faster adsorption.

4.2.5 Predictions of Dynamic Surface Tension

For the two nonionic surfactants considered, $C_{12}E_4$ and $C_{12}E_6$, DST profiles were predicted at several C_b values using the ESTC models which were shown to fit both the equilibrium surface tension measurements as well as the surface-expansion measurements, for the range of D values discussed in Section 4.2.3 and for a r_0 value of 0.10 cm.

Specifically, Figure 4-3(a-d) shows the predicted DST profiles for $C_{12}E_4$ at: (a) 0.4 x 10^{-8} mol/cm^3, (b) 0.6 x 10^{-8} mol/cm^3, (c) 1.0 x 10^{-8} mol/cm^3, and (d) 2.0 x 10^{-8} mol/cm^3. Similarly, Figure 4-4(a-d) shows the predicted DST profiles for $C_{12}E_6$ at: (a) 0.2 x 10^{-8} mol/cm^3, (b) 0.6 x 10^{-8} mol/cm^3, (c) 1.3 x 10^{-8} mol/cm^3, and (d) 2.0 x 10^{-8} mol/cm^3. The experimental DST data measured using the pendant-bubble apparatus for $C_{12}E_4$ and $C_{12}E_6$ [3, 5] at the corresponding C_b values are also shown in Figures 4-3(a-d) and 4-4(a-d). In Figures 4-3(a-d) and 4-4(a-d), the solid lines correspond to the predicted DST profiles at the nominal values of D, the dashed lines correspond to the predicted DST profiles at the lower bound values of D, the dotted lines correspond to the predicted DST profiles at the upper bound values of D, and the filled circles correspond to the experimental DST data reported in Refs.[3] and [5].

Note that in Figures 4-3(d) and 4-4(d), DST predictions are reported only for $\gamma > 40$ mN/m and
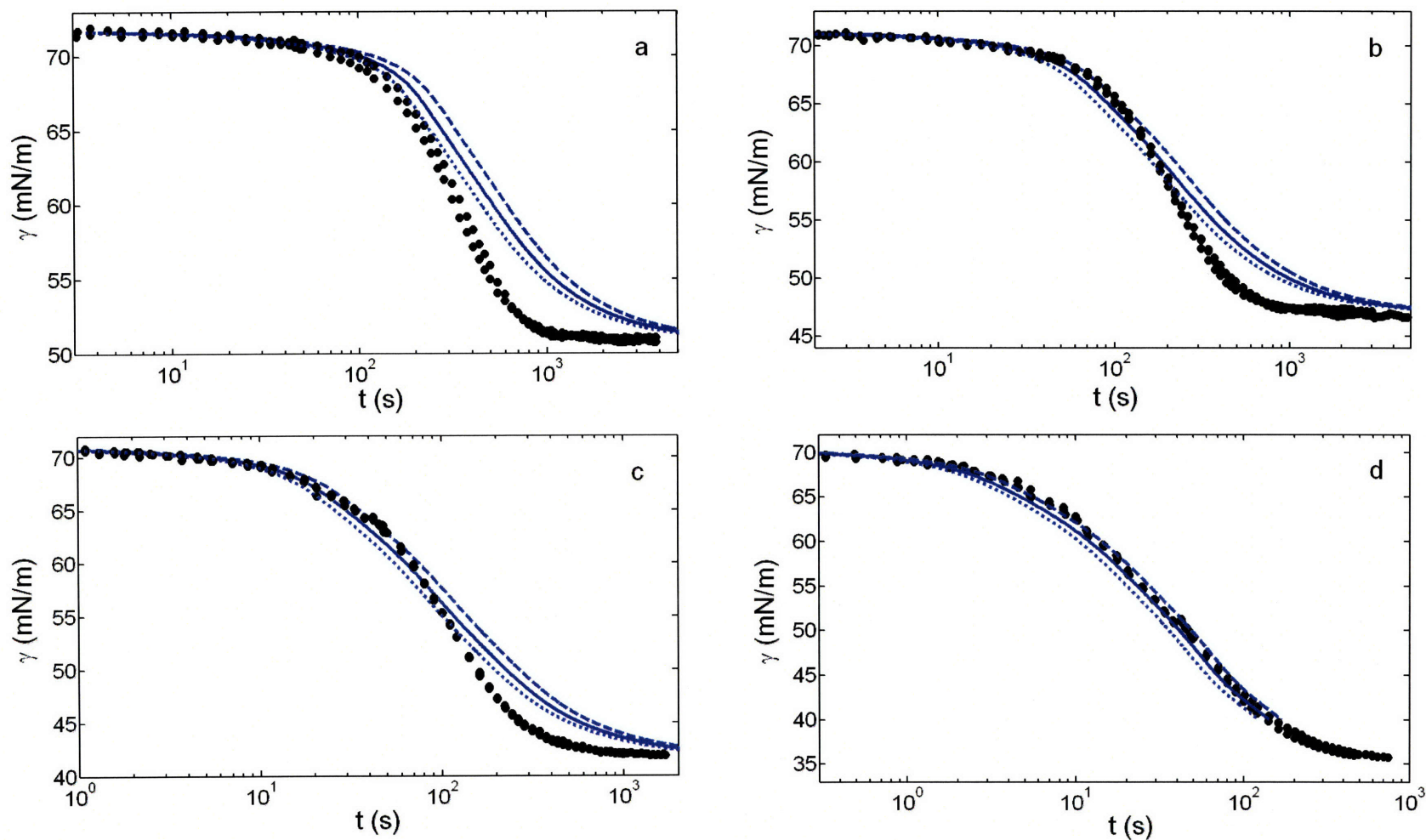
Figure 4-3: Comparison of the predicted dynamic surface tension, $\gamma(t)$, as a function of time, t, using the diffusion-controlled adsorption model with the experimentally observed DST behavior for $C_{12}E_4$ at: (a) 0.4 x 10^{-8} mol/cm^3, (b) 0.6 x 10^{-8} mol/cm^3, (c) 1.0 x 10^{-8} mol/cm^3, and (d) 2.0 x 10^{-8} mol/cm^3. In these figures, the solid, dashed, and dotted lines correspond to the nominal, lower, and upper bound values of D, respectively. The filled circles correspond to the experimental DST data reported in Ref.[3].
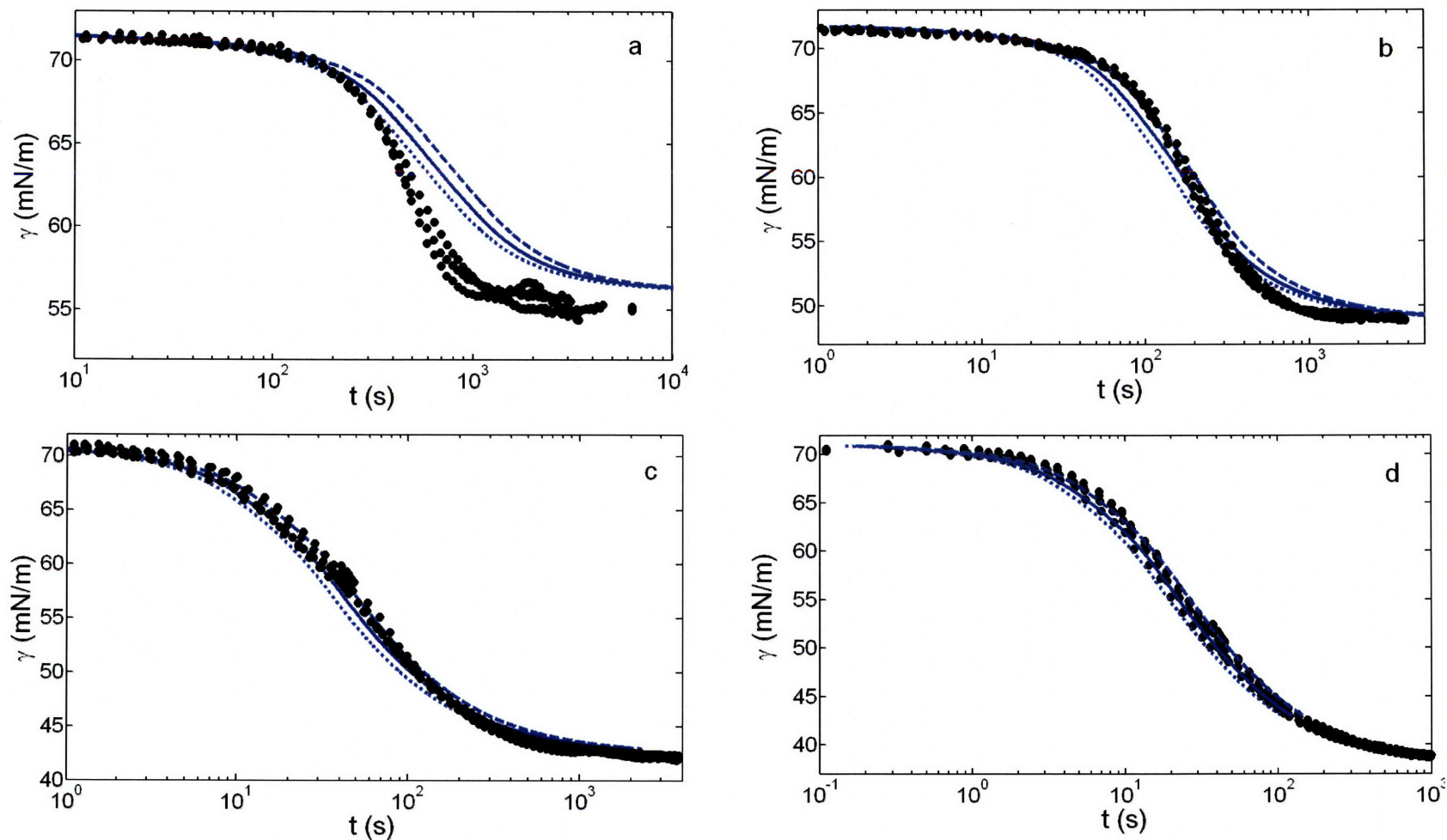
Figure 4-4: Comparison of the predicted dynamic surface tension, $\gamma(t)$, as a function of time, t, using the diffusion-controlled adsorption model with the experimentally observed DST behavior for $C_{12}E_6$ at: (a) 0.2 x 10^{-8} mol/cm^3, (b) 0.6 x 10^{-8} mol/cm^3, (c) 1.3 x 10^{-8} mol/cm^3, and (d) 2.0 x 10^{-8} mol/cm^3. In these figures, the solid, dashed, and dotted lines correspond to the nominal, lower, and upper bound values of D, respectively. The filled circles correspond to the experimental DST data reported in Ref.[5].

$\gamma > 43$ mN/m, respectively, since reliable EOS data was available only over this range of γ values (see Figures 4-1(a) and 4-2(a)). Note also that in Figures 4-3(a-d) and 4-4(a-d), the experimental DST data does not approach the expected pure water/air surface tension value of 72.0 mN/m at 298 K as $t \to 0$. This behavior is interpreted to indicate the presence of trace quantities of adsorbed surfactant molecules at the beginning of the adsorption process. Accordingly, in order to set the proper initial conditions for the predictions made that best represent the experimental initial conditions, the initial surfactant surface concentration values, Γ_0, were chosen such that the resulting predicted initial surface tensions agreed with the experimental DST data as $t \to 0$.

As can be seen from Figures 4-3(a-d) and 4-4(a-d), there are *systematic deviations* between the predicted DST profiles and the experimentally observed DST behavior for both $C_{12}E_4$ and $C_{12}E_6$, where the experimental DST appears to decrease faster with time relative to the predictions of the diffusion-controlled model. In Section 4.3 below, I analyze possible causes for the observed 'super-diffusion' adsorption kinetics behavior of $C_{12}E_4$ and $C_{12}E_6$.

4.3 Analysis of Possible Causes for the Observed Systematic Deviations

In this Section, I analyze possible causes for the systematic deviations observed between the predicted DST profiles and the experimental DST behavior for $C_{12}E_4$ and $C_{12}E_6$ reported in Figures 4-3(a-d) and 4-4(a-d). Based on these figures, the following four observations can be made:

Observation 1: While the predictions agree well with the experimentally measured DST behavior at the higher C_b values, systematic deviations occur at the lower C_b values. Figures 4-3(a-d) and 4-4(a-d) clearly show that, for both $C_{12}E_4$ and $C_{12}E_6$, the agreement between the predicted DST profiles and the experimental DST data becomes progressively better as C_b increases.

Observation 2: At low C_b values, while the predictions agree well with the experimental DST behavior at the initial times, they begin to deviate at the later times. Specifically, it appears that the deviations become significant beyond a time of $t \approx 100$ - 200 s for both $C_{12}E_4$ and $C_{12}E_6$.

160

Observation 3: For those deviations that occur beyond $t \approx 100$ - 200 s, the experimental DST data is consistently *lower* than the predicted DST profiles.

Observation 4: Although the experimental DST behavior and the predicted DST profiles deviate at low C_b values at later times, both the experimental DST behavior and the predicted DST profiles approach the same equilibrium surface tension values.

My analysis of the observed systematic deviations considers two types of causes: (i) inaccuracies in the model specifications (Section 4.3.1), and (ii) breakdown of key modeling assumptions (Section 4.3.2).

4.3.1 Inaccuracies in the Model Specifications

As discussed in Section 4.2.1, the diffusion-controlled model requires the following key specifications:

1. The surfactant ESTC model.
2. The diffusion coefficient of the surfactant molecule, D.
3. The radius of the spherical bubble, r_0.

Below, I consider the effect of possible errors in specifications 1-3 in the context of the observed systematic deviations.

The Surfactant Equilibrium Surface Tension vs. Bulk Solution Concentration (ESTC) Model

Recall that in Refs.[14, 15] it was demonstrated that the accuracy of the ESTC model used significantly affects the DST predictions of the diffusion-controlled model. The observed high sensitivity to the ESTC was attributed to using solely the equilibrium surface tension measurements (γ_e vs. C_b^e) to fit the ESTC model, and then *differentiating* the fitted ESTC model to estimate Γ_e using the Gibbs adsorption equation (Eq.(4.10)). It is for this reason that surface-expansion measurements were introduced to relate Γ_e directly to γ_e using one unknown reference value, Γ_{ref} (see Eq.(4.11)). On the other hand, in the approach proposed here to identify the ESTC models for $C_{12}E_4$ and $C_{12}E_6$, I first use the surface-expansion measurements to identify the surfactant EOS, and then *integrate* the Gibbs adsorption equation (Eq.(4.10)) to determine the ESTC model (see Section 4.2.2). Therefore, it is less likely that the input ESTC models used here contain significant inaccuracies.

In fact, if the input ESTC model was inaccurate, it would not have yielded good agreement between the predicted DST profiles and the experimental DST behavior at any of the C_b values considered. This, in turn, is at odds with Observation 1, since one does observe good agreement between the predicted DST profiles and the experimental DST behavior at all the high C_b values considered.

Moreover, since the ESTC model involves a relation between C_b^e and γ_e, any inaccuracy of the ESTC model would result in deviations that are characterized by a specific $\gamma(t)$ value which is independent of the initial C_b value. On the other hand, the observed systematic deviations appear to be controlled by the time elapsed rather then by a specific $\gamma(t)$ value (see Observation 2).

Keeping all of the above in mind, I conclude that it is unlikely that the systematic deviations observed for *both* $C_{12}E_4$ and $C_{12}E_6$ are caused by inaccuracies in the surfactant ESTC models identified.

The Diffusion Coefficient, D

Recall that the ranges of D values used to generate the DST predictions for $C_{12}E_4$ and $C_{12}E_6$ are consistent with independent measurements conducted for structurally similar surfactants like $C_{12}E_5$. Figures 4-3(a-c) and 4-4(a-b) indicate that the DST predictions corresponding to the upper and lower bound values of D do not explain the observed deviations occurring at large values of t (> 100 - 200 s). In addition, it is noteworthy that any inaccuracy in the D value tends to shift the *entire predicted DST profile* to the left (if the D value is higher) or to the right (if the D value is lower) *at all the C_b values*. This is because when the D value is higher, it corresponds to faster adsorption at all times and at all C_b values, and therefore, the entire predicted DST profile shifts to the left. Similarly, when the D value is lower, it corresponds to slower adsorption at all times and at all C_b values, and therefore, the entire predicted DST profile shifts to the right. This observation is at odds with Observations 1 and 2, which state that the deviations occur *only at low C_b values*, and are more pronounced for t > 100 - 200 s.

The Radius of the Pendant Bubble, r_0

As discussed in Section 4.2.1, Eq.(4.5) models surfactant adsorption onto a spherical pendant bubble surface, where the term containing the factor D/r_0 models the effect of curvature ($1/r_0$) on the rate of surfactant adsorption. Equation (4.5) indicates that as the curvature increases, or as r_0

162

decreases, the rate of surfactant adsorption increases [16].

Recall that in the pendant-bubble DST measurements for $C_{12}E_4$ and $C_{12}E_6$, the radius of the pendant-bubble, r_0, was varied between 0.10 cm to 0.15 cm for the range of C_b values considered (see Section 4.2.4). Therefore, the value of $r_0 = 0.10$ cm used here to predict the DST profiles reported in Figures 4-3(a-d) and 4-4(a-d) corresponds to the *lower estimate* of the r_0 value. As a result, the predicted DST profiles correspond to the limit of faster surfactant adsorption. However, Observation 3 indicates that the experimental DST decreases at a rate which is even faster than the rate at which the predicted DST profiles decrease. Consequently, I conclude that it is unlikely that the observed systematic deviations are caused by inaccuracies in the r_0 value.

Based on the arguments presented in Section 4.3.1, I conclude that it is unlikely that the observed systematic deviations are caused by inaccuracies in specifications 1-3 associated with the diffusion-controlled model.

4.3.2 Breakdown of Key Modeling Assumptions

In this section, I investigate if the observed systematic deviations can be explained by the breakdown of any of the key modeling assumptions made in the development of the diffusion-controlled model. For a discussion of the four key assumptions made in the development of the diffusion-controlled model, see Section 4.2.1.

First, I will discuss why any breakdown of Assumptions 2 and 4 cannot explain the observed systematic deviations. Subsequently, I will present arguments which indicate that *Assumption 3 is valid* for the two nonionic surfactants considered here. Finally, I will hypothesize the breakdown of Assumption 1, and demonstrate how this hypothesis may explain the observed systematic deviations.

Analysis of Assumption 2

This assumption specifies that the adsorption of the surfactant molecules from the sub-surface onto the surface is instantaneous. Breakdown of this assumption would imply that the surfactant molecules at the sub-surface require a finite time to adsorb onto the surface. This, in turn, would effectively reduce the rate of surfactant adsorption onto the surface, and result in a DST reduction which is *slower* than that predicted by the diffusion-controlled model. On the other hand,

Observation 3 indicates that the experimental DST decreases at a rate which is faster than that of the DST profiles predicted by the diffusion-controlled model. Therefore, I conclude that it is unlikely that the observed deviations are caused by the breakdown of Assumption 2 underlying the diffusion-controlled model.

Analysis of Assumption 4

This assumption specifies that the adsorption of the surfactant molecules onto the pendant-bubble surface can be modeled as adsorption onto a spherical surface. Practically, this assumption is clearly not valid in the case of the pendant-bubble experiment, since the very basis of measuring the DST involves monitoring changes in the bubble shape with time [16]. However, here I attempt to answer the question: can the breakdown of this assumption explain the observed systematic deviations? First, using a qualitative argument, I show that, in general, the rate of surfactant adsorption onto a *spherical* surface provides an *upper bound* to the rate of surfactant adsorption onto the actual pendant-bubble surface. Subsequently, I discuss if this upper bound estimate is consistent with the observed systematic deviations.
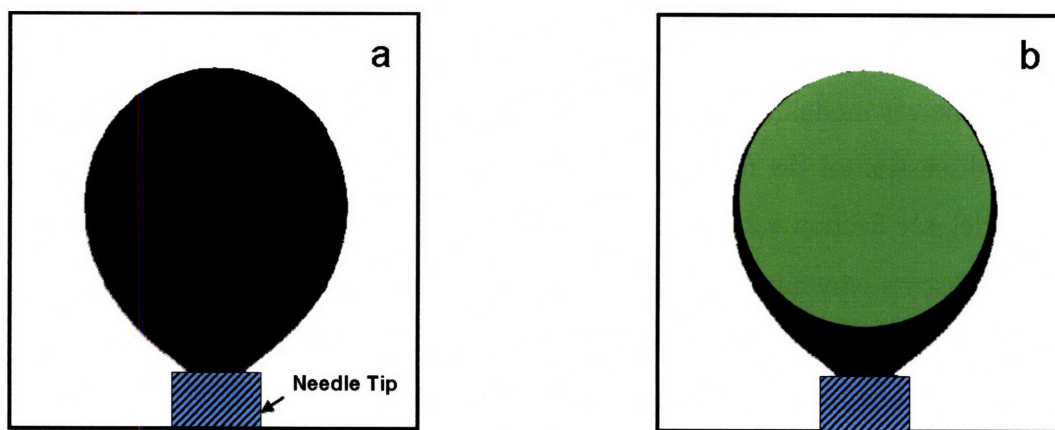
Figure 4-5: Effect of the spherical approximation of a pendant-bubble surface: (a) Actual snapshot of a pendant-bubble profile, and (b) spherical approximation of the pendant bubble in (a), where the sphere radius is equal to the radius of curvature of the pendant bubble at the apex. The spherical approximation corresponds to the green circle.

Note that the shape of the actual pendant bubble deviates from the energy-minimizing spherical shape due to the action of the buoyant force that elongates the bubble at the tip of the needle. Figure 4-5(a) shows a typical shape of a pendant bubble [22]. Recall that the radius of the sphere, r_0, associated with the pendant bubble is computed as the the radius of curvature of the pendant

bubble measured at the apex [2]. Figure 4-5(b) shows the spherical approximation of the actual pendant bubble in Figure 4-5(a) as the green circle. Figure 4-5(b) reveals that the radius of curvature of the pendant bubble at the apex represents a *lower bound* to the radius of curvature at other sites on the pendant-bubble surface. Clearly, by modeling the actual pendant-bubble surface as a spherical surface, one is assuming a constant value of the radius of curvature, r_0, at all sites on the pendant-bubble surface. Recall that the rate of surfactant adsorption increases as the radius of curvature decreases (see Eq.(4.5)). Consequently, by assuming a constant (lower bound) value of r_0 at all sites on the pendant-bubble surface, the predicted rate of surfactant adsorption provides a higher estimate of the rate of surfactant adsorption onto the pendant-bubble surface. Therefore, the predicted DST behavior corresponds to a faster reduction of the surface tension. On the other hand, Observation 3 indicates that the experimental DST decreases at a rate which is faster than that of the predicted DST profiles. Accordingly, I conclude that it is unlikely that the observed deviations are caused by the breakdown of Assumption 4 underlying the diffusion-controlled model.

Analysis of Assumption 3

This assumption specifies that the adsorbed surfactant molecules either do not undergo any reorganization at the surface or that the reorganization is instantaneous. This assumption is likely valid, since molecular dynamics simulations of several C_iE_j nonionic surfactants at an air/water surface are typically run for a duration of about 4 ns in order to study *equilibrium* surface properties. Specifically, in Refs.[23] and [24], molecular dynamics simulations were conducted to study the adsorption properties of $C_{12}E_5$ and $C_{12}E_6$, respectively. In these studies, the surfactants molecules were initially placed at the water/air surface (to simulate adsorbed surfactant molecules), and the simulation was run for about 4 ns. Based on the results gathered during this simulation time, equilibrium adsorption structural properties, including the angle of orientation of the surfactant hydrophobic chains with respect to the water/air surface, were computed. These simulation studies report good agreement between the predicted structural properties and the experimentally measured *equilibrium* structural properties. On the other hand, typical time scales associated with the adsorption kinetics of the $C_{12}E_4$ and $C_{12}E_6$ nonionic surfactants considered here vary from seconds to hours depending on their initial bulk solution concentration, C_b (see Figures 4-3(a-d) and Figures 4-4(a-d)). Therefore, Assumption 3 specifying instantaneous reorganization at the surface

is likely valid for the $C_{12}E_4$ and $C_{12}E_6$ nonionic surfactants considered. Therefore, I conclude that it is unlikely that the observed systematic deviations are caused by the breakdown of Assumption 2 underlying the diffusion-controlled model.

Analysis of Assumption 1

This assumption specifies that transport of the surfactant molecules in the bulk solution is governed by Fickian diffusion. Keeping the analysis of Assumptions 2, 3, and 4 presented above in mind, I hypothesize that the observed deviations are caused by the breakdown of Assumption 1. Specifically, I hypothesize the onset of natural convection in the system driven by evaporative cooling at the pendant-bubble surface, which in turn, invalidates Assumption 1. Note that evaporative cooling is a physical phenomenon in which evaporation of a liquid, typically into the surrounding air, cools the liquid surface [25]. In such cases, depending on the properties of the liquid, the resulting temperature gradients in the liquid can cause local density gradients that are sufficiently strong to induce natural convection (nc) in the fluid. In such cases, there is a characteristic time scale, τ_{nc}, after which the fluid ceases to be stagnant and after which natural convection sets in. The onset of natural convection due to evaporative cooling when stagnant water is exposed to still air was demonstrated experimentally by Spangenberg and Rowland in Ref.[26]. These authors observed the onset of natural convection after about 70 s when stagnant water at an initial temperature of 25.9° C was exposed to still air and the water surface temperature decreased to about 25.5° C.

Below, I first discuss how the natural convection hypothesis is consistent with the four observations discussed in Section 4.3, and then provide additional independent evidence to demonstrate the validity of this hypothesis.

Observation 1: This observation specifies that the agreement between the predicted DST profiles and the experimental DST data becomes progressively better as C_b increases for both $C_{12}E_4$ and $C_{12}E_6$.

Recall that surfactant adsorption occurs faster at higher C_b values and is slower at lower C_b values. Therefore, at higher C_b values, it is possible that the adsorption process is close to equilibrium even before natural convection sets in. As a result, one observes good agreement between the DST predictions of the diffusion-controlled model and the experimental DST behavior at the higher C_b values. On the other hand, at lower C_b values, the adsorption

process takes place during a longer time period, and therefore, during the hypothesized onset of natural convection, the system is significantly away from the equilibrium conditions. Consequently, at lower C_b values one observes deviations between the predicted DST profiles (based on the premise that only diffusive transport of surfactant molecules occur in the bulk solution) and the experimental DST behavior.

Observation 2: This observation specifies that at low C_b values (see Figure 4-3(a-c) and Figure 4-4(a-b)), systematic deviations are observed when $t > 100$ - 200 s.

This observation is consistent with the natural convection hypothesis which involves a characteristic time scale τ_{nc}. Note that the observed time of 100 - 200 s beyond which deviations between the experimental DST behavior and the predicted DST profiles become significant is consistent with the observed time scale for the onset of natural convection when stagnant water is exposed to still air, which is about 70 s [26]. To our knowledge, the onset of natural convection when a *spherical air bubble* is introduced into a stagnant aqueous solution has not been studied experimentally. With this in mind, in Appendix 4.A, I apply the theoretical approach developed in Refs.[27, 28] to estimate the time scale, τ_{nc}, in the case of a spherical bubble in a stagnant aqueous solution. Specifically, I consider the case of a spherical air bubble at temperature T_0 which is brought in contact with an aqueous solution at a temperature T_1, and apply the theoretical approach presented in Refs. [27, 28] to estimate τ_{nc}. The results derived in Appendix 4.A clearly show that τ_{nc} can vary between 250 s to 120 s seconds as $\Delta T = T_1 - T_0$ varies between 0.5 to 1.0 ° C. Note that the estimated scale value of τ_{nc} is consistent with the observed time scales of 100 - 200 s associated with the systematic deviations observed in Figures 4-3(a-c) and 4-4(a-b).

Observation 3: This observation specifies that when systematic deviations occur at the later times ($t > 100$ - 200 s) in Figures 4-3(a-c) and 4-4 (a-b), the experimental DST data is consistently *lower* than the predicted DST profiles.

This observation is consistent with the natural convection hypothesis, since, similar to diffusion, convection also helps create more uniformity in the bulk solution. Due to the combined action of diffusion and convection, surfactant molecules are more readily available at

the sub-surface to adsorb onto the surface after the onset of natural convection. This, in turn, results in an increased rate of surfactant adsorption relative to that resulting from the diffusion-controlled model. Accordingly, one observes a faster reduction of the experimental DST relative to the predictions of the diffusion-controlled model.

Observation 4: This observation specifies that both the experimental DST behavior and the DST profiles predicted by the diffusion-controlled model approach the same equilibrium surface tension value.

This observation is consistent with the natural convection hypothesis since convection affects solely the *transport* of the surfactant molecules within the bulk solution, and does not affect the equilibrium state of the system. Consequently, the experimental DST behavior and the DST profiles predicted by the diffusion-controlled model should yield the same equilibrium surface tension value.

Note that the possible onset of natural convection in DST experiments has also been noted in Ref.[29], where dynamic ellipsometry experiments were conducted, in addition to DST measurements, in order to directly measure the dynamic surface concentration, $\Gamma(t)$, for $C_{12}E_5$. The authors in Ref.[29] observed that at lower C_b values, $\Gamma(t)$ measured using the dynamic ellipsometry experiment was higher than $\Gamma(t)$ predicted by the diffusion-controlled adsorption model. These authors commented that the observed high dynamic surfactant surface concentration was obtained because of the onset of natural convection. Interestingly, the deviations between the predicted and the experimental $\Gamma(t)$ values reported in Ref.[29] began at $t \approx 5$ min (= 300 s). Note that this time scale is consistent with the time scales at which systematic deviations are observed in the DST analysis presented here (see Figures 4-3(a-d) and 4-4(a-d)).

4.4 Conclusions

In this chapter, I analyzed the experimental DST data of the two nonionic surfactants, $C_{12}E_4$ and $C_{12}E_6$, measured using the pendant-bubble apparatus. Using ESTC models that fit both the equilibrium surface tension measurements as well as the surface-expansion measurements, and using a range of acceptable diffusion coefficient values, I predicted the DST profiles corresponding to

the diffusion-controlled model at several initial surfactant bulk solution concentrations for the two nonionic surfactants considered. Systematic deviations were observed when comparing the predicted DST profiles with the experimental DST data measured using the pendant-bubble apparatus for both $C_{12}E_4$ and $C_{12}E_6$. Specifically, the experimental DST behavior decreased at a rate that is higher than the rate predicted by the diffusion-controlled model. Interestingly, this 'super-diffusion' adsorption behavior appeared to occur, consistently at later time values ($t > 100$ - 200 seconds) for both $C_{12}E_4$ and $C_{12}E_6$. I investigated possible causes for the observed systematic deviations, including analyzing the effect of possible errors in the diffusion-controlled model input specifications, and the breakdown of key assumptions underlying the diffusion-controlled model. My analysis pointed to the breakdown of the assumption of diffusive-transport of surfactant molecules in the bulk solution as being the likely cause for the observed systematic deviations. Accordingly, I hypothesized the onset of natural convection resulting from the evaporative cooling of water at the pendant-bubble surface, including demonstrating that this hypothesis could explain all the features associated with the observed systematic deviations. It is noteworthy that I was unable to find any direct evidence in the literature to validate or invalidate this hypothesis. Clearly, additional experimental analysis of the pendant-bubble technique is required to understand possible natural convection effects. For example, analyzing the experimental DST results when the air bubble is introduced at different temperatures and at different humidity conditions may shed light on the existence of natural convection in the pendant-bubble apparatus, and if it does, experiments of this type will also help to quantify the effect of natural convection on the adsorption kinetics behavior of surfactant molecules.

It is important to recognize that one of the key applications of the pendant-bubble technique is to investigate the adsorption kinetics behavior of surfactant molecules onto liquid/liquid interfaces, and therefore, knowledge and characterization of the underlying transport mechanism is essential in order to carry out a reliable analysis of the experimental DST data reliably.

In Chapter 5, I explore a novel approach to predict equilibrium adsorption properties from experimental DST data and the known adsorption kinetics rate-limiting mechanism. Specifically, I develop a novel methodology to predict the ESTC behavior of C_iE_j nonionic surfactants from experimental pendant-bubble DST data when the adsorption kinetics is diffusion-controlled. Keeping

the results presented in Chapter 4 in mind, I only use experimental DST data corresponding to $t < 200$ s to demonstrate the utility of the novel methodology developed in Chapter 5.

Appendix 4.A: Estimation of time for the onset of natural convection

In this appendix, I apply the theoretical approach developed by Tan and Thorpe in Refs.[27, 28] to estimate the time for the onset of natural convection (nc) when a spherical air bubble of radius r_0 and having a Fixed Surface Temperature (FST) T_0 is introduced into an aqueous solution at temperature T_1.

The literature in the area of natural convection defines the *Rayleigh number*, Ra, as the nondimensionless number that determines the onset of natural convection in a fluid. Specifically, when Ra is smaller than a critical value, Ra_c, the transfer of heat in the fluid is primarily in the form of conduction, and when Ra is larger than Ra_c, natural convection sets in the fluid. The theoretical approach developed in Refs.[27, 28] to predict the time for the onset of natural convection involves the following three steps:

1. Defining a *transient (t) Rayleigh number* (Ra_t) for the system of interest.

2. Estimating the maximum value of Ra_t $(Ra_t^{\max})$ at any given time instant.

3. Estimating the time when $Ra_t^{\max}$ reaches the critical value, Ra_c, corresponding to the onset of natural convection in the system.

The theoretical approach outlined above has been implemented successfully to predict the onset of natural convection when stagnant water is exposed to a *flat* air surface [27]. Since the pendant-bubble measurement involves introducing an air bubble into an aqueous surfactant solution, it is possible that the spherical nature of the bubble may affect the time for the onset of natural convection. With the above in mind, in this Appendix, I predict the time for the onset of natural convection, τ_{nc}, when a *spherical surface* of radius, r_0, is introduced into water by following the three steps listed above. Note that the mole fractions of surfactants in the aqueous surfactant solutions used for the DST experiments reported in Figures 4-3(a-d) and 4-4(a-d) are extremely small ($\sim 10^{-10}$). Therefore, I assume that the thermal properties of the surfactant solution are similar to those of pure water. With this in mind, I consider pure water in order to estimate the time scale for the onset of natural convection, τ_{nc}.

Step 1: Defining a Transient Rayleigh Number, Ra_t

The time-dependent Rayleigh number at a radial distance r is defined as follows [28]:

$$Ra_t(r,t) = \frac{g\alpha r^4}{\nu\kappa}\left(\frac{\partial T}{\partial r}\right)_t \tag{4.A.1}$$

where g is the gravitational acceleration, α is the volumetric coefficient of thermal expansion, ν is the fluid kinematic viscosity, κ is the fluid thermal diffusivity, and T is the absolute temperature.

When a solution initially at temperature T_1 is exposed to a spherical surface at constant temperature T_0, the transient temperature profile in the bulk fluid is given by [30]:

$$\frac{T(r,t)-T_1}{\Delta T} = -\frac{r_0}{r}\text{erfc}\left(\frac{r-r_0}{2\sqrt{\kappa t}}\right) \tag{4.A.2}$$

where $\Delta T = T_1 - T_0$. The temperature gradient can be found by differentiating Eq.(4.A.2) with respect to r as follows:

$$\left(\frac{\partial T}{\partial r}\right)_t = \Delta T\frac{r_0}{r}\left\{\frac{1}{r}\text{erfc}\left(\frac{r-r_0}{2\sqrt{\kappa t}}\right) + \frac{1}{\sqrt{\pi\kappa t}}\exp\left(-\frac{(r-r_0)^2}{4\kappa t}\right)\right\} \tag{4.A.3}$$

Substituting Eq.(4.A.3) in Eq.(4.A.1) yields the transient Rayleigh number as follows:

$$Ra_t(r,t) = \frac{g\alpha r_0 r^3 \Delta T}{\nu\kappa}\left\{\frac{1}{r}\text{erfc}\left(\frac{r-r_0}{2\sqrt{\kappa t}}\right) + \frac{1}{\sqrt{\pi\kappa t}}\exp\left(-\frac{(r-r_0)^2}{4\kappa t}\right)\right\} \tag{4.A.4}$$

Step 2: Estimating the Maximum Value of Ra_t ($Ra_t^{max}(t)$)

The maximum value of $Ra_t(r,t)$ at any given time instant, $Ra_t^{max}(t)$, can be determined by differentiating Eq.(4.A.4) with respect to r, setting the derivative equal to zero, solving the resulting equation for the value of r, and verifying that the second order derivative condition for a maximum is satisfied at the value of r corresponding to the solution of the first derivative. Specifically, differentiating Eq.(4.A.4) and setting the derivative equal to zero yields:

$$\frac{\partial Ra_t(r,t)}{\partial r} = \frac{g\alpha r_0 r \Delta T}{\nu\kappa}\left\{2\text{erfc}\left(\frac{r-r_0}{2\sqrt{\kappa t}}\right) + \right.$$

$$\left.\frac{1}{2\sqrt{\pi}}\exp\left(-\frac{(r-r_0)^2}{4\kappa t}\right)\left[4\frac{r}{\sqrt{\kappa t}} - \left(\frac{r}{\sqrt{\kappa t}}\right)^2\frac{(r-r_0)}{\sqrt{\kappa t}}\right]\right\} = 0 \tag{4.A.5}$$

Note that an exact solution of Eq.(4.A.5) can only be obtained numerically. Nevertheless, in order to facilitate the derivation of an analytical solution of Eq.(4.A.5), I will assume that the value of r at which $Ra_t(r, t)$ reaches its maximum value is much larger than r_0. In other words, if r^* is such that $\frac{\partial Ra_t(r,t)}{\partial r}\Big|_{r=r^*} = 0$, then I assume that $r^* \gg r_0$. Note that I will also solve Eq.(4.A.5) numerically to compute the exact value of r^*, and the corresponding exact maximum value of $Ra_t(r, t)$, and compare the two results.

Making the assumption that $r^* \gg r_0$ in Eq.(4.A.5), and defining $z = r^*/\sqrt{\kappa t}$ yields:

$$\frac{\partial Ra_t(z, t)}{\partial z}\Big|_{z=z^*} = \frac{g\alpha r_0 z^* t \Delta T}{\nu} \left\{ 2\mathrm{erfc}(z^*/2) + \frac{1}{2\sqrt{\pi}} \exp(-z^{*2}/4) \left[4z^* - z^{*3} \right] \right\} = 0 \qquad (4.A.6)$$

Solving Eq.(4.A.6) and requiring that the resulting solution satisfies the second derivative test for the maximum of $Ra_t(z, t)$ yields the solution $z^* = 2.28$. The value of r at which $Ra_t(r, t)$ attains its maximum value, denoted as $r^*(t)$, is then given by:

$$r^*(t) = 2.28\sqrt{\kappa t} \qquad (4.A.7)$$

Using the assumption that $r^* \gg r_0$, and substituting $r^* = 2.28\sqrt{\kappa t}$ in Eq.(4.A.4) yields the maximum transient Rayleigh number, $Ra_t^{\mathrm{max}}(t)$, as follows:

$$Ra_t^{\mathrm{max}}(t) = \frac{2.37 g\alpha t r_0 \Delta T}{\nu} \qquad (4.A.8)$$

Step 3: Estimating τ_{nc} when $Ra_t^{\mathrm{max}} = Ra_c$

The time, $t = \tau_{nc}$, when the maximum value of the transient Rayleigh number equals the critical value, Ra_c, can be determined from Eq.(4.A.8) as follows:

$$\tau_{nc} = \frac{Ra_c \nu}{2.37 g\alpha r_0 \Delta T} \qquad (4.A.9)$$

An estimate of the critical Rayleigh number for the Fixed Surface Temperature (FST) boundary condition is about 1100 [28]. Therefore, using $Ra_c = 1100$, $g = 9.8$ m^2/s, the following values for the required properties of water [28]: $\nu = 8.76 \times 10^{-7}$ m^2/s, $\alpha = 2.65 \times 10^{-4}$ K^{-1}, $\kappa = 1.44 \times 10^{-7}$ m^2/s, and a typical value of $r_0 = 1 \times 10^{-3}$ m, τ_{nc} was computed for a range of ΔT

173
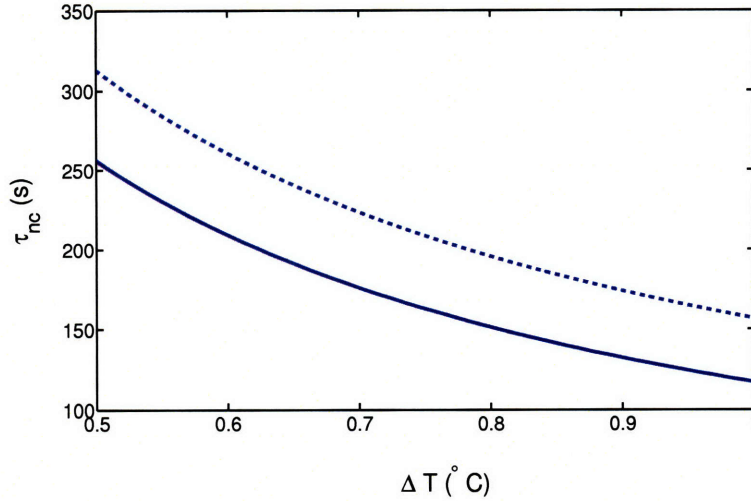
Figure 4-6: Estimated time for the onset of natural convection, τ_{nc}, as function of the difference between the water and air temperatures, ΔT. The solid line corresponds to the exact numerical solution of Eq.(4.A.5) and the dashed line corresponds to the approximate solution, Eq.(4.A.9).

values using Eq.(4.A.9). The resulting τ_{nc} is plotted as a function of ΔT in Figure 4-6 (see the dashed line). In Figure 4-6, I have also plotted the exact τ_{nc} versus ΔT calculated by numerically solving Eq.(4.A.5) for r^*, and then using Eq.(4.A.4) to determine $Ra_t^{max}(t)$ (see the solid line). The exact numerical solution predicts that τ_{nc} ranges between 250 to 120 s as the difference in temperature between the air bubble and water vary between 0.5 to 1 °C. Note that the estimated time for the onset of natural convection is of the same order of magnitude as the observed time scale ($\approx$ 100 - 200 s) at which the systematic deviations between the predicted DST profiles and the experimental DST behavior begin to become significant (see Figures 4-3(a-d) and 4-4(a-d)). Comparing the dashed and solid lines in Figure 4-6 reveals that τ_{nc} predicted using Eq.(4.A.9) and τ_{nc} obtained from the exact numerical solution of Eq.(4.A.5) are consistent both in magnitude and trend. Therefore, I suggest that Eq.(4.A.9) can be used to make quick and approximate estimates of τ_{nc} when conducting pendant-bubble experiments.

In summary, in this Appendix, I estimated the time for the onset of natural convection, τ_{nc}, when a spherical air bubble at fixed surface temperature T_0 is introduced into an aqueous solution at an initial uniform temperature T_1 by applying the theoretical approach developed by Tan and Thorpe in Refs. [27, 28]. Using typical values for the physical properties of water, as well as a

typical value for the radius of the pendant bubble, the results indicate that τ_{nc} ranges between 250 s to 120 s as $\Delta T = T_1 - T_0$ varies between 0.5 to 1 °C.

Bibliography

[1] J. Eastoe and J. S. Dalton. Dynamic surface tension and adsorption mechanisms of surfactants at the air-water interface. *Advances in Colloid and Interface Science*, 85:103–144, 2000.

[2] S-Y. Lin, K. McKeigue, and C. Maldarelli. Diffusion-controlled surfactant adsorption studied by pendant drop digitization. *AIChE Journal*, 36:1785 – 1795, 1990.

[3] C-T. Hsu, M-J. Shao, and S-Y. Lin. Adsorption kinetics of $C_{12}E_4$ at the air-water interface: Adsorption onto a fresh interface. *Langmuir*, 16:3187–3194, 2000.

[4] Y-C. Lee, H-S. Liu, and S-Y. Lin. Adsorption kinetics of $C_{10}E_4$ at the air/water interface: consider molecular interaction or reorientation. *Colloids and Surfaces A: Physicochemical and Engineering Aspects*, 212:123–134, 2003.

[5] Y-C. Lee, S-Y. Lin, and M-J. Shao. Adsorption kinetics of $C_{12}E_6$ at the air-water interface. *Journal of Chinese Institute of Chemical Engineers*, 33(6):631–643, 2002.

[6] R. Pan, J. Green, and C. Maldarelli. Theory and experiment on the measurement of kinetic rate constants for surfactant exchange at an air/water interface. *Journal of Colloid and Interface Science*, 205:213–230, 1998.

[7] H-C. Chang, C-T. Hsu, and S-Y. Lin. Adsorption kinetics of $C_{10}E_8$ at the air-water interface. *Langmuir*, 14:2476–2484, 1998.

[8] S-Y. Lin, R-Y. Tsay, L-W. Lin, and S-I. Chen. Adsorption kinetics of $C_{12}E_8$ at the air-water interface: Adsorption onto a clean interface. *Langmuir*, 12:6530–6536, 1996.

[9] S-Y. Lin, Y-C. Lee, M-J. Shao, and C-T. Hsu. A study on surfactant adsorption kinetics: The role of the data of equation of state for $C_{14}E_8$. *Journal of Colloid and Interface Science*, 244:372–376, 2001.

[10] S-Y. Lin, T-L. Lu, and W-B. Hwang. Adsorption kinetics of decanol at the air-water interface. *Langmuir*, 11:555–562, 1995.

[11] Y-C. Lee, Y-B. Liou, R. Miller, H-S. Liu, and S-Y. Lin. Adsorption kinetics of nonanol at the air-water interface: Considering molecular interaction or aggregation within surface layer. *Langmuir*, 18:2686–2692, 2002.

[12] S-Y. Lin, K. McKeigue, and C. Maldarelli. Diffusion-limited interpretation of the induction period in the relaxation in surface tension due to the adsorption of straight chain, small polar group surfactants: Theory and experiment. *Langmuir*, 7:1055–1066, 1991.

[13] S-Y. Lin, W-J. Wang, and C-T. Hsu. Adsorption kinetics of 1-octanol at the air-water interface. *Langmuir*, 13:6211 – 6218, 1997.

[14] C-T. Hsu, C-H. Chang, and S-Y. Lin. Comments on the adsorption isotherm and determination of adsorption kinetics. *Langmuir*, 13:6204–6210, 1997.

[15] Y-C. Lee, S-Y. Lin, and H-S. Liu. Role of equation of state on studying surfactant adsorption kinetics. *Langmuir*, 17:6196–6202, 2001.

[16] J. K. Ferri, S. Y. Lin, and K. J. Stebe. Curvature effects in the analysis of Pendant bubble data: Comparison of numerical solutions, asymptotic arguments, and data. *Journal of Colloid and Interface Science*, 241:154–168, 2001.

[17] M. J. Rosen. *Surfactants and Interfacial Phenomena*. Wiley Interscience, 1989.

[18] S-Y. Lin, Y-C. Lee, M-W Yang, and H-S Liu. Surface equation of state of nonionic C_mE_n surfactants. *Langmuir*, 19:3164 – 3171, 2003.

[19] C. R. Wilke and P. Chang. Correlation of diffusion coefficients in dilute solutions. *AIChE Journal*, 1:264–270, 1955.

[20] S. N. Moorkanikkara and D. Blankschtein. New methodology to determine the adsorption kinetics rate limiting mechanism from experimental dynamic surface tension data. *Journal of Colloid and Interface Science*, 302:1–19, 2006.

[21] M. Schonhoff and O. Soderman. PFG-NMR diffusion as a method to investigate the equilibrium adsorption dynamics of surfactants at the solid/liquid interface. *J. Phys. Chem. B*, 101:8237–8242, 1997.

[22] S-Y. Lin, W-J. Wang, L-W. Lin, and L-J. Chen. Systematic effects of bubble volume on the surface tension measured by pendant bubble profiles. *Colloids and Surfaces A: Physicochemical and Engineering Aspects*, 114:31–39, 1996.

[23] H. Kuhn and H. Rehage. Molecular orientation of monododecyl pentaethylene glycol at water/air and water/oil interfaces. A molecular dynamics computer simulation study. *Colloid and Polymer Science*, 278:114–118, 2000.

[24] J. Chanda and S. Bandyopadhyay. Molecular dynamics study of a surfactant monolayer adsorbed at the air/water interface. *Journal of Chemical Theory and Computation*, 1:963–971, 2005.

[25] W. M. Deen. *Analysis of Transport Phenomena*. Oxford University Press, 1998.

[26] W. G. Spangenberg and W. R. Rowland. Convective circulation in water induced by evaporative cooling. *The Physics of Fluids*, 4:743–750, 1961.

[27] K. K. Tan and R. B. Thorpe. The onset of convection caused by buoyancy during transient heat conduction in deep fluids. *Chemical Engineering Science*, 51:4127–4136, 1996.

[28] K. K. Tan and R. B. Thorpe. The onset of convection driven by buoyancy effects caused by various modes of transient heat conduction: Part 1. Transient Rayleigh numbers. *Chemical Engineering Science*, 54:225–238, 1999.

[29] B. P. Binks, P. D. I. Fletcher, V. N. Paunov, and D. Segal. Equilibrium and dynamic adsorption of $C_{12}E_5$ at the air-water surface investigated usin ellipsometry and tensiometry. *Langmuir*, 16:8926–8931, 2000.

[30] H. S. Carslaw. *Introduction to the mathematical theory of the conduction of heat in solids.* Macmillan and Company (London), 1954.

Chapter 5

New Methodology to Determine Equilibrium Surfactant Adsorption Properties from Experimental Dynamic Surface Tension Data

5.1 Introduction

In Chapter 3, I emphasized that the existing procedure to determine the rate-limiting adsorption kinetics mechanism requires: (a) experimental Dynamic Surface Tension (DST) data corresponding to the *entire relaxation process*, and (b) knowledge of the equilibrium surfactant adsorption behavior. Instead, the new methodology presented in Chapter 3 requires only the *short-time* DST data to predict the rate-limiting adsorption kinetics mechanism. Since the new methodology allows determination of the rate-limiting adsorption kinetics mechanism *without using any information about the equilibrium surfactant adsorption behavior*, in this chapter, I explore a novel approach to predict equilibrium surfactant adsorption properties using: (i) the experimental DST data corresponding to the entire relaxation process, and (ii) the known rate-limiting adsorption kinetics mechanism. Note that the rate-limiting adsorption kinetics mechanism can be determined from the experimental DST data using either the asymptotic behavior of the DST [1] or the new methodology presented

in Chapter 3.

As proof-of-principle, I present a new methodology to predict the Equilibrium Surface Tension versus bulk solution Concentration (*referred to hereafter as the ESTC*) behavior of nonionic surfactants from the experimental pendant-bubble DST data when the adsorption kinetics process is *diffusion-controlled*. I consider the case of diffusion-controlled adsorption because it has been found to be applicable to a broad class of surfactant systems [2–4]. Basically, the new methodology involves transforming the classical diffusion-controlled model such that the experimental DST profile is the input and the ESTC is the output. This should be contrasted with the traditional approach where the experimental equilibrium adsorption behavior is the input and the DST is the output[2–4]. Implementation of the new methodology requires the following three inputs:

1. Experimental pendant-bubble DST data corresponding to the entire relaxation process measured at a *single* surfactant bulk (*b*) solution concentration, C_b.

2. The diffusion coefficient of the surfactant molecule, D.

3. An experimental equilibrium surface tension value at a *single* surfactant bulk solution concentration, $C_{b,1}$, where $C_{b,1} < C_b$.

With these three inputs, the new methodology can predict the *entire equilibrium surface tension vs. surfactant bulk solution concentration (ESTC) curve* corresponding to surfactant bulk solution concentrations which are smaller than, or equal to, C_b.

Note that this prediction is possible because, for a diffusion-controlled adsorption process, the sub-surface is assumed to be in equilibrium with the surface at all times [5]. Therefore, at any time t, the dynamic surface tension, $\gamma(t)$, corresponds to the equilibrium surface tension associated with the instantaneous surfactant sub-surface (*s*) concentration, $C_s(t)$. Consequently, when $\gamma(t)$ varies from an initial value, γ_0, to the equilibrium surface tension value, γ_b^e, corresponding to the surfactant bulk solution concentration C_b, it traces the variation of $C_s(t)$ from the equilibrium surfactant bulk solution concentration corresponding to γ_0, $C_b^e(\gamma_0)$, to $C_b^e = C_b$. In other words, as surfactant adsorption takes place, the relation between $\gamma(t)$ and $C_s(t)$ 'sweeps' through the entire ESTC curve between $C_b^e(\gamma_0)$ and $C_b^e = C_b$. The new methodology presented here uses this feature of the diffusion-controlled model to predict the ESTC curve from the experimental DST data (input 1), the D value (input 2), and a known value of $C_b^e(\gamma_0)$ which serves as the 'starting point' for the

prediction of the ESTC curve. Since $C_b^e(\gamma_0)$ is typically unknown, the new methodology uses input 3 above to fit for the value of $C_b^e(\gamma_0)$. Specifically, the new methodology predicts ESTC curves using inputs 1 and 2 above for different guesses of $C_b^e(\gamma_0)$, and uses input 3 (a single equilibrium surface tension measurement) to select the value of $C_b^e(\gamma_0)$ such that the resulting ESTC curve passes through the single measured equilibrium surface tension value (input 3). Considering that $C_s(t)$ varies from $C_b^e(\gamma_0)$ to C_b during the surfactant adsorption process, the ESTC curve obtained should be applicable over the range of equilibrium surfactant bulk solution concentrations, C_b^e, given by: $C_b^e(\gamma_0) \leq C_b^e \leq C_b$. With this in mind, one requires that the surfactant bulk solution concentration, $C_{b,1}$, corresponding to the single measured equilibrium surface tension value, be less than C_b.

Note that the existing procedure to determine the ESTC of surfactants involves performing actual equilibrium surface tension measurements at various C_b^e values, and then generating the best-fit curve that passes through the various experimental data points based on empirical model equations [1]. In Refs.[6, 7], it was pointed out that different ESTC models that fit the equilibrium experimental surface tension data well result in very different predictions of the corresponding Equation Of State (EOS). As a result, in order to further test the validity of the different ESTC models, novel surface-expansion measurements were introduced to predict EOS information [8–10]. In such cases, the EOS predictions of different ESTC models can be directly compared with the EOS information obtained from the surface-expansion measurements[10]. When compared to the existing procedure to determine and verify the ESTC behavior of surfactants, the new methodology presented here is practically advantageous for the following two reasons:

1. The existing procedure requires measuring the equilibrium surface tension at several C_b^e values, which is very tedious and time consuming, with each measurement corresponding to only a single data point on the underlying ESTC curve. On the other hand, the new methodology requires the experimental DST data measured at a single C_b value, as well as one equilibrium surface tension value measured at a single $C_{b,1}$ value, in order to predict the *entire ESTC curve* of the surfactant over a wide range of surfactant bulk solution concentrations, $C_b^e(\gamma_0) \leq C_b^e \leq C_b$.

2. In Refs. [6, 7], it was shown that the predicted DST behavior of surfactants is very sensitive to the accuracy of the model used to describe the equilibrium adsorption behavior of the

surfactants. As a result, one may anticipate that the ESTC information deduced using the experimental DST data should be very accurate.

Recall that, in Chapter 3, an analysis of the short-time DST data of several alkyl poly(ethylene) oxide, C_iE_j, nonionic surfactants was carried out using a new theoretical methodology, and the rate-limiting adsorption kinetics mechanism of two of the nonionic surfactants considered, $C_{12}E_4$ and $C_{12}E_6$, was found to be diffusion-controlled at their premicellar C_b values. Therefore, I will demonstrate the applicability of the new methodology presented here by predicting the ESTC behavior of $C_{12}E_4$ and $C_{12}E_6$ using the experimental pendant-bubble DST data published in Refs.[11] and [12], respectively. For both $C_{12}E_4$ and $C_{12}E_6$, I will validate the ESTC behaviors predicted using the new methodology by: (a) comparing the predicted ESTC behaviors with independent experimental equilibrium surface tension measurements, and (b) comparing the EOS information corresponding to the predicted ESTC behaviors with independent experimental surface-expansion measurements. For both $C_{12}E_4$ and $C_{12}E_6$, I will show that the agreement between the predicted equilibrium adsorption properties and the experimental measurements in (a) and (b) above is very good.

The remainder of the chapter is organized as follows. In Section 5.2, I develop the new methodology to predict the ESTC behavior of nonionic surfactants from experimental pendant-bubble DST data when the adsorption kinetics mechanism is diffusion-controlled. In Section 5.3, I utilize the new methodology to predict the ESTC behaviors of $C_{12}E_4$ and $C_{12}E_6$ using experimental DST data published in Refs.[11] and [12], respectively, and validate the results using independent equilibrium surface tension measurements and surface-expansion measurements. Finally, in Section 5.4, I summarize the main results of the chapter. In addition, in Appendix 5.A, I demonstrate the reliability of the new methodology, and in Appendix 5.B, I investigate the sensitivity of the ESTC curve predicted using the new methodology to the three inputs introduced earlier.

5.2 Development of the New Methodology

5.2.1 New Methodology to Analyze Experimental Pendant-Bubble DST Data

The key step in the development of the new methodology involves transforming the classical diffusion-controlled model such that the experimental DST profile is the input and the ESTC behavior is the output. For completeness, below, I summarize the four key assumptions underlying the diffusion-controlled model as it applies when nonionic surfactants adsorb onto a pendant-bubble surface (for additional details, see Section 4.2.1):

Assumption 1: Transport of the surfactant molecules in the bulk solution is governed by Fickian diffusion.

Assumption 2: Adsorption of the surfactant molecules from the sub-surface onto the surface is instantaneous, that is, the sub-surface and the surface reach equilibrium instantaneously.

Assumption 3: The adsorbed surfactant molecules either do not undergo any reorganization at the surface or the reorganization is instantaneous.

Assumption 4: Adsorption of the surfactant molecules onto the pendant-bubble surface can be modeled as adsorption onto a spherical surface.

The following governing equations and associated boundary and initial conditions apply to the diffusion-controlled model in the case of a pendant bubble (see Section 4.2.1):

- The surfactant diffusive transport along the radial direction, r, towards the spherical surface is given by:

$$\frac{\partial C}{\partial t} = \frac{D}{r^2} \frac{\partial}{\partial r} \left(r^2 \frac{\partial C}{\partial r} \right), \qquad r \geq r_0, \ t \geq 0 \tag{5.1}$$

where C is the surfactant concentration, D is the surfactant diffusion coefficient, and r_0 is the radius of the pendant bubble.

- The rate of surfactant adsorption at the surface is equal to the net flux of surfactant molecules leaving the sub-surface towards the surface, that is,

$$\frac{d\Gamma}{dt} = D \left. \frac{\partial C}{\partial r} \right|_{r=r_0} \tag{5.2}$$

where Γ is the surfactant surface concentration.

- Assuming that the far field ($r \to \infty$) surfactant concentration is uniform at a value C_b, the boundary condition for Eq.(5.1) is given by:

$$C(t, r \to \infty) = C_b, \qquad t \geq 0 \tag{5.3}$$

- Assuming a surfactant surface concentration, Γ_0, and a homogeneous bulk solution at the beginning of the adsorption process ($t = 0$), the initial conditions associated with the governing equations (Eqs.(5.1) and (5.2)) can be expressed as follows:

$$\Gamma(t = 0) = \Gamma_0 \qquad \text{and} \qquad C(t = 0, r) = C_b, \qquad r \geq r_0 \tag{5.4}$$

Equations (5.1) - (5.4) can be solved using the method of Laplace Transforms to yield[13]:

$$\Gamma(t) = \Gamma_0 + \frac{D}{r_0} \left[C_b t - \int_0^t C_s(t) dt \right] + 2\sqrt{\frac{D}{\pi}} \left[C_b \sqrt{t} - \int_0^{\sqrt{t}} C_s(t - \eta) d\sqrt{\eta} \right] \tag{5.5}$$

where $C_s(t)$ is the instantaneous surfactant sub-surface concentration (that is, $C(t, r = r_0)$). Equation (5.5) enables the prediction of the dynamic surface concentration, $\Gamma(t)$, when the dynamic sub-surface concentration, $C_s(t)$, is known.

In the case of the diffusion-controlled model, since the sub-surface and the surface reach equilibrium instantaneously (see Assumption 2), the instantaneous surface concentration, $\Gamma(t)$, and the instantaneous sub-surface concentrations, $C_s(t)$, are related by the equilibrium (e) adsorption isotherm relation between Γ_e and C_b^e. In other words, if the equilibrium adsorption isotherm relating Γ_e to C_b^e is given by:

$$\Gamma_e = g(C_b^e) \tag{5.6}$$

then, in the case of the diffusion-controlled model, the relation between $\Gamma(t)$ and $C_s(t)$ in Eq.(5.5) is given by:

$$\Gamma(t) = g(C_s(t)) \tag{5.7}$$

Note that the existing procedure in the DST area involves: (i) assuming a known equilibrium adsorption isotherm, $g(C_b^e)$, for use in Eq.(5.7), (ii) predicting $\Gamma(t)$ by solving simultaneously

186

Eqs.(5.5) and (5.7), and (iii) using the Equation Of State (EOS) corresponding to the assumed equilibrium adsorption isotherm, $g(C_b^e)$, to predict the dynamic surface tension, $\gamma(t)$, from the predicted $\Gamma(t)$ [2–4].

Instead, in the new methodology presented here, imagine that $\Gamma(t)$ is known *a priori* at a specific C_b value, and that the values of D and r_0 are also known. In that case, Eq.(5.5) becomes a fully defined integral equation in $C_s(t)$, which can be solved numerically. Once $C_s(t)$ is predicted in this manner, one can make the assumption of instantaneous equilibrium between the sub-surface and the surface underlying the diffusion-controlled model (see Assumption 2) to predict the equilibrium adsorption isotherm by relating the instantaneous values of $\Gamma(t)$ and $C_s(t)$ using Eq.(5.7). However, unfortunately, $\Gamma(t)$ is not typically measured experimentally. Instead, one measures the dynamic surface tension, $\gamma(t)$. With this in mind, I transform Eq.(5.5) into a form that involves $\gamma(t)$ instead of $\Gamma(t)$. For this purpose, recall that the Gibbs adsorption equation relates the differential change in the equilibrium value of the surface tension (γ_e) with respect to C_b^e to Γ_e as follows [1]:

$$\Gamma_e = -\frac{C_b^e}{RT}\left[\frac{d\gamma_e}{dC_b^e}\right] \tag{5.8}$$

where R is the gas constant, and T is the absolute temperature. In the case of diffusion-controlled adsorption, since the sub-surface and the surface are in equilibrium at all times, the Gibbs adsorption equation (Eq. (5.8)) can also be used to relate $\Gamma(t)$, $\gamma(t)$, and $C_s(t)$. Specifically,

$$\Gamma(t) = -\frac{C_s(t)}{RT}\left[\frac{d\gamma(t)}{dC_s(t)}\right] \tag{5.9}$$

Substituting Eq.(5.9) in Eq.(5.5), one obtains:

$$-\frac{C_s(t)}{RT}\left[\frac{d\gamma(t)}{dC_s(t)}\right] = \Gamma_0 + \frac{D}{r_0}\left[C_b t - \int_0^t C_s(t)dt\right] + 2\sqrt{\frac{D}{\pi}}\left[C_b\sqrt{t} - \int_0^{\sqrt{t}} C_s(t-\eta)d\sqrt{\eta}\right] \tag{5.10}$$

At any given T value, Eq.(5.10) is a fully *defined* integro-differential equation in $C_s(t)$ given the following two inputs:

Input 1: The dynamic surface tension, $\gamma(t)$, measured at known values of C_b and r_0.

Input 2: The diffusion coefficient of the surfactant molecule, D.

Considering that in typical experimental pendant-bubble DST data the value of $\gamma(t)$ as $t \to 0$, γ_0, is smaller than the water/air surface tension value ($\gamma_{w/a}$) by only about 0.5 mN/m (see Chapter 4), the value of Γ_0 in Eq.(5.10) can be estimated by assuming that the very small surface pressure, $\gamma_{w/a} - \gamma_0$, is related to Γ_0 by the Ideal Gas EOS. Specifically,

$$\gamma_{w/a} - \gamma_0 = RT\Gamma_0 \tag{5.11}$$

Therefore, by specifying the two inputs listed above, Eq.(5.10) is a fully defined integro-differential equation in the variable $C_s(t)$, which can be solved numerically given the initial value of $C_s(t)$. Note that once $C_s(t)$ is determined, one can then make the assumption of instantaneous equilibrium between the sub-surface and the surface underlying the diffusion-controlled model (see Assumption 2) to relate the instantaneous values of $\gamma(t)$ and $C_s(t)$ to predict the relation between the equilibrium surface tension, γ_e, and the surfactant bulk solution concentration, C_b^e, (that is, the ESTC curve) of the nonionic surfactant of interest.

Using Eq.(5.4), it follows that $C_s(t = 0) = C(t = 0, r = r_0) = C_b$. However, note that immediately after the adsorption process begins, at $t = 0^+$, in view of the assumption of instantaneous equilibrium between the sub-surface and the surface underlying the diffusion-controlled model (see Assumption 2), the sub-surface concentration *reduces instantaneously* from $C_s = C_b$ to an unknown value, $C_s = C_b^e(\gamma_0)$, in order to remain in equilibrium with the initial value of the surface tension, γ_0, and the associated surfactant surface concentration, Γ_0. Note that Eq.(5.10) assumes the existence of equilibrium between $C_s(t)$ and $\gamma(t)$ *at all times*, and therefore, the unknown $C_b^e(\gamma_0)$, rather than C_b, is the appropriate initial condition for $C_s(t)$ in Eq.(5.10). Since $C_b^e(\gamma_0)$ is not measured experimentally, it is considered as a fitting parameter in the new methodology presented here. Therefore, in addition to the 2 inputs listed above, the methodology requires an additional input:

Input 3: One experimental equilibrium surface tension value ($\gamma_{b,1}^e$) measured at a *single* surfactant bulk solution concentration, $C_{b,1}$.

Specifically, for given inputs 1 and 2: (i) Eq. (5.10) is solved numerically using different guesses for the initial value of $C_s(t = 0) = C_b^e(\gamma_0)$, (ii) ESTC curves are predicted for each guess of $C_b^e(\gamma_0)$ by relating $C_s(t)$, determined through the solution of Eq.(5.10), and the input DST, $\gamma(t)$, and (iii)

the value of $C_b^e(\gamma_0)$ is identified such that the corresponding ESTC curve passes through the given equilibrium surface tension data point $(C_{b,1}, \gamma_{b,1}^e)$.

Note that when the dynamic surface tension decreases from γ_0 to γ_b^e (corresponding to the equilibrium surface tension value of C_b), the surfactant sub-surface concentration increases from $C_b^e(\gamma_0)$ and C_b. Accordingly, using the new methodology proposed here, one can predict the *entire ESTC curve* for $C_b^e(\gamma_0) \leq C_b^e \leq C_b$. Since the value of $C_b^e(\gamma_0)$ is chosen such that the resulting ESTC curve passes through the given equilibrium surface tension data point $(C_{b,1}, \gamma_{b,1}^e)$, $C_{b,1}$ must be smaller than C_b.

5.2.2 Reliability and Input Sensitivity of the New Methodology

To demonstrate the reliability of the new methodology, I: (a) artificially generate experimental DST data corresponding to a specific ESTC model, (b) apply the new methodology to the artificially generated experimental DST data to predict the ESTC behavior of the surfactant, and (c) compare the ESTC behavior, predicted using the new methodology in (b), with the one that was used to generate the DST data in (a). A detailed description of the artificially generated experimental DST data, including the various steps associated with implementing the new methodology to analyze the DST data, is presented in Appendix 5.A. Based on the results presented in Appendix 5.A, I find that the new methodology is indeed able to reliably predict the *entire ESTC curve*, using: (1) the DST data measured at a single surfactant bulk solution concentration, (2) the known value of the diffusion coefficient of the surfactant molecule, and (3) a single experimental equilibrium surface tension data point.

In addition, to study the sensitivity of the ESTC curve predicted using the new methodology to typical inaccuracies in inputs 1 to 3 above in the case of the artificially generated experimental DST data, I examine the extent to which the ESTC curve shifts as inputs 1, 2, and 3 are separately varied over a range of appropriate values. A detailed description of the sensitivity analysis is presented in Appendix B. The results presented in Appendix B indicate that the ESTC curve is most sensitive to the value of the diffusion coefficient of the surfactant molecule (input 2), and less sensitive to the experimental dynamic surface tension data (input 1) and to the experimental equilibrium surface tension data point (input 3). Specifically, the maximum shifts of the ESTC curve for typical uncer-

tainties in inputs 1 to 3 are as follows: about $\pm$ 0.5 mN/m for input 1, about $\pm$ 1.5 mN/m for input 2, and about $\pm$ 0.4 mN/m for input 3. Having established that the value of the diffusion coefficient of the surfactant molecule, D, affects the ESTC curve the most, in Section 5.3, I analyze specifically the effect of D on the ESTC curve when using the new methodology to analyze experimental DST data.

5.3 Application of the New Methodology

In this Section, I utilize the new methodology presented in Section 5.2.1 to determine the Equilibrium Surface Tension vs. surfactant bulk solution Concentration (ESTC) behavior of the two nonionic surfactants, $C_{12}E_4$ and $C_{12}E_6$. Specifically, I use the experimental pendant-bubble DST data of $C_{12}E_4$ and $C_{12}E_6$ reported in Refs.[11] and [12], respectively, in order to predict their respective ESTC behaviors. As already stressed in Section 3.3.1, the adsorption kinetics mechanism for both $C_{12}E_4$ and $C_{12}E_6$ is diffusion-controlled at all premicellar surfactant bulk solution concentrations.

Recall that when experimental DST data measured at an initial surfactant bulk solution concentration C_b is used in the new methodology, it follows that the deduced ESTC behavior is applicable for surfactant bulk solution concentrations in the range, $C_b^e(\gamma_0) \leq C_b^e \leq C_b$. With this observation in mind, I have chosen a high initial surfactant bulk solution concentration at which the DST was measured, $C_b = 2.0$ x 10^{-8} mol/cm^3, for both $C_{12}E_4$ and $C_{12}E_6$. Recall that the analysis presented in Chapter 4 demonstrated that the assumption of diffusive transport of $C_{12}E_4$ and $C_{12}E_6$ in the bulk solution appears to break down about 100-200 s after the creation of the pendant bubble due to the onset of natural convection. Keeping this important finding in mind, only experimental DST data corresponding to $t < 200$ s was considered for input 1 when utilizing the new methodology. The input DST data for $C_{12}E_4$ and $C_{12}E_6$, including the best-fit curve representations of the experimental DST data using the modified Rosen functional form (see Eq.(5.A.3)) are shown in Figures 5-1(a) and 5-1(b), respectively. In both Figures 5-1(a) and 5-1(b), the filled circles correspond to the experimental pendant-bubble DST data, and the solid lines correspond to the best-fit curve representations of the modified Rosen functional form for (a) $C_{12}E_4$ and (b) $C_{12}E_6$. Note that the standard deviation of the residuals corresponding to the best-fit representation is 0.3 mN/m for
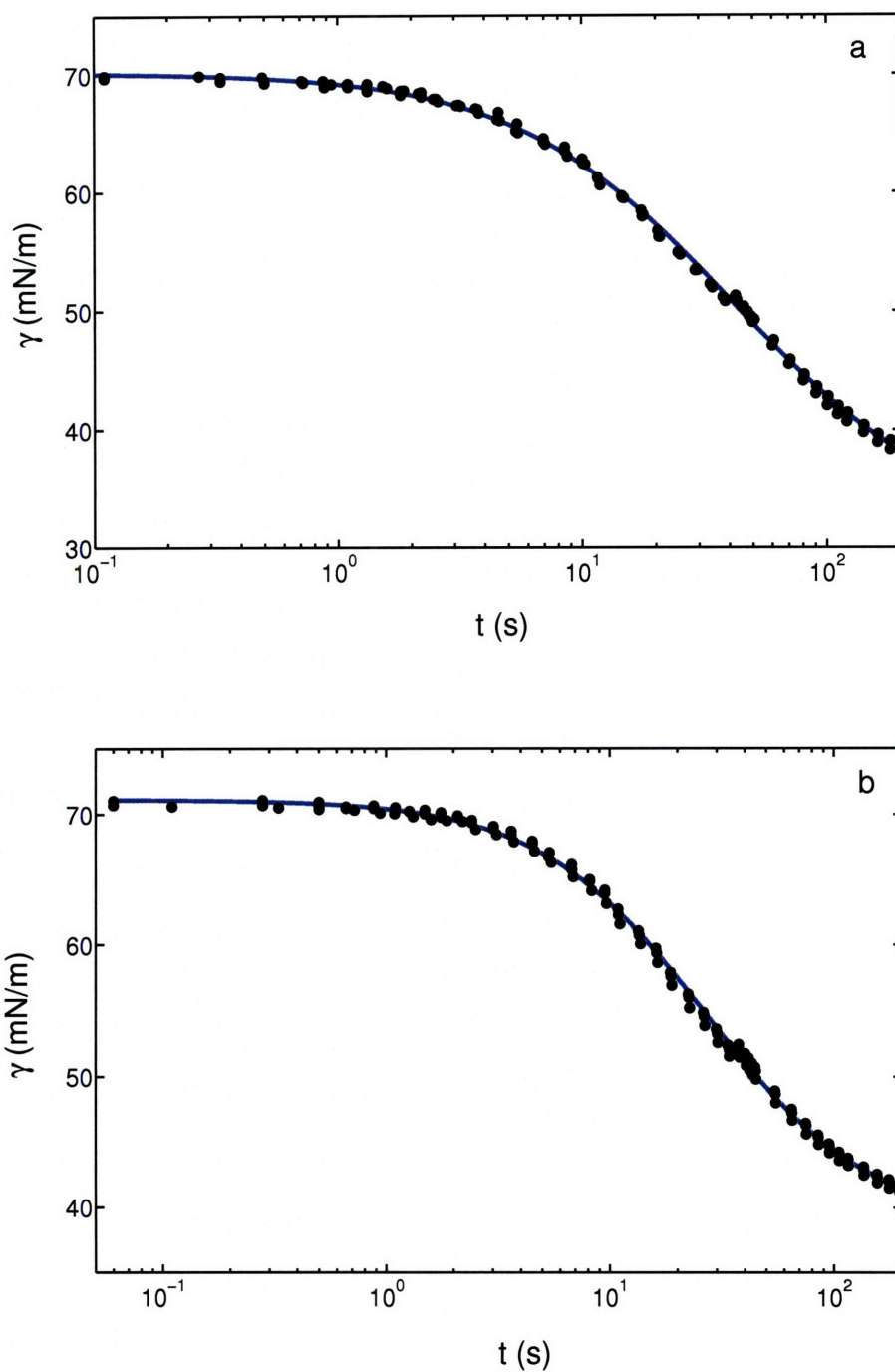
Figure 5-1: Experimental DST data used as input 1 to apply the new methodology, and the best-fit representation of the experimental DST data for: (a) $C_{12}E_4$, measured at $C_b = 2.0$ x 10^{-8} mol/cm^3, and (b)$C_{12}E_6$, measured at $C_b = 2.0$ x 10^{-8} mol/cm^3. The filled circles correspond to the experimental DST data and the solid lines correspond to the best-fits using the modified Rosen functional form given in Eq.(5.A.3).

$C_{12}E_4$ and 0.36mN/m for $C_{12}E_6$, which are both comparable to the typical accuracy of DST measurements conducted using the pendant-bubble apparatus (0.3 mN/m [14]). Values of inputs 1-3 used to apply the new methodology to $C_{12}E_4$ and $C_{12}E_6$, including relevant references, are summarized in Table 5.1. Note that the values of $C_{b,1}$ corresponding to input 3 were chosen keeping in mind that: (i) $C_{b,1} < C_b$ (see Section 5.2.1) and (ii) the equilibrium surface tension corresponding to $C_{b,1}$ should be significantly lower than the pure water/air surface tension value (in order to minimize possible inaccuracies in the experimental equilibrium surface tension value [15]).

Table 5.1: Values of the three inputs used to apply the new methodology to predict the ESTC behaviors of $C_{12}E_4$ and $C_{12}E_6$.

Nonionic	Input 1		Input 2	Input 3	
Surfactants	C_b(mol/cm^3)	r_0 (cm)	D (cm^2/s)	$C_{b,1}$ (mol/cm^3)	$\gamma^e_{b,1}$ (mN/m)
$C_{12}E_4$	2.0 x 10^{-8}	0.1 [11]	3.9 ± 0.6 x 10^{-6}[16]	0.6 x 10^{-8}	47.2[11]
$C_{12}E_6$	2.0 x 10^{-8}	0.1 [11]	3.8 ± 0.6 x 10^{-6}[16]	1.0 x 10^{-8}	45.0[11]

Recognizing that the value of the surfactant diffusion coefficient, D, was found to be the most sensitive of the three inputs (see Appendix 5.B), the new methodology was used separately using the nominal value of D, as well as the upper and the lower bound values of D, reported in Table 5.1. For both $C_{12}E_4$ and $C_{12}E_6$, validation of the predicted ESTC behavior was carried out by : (a) comparing the predicted ESTC behavior with experimental equilibrium surface tension data, (b) comparing the EOS corresponding to the predicted ESTC behavior with experimental surface-expansion data, and (c) using the predicted ESTC behavior to predict the DST behavior at several other C_b values, and then comparing the predicted DST with the experimentally measured DST.

Equilibrium Surface Tension versus Surfactant Bulk Solution Concentration (ESTC) Behavior

Figures 5-2(a) and 5-2(b) compare the ESTC behavior predicted using the new methodology with the experimental equilibrium surface tension measurements reported in Refs.[11] and [12] for $C_{12}E_4$ and $C_{12}E_6$, respectively. In both Figures 5-2(a) and 5-2(b), the solid, dashed, and dotted lines correspond to the ESTC behaviors predicted using the new methodology with the nominal, upper, and lower bound values of D, respectively, and the filled circles correspond to the experi-
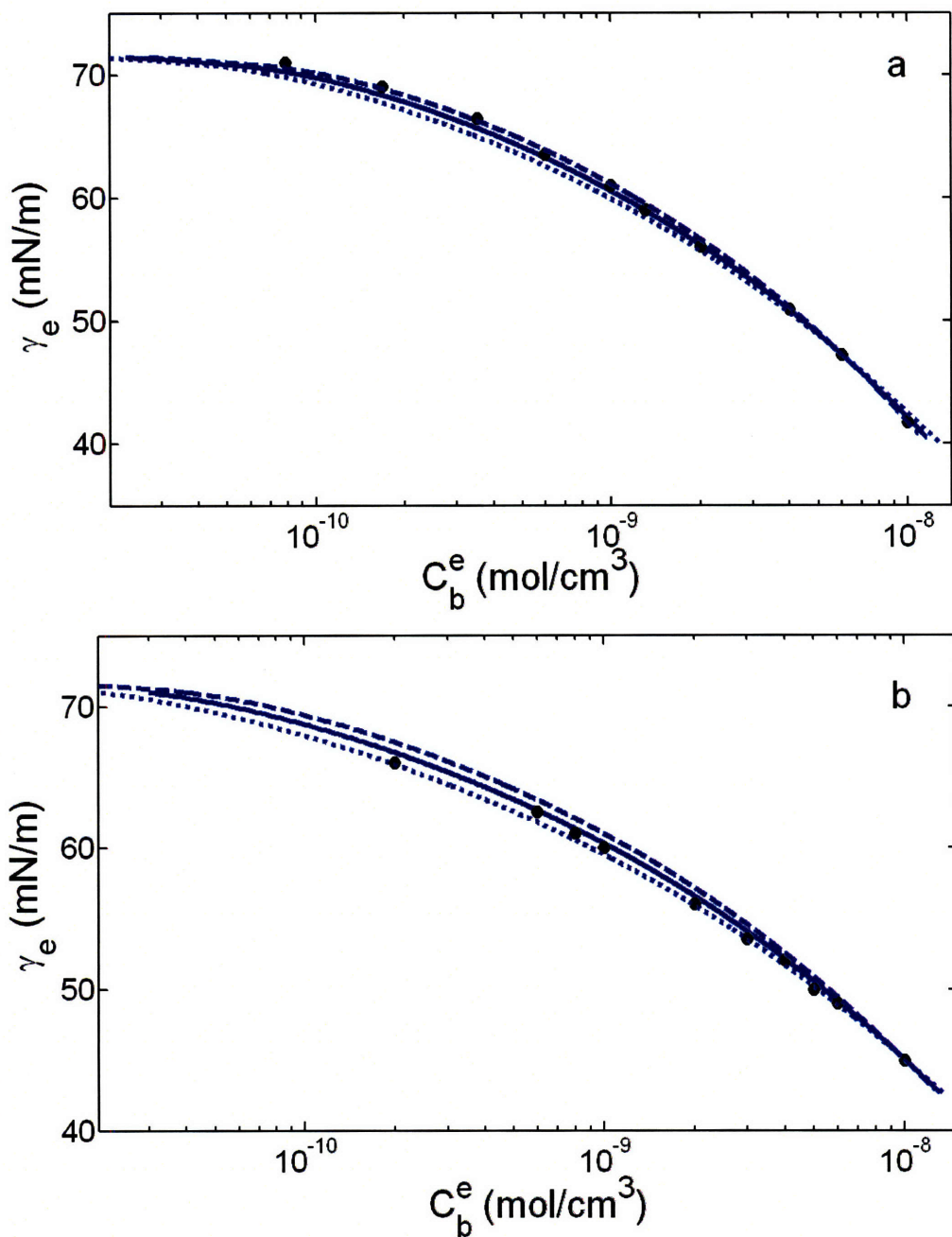
Figure 5-2: Comparison of the ESTC behavior predicted using the new methodology with the experimental equilibrium surface tension data for: (a) $C_{12}E_4$ and (b) $C_{12}E_6$. The filled circles in (a) and (b) correspond to the experimental equilibrium surface tension data reported in Refs. [11] and [12], respectively. In both (a) and (b), the solid lines correspond to the ESTC behavior predicted using the nominal values of D, the dashed lines correspond to the higher bound values of D, and the dotted lines correspond to the lower bound values of D.

193

mental equilibrium surface tension data. Figures 5-2(a) and 5-2(b) indicate that for both $C_{12}E_4$ and $C_{12}E_6$, there is very good agreement between the ESTC behavior predicted using the new methodology and the experimental equilibrium surface tension values. Specifically, consider the predicted ESTC curves corresponding to the nominal values of D for $C_{12}E_4$ and $C_{12}E_6$. Note that the nominal D values used for $C_{12}E_4$ (3.9 x 10^{-6} cm^2/s) and for $C_{12}E_6$ (3.8 x 10^{-6} cm^2/s) are in close agreement with the measured D value for a structurally similar solute $C_{12}E_5$ (3.9 x 10^{-6} cm^2/s) [17]. Figures 5-2(a) and 5-2(b) reveal that the maximum deviation between the predicted ESTC behavior corresponding to the nominal value of D and the experimental equilibrium surface tension value is only about 0.4 mN/m for both $C_{12}E_4$ and $C_{12}E_6$. Note that the existing procedure to determine the ESTC curve requires measuring the equilibrium surface tension at several specific C_b values, which makes its use tedious and time consuming. On the other hand, the new methodology presented here requires only the experimental DST data measured at a single C_b value and one experimental equilibrium surface tension value measured at a single $C_{b,1}$ value in order to predict the ESTC curves shown in Figures 5-2(a) and 5-2(b).

Equation of State (EOS)

The EOS corresponding to the predicted ESTC is determined by applying the Gibbs adsorption equation (Eq.(5.8)) to the ESTC curves predicted in Figures 5-2(a) and 5-2(b). The EOS predicted for $C_{12}E_4$ and $C_{12}E_6$ for each of the ESTC curves corresponding to the nominal, the upper, and the lower bound values of D are shown in Figure 5-3. In Figure 5-3, the black lines correspond to the EOS of $C_{12}E_4$, and the blue lines correspond to the EOS of $C_{12}E_6$, where the solid lines correspond to the nominal values of D, and the dashed and dotted lines correspond to the upper and the lower bound values of D, respectively.

Figure 5-3 reveals that for both $C_{12}E_4$ and $C_{12}E_6$ the predicted EOS corresponding to a higher D value is higher than that corresponding to a lower D value. Note that for a high value of D, surfactant adsorption occurs faster, and the dynamic surfactant surface concentration, $\Gamma(t)$, is higher than that corresponding to a lower D value. Therefore, for a given input experimental DST data, the new methodology presented here reduces the ability of $\Gamma(t)$ to decrease the surface tension when $\Gamma(t)$ increases at a faster rate, while it increases the ability of $\Gamma(t)$ to decrease the surface tension when $\Gamma(t)$ increases at a slower rate. This, in turn, ensures that the resulting rate

194
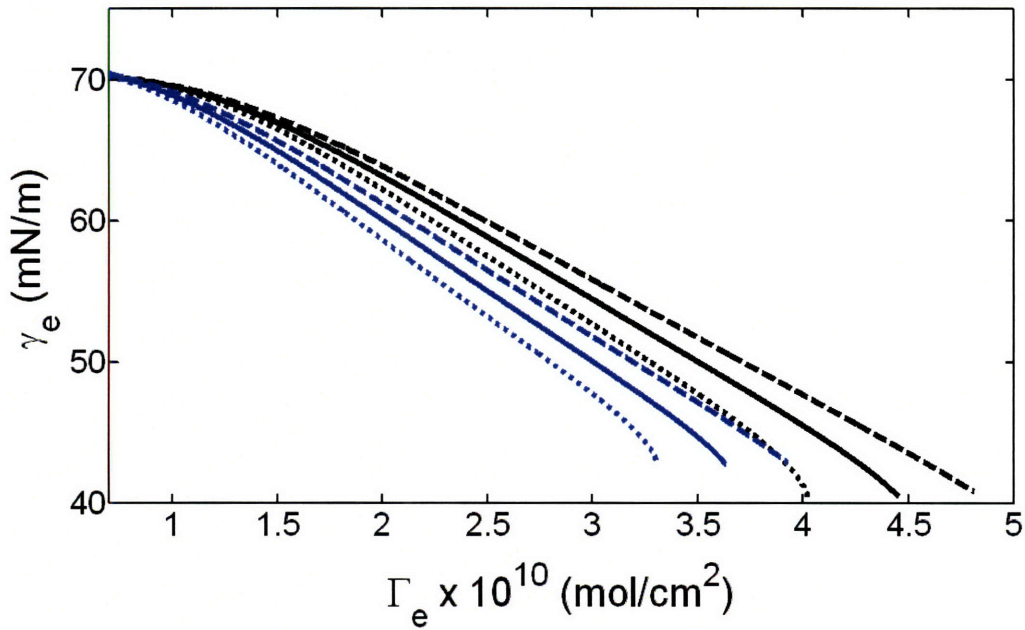
Figure 5-3: Comparison of the EOS predicted using the new methodology for $C_{12}E_4$ and $C_{12}E_6$. The various black lines correspond to the EOS of $C_{12}E_4$ and the various blue lines correspond to the EOS of $C_{12}E_6$. For both $C_{12}E_4$ and $C_{12}E_6$, the solid, dashed, and dotted lines correspond to the EOS obtained using the nominal, upper, and lower bound values of D, respectively.

of surface tension reduction agrees with the experimental DST data. Accordingly, the EOS is higher (that is, γ_e is larger) when D is larger (see the black and blue dashed lines in Figure 5-3).

I have validated the EOS of $C_{12}E_4$ and $C_{12}E_6$ predicted using the new methodology by comparing these EOS with the surface-expansion measurements for $C_{12}E_4$ and $C_{12}E_6$ reported in Refs.[11] and [12], respectively. Note that surface-expansion measurements relate γ_e to Γ_e/Γ_{ref}, where Γ_{ref} is a reference value for the equilibrium surfactant surface concentration which is typically chosen as $\Gamma_e(\gamma_{ref})$ corresponding a reference value γ_{ref}. The experimental surface-expansion measurements for $C_{12}E_4$ and $C_{12}E_6$ reported in Ref.[11] and [12] are plotted as filled circles in Figures 5-4(a) and 5-4(b), respectively, where $\Gamma_{ref} = \Gamma_e(\gamma_{ref} = 64\text{mN/m})$ for $C_{12}E_4$ and $\Gamma_{ref} = \Gamma_e(\gamma_{ref} = 60 \text{ mN/m})$ for $C_{12}E_6$. The relation between γ_e and Γ_e/Γ_{ref}, corresponding to the predicted EOS for $C_{12}E_4$ and $C_{12}E_6$ in Figure 5-3, was determined by using the predicted value of $\Gamma_e(\gamma_{ref} = 64 \text{ mN/m})$ as Γ_{ref} for $C_{12}E_4$, and the predicted value of $\Gamma_e(\gamma_{ref} = 60 \text{ mN/m})$ as Γ_{ref} for $C_{12}E_6$. The predicted relation between γ_e and Γ_e/Γ_{ref} corresponding to the nominal, upper, and lower bound values of D are plotted as the solid, dashed, and dotted lines in Figures 5-4(a) and 5-4(b). Figures 5-4(a)
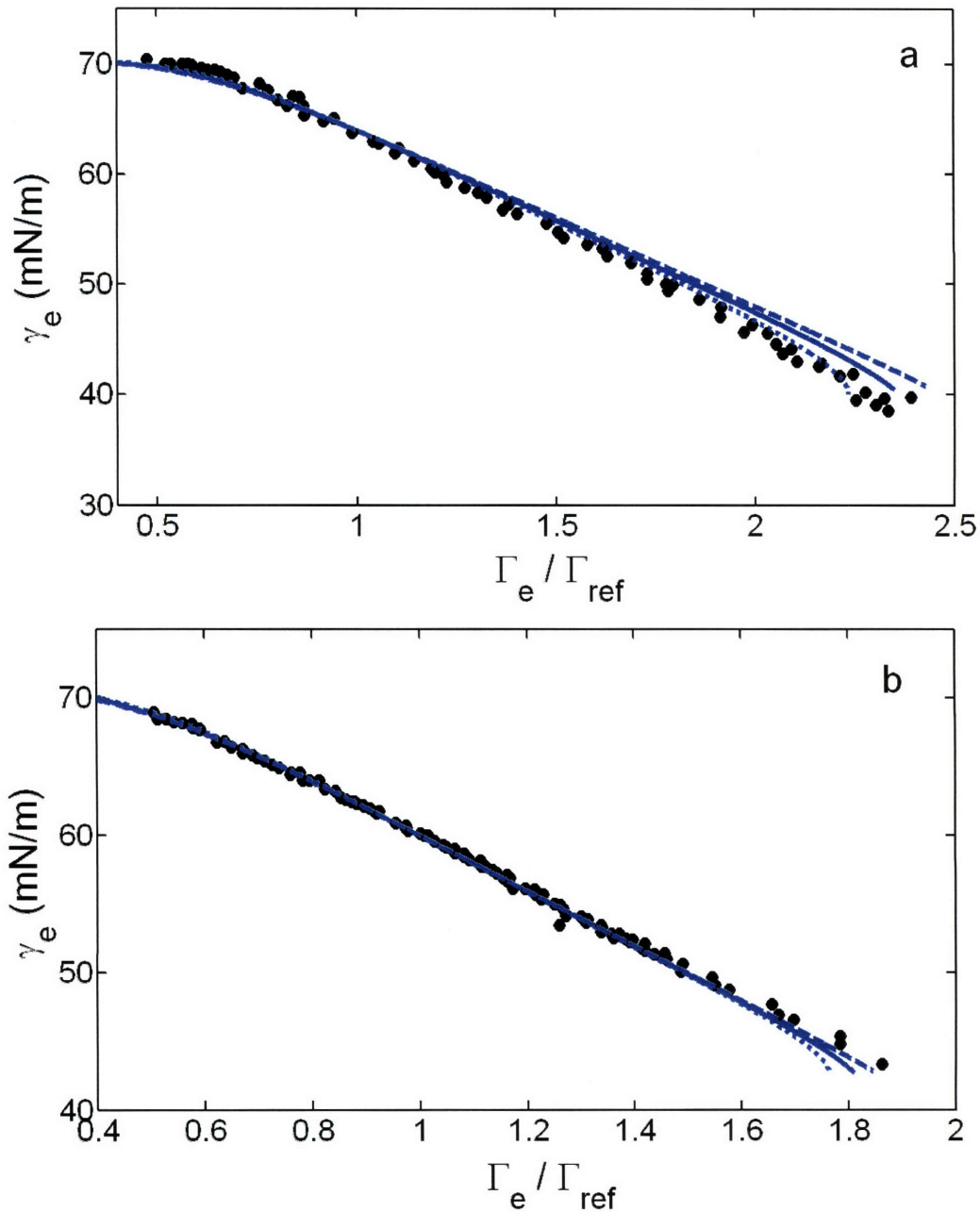
Figure 5-4: Comparison of the EOS information predicted using the new methodology with experimental surface-expansion measurements for: (a) $C_{12}E_4$ and (b) $C_{12}E_6$. The filled circles correspond to the experimental data, the solid lines correspond to the EOS information predicted using the nominal values of D, the dashed lines correspond to the EOS information predicted using the higher bound values of D, and the dotted lines correspond to the EOS information predicted using the lower bound values of D.

and 5-4(b) show that the EOS information predicted using the new methodology agrees very well with the results of the surface expansion measurements, thus validating the accuracy of the new methodology.

In addition, I conducted the following *qualitative* validation of the EOS predicted using the new methodology: Figure 5-3 shows that the EOS corresponding to $C_{12}E_6$ lies below the EOS corresponding to $C_{12}E_4$, except at large values of Γ where the $C_{12}E_6$ EOS corresponding to the upper bound of D appears to overlap with the $C_{12}E_4$ EOS corresponding to the lower bound of D (see the black dotted line and the blue dashed line). In other words, overall, Figure 5-3 reveals that for any given equilibrium surfactant surface concentration, Γ_e, $C_{12}E_6$ has a greater potential to reduce surface tension relative to $C_{12}E_4$. This observation is consistent with the expected trend based on the nature of the interactions between the adsorbed C_iE_j nonionic surfactant molecules. Specifically, consider the molecular-based theoretical framework to model the equilibrium adsorption isotherm behavior of the adsorbed C_iE_j nonionic surfactant molecules presented in Ref.[18]. According to this theoretical framework, the interactions between the C_i hydrocarbon tails of the adsorbed C_iE_j surfactant molecules are modeled in terms of attractive van der Waals interactions, and the interactions between the E_j heads of the adsorbed C_iE_j surfactant molecules are modeled in terms of repulsive hard-disc interactions. In this theoretical description, as the size of the E_j head increases, for a given C_i tail, the repulsive interactions between the adsorbed C_iE_j surfactant molecules become stronger. As a result, for a given surfactant surface concentration, Γ_e, $C_{12}E_6$ produces a higher surface pressure ($\gamma_{w/a} - \gamma_e$) than that produced by $C_{12}E_4$ [18]. Consequently, for a given Γ_e value, $C_{12}E_6$ induces a greater reduction in surface tension than that induced by $C_{12}E_4$, a prediction which is consistent with the results shown in Figure 5-3.

DST Predictions at other Surfactant Bulk Solution Concentrations

Recall that the new methodology presented here uses the DST data measured at a *single* C_b value in order to predict the ESTC behavior. Therefore, I have further tested the ESTC behavior predicted using the new methodology by predicting the DST behavior at other C_b values, and subsequently, by comparing the predicted DST profiles with the corresponding experimentally measured DST data for both $C_{12}E_4$ and $C_{12}E_6$.

The ESTC behavior corresponding to the nominal values of D for both $C_{12}E_4$ and $C_{12}E_6$ pre-

197

dicted using the new methodology (see Figures 5-2(a) and 5-2(b)) was used to predict DST profiles at several C_b values assuming a diffusion-controlled adsorption model. In Figures 5-5 and 5-6, I compare the predicted DST profiles for $C_{12}E_4$ and $C_{12}E_6$ with the experimental DST data reported in Ref.[11] and [12], respectively. Specifically, Figure 5-5 compares the predicted DST profiles with the experimental DST data for $C_{12}E_4$ at: (a) 2.0 x 10^{-8} mol/cm^3, (b) 1.0 x 10^{-8} mol/cm^3, (c) 0.6 x 10^{-8} mol/cm^3, and (d) 0.4 x 10^{-8} mol/cm^3, and Figure 5-7 compares the predicted DST profiles with the experimental DST data for $C_{12}E_6$ at: (a) 2.0 x 10^{-8} mol/cm^3, (b) 1.3 x 10^{-8} mol/cm^3, (c) 0.6 x 10^{-8} mol/cm^3, and (d) 0.2 x 10^{-8} mol/cm^3. In both Figures 5-5 and 5-6, the solid lines correspond to the predicted DST profiles and the filled circles correspond to the experimental DST data.
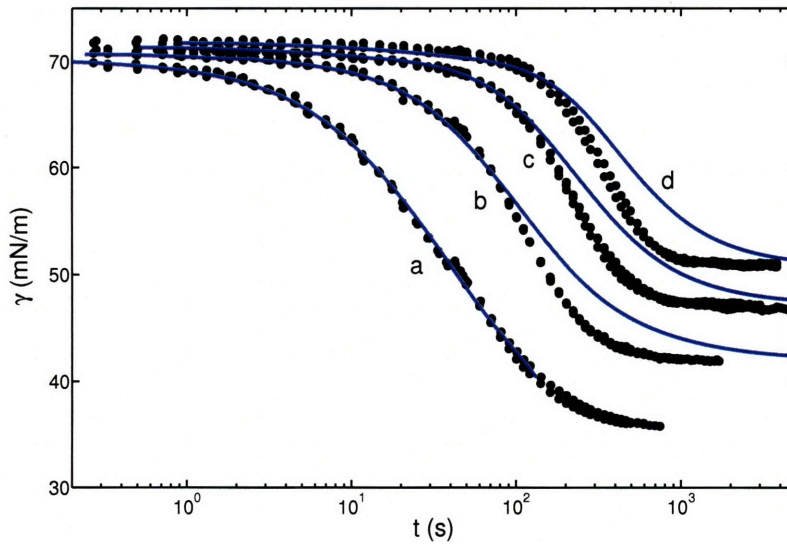
Figure 5-5: Comparison of the predicted dynamic surface tension, $\gamma(t)$, as a function of time, t, using the diffusion-controlled adsorption model and the ESTC behavior deduced using the new methodology with the experimentally measured DST data for $C_{12}E_4$ at: (a) 2.0 x 10^{-8} mol/cm^3, (b) 1.0 x 10^{-8} mol/cm^3, (c) 0.6 x 10^{-8} mol/cm^3, and (d) 0.4 x 10^{-8} mol/cm^3. In the figure, the solid lines correspond to the predicted DST profiles and the filled circles correspond to the experimental DST data reported in Ref.[11].

Recall that the experimental DST data measured at C_b = 2.0 x 10^{-8} mol/cm^3 was originally used to predict the ESTC behavior of $C_{12}E_4$ and $C_{12}E_6$ using the new methodology (see Figures 5-1(a) and 5-1(b)). In Figures 5-5 (case (a)) and 5-6 (case (a)), I compare the DST predictions at this C_b value in order to verify if the predicted ESTC curve is indeed consistent with the original
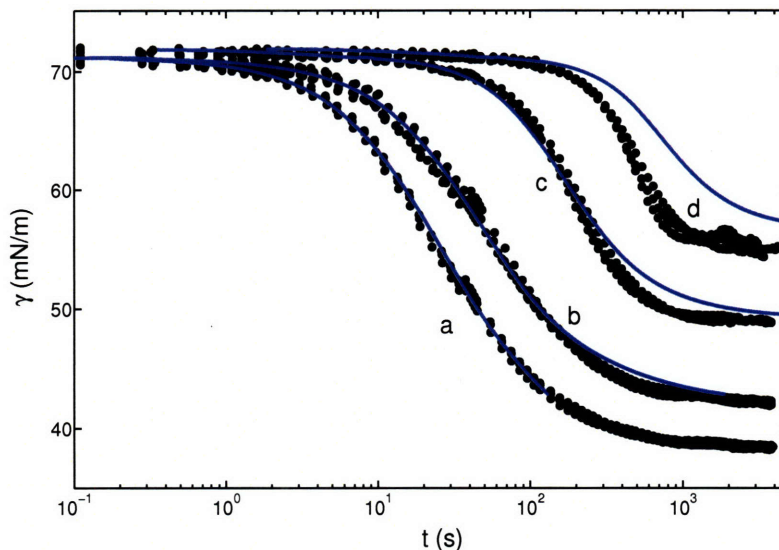
Figure 5-6: Comparison of the predicted dynamic surface tension, $\gamma(t)$, as a function of time, t, using the diffusion-controlled adsorption model and the ESTC behavior deduced using the new methodology with the experimentally measured DST data for $C_{12}E_6$ at: (a) 2.0 x 10^{-8} mol/cm^3, (b) 1.3 x 10^{-8} mol/cm^3, (c) 0.6 x 10^{-8} mol/cm^3, and (d) 0.2 x 10^{-8} mol/cm^3. In the figure, the solid lines correspond to the predicted DST profiles and the filled circles correspond to the experimental DST data reported in Ref.[12].

DST data used to generate the ESTC curve. As can be seen from Figures 5-5 (case (a)) and 5-6 (case (a)), the predicted DST profiles are indeed consistent with the original DST data. Additional comparison of the predicted DST profiles with the experimental DST data in Figures 5-5 and 5-6 for cases (b), (c), and (d) reveals the existence of *systematic deviations*, where the experimental DST data decreases faster with time than the DST predicted using to the diffusion-controlled adsorption model and the ESTC behavior deduced using the new methodology for t greater than about 100 to 200 seconds. Note that this finding is consistent with the results of the analysis presented in Chapter 4, where I hypothesized and demonstrated that the assumption of diffusive transport of surfactant molecules in the bulk solution may not be valid for $t > 100$ - 200 s due to the onset of natural convection. Keeping this important observation in mind, one should compare the predicted DST profiles with the experimentally observed DST behavior only when $t < 100$ - 200 s. A reexamination of Figures 5-5 and 5-6 for $t < 100$ - 200 s reveals that the predicted DST profiles for cases (b), (c), and (d) agree very well with the experimentally measured DST data for these three cases.

5.4 Conclusions

In this chapter, I explored a novel approach to determine equilibrium adsorption properties using experimental dynamic surface tension data and the known adsorption kinetics rate-limiting mechanism. Specifically, I developed a new methodology to determine the Equilibrium Surface Tension vs. surfactant bulk solution Concentration (ESTC) behavior of nonionic surfactants from experimental pendant-bubble DST when the adsorption kinetics is diffusion-controlled. Implementation of the new methodology requires the following inputs: (1) experimental DST data measured at a *single* surfactant bulk solution concentration, C_b, (2) the diffusion coefficient of the surfactant molecule, D, and (3) one equilibrium surface tension value measured at a single surfactant bulk solution concentration, $C_{b,1} < C_b$. Using inputs 1-3, the new methodology can be used to predict the *entire ESTC curve* applicable over a wide range of surfactant bulk solution concentrations. Note that the existing procedure to determine the ESTC behavior of surfactants requires performing tedious and time consuming equilibrium surface tension measurements at various C_b^e values, and then generating the best-fit curve that passes through the various experimental data points based on empirical model equations [1].

I demonstrated the applicability of the new methodology by predicting the ESTC curves of $C_{12}E_4$ and $C_{12}E_6$ using experimental pendant-bubble DST data reported in Ref.[11] and [12], respectively. For both $C_{12}E_4$ and $C_{12}E_6$, I validated the predicted ESTC curves by: (a) comparing the predicted ESTC with independent equilibrium surface tension measurements, (b) comparing the predicted equations of state associated with the predicted ESTC curves with surface-expansion measurements, and (c) predicting DST profiles at other C_b values and comparing the predicted DST profiles with the experimental DST data. I observed very good agreement between the predicted equilibrium adsorption behavior and the experimental measurements for (a) and (b) for both $C_{12}E_4$ and $C_{12}E_6$. For (c), while the predicted DST profiles agreed with the experimental DST data for t values less than about 100-200 seconds at all the C_b values considered, *systematic deviations* were observed at large values of t. These systematic deviations are similar to those observed in Chapter 4, where I hypothesized and demonstrated that the assumption of diffusive transport of surfactant molecules in the bulk solution may cease to be valid for t values which are greater than 100 - 200 s due to the onset of natural convection in the system. Overall, considering the agreement for (a) and

(b), and the agreement between the predicted DST profiles and the experimental DST data for $t <$ 100 - 200 s, I conclude that the new methodology presented in this chapter represents an efficient and reliable method to determine the equilibrium adsorption behavior of nonionic surfactants using experimental dynamic surface tension data.

In the next chapter, Chapter 6, I consider the problem of designing nonionic surfactant formulations that need to meet specific adsorption kinetics requirements, and develop a novel approach that involves the combined use of predictive dynamic surface tension models and optimization algorithms to identify the optimal surfactant formulations.

Appendix 5.A: Reliability of the New Methodology

In this appendix, I demonstrate the reliability of the new methodology by: (i) artificially generating experimental DST data corresponding to a specific ESTC model, (ii) applying the new methodology to the artificially generated DST data, and (iii) comparing the ESTC obtained using the new methodology with the ESTC that was used to artificially generate the DST data.

5.A.1 Generation of Artificial Experimental DST Data

To artificially generate the experimental DST data, consider the diffusion-controlled adsorption of a nonionic surfactant characterized by a 'representative' value of $D = 5.0 \times 10^{-6}$ cm^2/s onto a pendant bubble surface having a 'representative' radius $r_0 = 0.10$ cm [10]. Let the equilibrium adsorption behavior of the nonionic surfactant satisfy the Generalized Frumkin Equilibrium Adsorption Isotherm (EAI), that is:

$$\frac{\Gamma_e}{\Gamma_\infty} = x = \frac{C_b^e}{C_b^e + a \exp(Kx^n)} \tag{5.A.1}$$

where $\Gamma_\infty = 5.0 \times 10^{-10}$ mol/cm^2, $a = 2.0 \times 10^{-10}$ mol/cm^3, $K = 2.0$, and $n = 0.5$, which correspond to typical parameter values of several $C_i E_j$ nonionic surfactants [10], and Γ_e is the equilibrium surfactant surface concentration corresponding to the surfactant bulk solution concentration C_b^e. The EOS corresponding to the Generalized Frumkin EAI in Eq.(5.A.1) is given by [10]:

$$\gamma_{w/a} - \gamma_e = -\Gamma_\infty RT \left[\log(1 - x) - \frac{Knx^{n+1}}{1 + n} \right] \tag{5.A.2}$$

where $\gamma_{w/a}$ is the surface tension of the water/air surface taken to be 72.0 mN/m at $T = 298$ K, R is the gas constant = 8.314 J/(mol· K), and γ_e is the equilibrium surface tension corresponding to Γ_e.

Assuming a trace quantity for the initial amount of adsorbed surfactant molecules at the pendant-bubble surface, $\Gamma_0 = 2.0 \times 10^{-11}$ mol/cm^2 (corresponding to the value $\gamma_0 = 71.5$ mN/m which is typically observed in experimental pendant-bubble DST data), a DST profile can be generated at an initial surfactant bulk solution concentration of $C_b = 3.0 \times 10^{-8}$ mol/cm^3. Since the measure-

ment of DST typically involves determining the surface tension at specific t values, DST values are obtained for specific t values from the generated DST profile. With this in mind, the t values used to generate the artificial experimental DST data were obtained by generating random numbers satisfying a uniform distribution in the range -1 to 2 in the $\log t$ axis, corresponding to t values in the range of 0.1 s to 100 s. Note that this range of t values was selected keeping in mind that:

- The shortest time encountered in typical DST measurements using the pendant-bubble apparatus is about 0.1 s.

- The time scale associated with the validity of the assumption of diffusive transport of the surfactant molecules in the bulk solution for a pendant-bubble apparatus was found to be about 100 to 200 seconds (see Chapter 4).

In order to generate a realistic artificial representation of the actual experimental DST data, random errors were introduced in the generated DST values. For this purpose, random numbers were generated that satisfy a normal distribution with a mean value of 0, and a standard deviation value of 0.3. A value of 0.3 was chosen since the typical reproducibility of the DST measurements using the pendant-bubble apparatus is about 0.3 mN/m [14]. The artificially generated experimental DST data is shown as the filled circles in Figure 5-7. For a description of the two lines shown in Figure 5-7, see Section 5.A.2 below.

5.A.2   Application of the New Methodology

Recall that the application of the new methodology requires solving Eq.(5.10) for $C_s(t)$ given the following three inputs (for details, see Section 5.2.1):

1. The dynamic surface tension, $\gamma(t)$, at a single known initial surfactant bulk solution concentration, C_b.

2. The diffusion-coefficient, D, of the surfactant molecule.

3. A single equilibrium surface tension data point $(C_{b,1}, \gamma_{b,1}^e)$, where $C_{b,1} < C_b$.

Note that while the experimental DST data is measured at specific t values, the numerical solution of Eq.(5.10) requires inputting $\gamma(t)$ at t values which can be arbitrarily close. For this purpose, one needs to interpolate the experimental DST data to obtain $\gamma(t)$ at t values for which
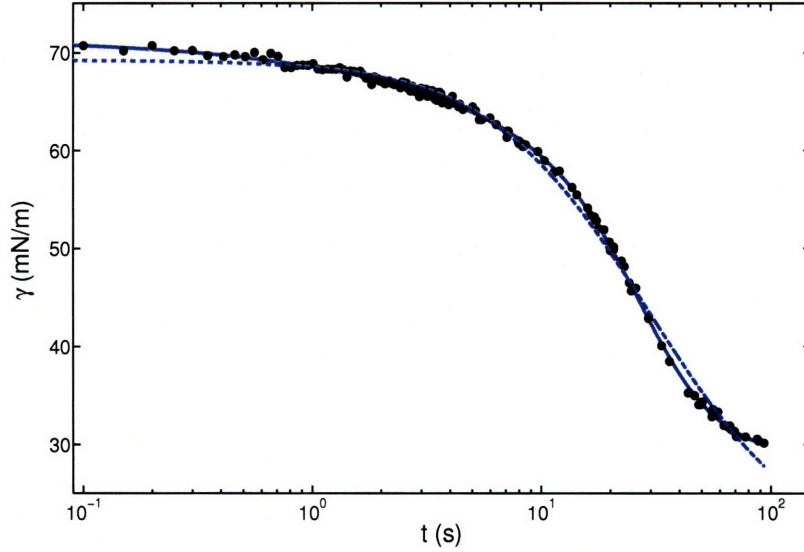
Figure 5-7: Functional form representation of the artificially generated experimental DST data: A comparison between the artificially generated experimental DST data, the best-fit corresponding to the modified Rosen functional form, Eq.(5.A.3), and the best-fit corresponding to the Rosen functional form, Eq.(5.A.4). The filled circles correspond to the artificially generated experimental DST data, the solid line corresponds to the best-fit of the modified Rosen functional form, and the dashed line corresponds to the best-fit of the Rosen functional form.

the experimental DST values are not available. Specifically, I have regressed the experimental DST data with a known functional form for the DST, and have subsequently used the regressed function as input 1 in the new methodology. To regress the artificially generated experimental DST data shown in Figure 5-7, I have used the following parameterized functional form of the DST:

$$\frac{\gamma_0 - \gamma(t)}{\gamma(t) - \gamma_e} = \frac{1}{2}\left[\left(\frac{t}{t^*}\right)^{n_1} + \left(\frac{t}{t^*}\right)^{n_2}\right] \tag{5.A.3}$$

having five parameters: γ_0, γ_e, t^*, n_1, and n_2. Note that the functional form in Eq.(5.A.3) is inspired by the work of Rosen and co-workers who conducted extensive DST measurements for several nonionic and ionic surfactants, including their mixtures, and observed that the following parameterized functional form yielded a good fit of the experimental DST behavior for all the surfactant systems that they considered [19–23]:

$$\frac{\gamma_0 - \gamma(t)}{\gamma(t) - \gamma_e} = \left(\frac{t}{t^*}\right)^{n_1} \tag{5.A.4}$$

In the case of the artificially generated experimental DST data, the functional form in Eq.(5.A.4)[1] did not result in a good fit, as shown by the dashed line in Figure 5-7. However, by adding the parameter n_2 to the original Rosen functional form (see Eq.(5.A.3)[2]) an excellent fit was obtained, as shown by the solid line in Figure 5-7. Quantitatively, the standard deviation of the residuals for the best-fit corresponding to the original Rosen functional form is 0.79 mN/m, while it is only 0.32 mN/m for the modified Rosen functional form. Note that the value of the standard deviation of the residuals for the modified Rosen functional form (0.32 mN/m) is consistent with the value of 0.3 mN/m associated with the standard deviation of the measurement errors used to artificially generate the experimental DST data.

It is important to recognize that the actual functional form used to represent the experimental DST data is arbitrary, as long as the chosen functional form and the resulting best-fit capture the essential features of the experimental DST behavior[3]. The effect of the DST measurement errors on the predicted ESTC is investigated in Appendix B.1.

The new methodology was applied using: (1) the best-fit DST curve corresponding to the modified Rosen functional form as input 1, (2) $D = 5.0 \times 10^{-6}$ cm^2/s as input 2, and (3) $\gamma_{b,1}^e = 38.4$ mN/m at $C_{b,1} = 1.0 \times 10^{-8}$ mol/cm^3 as input 3. Figure 5-8 compares the ESTC behavior predicted using the new methodology with the original ESTC model used to artificially generate the DST data. In the figure, the solid line corresponds to the ESTC predicted using the new methodology, the dashed line corresponds to the original ESTC model used to artificially generate the experimental DST data, and the filled circle corresponds to the single equilibrium surface tension data point $(C_{b,1}, \gamma_{b,1}^e)$ used as input 3. Figure 5-8 clearly shows that the *entire ESTC curve* predicted using the new methodology is consistent with the original ESTC used to artificially generate the experimental DST data. In fact, the maximum difference between the equilibrium surface tension, γ_e, using the predicted ESTC and using the original ESTC is only about 0.2 mN/m.

---

[1]Hereafter, Eq.(5.A.4) will be referred to as the *Rosen functional form*.

[2]Hereafter, Eq.(5.A.3) will be referred to as the *modified Rosen functional form*.

[3]I have also implemented the new methodology using other functional forms like a 13-degree polynomial ,and found that it did not result in any significant difference with the ESTC curve predicted using the modified Rosen functional form.
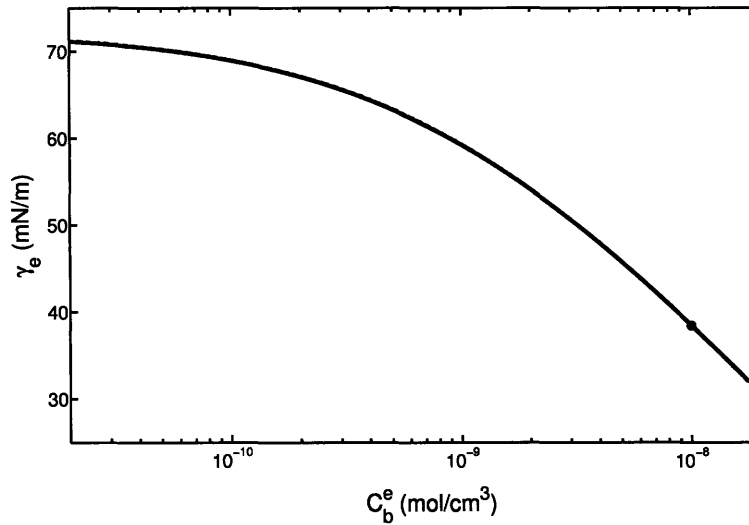
Figure 5-8: Comparison of the ESTC predicted by applying the new methodology to the artificially generated experimental DST data with the ESTC model that was originally used to artificially generate the experimental DST data. The solid line corresponds to the ESTC predicted using the new methodology, the dashed line corresponds to the original ESTC, and the filled circle corresponds to the single equilibrium surface tension data point used as input 3.

5.A.3 Comment on the Value of $C_b^e(\gamma_0)$

In implementing the new methodology using the artificially generated experimental DST data, I find that the numerical solution of Eq.(5.10) depends strongly on the initial value of C_s, $C_s(t = 0) = C_b^e(\gamma_0)$. This is because the numerical solution of Eq.(5.10) requires recursively solving for the value of the surfactant sub-surface concentration $(C_s(t_n))$ at the nth time step (t_n), based on all the previously computed values of C_s from $C_s(t = 0)$ to $C_s(t_{n-1})$, starting from $n = 1$. Therefore, any error in the initial value, $C_s(\gamma_0)$, gets amplified as the time step index, n, increases. As a result, the resulting ESTC curve depends strongly on the value of $C_b^e(\gamma_0)$. However, specifying the single equilibrium surface tension data point, $(C_{b,1}, \gamma_{b,1}^e)$ (see input 3), helps to 'pin-down' the resulting ESTC curve by adjusting for the value of $C_b^e(\gamma_0)$ appropriately.

Based on the results of the analysis presented in this Appendix, I conclude that the new methodology presented in this chapter can be used to reliably predict the ESTC behavior using: (1) the experimental DST data measured at a single surfactant bulk solution concentration using the pendant-bubble apparatus, (2) the diffusion coefficient of the surfactant molecule, and (3) a single equilibrium surface tension data point.

206

Appendix 5.B: Sensitivity Analysis of the ESTC to the Three Inputs Used

In this Appendix, I investigate the sensitivity of the ESTC curve predicted using the new methodology to typical uncertainties in each of the three inputs in the context of the artificial experimental DST data examined in Appendix A. Such a sensitivity analysis assists in identifying those inputs that most significantly affect the ESTC curve predicted using the new methodology, as well as in determining confidence regions for the predicted ESTC curve. Specifically, I have investigated the sensitivity of each input by determining the extent to which the ESTC curve shifts as each input is varied over a relevant range of values, while the other inputs remain constant.

5.B.1 Sensitivity to Input 1: Dynamic Surface Tension, $\gamma(t)$

Note that the input DST, $\gamma(t)$, is a *function*, and therefore, the sensitivity analysis should consider a *set of functions* that form acceptable representations of the experimental DST data. One useful procedure to perform a sensitivity analysis of functions is to consider the original function as a combination of a set of basis functions, and to perform a regular sensitivity analysis of the weights of each basis function over a range of values [24]. Keeping this procedure in mind, I have performed a sensitivity analysis of the input DST with respect to each of the 5 parameters of the modified Rosen functional form (see Eq.(5.A.3)). In other words, I have performed the sensitivity analysis of the input DST function, $\gamma(t)$, by: (i) generating a set of acceptable representations of the input DST, and (ii) determining how the predicted ESTC curve shifts for each of the representations of the input DST. Using an approach which is analogous to the basis function approach, I have generated the set of acceptable representations of the input DST by varying the five parameters of the modified Rosen functional form separately.

Determining the Range of the Five Parameter Values

Note that as the value of each of the five parameters in Eq.(5.A.3) changes, it generates different DST profiles to represent the experimental DST data. In order to determine acceptable ranges for the variation of each of the five parameters in Eq.(5.A.3), I have:

1. Estimated the error in the experimental DST data using the standard deviation of the residuals

corresponding to the best-fit modified Rosen functional form, ϵ.

2. Considered a prediction envelope defined as $\pm\ \epsilon$ about the best-fit DST profile.

3. Found the limiting value of each parameter when the predicted DST profile falls just outside the envelope defined in item 2, by varying each of the five parameters of Eq.(5.A.3) separately (keeping the remaining four parameters at their best-fit value).

In other words, I have considered all the DST profiles that fall within the estimated magnitude of error in the experimental DST data as acceptable representations of the experimental DST data, and generated different representative DST profiles by separately varying each of the five parameters.

In the case of the artificial experimental DST data, keeping in mind that the standard deviation of the residuals was estimated to be 0.32 mN/m (see Appendix A), the prediction envelope is defined as $\gamma(t) = \gamma_{\text{Best-Fit}}(t) \pm 0.32$ mN/m. The best-fit values of the five parameters, as well as the range of values over which each of the five parameters can vary such that the resulting DST profiles lie within the defined prediction envelope, are reported in Table 5.2. Subsequently, DST

Table 5.2: The best-fit values of the five parameters of the modified Rosen functional form (Eq.(5.A.3)) used to represent the artificial experimental DST data, and the lower and upper limit values over which each of these parameters can vary such that the resulting DST profiles lie within a prediction envelope defined by $\gamma_{\text{Best-Fit}} \pm 0.32$ mN/m.

Parameter	Nominal Value	Lower Limit	Upper Limit
γ_0	71.56	71.14	71.78
γ_e	29.45	29.13	29.77
t^*	20.10	19.80	20.40
n_1	2.74	2.66	2.82
n_2	0.65	0.61	0.69

profiles were generated for the lower and upper limiting values of each of the five parameters, that is, a total of 5x2 = 10 DST profiles. Following that, with each DST profile as an input (input 1), and using the nominal values for inputs 2 and 3, the ESTC curves were predicted. The ten DST profiles considered are shown as solid lines in Figure 5-9, where the filled circles correspond to the experimental DST data points. The ten ESTC curves predicted using each of the 10 DST profiles as input 1 are shown as solid lines in Figure 5-10, where the filled circle corresponds to
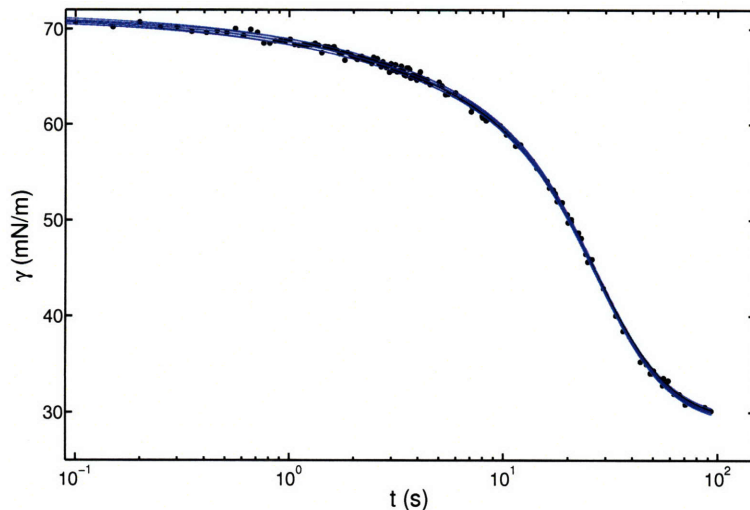
Figure 5-9: DST profiles generated by separately varying the five parameters of the modified Rosen functional form, Eq.(5.A.3), such that the resulting DST profile falls within the $\pm\epsilon$ prediction envelope. There are a total of 10 profiles corresponding to the upper and lower limits for each of the five parameters. The solid lines correspond to different limiting DST profiles, and the filled circles correspond to the artificial experimental DST data.
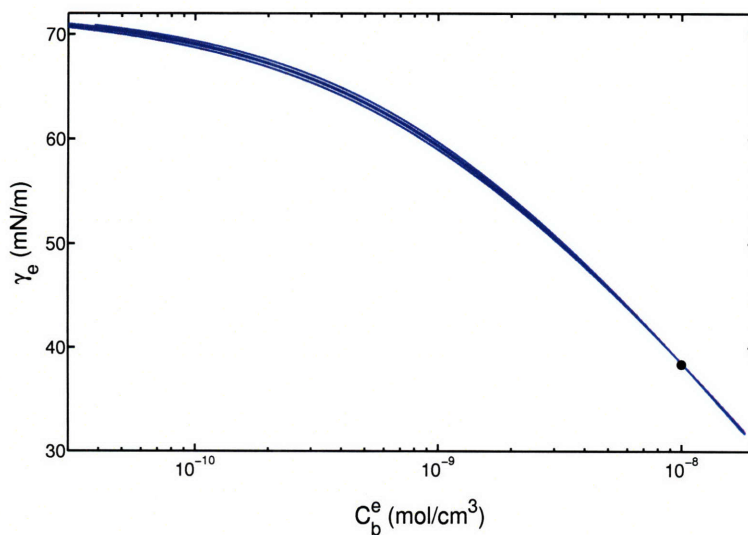
Figure 5-10: ESTC curves predicted using the new methodology for each of the ten different DST profiles shown in Figure 5-9. The solid lines correspond to the ten ESTC curves, and the filled circle corresponds to the single equilibrium surface tension data point used as input 3.

209

the single equilibrium surface tension data point used as input 3. Note that the ten DST profiles in Figure 5-9 appear to overlap because they deviate from the best-fit representation only by 0.32 mN/m. The ten ESTC curves shown in Figure 5-10, together, define the envelope of variability of the ESTC curve resulting from the measurement errors in the input experimental DST data considered. A quantitative examination of Figure 5-10 shows that accounting for a variability of $\pm\epsilon$ in the experimental DST measurements results in a shift of the ESTC curve by a maximum of about $\pm$ 0.5 mN/m.

5.B.2   Sensitivity to Input 2: The Surfactant Molecule Diffusion Coefficient, D

Note that estimates of the diffusion coefficient of surfactant molecules can vary by about ± 1.0 x 10^{-6} cm^2/s [11, 14]. Therefore, the sensitivity analysis of this input was carried out by varying the D value by ± 1.0 x 10^{-6} cm^2/s from the nominal value of 5.0 x 10^{-6} cm^2/s. Accordingly, I predicted the ESTC curves by applying the new methodology separately for $D = 4.0$ x 10^{-6} cm^2/s and $D = 6.0$ x 10^{-6} cm^2/s, and the results are shown in Figures 5-11. In the figure, the solid line
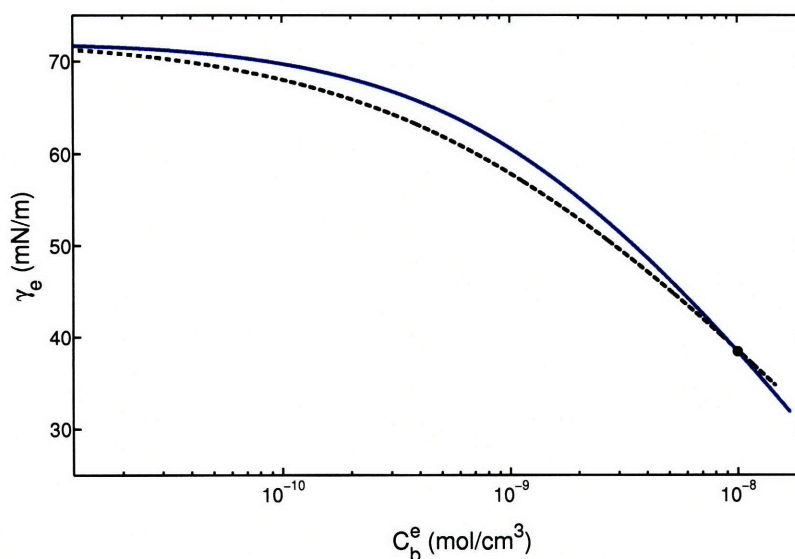
Figure 5-11: Effect of the value of the diffusion coefficient, D, (input 2) on the ESTC curve predicted using the new methodology. The solid line corresponds to the upper bound value value of $D = 6.0$ x 10^{-6} cm^2/s, the dashed line corresponds to the lower bound value of $D = 4.0$ x 10^{-6} cm^2/s, and the filled circle corresponds to the single equilibrium surface tension data point used as input 3.

corresponds to the upper bound value of $D = 6.0 \times 10^{-6}$ cm^2/s, the dashed line corresponds to the lower bound value of $D = 4.0 \times 10^{-6}$ cm^2/s, and the filled circle corresponds to the single equilibrium surface tension data point used as input 3. Figure 5-11 reveals that the ESTC curve corresponding to the upper bound value of D lies consistently above the ESTC curve corresponding to the lower bound value of D for $C_b^e < C_{b,1}$. This is because when D is higher, the sub-surface is replenished with surfactant molecules from the bulk solution interior at a higher rate leading to a larger value of $C_s(t)$. For a given input DST behavior (input 1), with a higher D value, the new methodology presented here reduces the effectiveness of the surfactant molecules to decrease the surface tension. As a result, the ESTC curve corresponding to the upper bound value of D lies above the ESTC curve corresponding to the lower bound value of D. Figure 5-11 shows that for the range of D values considered, the maximum variation in the predicted equilibrium surface tension, γ_e, is about $\pm$ 1.5 mN/m.

5.B.3 Sensitivity to Input 3: The Single Equilibrium Surface Tension Data Point

Note that the typical accuracy associated with measuring equilibrium surface tensions is about $\pm$ 0.3 mN/m [1]. Accordingly, the sensitivity analysis to input 4 was done by varying the single equilibrium surface tension data point used ($C_{b,1}^e = 1.0 \times 10^{-8}$ mol/cm^3, $\gamma_{b,1}^e = 38.4$ mN/m) by $\pm$ 0.3 mN/m. With this in mind, I predicted the ESTC curves using the new methodology separately for $\gamma_{b,1}^e = 38.7$ mN/m and for $\gamma_{b,1}^e = 38.1$ mN/m. The predicted ESTC curves are shown in Figure 5-12, where the solid line corresponds to the upper bound value of $\gamma_{b,1}^e = 38.7$ mN/m and the dashed line corresponds to the lower bound value of $\gamma_{b,1}^e = 38.1$ mN/m. Figure 5-12 reveals that the ESTC curves shift by a maximum of about $\pm$ 0.4 mN/m as $\gamma_{b,1}^e$ varies over the range of values considered.

In summary, the results of the sensitivity analysis presented in this Appendix show that the ESTC curve predicted using the new methodology is most sensitive to variations in the value of surfactant molecule diffusion coefficient, D (input 2), as quantified in terms of the maximum shift in the ESTC curve.
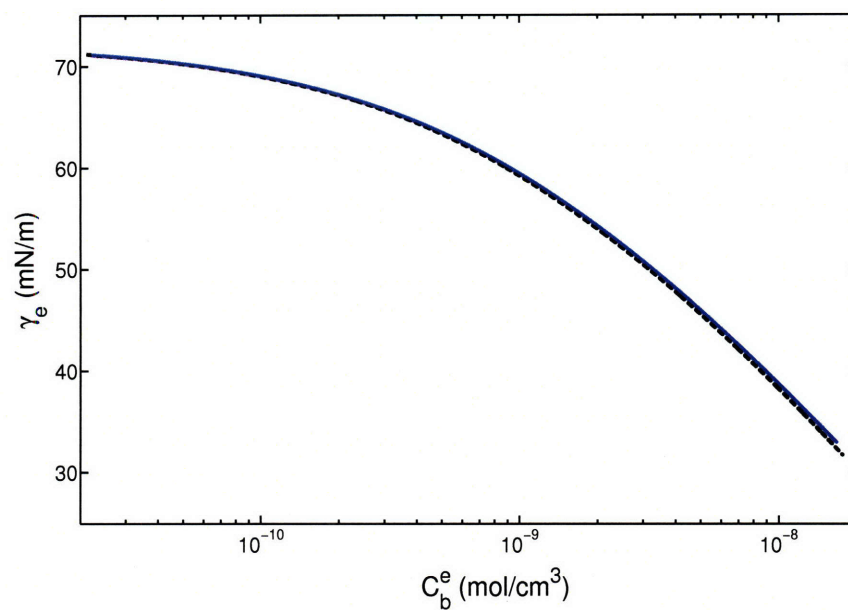
Figure 5-12: Effect of the value of the single equilibrium surface tension data point, $\gamma_{b,1}^e$, (input 3) on the ESTC curve predicted using the new methodology. The solid line corresponds to $\gamma_{b,1}^e = 38.7$ mN/m, and the dashed line corresponds to $\gamma_{b,1}^e = 38.1$ mN/m.

Bibliography

[1] M. J. Rosen. *Surfactants and Interfacial Phenomena*. Wiley Interscience, 1989.

[2] J.Eastoe, A.Rankin, R.Wat, and C. D. Bain. Surfactant adsorption dynamics. *International Reviews in Physical Chemistry*, 20(3):357–386, 2001.

[3] C-H. Chang and Elias I. Franses. Adsorption dynamics of surfactants at the air/water interface: a critical review of mathematical models, data, and mechanisms. *Colloids and Surfaces A: Physicochemical and Engineering Aspects*, 100:1–45, 1995.

[4] R. Miller, P. Joos, and V. B. Fainerman. Dynamic surface and interfacial tensions of surfactant and polymer solutions. *Advances in Colloid and Interface Science*, 49:249–302, 1994.

[5] J. Eastoe and J. S. Dalton. Dynamic surface tension and adsorption mechanisms of surfactants at the air-water interface. *Advances in Colloid and Interface Science*, 85:103–144, 2000.

[6] C-T. Hsu, C-H. Chang, and S-Y. Lin. Comments on the adsorption isotherm and determination of adsorption kinetics. *Langmuir*, 13:6204–6210, 1997.

[7] Y-C. Lee, S-Y. Lin, and H-S. Liu. Role of equation of state on studying surfactant adsorption kinetics. *Langmuir*, 17:6196–6202, 2001.

[8] S-Y. Lin, Y-C. Lee, M-J. Shao, and C-T. Hsu. A study on surfactant adsorption kinetics: The role of the data of equation of state for $C_{14}E_8$. *Journal of Colloid and Interface Science*, 244:372–376, 2001.

[9] R. Pan, J. Green, and C. Maldarelli. Theory and experiment on the measurement of kinetic

rate constants for surfactant exchange at an air/water interface. *Journal of Colloid and Interface Science*, 205:213–230, 1998.

[10] S-Y. Lin, Y-C. Lee, M-W Yang, and H-S Liu. Surface equation of state of nonionic C_mE_n surfactants. *Langmuir*, 19:3164 – 3171, 2003.

[11] C-T. Hsu, M-J. Shao, and S-Y. Lin. Adsorption kinetics of $C_{12}E_4$ at the air-water interface: Adsorption onto a fresh interface. *Langmuir*, 16:3187–3194, 2000.

[12] Y-C. Lee, S-Y. Lin, and M-J. Shao. Adsorption kinetics of $C_{12}E_6$ at the air-water interface. *Journal of Chinese Institute of Chemical Engineers*, 33(6):631–643, 2002.

[13] J. K. Ferri, S. Y. Lin, and K. J. Stebe. Curvature effects in the analysis of Pendant bubble data: Comparison of numerical solutions, asymptotic arguments, and data. *Journal of Colloid and Interface Science*, 241:154–168, 2001.

[14] S-Y. Lin, K. McKeigue, and C. Maldarelli. Diffusion-controlled surfactant adsorption studied by pendant drop digitization. *AIChE Journal*, 36:1785 – 1795, 1990.

[15] T. Gilanyi, I. Varga, M. Gilanyi, and R. Meszaros. Adsorption of poly(ethylene oxide) at the air/water interface: A dynamic and static surface tension study. *Journal of Colloid and Interface Science*, 301:428 – 435, 2006.

[16] S. N. Moorkanikkara and D. Blankschtein. New methodology to determine the rate-limiting adsorption kinetics mechanism from experimental dynamic surface tension data. *Journal of Colloid and Interface Science*, 302:1–19, 2006.

[17] W. S. Schonhoff and O. Soderman. Self-diffusion coefficients of some hydrocarbons in water: Measurements and scaling relations. *J. Phys. Chem. A*, 104:5892 – 5894, 2000.

[18] Y. J. Nikas, S. Puvvada, and D. Blankschtein. Surface tensions of aqueous nonionic surfactant mixtures. *Langmuir*, 8:2680–2689, 1992.

[19] X. Y. Hua and M. J. Rosen. Dynamic surface tension of aqueous surfactant solutions: 1. Basic parameters. *Journal of Colloid and Interface Science*, 124:652–659, 1988.

[20] M. J. Rosen and X. Y. Hua. Dynamic surface tension of aqueous surfactant solutions: 2. PARAMETERS at 1 s and at mesoequilibrium. *Journal of Colloid and Interface Science*, 139:397–407, 1990.

[21] X. Y. Hua and M. J. Rosen. Dynamic surface tension of aqueous surfactant solutions: 3. Some effects of molecular structure and environment. *Journal of Colloid and Interface Science*, 141:180–190, 1991.

[22] T. Gao and M. J. Rosen. Dynamic surface tensions of aqueous surfactant solutions: 6. Mixtures of different charge type surfactants. *Journal of Colloid and Interface Science*, 173:42–48, 1995.

[23] T. Gao and M. J. Rosen. Dynamic surface tensions of aqueous surfactant solutions: 7. Physical significance of the dynamic parameters and the induction period. *Journal of Colloid and Interface Science*, 172:242–248, 1995.

[24] D. G. Cacuci. *Sensitivity and Uncertainty Analysis*. CRC Press, 2003.

Chapter 6

New Theoretical Framework to Design Optimal Nonionic Surfactant Formulations that Exhibit a Desired Dynamic Surface Tension Behavior

6.1 Introduction

In Chapters 2-5, I developed several theoretical methodologies to address various *fundamental* aspects of the kinetics of surfactant adsorption. In this chapter, I consider the following *practical* aspect associated with the kinetics of surfactant adsorption: How to design optimal nonionic surfactant formulations for applications in which the surfactant adsorption kinetics plays a significant role. Applications like ink-jet printing [1], pesticide sprays [2], and foam and emulsion formation [3–5], all involve the rapid formation of fluid/fluid interfaces. Surfactants are used in these applications in order to stabilize the freshly-formed interfaces by adsorbing at a desired rate. In these applications, the kinetics of surfactant adsorption is expected to play a significant role in determining the performance and effectiveness of the surfactant formulations [6, 7]. The current procedure for designing surfactant formulations in these applications involves: (i) preparing several sample formulations by mixing the constituent surfactants at different concentrations, and (ii)

217

measuring the adsorption kinetics behavior of each individual sample formulation in order to screen for the formulations that are most efficient. Considering the large number of commercially available surfactant components (for example, alkyl poly(ethylene) oxide, C_iE_j, nonionic surfactants, n-alcohols, and sodium dodecyl sulfate) that can potentially be chosen to prepare the surfactant formulation, the time and effort required to design surfactant formulations that meet a desired adsorption kinetics behavior can be very significant. Furthermore, this trial-and-error experimental procedure does not guarantee identification of the most efficient or most economical surfactant formulation.

With the above in mind, in this chapter, I propose a new theoretical framework to identify the optimal nonionic surfactant formulation that most closely meets a desired adsorption kinetics behavior. Specifically, the new theoretical framework poses the design of the surfactant formulation as an *optimization problem* using predictive models, and finds the solution of the formulated optimization problem using numerical algorithms implemented in a commercial optimization package (see Figure 6-1).
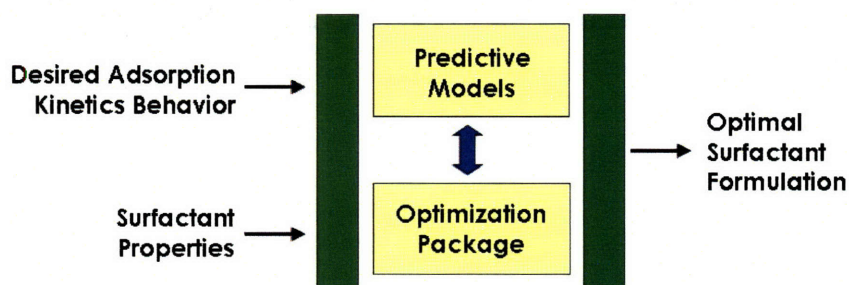
Figure 6-1: Proposed new theoretical framework for the design of optimal surfactant formulations.

The formulation of the optimization problem involves:

(i) Choosing an *objective function* that quantifies the deviation (or the agreement[1]) between the desired adsorption kinetics behavior and the adsorption kinetics behavior corresponding to a specific formulation condition.

(ii) Defining the optimization *decision variables* as the bulk solution concentrations of the individual surfactants comprising the formulation.

---

[1]If the objective function chosen quantifies the *deviation*, then the optimization problem is posed as a *minimization* problem. On the other hand, if the objective function chosen quantifies the *agreement*, then the optimization problem is posed as a *maximization* problem.

(iii) Relating the decision variables to the objective function using models that predict the adsorption kinetics behavior of formulations given the bulk solution concentrations of the individual surfactants comprising the formulation.

(iv) Including any *constraints* on the decision variables (see (ii) above) to account for model limitations on the concentrations of the individual surfactants comprising the formulation.

As proof of technical feasibility of the proposed new theoretical framework, I: (a) consider the problem of identifying the *nonionic* surfactant formulation that optimally satisfies a desired adsorption kinetics behavior specified in terms of a desired *dynamic surface tension profile*, (b) formulate the problem defined in (a) as an optimization problem using the Mulqueen-Stebe-Blankschtein (MSB) adsorption kinetics model[8], and (c) develop a framework to find the solution of the optimization problem formulated in (b) using the Sequential Nonlinear OPTimization (SNOPT) package [9]. In addition, I demonstrate the effectiveness of the new theoretical framework through a representative case study.

The remainder of this chapter is organized as follows. In Section 6.2, I develop the new theoretical framework to design optimal nonionic surfactant formulations that most closely meet a desired surfactant adsorption kinetics behavior. In Section 6.3, I demonstrate the reliability of the developed framework, and subsequently, I demonstrate its effectiveness by analyzing a representative case study. Finally, in Section 6.4, I summarize the main results of this chapter. In addition, in Appendix 6.A, I describe the evaluation of the objective function at a given set of values for the decision variables using the MSB adsorption kinetics model. Finally, in Appendix 6.B, I describe the calculation of the sensitivity of the objective function with respect to the decision variables.

6.2   Development of the New Theoretical Framework to Design Optimal Nonionic Surfactant Formulations that Most Closely Meet a Desired Surfactant Adsorption Kinetics Behavior

Consider the following *design problem*: If a nonionic surfactant formulation can be prepared by mixing a given set of nonionic surfactants, how does one identify the individual bulk solution concentrations of these surfactants that results in a Dynamic Surface Tension (DST) behavior that

optimally satisfies a desired DST profile? Let the desired (d) DST profile be $\gamma_d(t)$, and let the range of time over which the desired DST profile is specified be $t_L \le t \le t_U$, where L denotes lower and U denotes upper. Let the total number of nonionic surfactants used to prepare the formulation be n. With these specifications in mind, I: (i) formulate the above design problem as an optimization problem using the MSB adsorption kinetics model (Section 6.2.1), and (ii) find the optimal solution of the formulated optimization problem using SNOPT (Section 6.2.2).

6.2.1 Formulation of the Optimization Problem

The formulation of the optimization problem to address the design problem defined above using the MSB adsorption kinetics model involves the following four steps:

1. Choosing an *objective function* (M) that quantifies the deviation between the desired DST profile ($\gamma_d(t)$) and the DST profile corresponding to a specific surfactant mixture ($\gamma(t)$).

2. Defining a set of optimization *decision variables* that are related to the bulk solution concentrations of the n surfactants (see the section on Decision Variables below). For notational simplicity, let $\mathbf{C}_b$ denote the set of bulk solution concentrations of the n surfactants, that is,

$$\mathbf{C}_b = \{C_{b,1}, C_{b,2}, \ldots, C_{b,n}\} \tag{6.1}$$

where $C_{b,i}$ denotes the bulk solution concentration of surfactant i.

3. Using the MSB adsorption kinetics model to relate the decision variables to the objective function. Specifically, using the MSB adsorption kinetics model to first predict $\gamma(t)$ at the given $\mathbf{C}_b$, and then evaluating M using the predicted $\gamma(t)$.

4. Including *constraints* on the decision variables to account for limitations of the MSB adsorption kinetics model (see the section on Constraints on the Decision Variables below).

Objective Function

The goal of optimally satisfying the desired DST profile is expressed as the following objective function:

$$\min \; M = \int_{t_L}^{t_U} \left[\frac{\gamma_d(t) - \gamma(t)}{\gamma^*} \right]^2 w(t) \mathrm{d}t \tag{6.2}$$

220

where γ^* is a factor included to non-dimensionalize the term $(\gamma_d(t)-\gamma(t))$, and $w(t)$ is the weighting function.

The following points are noteworthy regarding the specific choice of the objective function in Eq.(6.2):

1. The objective function (M) measures the deviation between the desired DST profile $(\gamma_d(t))$ and the DST corresponding to a specific surfactant mixture $(\gamma(t))$. Therefore, by *minimizing* M, one determines the formulation conditions for which the deviation between $\gamma_d(t)$ and $\gamma(t)$ is minimum. Furthermore, M can also be interpreted as the continuous function-equivalent to the sum-of-squared-error minimization (which involves discrete points) performed in a typical regression analysis [10]. In other words, the objective function defined in Eq.(6.2) is equivalent to finding the formulation conditions for which the 'sum-of-squared-errors' between $\gamma_d(t)$ and $\gamma(t)$ is minimal.

2. The weighting function $w(t)$ accounts for the rate (logarithmic vs. linear) at which $\gamma_d(t)$ changes with time (t). In other words, if the desired $\gamma_d(t)$ inherently varies on the $\log(t)$ scale (which is typical of the DST behavior observed for surfactants), then, $w(t)$ can be chosen to be $1/[t\ln(10)]$. In this case, Eq.(6.2) becomes:

$$\min\ M = \int_{\log t_L}^{\log t_U} \left[\frac{\gamma_d(t) - \gamma(t)}{\gamma^*}\right]^2 \mathrm{d}\log t \tag{6.3}$$

The objective function in Eq.(6.3) has a clear physical interpretation: M is proportional to the area between the profiles $\gamma_d(t)$ and $\gamma(t)$, when these two profiles are plotted as a function of $\log(t)$. On the other hand, if $\gamma_d(t)$ varies on the linear t scale, then, $w(t)$ can be chosen to be a *constant* value, say, $1/t_U$, and Eq.(6.2) becomes:

$$\min\ M = \int_{t_L}^{t_U} \left[\frac{\gamma_d(t) - \gamma(t)}{\gamma^*}\right]^2 \frac{\mathrm{d}t}{t_U} \tag{6.4}$$

Note that this choice of $w(t)$ helps to retain the non-dimensional nature of the objective function. In addition, note that in this case, M is proportional to the area between the curves $\gamma_d(t)$ and $\gamma(t)$ when they are plotted on the linear t scale.

3. The factor γ^*, which is included in Eqs.(6.2) - (6.4) to non-dimensionalize the term $(\gamma_d(t) -$

$\gamma(t)$), is chosen to be a *constant*, recognizing that surface tension values typically vary on a *linear* scale (for example, from 72.0 mN/m to 35 mN/m).

Decision Variables

Since the original design problem involves identifying the optimal bulk solution concentrations of the n surfactants in the nonionic surfactant mixture, it follows that the optimization *decision variables* should be related to the bulk solution concentrations of the n surfactants, $\mathbf{C}_b$. However, it is not convenient to choose $\mathbf{C}_b$ as the actual decision variables for the following practical reason: The objective function (M) depends on the 'variable' $\gamma(t)$ (see Eq.(6.2)), which, in turn, depends on $\mathbf{C}_b$. For a typical surfactant, both the equilibrium and the dynamic surface tensions vary on a *linear* scale (for example, from 72 mN/m to 35 mN/m) as the surfactant bulk solution concentration varies on the *logarithmic* scale (for example, from 10^{-15} mol/cm^3 to 10^{-6} mol/cm^3) [11]. Since the objective function (M) in Eq.(6.2) is $\sim \mathcal{O}(\gamma(t)^2)$, the value of M can be expected to vary on a 'quadratic scale' as C_b varies on the logarithmic scale. However, note that the Sequential Quadratic Programming (SQP) algorithm that is implemented in the SNOPT package constructs a local *quadratic* relationship between the objective function and the decision variables while numerically finding the solution of the optimization problem [9]. Considering this numerical aspect, I have chosen the *logarithm* of the bulk solution concentrations of the n surfactants (denoted hereafter as $\log \mathbf{C}_b = \{\log C_{b,1}, \log C_{b,2}, \ldots, \log C_{b,n}\}$) as the optimization decision variables. Note that with this choice, the values of the decision variables vary on a linear scale (for example, from -15 to -6) rather than on the logarithmic scale (for example, from 10^{-15} mol/cm^3 to 10^{-6} mol/cm^3)^2, and that the objective function varies on the quadratic scale with respect to the decision variables.

Relation between the Decision Variables and the Objective Function

The evaluation of the objective function (M) for a given set of values of the decision variables ($\log \mathbf{C}_b$) requires knowing the dynamic surface tension ($\gamma(t)$) corresponding to the given $\log \mathbf{C}_b$ (see Eq.(6.2)). For this purpose, I have used the molecularly-based Mulqueen-Stebe-Blankschtein (MSB) adsorption kinetics model [8] to predict $\gamma(t)$ for a given $\log C_b$, and subsequently, have evaluated

---

^{2}Note that the optimal surfactant concentrations corresponding to the minimum value of M in Eq.(6.2) will not be affected by choosing $\log \mathbf{C}_b$ as the decision variables. This follows because the logarithm operator represents a continuous one-to-one mapping. In other words, since $\mathbf{C}_b$ and $\log \mathbf{C}_b$ form a *unique one-to-one relation*, if $\mathbf{C}_b^*$ is the optimal solution to Eq.(6.2) when $\mathbf{C}_b$ are chosen as the decision variables, then $\log \mathbf{C}_b^*$ is the optimal solution to Eq.(6.2) when $\log \mathbf{C}_b$ are chosen as the decision variables, and vice versa.

M using the predicted $\gamma(t)$ in Eq.(6.2). Note that the MSB adsorption kinetics model describes the adsorption kinetics of nonionic surfactant mixtures at premicellar surfactant concentrations [8]. The specific steps involved in evaluating M at a given $\log C_b$ using the MSB adsorption kinetics model are discussed in Appendix 6.A. The MSB adsorption kinetics model requires as inputs the following parameters for each surfactant i comprising the nonionic surfactant formulation: (i) a_i – the head cross-sectional area of surfactant i, (ii) B_{ij} ($j = 1, \ldots, n$) – the second virial coefficient[3] between surfactant i and surfactant j, (iii) $\Delta\bar{\mu}_i^0$ – the difference between the standard-state chemical potentials of surfactant i at the interface and in the bulk solution, and (iv) D_i – the diffusion coefficient of surfactant i.

Constraints on the Decision Variables

The MSB adsorption kinetics model considered here can be used to predict the adsorption kinetics behavior of nonionic surfactant mixtures only at *premicellar* surfactant concentrations[8]. Let $C_{b,i}^{\mathrm{u}}$ denote the upper bound value of $C_{b,i}$ ($i = 1, \ldots, n$) below which micelles do not form in the bulk solution, and let $\mathbf{C}_b^{\mathrm{u}} = \{C_{b,1}^{\mathrm{u}}, C_{b,2}^{\mathrm{u}}, \ldots, C_{b,n}^{\mathrm{u}}\}$ denote the set containing these values. Recalling that the decision variables were chosen as $\log \mathbf{C}_b$, the MSB adsorption kinetics model limitation is specified by the following *constraints*:

$$\log C_{b,i} \leq \log C_{b,i}^{\mathrm{u}}, \qquad i = 1, \ldots, n \tag{6.5}$$

Since there is no specific lower surfactant bulk solution concentration limit for the applicability of the MSB adsorption kinetics model[8], the lower bound values for $C_{b,i}$ ($i = 1, \ldots, n$) = 0. Accordingly, the lower bound for the chosen decision variables $\log \mathbf{C}_b$ are $-\infty$, or in other words, the decision variables $\log \mathbf{C}_b$ are unbounded from below.

Table 6.1 summarizes the various specifications associated with the formulation of the optimization problem.

6.2.2 Solution of the Formulated Optimization Problem Using SNOPT

The optimization problem formulated in Section 6.2.1 belongs to the class of *nonlinear* optimization problems since the decision variables and the objective function are related through the MSB

---

[3]Since B_{ij} accounts for *pairwise* interactions, $B_{ij} = B_{ji}$.

Table 6.1: List of specifications for the formulation of the optimization problem.

Optimization Problem Component	Specifications
Objective Function	Desired dynamic surface tension profile, $\gamma_d(t)$
	Non-dimensionalization factor, γ^*
	Weighting function, $w(t)$
	Lower time limit of interest, t_L
	Upper time limit of interest, t_U
Variables	Total number of nonionic surfactants, n
	MSB adsorption kinetics model parameters for each surfactant
Constraints	Upper bound surfactant bulk solution concentrations, $\mathbf{C}_b^u$

adsorption kinetics model which is nonlinear (see Appendix 6.A). Considering that the Sequential Nonlinear OPTimization (SNOPT) package has been shown to be effective in numerically solving several types of nonlinear optimization problems in a variety of areas [9], I have chosen the SNOPT package to find the optimal solution to the optimization problem formulated in Section 6.2.1. In essence, SNOPT incorporates the Sequential Quadratic Programming (SQP) algorithm to find the optimal solution through numerical iterations. A schematic of the implementation of the SNOPT package to find the solution of the optimization problem formulated in Section 6.2.1 is shown in Figure 6-2.

Optimization Problem Formulation

New Guess of the Optimal Solution

1. Objective Function (M)
2. Sensitivity (S)
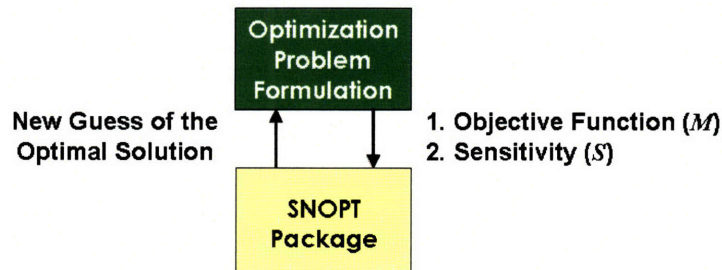
SNOPT Package

Figure 6-2: Schematic of the implementation of the SNOPT package to find the optimal solution to the optimization problem formulated in Section 6.2.1.

The procedure for the interaction between the SNOPT package and the Optimization Problem

Formulation (OPF) is as follows:

Step 1: SNOPT supplies a guess of the optimal solution to the OPF, including a set of values of the decision variables, that is, the set of $\log C_b$ values.

Step 2: For the given guess of the optimal solution, the OPF evaluates: (a) the objective function, M, using the MSB adsorption kinetics model (see Appendix 6.A), and (b) the sensitivity of the decision variables, which is the rate of change of the objective function with respect to each of the decision variables. Specifically, if S_i denotes the sensitivity of a decision variable $\log C_{b,i}$, then:

$$S_i = \frac{\partial M}{\partial \log C_{b,i}} \quad \text{and} \quad \mathbf{S} = \{S_1, S_2, \dots, S_n\} \tag{6.6}$$

Note that: (i) the *sign* of S_i indicates if the objective function, M, increases, or decreases, when $\log C_{b,i}$, increases, and (ii) the *magnitude* of S_i indicates the *extent* to which the objective function, M, increases, or decreases, when $\log C_{b,i}$ increases. Since the formulated optimization problem involves finding the *minimum* value of M (see Eq.(6.2)), the S_i values indicate if the given values of the decision variables need to be increased, or decreased, to further reduce the value of M. As such, the S_i values at a given guess of the optimal solution play a key role in determining the direction in which the search for the optimal solution continues (see Step 4 below). The various steps involved in the calculation of the S_i values at a given set of values of the decision variables, $\log C_b$, are discussed in Appendix 6.B.

Step 3: The OPF provides the value of the objective function (M) and the sensitivity $(\mathbf{S})$ at the given guess of the optimal solution to SNOPT.

Step 4: Based on the values of M and $\mathbf{S}$, SNOPT checks if the guess supplied to the OPF in Step 1 is indeed the optimal solution. If the check is positive, the iterations are terminated and the optimal solution is declared. If the check is negative, SNOPT applies the SQP algorithm to find the next guess for the optimal solution, and the procedure goes back to Step 1.

While the optimization problem formulation in Section 6.2.1 seeks to find the *global* optimal solution, the optimal solution found using numerical optimization solvers (like SNOPT) corresponds to a *local* optimal solution which may, or may not, be globally optimal [9]. The success of finding the global optimal solution depends on [12]: (i) the convex nature of the objective function with

respect to the decision variables, and (ii) the initial guess of the optimal solution. One common procedure to increase the likelihood of finding the global optimal solution is to find the local optimal solutions starting at randomly chosen initial guesses for the optimal solution [12]. If one observes convergence to a unique local optimal solution with each of the initial guesses, then, that local optimal solution is considered as the likely global optimum. However, if one observes different local optimal solutions with different initial guesses, then, the objective function values corresponding to each of the local optimal solutions are compared to determine the likely global optimum. Accordingly, when implementing the theoretical framework to identify the nonionic surfactant formulation that most closely meets a desired dynamic surface tension behavior, it is necessary to study the local optimal solutions obtained by utilizing the framework starting at randomly chosen initial guesses for the bulk solution concentrations of the various nonionic surfactants comprising the formulation.

6.3 Analysis

In this section, I: (i) demonstrate the reliability of the theoretical framework developed in Section 6.2 (Section 6.3.1), and (ii) demonstrate the effectiveness of the theoretical framework by analyzing a representative case study (Section 6.3.2). In order to demonstrate the reliability of the theoretical framework in Section 6.3.1, as well as its effectiveness in Section 6.3.2, I consider surfactant formulations which consists of *four* model nonionic surfactants, that is, $n = 4$. The nonionic surfactants were chosen such that they encompass four distinct types. Specifically, (i) the first one possesses a small head and a short tail, (ii) the second one possesses a large head and a short tail, (iii) the third one possesses a small head and a long tail, and (iv) the fourth one possesses a large head and a long tail. Recall that the MSB adsorption kinetics model used here utilizes the molecular Equilibrium Adsorption Isotherm (EAI) developed in Ref.[13], which models interactions between the nonionic surfactant molecules at the surface in terms of: (a) excluded-volume repulsions between the surfactant heads, and (b) van der Waals attractions between the surfactant tails. In the case study presented here, I will assume that the four nonionic surfactants considered interact solely through excluded-volume repulsions between the surfactant heads. In other words, I will assume that the van der Waals interactions between the surfactant tails are negligible. This will allow me to provide a physical rationalization of the predicted optimal DST behavior in the

case study presented in Section 6.3.2. The specific case study considered here will illustrate that it is possible to realize an interesting and non-intuitive DST profile even when the surfactants comprising the formulation interact solely through excluded-volume repulsions between the surfactant heads.

Recall that in the formulation of the optimization problem (see Section 6.2.1), the properties of the various surfactants comprising the mixture are specified through the MSB adsorption kinetics model parameters (see section on Relation between the Decision Variables and the Objective Function above). For the four nonionic surfactants considered: (i) a_i ($i = 1, \ldots, n$) depends solely on the head size of surfactant i, (ii) B_{ij} ($i, j = 1, \ldots, n$) = 0, since van der Waals interactions are neglected, (iii) $\Delta\bar{\mu}_i^0$ ($i = 1, \ldots, n$) is assumed to depend solely on the length of surfactant tail[4] i, and (iv) D_i ($i = 1, \ldots, n$) increases as the length of the surfactant tail decreases, and as the size of the surfactant head decreases [14]. The specific values chosen for a_i, $\Delta\bar{\mu}_i^0$, and D_i ($i = 1, \ldots, n$) are listed in Table 6.2. The values of a_i and $\Delta\bar{\mu}_i^0$ were chosen based on the reported values corresponding to typical alkyl poly(ethylene) oxide, C_iE_j, nonionic surfactants [13, 15, 16]. The D_i values were chosen keeping in mind that typical diffusion coefficients of C_iE_j nonionic surfactants are of the order of 1 x 10^{-6} cm^2/s [17–19].

Table 6.2: Values of: (i) head cross-sectional areas (a_i) (ii) standard-state chemical potential differences ($\Delta\bar{\mu}_i^0$), and (iii) diffusion coefficients (D_i) chosen for the four nonionic surfactant types considered in the case study.

Surfactant Type	i	a_i (Å^2)	$\Delta\bar{\mu}_i^0$ (RT)	D_i x 10^6 (cm^2/s)
Small head-short tail	1	25	-21	8
Large head-short tail	2	50	-21	6
Small head-long tail	3	25	-24	4
Large head-long tail	4	50	-24	2

[4]Note that $\Delta\bar{\mu}_i^0$ reflects the driving force for surfactant i to adsorb at the surface from the bulk solution. Recognizing that surfactant adsorption from aqueous solution onto surfaces is driven primarily by the hydrophobic effect, it is reasonable to assume that $\Delta\bar{\mu}_i^0$ depends primarily on the length of the hydrophobic tail of surfactant i.

6.3.1 Demonstration of the Reliability of the New Theoretical Framework

In this section, I demonstrate the reliability of the new theoretical framework developed in Section 6.2 by: (i) using the MSB adsorption kinetics model to generate a DST behavior corresponding to a specific surfactant formulation, that is, to a formulation having known C_b values of the four surfactants, (ii) considering the DST profile generated in (i) as the desired DST profile, and using the theoretical framework to determine the optimal surfactant formulation, and (iii) comparing the optimal surfactant formulation determined in (ii) with the original surfactant formulation used to generate the DST behavior in (i). Since the desired DST profile was generated using known specific values of the four surfactant bulk solution concentrations, this situation corresponds to the case where the global optimal solution of the optimization problem in Eq.(6.2) is known *a priori*. As a result, by performing the analysis described above, one can validate the reliability (and effectiveness) of the new theoretical framework in identifying the surfactant formulation that optimally meets a desired adsorption kinetics behavior.

Generation of the Desired DST Behavior

For the four-component nonionic surfactant mixture considered, I predicted the DST corresponding to the C_b values specified in Table 6.3 at $T = 295$ K using the MSB adsorption kinetics model. The predicted DST profile is shown in Figure 6-3. Note that the C_b values in Table 6.3

Table 6.3: Bulk solution concentrations of the four nonionic surfactants (C_b) for which the DST was predicted using the MSB adsorption kinetics model.

Surfactant Type	i	$C_{b,i}$ (mol/cm^3)
Small head-short tail	1	8×10^{-8}
Large head-short tail	2	6×10^{-9}
Small head-long tail	3	4×10^{-10}
Large head-long tail	4	0

were chosen such that: (i) they differ by one or two orders of magnitude ($\sim 10^{-8}$, 10^{-9}, and 10^{-10} mol/cm^3), and (ii) at least one of the surfactants has a bulk solution concentration which is equal to zero. Item (i) was examined to verify that the optimization problem formulation and the SNOPT package can identify the effect of surfactants whose concentrations are low ($\sim 10^{-10}$ mol/cm^3)

228

relative to those of other surfactants ($\sim 10^{-8}$ mol/cm^3) comprising the mixture. Item (ii) was examined to study the numerical behavior of the theoretical framework when the concentration of any of the surfactants is equal to zero [5].
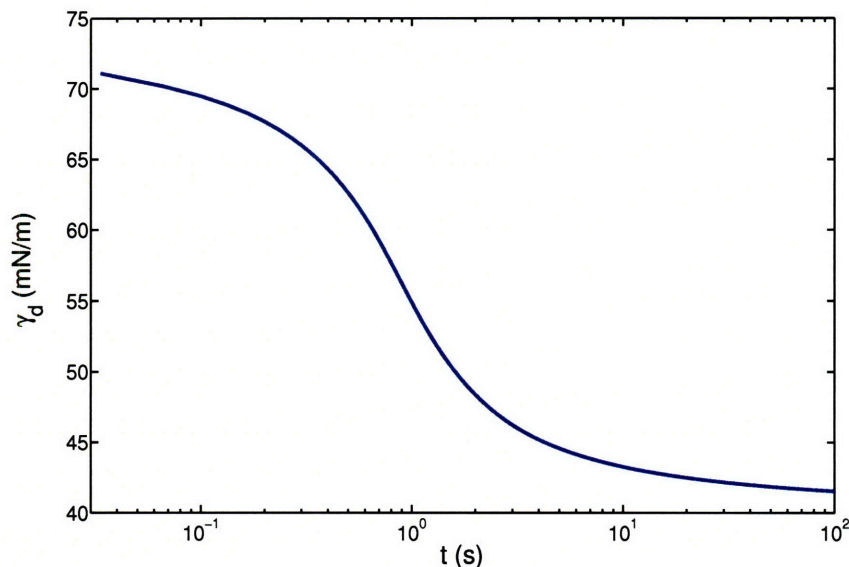
Figure 6-3: Desired dynamic surface tension profile, $\gamma_d(t)$, predicted using the MSB adsorption kinetics model.

Application of the New Theoretical Framework

Recall that the formulation of the optimization problem involves a set of specifications summarized in Table 6.1. Table 6.4 lists the specifications used in implementing the theoretical framework utilizing the predicted DST profile shown in Figure 6-3. The following observations apply to the entries in Table 6.4: (i) the non-dimensionalization factor, γ^*, was chosen to be the surface tension of pure water at $T = 295$ K, and is specified in units of mN/m consistent with the units used to predict the desired DST profile shown in Figure 6-3, (ii) $w(t)$ was chosen as $1/(t \ln 10)$ recognizing that the desired $\gamma_d(t)$ profile varies on the log t scale (see Figure 6-3), and (iii) a constant upper bound value of $C_{b,i}^{\mathrm{u}} = 1 \times 10^{-6}$ mol/cm^3 ($i = 1, \ldots, 4$) was chosen since it corresponds to a typical value of critical micellar concentrations of $C_i E_j$ nonionic surfactants [18].

---

[5]Recall that the decision variables for the optimization problem have been chosen to be $\log \mathbf{C}_b$, and therefore, when $C_{b,i} \to 0$, $\log C_{b,i} \to -\infty$. As a result, by considering a case when the known global optimal solution corresponds to one for which one of the $C_{b,i}$ values is equal to zero (or $\log C_{b,i}$ is equal to $-\infty$), one can study the robustness of the theoretical framework in handling such extreme situations.

Table 6.4: List of specifications used when utilizing the new theoretical framework to attain the desired DST profile shown in Figure 6-3.

Optimization Problem Component	Specifications	Values Used
Objective Function	$\gamma_d(t)$	See Figure 6-3
	γ^*	72.0 (mN/m)
	$w(t)$	$1/(t \ln 10)$ s^{-1}
	t_L	0.3 (s)
	t_U	100.0 (s)
Variables	n	4
	MSB adsorption kinetics model parameters	See Table 6.2
Constraints	$C_{b,i}^u (i = 1, \ldots, 4)$	1×10^{-6} (mol/cm^3)

Analysis of the Optimal Solution

SNOPT was implemented to find the optimal solution of the formulated optimization problem, corresponding to the specifications reported in Table 6.4, starting at different initial guesses for the optimal solution. Specifically, the optimal solution was found starting at 10 initial guesses[6] that were chosen at random. In each case, I found that the iterations converged to an 'apparent' unique optimal solution: Even though the concentrations of the three surfactants that were present in the original surfactant formulation (see Table 6.3) converged to 'apparent' unique values (to within the fifth decimal place accuracy), the concentration of the fourth surfactant (consisting of the large head and the long tail), which was set to zero in the original surfactant formulation, converged to extremely small values (10^{-14} - 10^{-15} mol/cm^3), but not to zero, for the different initial guesses. Table 6.5 lists the observed 'apparent' unique optimal solution.

The observed uncertainties in the $C_{b,i}$ values for $i = 1, 2$, and 3 reported in Table 6.5 indicate that the numerical accuracy associated with finding the solution of the optimization problem is

---

[6]A rigorous binary selection of the initial guesses for the four nonionic surfactants considered would lead to $2^4 = 16$ initial guesses. Therefore, it is reasonable that choosing 10 random initial guesses provides a sufficiently large sample to investigate the existence of multiple local minima for the formulated optimization problem.

Table 6.5: The 'apparent' unique optimal surfactant bulk solution concentrations obtained with the new theoretical framework using the predicted dynamic surface tension (DST) profile shown in Figure 6-3 as the desired DST profile.

Surfactant Type	i	$C_{b,i}$ (mol/cm^3)
Small head-short tail	1	$8 \pm 0.0000006 \times 10^{-8}$
Large head-short tail	2	$6 \pm 0.00002 \times 10^{-9}$
Small head-long tail	3	$4 \pm 0.00008 \times 10^{-10}$
Large head-long tail	4	$10^{-14} - 10^{-15}$

about $\pm 10^{-14}$ mol/cm^3. Since the optimal value of $C_{b,4}$ for different initial guesses was found to be about 10^{-14} mol/cm^3, it is likely that the observed optimal values of $C_{b,4} = 10^{-14} - 10^{-15}$ (see Table 6.5) is a numerical artifact due to limitations in the accuracy with which one can perform the calculations. In order to further validate this possibility, I estimated the maximum reduction in surface tension inducted by the fourth surfactant by predicting the *equilibrium* surface tension reduction corresponding to $C_{b,4} = 10^{-14}$ mol/cm^3, and then comparing this value with the accuracy with which the desired surface tension was specified (which is about 10^{-4} mN/m). Specifically, using the molecular Equilibrium Adsorption Isotherm (EAI) and the Equation of State (EOS) [13], the predicted reduction in the equilibrium surface tension induced by the fourth surfactant at $C_{b,4}$ = 10^{-14} mol/cm^3 was found to be about 10^{-3} mN/m. Since this value is comparable to the accuracy with which the desired surface tension was specified (about 10^{-4} mN/m), I conclude that the non-zero value of the concentration of the fourth surfactant is, most likely, numerically-based.

Considering that the new theoretical framework consistently identified unique optimal concentrations (to within the numerical accuracy) for the three surfactants ($i = 1$, 2, and 3) present in the surfactant formulation, whose values are in agreement with the original surfactant concentrations used to predict the desired DST profile, I conclude that the new theoretical framework can be used to reliably design optimal surfactant formulations that most closely meet a desired DST behavior.

6.3.2 Representative Case Study

Having demonstrated the reliability of the new theoretical framework presented in Section 6.3.1, in this section, I demonstrate its effectiveness by applying it to a representative case study. Specifically, I show how the framework can be used to identify optimal nonionic surfactant formulations that result in a *non-trivial* desired dynamic surface tension profile. I examine a case study involving surfactant formulations that consist of the four nonionic surfactants considered in Section 6.3.1.

Choosing the Desired DST Profile

Typical DST profiles of *single*-component surfactant solutions have a classic sigmoidal shape when the DST is plotted as a function of $\log(t)$, where the DST profile: (i) is relatively flat at the lower $\log(t)$ values, (ii) exhibits a significant decrease over a relatively narrow range of $\log(t)$ values, and (iii) becomes relatively flat again as it approaches the equilibrium surface tension value. This typical behavior of the DST has been rationalized based on a scaling analysis of the diffusion-controlled model in Refs.[8] and [20], where the authors identify a specific time scale at which significant surfactant adsorption takes place. Accordingly, when the DST is plotted as a function of $\log(t)$, one observes a specific region of $\log(t)$ values where the DST decreases significantly.

Keeping the above in mind, consider a case where the desired adsorption kinetics behavior consists of *a steadily decreasing DST profile as a function of* $\log(t)$ *over a time scale that spans about three orders of magnitude*. Specifically, consider the case where the desired DST profile corresponds to the *linear* $\gamma_d(t)$ vs. $\log(t)$ DST profile shown in Figure 6-4(a). In this case, the design problem involves identifying the specific concentrations of the four nonionic surfactants which results in a DST profile that optimally matches the desired DST profile shown in Figure 6-4(a).

Application of the New Theoretical Framework

The new theoretical framework was implemented by formulating the design problem posed above as an optimization problem with the specifications summarized in Table 6.6, and by finding the optimal solution of the formulated problem using the SNOPT package. Specifically, the SNOPT package was used to find the local optimal solutions starting at 10 different initial guesses chosen at random. In all the cases examined, the iterations converged to an 'apparent' unique optimal solution, and the corresponding bulk solution concentrations of the four surfactants are reported in Table 6.7. Specifically, in all the cases examined, the iterations converged to unique values (to
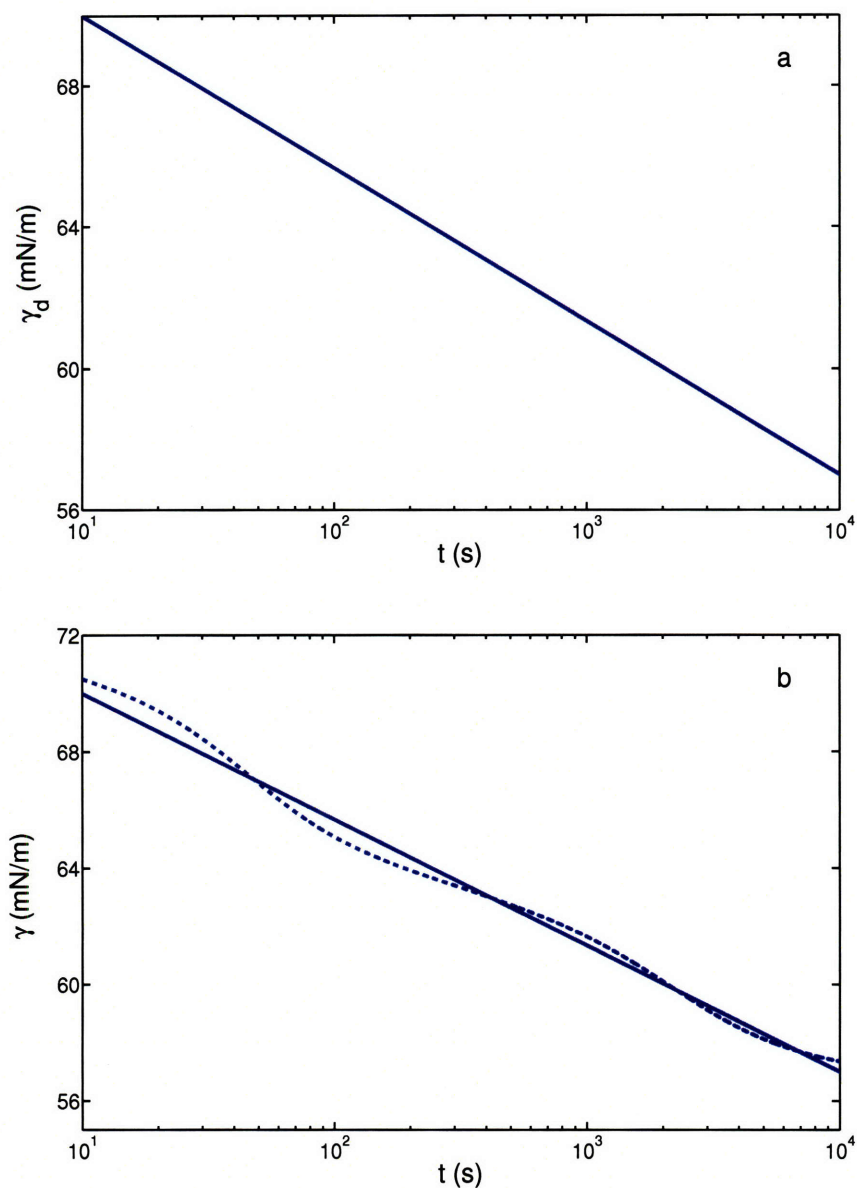
Figure 6-4: (a) Desired dynamic surface tension profile considered in the case study examined here: (b) Comparison between the desired dynamic surface tension profile and the dynamic surface tension profile corresponding to the optimal nonionic surfactant formulation. The solid lines in (a) and (b) correspond to the desired dynamic surface tension profile, and the dashed line in (b) corresponds to the dynamic surface tension profile associated with the optimal formulation.

Table 6.6: List of specifications associated with the formulation of the optimization problem where the desired DST profile is shown in Figure 6-4(a).

Optimization Problem Component	Specifications	Values Used
Objective Function	$\gamma_d(t)$	See Figure 6-4(a)
	γ^*	72.0 (mN/m)
	$w(t)$	$1/(t \ln 10)$ s^{-1}
	t_L	10 (s)
	t_U	10000 (s)
Variables	n	4
	MSB adsorption kinetics model parameters	See Table 6.2
Constraints	$C_{b,i}^u (i = 1, \ldots, 4)$	1 x 10^{-6} (mol/cm^3)

within numerical accuracy) for the bulk solution concentrations of three of the four surfactants ($C_{b,2}$ – large head-short tail, $C_{b,3}$ – small head-long tail, and $C_{b,4}$ – large head-long tail), but converged to different values ($C_{b,1}$) for the small head-small tail surfactant. Since the converged values of $C_{b,1}$ for the small head-small tail surfactant are extremely small ($\sim 10^{-13}$ mol/cm^3, corresponding to an equilibrium surface tension reduction of $\sim 10^{-3}$ mN/m), similar to the case discussed in Section 6.3.1, I have assumed that the actual optimal surfactant concentration, $C_{b,1}$, corresponding to the small head-small tail surfactant is equal to zero (denoted as trace in Table 6.7). The DST

Table 6.7: Surfactant bulk solution concentrations identified by the new theoretical framework to optimally meet the desired DST profile shown in Figure 6-4(a).

Surfactant Type	i	$C_{b,i}$ (mol/cm^3)
Small head-short tail	1	Trace
Large head-short tail	2	4.8 x 10^{-9}
Small head-long tail	3	1.5 x 10^{-10}
Large head-long tail	4	1.0 x 10^{-9}

profile corresponding to the optimal bulk solution concentrations in Table 6.7 is compared with the desired DST profile in Figure 6-4(b), where the solid line corresponds to the desired DST profile and the dotted line corresponds to the optimal DST profile. Figure 6-4(b) reveals that the DST profile corresponding to the optimal surfactant formulation results in a 'near-linear' DST profile which is very similar to the desired DST profile in Figure 6-4(a). Specifically, the average deviation of the DST profile corresponding to the optimal surfactant formulation and to the desired DST profile was calculated to be about 0.4 mN/m.

Rationalization of the Optimal Surfactant Bulk Solution Concentrations

To rationalize possible underlying physical mechanisms that result in the 'near-linear' optimal profile obtained using the new theoretical framework (see Figure 6-4(b)), as well as to understand the optimal surfactant formulation condition obtained, in Figure 6-5, I plot the dynamic surface concentrations of the three surfactants ($i = 2$, large head-short tail, $i = 3$, small head-long tail, and $i = 4$, large head-long tail) corresponding to the optimal formulation condition in Table 6-7. In Figure 6-5, the solid line corresponds to the large head-short tail surfactant ($i = 2$), the dashed line corresponds to the small head-long tail surfactant ($i = 3$), and the dotted line corresponds to the large head-long tail surfactant ($i = 4$). The dynamic surface concentration (DSC) profiles in Figure 6-5 reveal an interesting interplay of adsorption and desorption kinetics behavior of the three nonionic surfactants comprising the optimal surfactant formulation.

In order to rationalize the DSC profiles in Figure 6-5, as well as to understand the associated DST profile in Figure 6-4(b), it is helpful to keep in mind the following physical aspects associated with the effects of the surfactant tail and the surfactant head on the adsorption behavior of surfactants:

Effect of the Surfactant Tail: The adsorption of surfactant molecules onto a water/air surface is driven by the hydrophobic effect associated with the surfactant hydrophobic tail[21]. Therefore, as the surfactant tail length increases (for a given surfactant head), there is a *higher* incentive and drive for the surfactant molecules to adsorb at the surface.

Effect of the Surfactant Head: In the molecular EAI model adopted here [13], the effect of the surfactant head on the adsorption of surfactant molecules is accounted for in the form of steric (hard-sphere) repulsions between the heads of the adsorbed surfactant molecules. Ac-

235
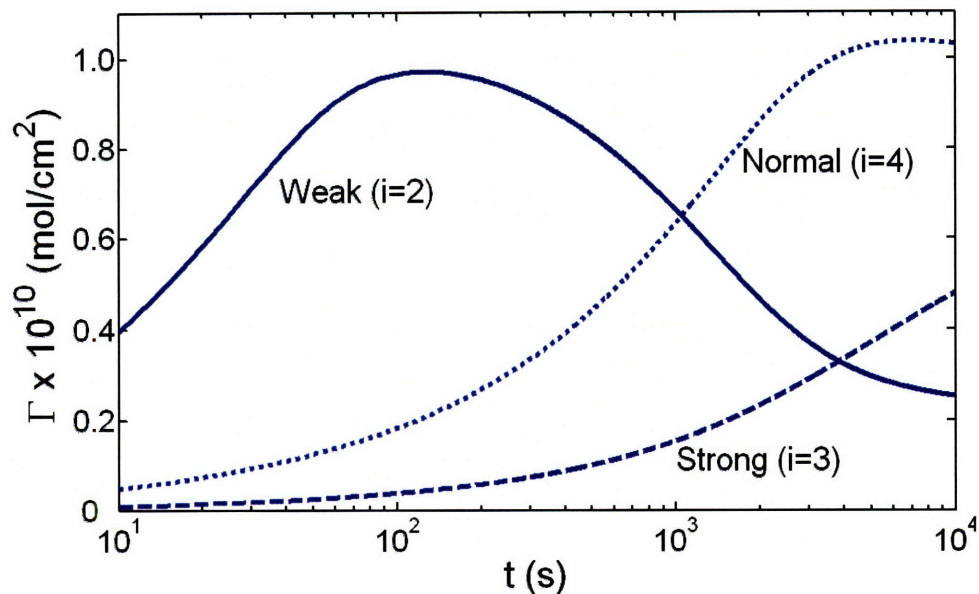
Figure 6-5: Dynamic surface concentrations (DSC's) of the three surfactants (i=2, 3, and 4, see Table 6.7) comprising the optimal surfactant formulation. The solid line corresponds to the large head-short tail surfactant ($i = 2$, the 'weak surfactant'), the dashed line corresponds to the small head-long tail surfactant ($i = 3$, the 'strong surfactant'), and the dotted line corresponds to the large head-long tail surfactant ($i = 4$, the 'normal surfactant').

cordingly, for surfactant molecules which posses a larger head (for a given surfactant tail), the steric repulsions are stronger, and this *reduces* the incentive and drive of the surfactant molecules to adsorb at the surface.

Based on the above physical understanding of the effects of the surfactant head and the surfactant tail on the 'adsorption tendency' of surfactants, the three surfactants comprising the optimal formulation can be *ranked* in decreasing order of 'adsorption tendency' as follows:

1. Small head-long tail surfactant ($i = 3$): Highest incentive to adsorb at the surface (referred to hereafter as the 'strong surfactant').

2. Large head-long tail surfactant ($i = 4$): Competing incentives to adsorb at the surface, since the long tail facilitates adsorption but the large head leads to stronger head-head repulsions at the surface (referred to hereafter as the 'normal surfactant').

3. Large head-short tail surfactant ($i = 2$): Lowest incentive to adsorb at the surface (referred to hereafter as the 'weak surfactant').

236

It is also very important to keep in mind the effect of the surfactant bulk solution concentration (C_b) on the dynamics of surfactant adsorption at the surface: The time scale associated with the dynamics of surfactant adsorption (τ_a) depends strongly on C_b [22]. A higher C_b value corresponds to a stronger driving force for surfactant adsorption. As a result, τ_a decreases as C_b increases. Specifically, for the case of diffusion-controlled (DC) adsorption kinetics of nonionic surfactant mixtures, the time scale associated with the adsorption kinetics of surfactant i ($\tau_{a,i}^{DC}$) is related to the surfactant i bulk solution concentration ($C_{b,i}$) as follows [8]:

$$\tau_{a,i}^{DC} = \frac{1}{D_i}\left(\frac{\Gamma_{e,i}}{C_{b,i}}\right)^2 \tag{6.7}$$

where D_i is the diffusion coefficient of surfactant i, and $\Gamma_{e,i}$ is the *equilibrium* surfactant surface concentration corresponding to a surfactant solution that contains solely surfactant i at a bulk solution concentration of $C_{b,i}$ [8].

Keeping the 'adsorption tendency' ranking for the three surfactants above in mind, the time scales for adsorption associated with each of the three surfactants at their respective optimal $C_{b,i}$ values (see Table 6-7) were calculated using Eq.(6.7) and are reported in Table 6-8.

Table 6.8: For each of the three nonionic surfactants identified by the new theoretical framework (see Table 6.7), the table reports: (a) their adsorption tendencies, (b) their bulk solution concentrations in the optimal formulation, and (c) the time scales for adsorption ($\tau_{a,i}^{DC}$) calculated using Eq.(6.7).

Surfactant Type	Adsorption Tendency	i	Optimal $C_{b,i}$ (mol/cm^3)	$\tau_{a,i}^{DC}$ (s)
Large head-short tail	Weak	2	4.8×10^{-9}	100
Large head-long tail	Normal	4	1.0×10^{-9}	11500
Small head-long tail	Strong	3	1.5×10^{-10}	406200

The $\tau_{a,i}^{DC}$ ($i = 2, 3, 4$) values reported in Table 6-8 clearly reveal that, at the optimal $C_{b,i}(i = 2, 3, 4)$ values, the weak surfactant adsorbs first, followed by the normal surfactant, and finally by the strong surfactant. The apparent 'quickness' in the adsorption behavior displayed by the weak surfactant is due to its *higher* bulk solution concentration relative to those of the normal and the strong surfactants. Conversely, the apparent 'slowness' in the adsorption behavior displayed by the

strong surfactant is due to its *lower* bulk solution concentration relative to those of the weak and the normal surfactants. These predictions are consistent with the observed DSC behavior in Figure 6-5 as described below:

At low t values ($\sim 10 - 50$ s), the surface concentration of the weak surfactant increases faster relative to those of the normal and the strong surfactants owing to its high initial bulk solution concentration. Subsequently, at $t \approx 80$ s, the rate of adsorption of the weak surfactant slows down as the adsorption of the normal surfactant starts becoming significant. As the adsorption of the normal surfactant continues, it displaces the weak surfactant from the surface, which results in the observed maximum in the surface concentration of the weak surfactant at $t \approx 100$ s (see Figure 6-5). Note that this time scale is consistent with the estimated $\tau_{a,2}^{DC} = 100$ s for the weak surfactant (see Table 6.8). Figure 6-5 reveals that significant adsorption of the normal surfactant takes place in the time range of $t \sim 100 - 4000$ s until the strong surfactant begins to adsorb. As the strong surfactant begins to adsorb at time scales ~ 1000's of seconds, the rate of adsorption of the normal surfactant decreases, and subsequently it begins to desorb.

Based on the above understanding of the dynamic surface concentration profiles shown in Figure 6-5, the surfactant formulation which was identified to optimally satisfy the desired *linear* DST profile (see Table 6-7) can be rationalized as follows:

The desired DST profile shown in Figure 6-4(a) involves a *steady* decrease of the surface tension with time which spans about *three* orders of magnitude. Accordingly, the optimal formulation should involve at least *three* types of surfactants, since each surfactant type has a unique time scale associated with its adsorption process at a given bulk solution concentration ($\tau_{a,i}^{DC}$). Since $\tau_{a,i}^{DC}$ decreases as $C_{b,i}$ increases, it follows that (a) the surfactant corresponding to the highest $C_{b,i}$ value serves to satisfy the desired DST profile at small t values, (b) the surfactant corresponding to the intermediate $C_{b,i}$ value serves to satisfy the desired DST profile at the intermediate t values, and (c) the surfactant corresponding to the lowest $C_{b,i}$ value serves to satisfy the desired DST profile at the large t values. Since the adsorption process needs to be sustained over t values which three orders of magnitude, it requires that the *strong* surfactant *adsorb at the latest time*, since it cannot be displaced by the two other surfactant types (the normal and the weak) if it did adsorb at an earlier time. Accordingly, one can see why the strong surfactant should be present at the lowest

$C_{b,i}$ value (corresponding to the largest $\tau_{a,i}^{DC}$ value) in the optimal surfactant formulation. Using a similar argument, one can see why the normal surfactant should be present at the intermediate $C_{b,i}$ value, and why the weakest surfactant should be present at the highest $C_{b,i}$ value. All these results are fully consistent with the actual $C_{b,i}$ values corresponding to the optimal surfactant formulation (see Table 6-8).

It is important to stress that although the optimal surfactant formulation identified using the new theoretical framework could be rationalized qualitatively as above, the *specific quantitative* $C_{b,i}$ values that result in the 'near-linear' profile shown in Figure 6-4(b) cannot be inferred using this type of qualitative analysis. Indeed, the great value of the new theoretical framework presented here is its ability to identify *quantitatively* the specific surfactant formulation that results in a DST profile that is closest to the desired DST profile.

Through the representative case study analyzed above, I have demonstrated the effectiveness of the new theoretical framework in the case of surfactant formulations which consists of *four* nonionic surfactants. The choice of four surfactants was motivated by the desired to provide a physical rationalization of the optimal surfactant formulation identified using the new theoretical framework. However, it is important to recognize that the new theoretical framework presented here can potentially be used to design optimal formulations containing any number of nonionic surfactants, even though the qualitative rationalization of such optimal formulations may not be possible.

6.4 Conclusions

In this chapter, I proposed a new theoretical framework which involves using predictive models in conjunction with optimization packages to design surfactant formulations that optimally satisfy desired performance requirements. As proof of technical feasibility, I considered the problem of designing nonionic surfactant formulations to optimally meet a desired adsorption kinetics requirement specified in terms of a desired dynamic surface tension profile. I formulated the above problem as an optimization problem using the Mulqueen-Stebe-Blankschtein adsorption kinetics model, and developed a framework to find the optimal solution using the Sequential Nonlinear OPTimization (SNOPT) package. I demonstrated the reliability of the new theoretical framework

239

and its effectiveness using a representative case study. Although the effectiveness of the new theoretical framework was demonstrated when the desired adsorption kinetics behavior consists of the dynamic surface tension profile, the new theoretical framework can also be used when the desired adsorption kinetics behavior consists of the *dynamic surface concentration behavior* of surfactants by appropriately modifying the objective function underlying the optimization problem.

In the next chapter, Chapter 7, I summarize the key contributions made in this thesis, discuss possible future research directions, and present concluding remarks.

Appendix 6.A: Evaluation of the Objective Function Using the MSB Adsorption Kinetics Model

In this Appendix, I describe the evaluation of the objective function (M) for a given set of values of the decision variables ($\log C_b$) using the Mulqueen-Stebe-Blankschtein (MSB) adsorption kinetics model [8].

Note that the MSB adsorption kinetics model describes the adsorption kinetics of nonionic surfactant mixtures onto spherical surfaces and predicts the dynamic surface tension ($\gamma(t)$) at given premicellar bulk solution concentrations of the constituent nonionic surfactants. Specifically, the MSB adsorption kinetics model assumes that the diffusion of surfactant molecules from the bulk solution to the sub-surface controls the overall rate of surfactant adsorption, and : (i) uses Fick's law to describe the diffusive transport of surfactant molecules from the bulk solution to the sub-surface, and (ii) uses the molecular Equilibrium Adsorption Isotherm (EAI) developed by Nikas *et al.* [13] to describe the equilibrium between the sub-surface and the surface.

The evaluation of the objective function (M) at a given $\log C_b$ involves: (a) using the MSB adsorption kinetics model to predict $\gamma(t)$ at the C_b corresponding to the given $\log C_b$, and (b) substituting the predicted $\gamma(t)$ in the chosen expression for the objective function (Eq.(6.2)). Below, I describe the specific steps associated with implementing this procedure.

Step 1: At the bulk solution concentrations of the constituent surfactants (C_b) corresponding to the given set of values of the decision variables $\log C_b$, the dynamic surface concentrations of the constituent surfactants are predicted by solving the extended Ward-Tordai (WT) equation applicable for surfactant mixtures and the molecular EAI model. Specifically, the extended WT equation is given by [8]:

$$\Gamma_i(t) = \frac{D_i}{r_0}\left[C_{b,i}t - \int_0^t C_{s,i}(t)dt\right] + 2\sqrt{\frac{D_i}{\pi}}\left[C_{b,i}\sqrt{t} - \int_0^{\sqrt{t}} C_{s,i}(t-\eta)d\sqrt{\eta}\right]$$

$$i = 1,\ldots,n, \qquad t \geq 0 \qquad\qquad (6.A.1)$$

where for each surfactant i: (i) $\Gamma_i(t)$ is the dynamic surfactant surface concentration, (ii) D_i

is the diffusion coefficient, (iii) $C_{b,i}$ is the given surfactant bulk solution concentration, and (iv) $C_{s,i}(t)$ is the dynamic surfactant sub-surface concentration. In addition, r_0 is the radius of the spherical surface, and n is the total number of nonionic surfactant components in the mixture. For notational convenience, let $\Gamma(t)$ represent the set $\{\Gamma_1(t), \Gamma_2(t), \ldots, \Gamma_n(t)\}$, and let $\mathbf{C_s}(t)$ represent the set $\{C_{s,1}(t), C_{s,2}(t), \ldots, C_{s,n}(t)\}$. Note that Eq.(6.A.1) defines a set of n equations containing $2n$ unknowns ($\Gamma(t)$ and $\mathbf{C_s}(t)$).

Owing to the diffusion-controlled assumption of the MSB adsorption kinetics model, the surface and the sub-surface reach equilibrium instantaneously, and $\Gamma(t)$ and $\mathbf{C_s}(t)$ are further related by the molecular EAI model [13], which can be expressed as follows [7]:

$$
\frac{\Delta\bar{\mu}_i^0}{RT} + 1 + \ln\left[\frac{RT}{\Pi_0}\frac{\Gamma_i(t)}{1 - \sum_k \frac{\Gamma_k(t)}{\Gamma_{\infty,k}}}\right] + \frac{\frac{1}{\Gamma_{\infty,i}}\sum_k \Gamma_k(t) + \frac{2}{\sqrt{\Gamma_{\infty,i}}}\sum_k \frac{\Gamma_k(t)}{\sqrt{\Gamma_{\infty,k}}}}{1 - \sum_k \frac{\Gamma_k(t)}{\Gamma_{\infty,k}}}
$$

$$
+ \frac{\frac{1}{\Gamma_{\infty,i}}\left[\sum_k \frac{\Gamma_k(t)}{\sqrt{\Gamma_{\infty,k}}}\right]^2}{\left(1 - \sum_k \frac{\Gamma_k(t)}{\Gamma_{\infty,k}}\right)^2} + 2\sum_k \bar{B}_{ik}\Gamma_k(t)
$$

$$
= \ln\left(\frac{18}{\rho}C_{s,i}(t)\right) \qquad i = 1, \ldots, n, \qquad t \geq 0 \tag{6.A.2}
$$

where for each surfactant i: (i) $\Delta\bar{\mu}_i^0$ is the difference between the reference chemical potential of the surfactant molecule adsorbed at the surface ($\mu_i^{\sigma,0}$) and the standard-state chemical potential of the surfactant molecule in the bulk solution ($\mu_i^{b,0}$), (ii) $\Gamma_{\infty,i}$ is the maximum surfactant surface concentration, and (iii) $\bar{B}_{ik}$ is the second virial coefficient associated with the van der Waals attractions between surfactant molecules of type i and type k. In addition, Π_0 is the surface pressure at the reference state for the adsorbed surfactant molecules, ρ is the mass density of water (gram/volume), R is the Gas constant, and T is the absolute temperature.

Note that Eq.(6.A.2) forms another set of n equations relating $\Gamma(t)$ and $\mathbf{C_s}(t)$. Accordingly, $\Gamma(t)$ and $\mathbf{C_s}(t)$ are predicted by solving Eqs. (6.A.1) and (6.A.2) simultaneously.

Step 2: Once $\Gamma(t)$ is predicted, the molecular Equation of State (EOS) corresponding to the molec-

---

[7]Note that the original expression for the molecular EAI model presented in Ref.[13] is different from Eq.(6.A.2). For more details, see the comment at the end of this appendix.

ular EAI is used to predict $\gamma(t)$ as follows [8, 13]:

$$\frac{\gamma_{w/a} - \gamma(t)}{RT} = \frac{\sum_i \Gamma_i(t)}{1 - \sum_i \frac{\Gamma_i(t)}{\Gamma_{\infty,i}}} + \frac{\left[\sum_i \frac{\Gamma_i(t)}{\sqrt{\Gamma_{\infty,i}}}\right]^2}{\left(1 - \sum_i \frac{\Gamma_i(t)}{\Gamma_{\infty,i}}\right)^2} + \sum_{ij} \bar{B}_{ij} \Gamma_i(t) \Gamma_j(t) \qquad (6.A.3)$$

where $\gamma_{w/a}$ is the pure water/air surface tension.

Step 3: The objective function (M) is then evaluated by substituting $\gamma(t)$ predicted using Eq.(6.A.3) in Eq.(6.2), and using the known desired dynamic surface tension profile $(\gamma_d(t))$ and the weighting function $(w(t))$. Specifically,

$$M = \int_{t_L}^{t_U} \left[\frac{\gamma_d(t) - \gamma(t)}{\gamma^*}\right]^2 w(t) \mathrm{d}t \qquad (6.A.4)$$

Comment on the Expression for the Molecular EAI Model in Eq.(6.A.2)

The original expression for the molecular EAI presented in Ref.[13] is given by:

$$\frac{\Delta \mu_i^0}{k_B T} + \ln\left[\frac{x_i^\sigma}{a - \sum_k x_k^\sigma a_k}\right] + \frac{a_i + 2\pi r_i \sum_k x_k^\sigma r_k}{a - \sum_k x_k^\sigma a_k}$$

$$+ \frac{\pi a_i \left[\sum_k x_k^\sigma r_k\right]^2}{\left(a - \sum_k x_k^\sigma a_k\right)^2} + \frac{2}{a} \sum_k B_{ij} x_k^\sigma$$

$$= \ln X_i, \qquad i = 1, \ldots, n, \qquad t \geq 0 \qquad (6.A.5)$$

where for each surfactant i: (i) x_i^σ and X_i denote the surface concentration and the bulk solution concentration, respectively (expressed in terms of *mole fraction* units), (ii) a_i and r_i denote the head cross-sectional area, and the associated radius, respectively, (iii) B_{ij} is the second virial coefficient associated with the van der Waals attractions between the surfactant molecules of type i and j, and (iv) $\Delta \mu_i^0$ is defined as follows:

$$\frac{\Delta \mu_i^0}{k_B T} = \frac{\mu_i^{\sigma,0} - \mu_i^{b,0}}{k_B T} + 1 + \ln\left(\frac{k_B T}{\Pi_0}\right) \qquad (6.A.6)$$

and a is the average available area per surfactant molecule. Note that in Eq.(6.A.5), all the struc-

243

tural properties of the surfactant molecules, including, a_i, r_i, B_{ij}, and $\Delta\mu_i^0$, are expressed on a *per-molecule* basis.

In order to be consistent with the units used in the previous chapters of this thesis, and with the typical units in which EAI models are commonly expressed [18], the original expression for the molecular EAI was transformed from that in Eq.(6.A.5) to that in Eq.(6.A.2) by: (a) expressing all the terms representing surfactant surface and bulk solution concentrations from the original mole fraction units to mole/area and mole/volume, respectively, (b) defining $\Gamma_{\infty,i} = 1/(a_i N_A)$, where N_A is Avogadro's number, and (c) defining $\bar{B}_{ij} = B_{ij} N_A$.

Note that, in the original representation of the molecular EAI, the fraction in the natural logarithm on the right-hand side of Eq.(6.A.6) is *not dimensionless*, and so is the fraction in the natural logarithm on the left-hand side of Eq.(6.A.5). On the other hand, all the other terms in Eqs.(6.A.6) and (6.A.5) are *dimensionless*. Therefore, in order to use a dimensionally consistent representation of the molecular EAI, $\Delta\bar{\mu}_i^0$ in Eq.(6.A.2) was defined such that:

$$\Delta\bar{\mu}_i^0 = \mu_i^{\sigma,0} - \mu_i^{b,0} \tag{6.A.7}$$

and the two terms involving the natural logarithm in Eqs.(6.A.5) and (6.A.6) were combined to obtain a dimensionally consistent natural logarithm term on the left-hand side of Eq.(6.A.2).

Appendix 6.B: Calculation of the Sensitivity of the Objective Function

In this Appendix, I describe the calculation of the sensitivity (S_i) of the objective function (M) to changes in the values of the decision variables $\log C_{b,i}$. Recall that the sensitivity, S_i, is defined as the partial derivative of the objective function (M) with respect to the decision variable $\log C_{b,i}$ (see Eq.(6.6)), that is,

$$S_i = \frac{\partial M}{\partial \log C_{b,i}} \qquad \text{and} \qquad \mathbf{S} = \{S_1, S_2, \ldots, S_n\} \tag{6.B.1}$$

In essence, the procedure followed to calculate $S_i = \frac{\partial M}{\partial \log C_{b,i}}$ involves differentiating *all* the equations associated with the evaluation of M with respect to $\log C_{b,i}$, and solving the resulting sensitivity equations.

Recall that the procedure for evaluating the objective function (M) at a given set of values of the decision variables $\log \mathbf{C}_b$ involves the following steps (see Appendix 6.A):

Step 1: Calculating the dynamic surface concentration of all the surfactant components $(\Gamma(t))$ and the sub-surface concentrations of all the components $(\mathbf{C}_s(t))$ by solving the extended Ward-Tordai equation (Eq.(6.A.1)) and the molecular EAI (Eq.6.A.2) simultaneously.

Step 2: Using the predicted $\Gamma(t)$ along with the EOS corresponding to the molecular EAI (Eq.(6.A.3)) to calculate $\gamma(t)$.

Step 3: Using $\gamma(t)$ obtained in Step 2 in Eq.(6.2) to evaluate the objective function M.

Since the derivation of the sensitivity equations involves differentiating the equations in steps 1-3 above with respect to each of the decision variables $\log C_{b,i}$, the sensitivity equations will involve the differentials of the quantities involved in the calculation of M (that is, $\partial \Gamma(t) / \log C_{b,i}$, $\partial \mathbf{C}_s(t) / \partial \log C_{b,i}$, $\partial \gamma(t) / \partial \log C_{b,i}$, and $\partial M / \partial \log C_{b,i}$).

For notational simplicity, the following notation is introduced: Let $\mathbf{A}(t)$ and $\mathbf{B}(t)$ be matrices of

dimensions $n \times n$, such that their elements $A_{ij}(t)$ and $B_{ij}(t)$, respectively, are given by:

$$A_{ij}(t) = \left(\frac{\partial \Gamma_i(t)}{\partial \log C_{b,j}} \right)$$

and

$$B_{ij}(t) = \left(\frac{\partial C_{s,i}(t)}{\partial \log C_{b,j}} \right), \qquad i = 1, \ldots, n, \qquad j = 1, \ldots, n \tag{6.B.2}$$

Let $\gamma_{C_b}(t)$ be an n−dimensional vector, such that each element $\gamma_{C_{b,i}}(t)$ is given by:

$$\gamma_{C_{b,i}}(t) = \left(\frac{\partial \gamma(t)}{\partial \log C_{b,i}} \right), \qquad i = 1, \ldots, n \tag{6.B.3}$$

Having introduced this notation, below, I derive the sensitivity equations by differentiating each of the three steps above involved in the evaluation of M with respect to each of the decision variable $\log C_{b,j}$ $(j = 1, \ldots, n)$.

6.B.1 Step 1: Calculation of A(t) and B(t)

Differentiating the extended Ward-Tordai equation for component i (see Eq.(6.A.1)) with respect to $\log C_{b,j}$, yields:

$$A_{ij}(t) = \frac{D_i}{r_0} \left[\delta_{ij} C_{b,i} t - \int_0^t B_{ij}(t)dt \right] + 2\sqrt{\frac{D_i}{\pi}} \left[\delta_{ij} C_{b,i} \sqrt{t} - \int_0^{\sqrt{t}} B_{ij}(t - \eta)d\sqrt{\eta} \right],$$

$$i = 1, \ldots, n, \qquad j = 1, \ldots, n, \qquad t \geq 0 \tag{6.B.4}$$

where

$$\delta_{ij} = \begin{cases} 0 & \text{if } i \neq j \\ \\ 1 & \text{if } i = j \end{cases} \tag{6.B.5}$$

Equation (6.B.4) is the sensitivity-equivalent of the extended Ward-Tordai equation (6.A.1), and it corresponds to a set of n^2 equations in $2n^2$ unknowns ($A_{ij}(t)$ and $B_{ij}(t)$, with $i = 1, \ldots, n$ and $j = 1, \ldots, n$).

For the purpose of the derivation in this appendix, the molecular EAI in Eq.(6.A.2) can be expressed

as follows:

$$g_i(\mathbf{\Gamma}(t)) = C_{s,i}(t), \qquad i = 1, \ldots, n \tag{6.B.6}$$

where $g_i(\mathbf{\Gamma}(t))$ is proportional[8] to the exponential of the LHS of Eq.(6.A.2). Differentiating Eq.(6.B.6) with respect to $\log C_{b,j}$ yields:

$$\sum_k \left(\frac{\partial g_i}{\partial \Gamma_k} \right) A_{kj}(t) = B_{ij}(t), \qquad i = 1, \ldots, n, \quad j = 1, \ldots, n \tag{6.B.7}$$

Equation (6.B.7) is the sensitivity-equivalent of the molecular EAI (Eq.(6.A.2)), and it corresponds to another set of n^2 equations in $2n^2$ unknowns ($A_{ij}(t)$ and $B_{ij}(t)$, with $i = 1, \ldots, n$ and $j = 1, \ldots, n$).

In a manner similar to calculating $\mathbf{\Gamma}(t)$ and $\mathbf{C}_s(t)$ by solving the extended Ward-Tordai equation and the molecular EAI simultaneously (see Step 1 in Appendix 6.A), $\mathbf{A}(t)$ and $\mathbf{B}(t)$ are calculated by solving the sensitivity-equivalent of the extended Ward-Tordai equation (Eq.(6.B.4)) and the sensitivity-equivalent of the EAI (Eq.(6.B.7)) simultaneously.

6.B.2 Step 2: Calculation of $\gamma_{C_b}(t)$

Recall that in the original MSB adsorption kinetics model, $\gamma(t)$ was calculated from the predicted $\mathbf{\Gamma}(t)$ using the molecular EOS (see Eq.(6.A.3)). For the purpose of the derivation in this appendix, the molecular EOS (Eq.(6.A.3)) can be expressed as follows:

$$\gamma_{w/a} - \gamma(t) = f(\mathbf{\Gamma}(t)) \tag{6.B.8}$$

where the function $f(\mathbf{\Gamma}(t))$ is proportional[9] to the RHS of Eq.(6.A.3). The sensitivity-equivalent of the EOS is derived by differentiating Eq.(6.B.8) with respect to $\log C_{b,j}$, that is,

$$-\gamma_{C_{b,j}}(t) = \sum_k \left(\frac{\partial f}{\partial \Gamma_k} \right) A_{kj}(t), \qquad j = 1, \ldots, n \tag{6.B.9}$$

---

[8]Specifically, $g_i(\mathbf{\Gamma}(t))$ is $\frac{\rho}{18}$ times the exponential of the LHS of Eq.(6.A.2).

[9]Specifically, $f(\mathbf{\Gamma}(t))$ is RT times the RHS of Eq.(6.A.3).

Note that Eq.(6.B.9) enables computation of all the components of $\gamma_{C_b}(t)$ using $A(t)$ calculated in Step 1.

6.B.3 Step 3: Calculation of S

The sensitivity of M with respect to the decision variable $\log C_{b,j}$ is then computed by differentiating Eq.(6.A.4) with respect to $\log C_{b,j}$, which yields:

$$S_j = \int_{t_L}^{t_U} 2 \left[\frac{\gamma_d(t) - \gamma(t)}{\gamma^{*2}} \right] \{-\gamma_{C_{b,j}}(t)\} \frac{dt}{w(t)}, \qquad j = 1, \ldots, n \qquad (6.B.10)$$

Using the known $\gamma_{C_b}(t)$, and $\gamma(t)$ predicted using the MSB adsorption kinetics model (discussed in Section 6.A), all the components of $S = \{S_1, S_2, \ldots, S_n\}$ can be computed.

Bibliography

[1] Andrew M. Howe. Some aspects of colloids in photography. *Current Opinion in Colloid and Interface Science*, pages 288–300, 2000.

[2] C-H. Chang and Elias I. Franses. Adsorption dynamics of surfactants at the air/water interface: a critical review of mathematical models, data, and mechanisms. *Colloids and Surfaces A: Physicochemical and Engineering Aspects*, 100:1–45, 1995.

[3] J. J. Bikerman. *Foams*. Springer-Verlag, 1973.

[4] P. R. Garrett and P. L. Gratton. Dynamic surface tensions, foam and the transition from micellar solution to lamellar phase dispersion. *Colloids and Surfaces A: Physicochemical and Engineering Aspects*, 103:127–145, 1995.

[5] V. Schröder, O. Behrend, and H. Schubert. Effect of dynamic interfacial tension on the emulsification process using microporous, ceramic membranes. *Journal of Colloid and Interface Science*, 202:334–340, 1998.

[6] P. J. G. Stevens, M. O. Kimberly, D. S. Murphy, and G. A. Policello. Adhesion of spray droplets to foliage: The role of dynamic surface tension and advantages of organosilicone surfa ctants. *Pesticide Science*, 38:237–245, 1993.

[7] M. Buzzacchi, P. Schmiedel, and W. von Rybinski. Dynamic surface tension of surfactant systems and its relation to foam formation and liquid film drainage on soli d surfaces. *Colloids and Surfaces A: Physicochemical and Engineering Aspects*, 273:47–54, 2006.

[8] M. Mulqueen, K. J. Stebe, and D. Blankschtein. Dynamic interfacial adsorption in aqueous surfactant mixtures: Theoretical study. *Langmuir*, 17:5196–5207, 2001.

[9] P. E. Gill, W. Murray, and M. A. Saunders. SNOPT: An SQP algorithm for large-scale constrained optimization. *SIAM Review*, 47:99–131, 2005.

[10] G. E. P. Box, W. G. Hunter, and J. S. Hunter. *Statistics for experimenters*. John Wiley & Sons, 1978.

[11] M. J. Rosen. *Surfactants and Interfacial Phenomena*. Wiley Interscience, 1989.

[12] D. P. Bertsekas. *Nonlinear programming*. Athena Scientific, 1999.

[13] Y. J. Nikas, S. Puvvada, and D. Blankschtein. Surface tensions of aqueous nonionic surfactant mixtures. *Langmuir*, 8:2680–2689, 1992.

[14] E. L. Cussler. *Diffusion: Mass transfer in fluid systems*. Cambridge University Press, 1984.

[15] M. Mulqueen, S. S. Datwani, K. J. Stebe, and D. Blankschtein. Dynamic surface tension of aqueous surfactant mixtures: Experimental investigation. *Langmuir*, 17:5801–5812, 2001.

[16] M. Mulqueen and D. Blankschtein. Prediction of equilibrium surface tension and surface adsorption of aqueous surfactant mixtures containing ionic surfactants. *Langmuir*, 15:8832–8848, 1999.

[17] S. N. Moorkanikkara and D. Blankschtein. New methodology to determine the rate-limiting adsorption kinetics mechanism from experimental dynamic surface tension data. *Journal of Colloid and Interface Science*, 302:1–19, 2006.

[18] S-Y. Lin, Y-C. Lee, M-W Yang, and H-S Liu. Surface equation of state of nonionic C_mE_n surfactants. *Langmuir*, 19:3164 – 3171, 2003.

[19] R. Pan, J. Green, and C. Maldarelli. Theory and experiment on the measurement of kinetic rate constants for surfactant exchange at an air/water interface. *Journal of Colloid and Interface Science*, 205:213–230, 1998.

[20] J. K. Ferri and K. J. Stebe. Which surfactants reduce surface tension faster? A scaling argument for diffusion-controlled adsorption. *Advances in Colloid and Interface Science*, 85:61–97, 2000.

[21] C. Tanford. *The Hydrophobic Effect: Formation of Micelles and Biological membranes*. Wiley-Interscience, second edition, 1980.

[22] B. A. Noskov. Fast adsorption at the liquid-gas interface. *Advances in Colloid and Interface Science*, 69:63–129, 1996.

Chapter 7

Conclusions and Future Research Directions

In this Chapter, I: (i) summarize the key contributions made in this thesis (Section 7.1), (ii) discuss possible future research directions to expand the capabilities of the methodologies developed in this thesis (Section 7.2), (iii) propose new research projects in the general area of surfactant adsorption kinetics (Section 7.3), and (iv) present concluding remarks (Section 7.4).

7.1 Thesis Summary

In this thesis, I considered the adsorption kinetics of simple[1] nonionic surfactants at premicellar surfactant bulk solution concentrations. Traditionally, the adsorption kinetics of nonionic surfactants has been understood in the context of two models: (a) the diffusion-controlled model, which assumes that diffusion of surfactant molecules from the bulk solution to the sub-surface determines the overall rate of surfactant adsorption, and (b) the mixed-controlled model, which hypothesizes the existence of an energy barrier for surfactant adsorption from the sub-surface onto the surface, and assumes that that both diffusion and the energy barrier determine the overall rate of surfactant adsorption. Although the existence of the energy barrier was hypothesized about 50 years

---

[1]As stressed in Chapter 1, *simple surfactants* refers to surfactants that do not exhibit phase transitions or any form of aggregation at the surface. In this chapter, I will refer to surfactants that exhibit surface phase transitions as *complex surfactants*.

ago, the fundamental physical nature underlying the existence of the energy barrier has not yet been elucidated. The traditional procedure to study surfactant adsorption kinetics involves conducting Dynamic Surface Tension (DST) measurements at different initial surfactant bulk solution concentrations, C_b's, and analyzing the resulting DST behaviors in order to determine the adsorption kinetics rate-limiting mechanism, including deducing relevant adsorption kinetics parameter values. One of the major drawbacks with the traditional procedure to analyze experimental DST data is that it requires a model for the *equilibrium* adsorption behavior of the surfactant, and unfortunately, the deduced results were found to be very sensitive to the accuracy of the equilibrium model used. As a result, it has not been possible to deduce the nature of the energy barrier by analyzing the experimental DST data of nonionic surfactants. On the other hand, in spite of the significant progress made in developing a fundamental understanding of the kinetics of surfactant adsorption, researchers in industry still follow a time-consuming, trial-and-error surfactant selection approach to design surfactant formulations for applications in which the kinetics of surfactant adsorption plays a significant role.

With the above in mind, the central goal of this thesis was to develop a number of novel methodologies to analyze the adsorption kinetics of nonionic surfactants. Specifically, I developed several novel methodologies to: (a) analyze the experimental DST data to efficiently determine reliable adsorption *kinetics* properties and *equilibrium* adsorption properties, and (b) design optimal surfactant formulations that meet a desired adsorption kinetics requirement.

In Chapter 2, I reconciled a long-standing, apparent contradiction between theoretical prediction and experimental observations on the adsorption kinetics mechanism at short times: while the mixed-controlled model predicts a barrier-controlled adsorption, as well as the impossibility of a diffusion-controlled adsorption at asymptotic short times, the short-time experimental DST behavior of many nonionic surfactants has been interpreted to result from diffusion-controlled adsorption at asymptotic short times. This is because the short-time experimental DST of these surfactants displays a $\sqrt{t}$ variation, which is considered as a fingerprint for the existence of diffusion-controlled adsorption, based on the short-time asymptotic behavior of the diffusion-controlled adsorption model. As a result of this interpretation, the fundamental physical nature of the energy barrier has been proposed to be associated with high surfactant surface concentrations. In Chapter 2, I derived

a new nonasymptotic short-time formalism of the mixed-controlled model to describe surfactant adsorption onto a spherical pendant-bubble surface, including determining the ranges of time and surfactant surface concentration values where the short-time formalism is applicable. Based on this formalism, I demonstrated that one can expect to observe an apparent $\sqrt{t}$ variation of the DST at short times even for the mixed-controlled adsorption model. I analyzed the consequence of this important finding by re-evaluating the existing notions of the energy barrier, and concluded that the energy barrier is associated with the adsorption of a *single* surfactant molecule onto a *clean surface*.

In Chapter 3, I developed a new methodology to determine the rate-limiting adsorption kinetics mechanism (diffusion-controlled vs mixed-controlled), including deducing the kinetics parameters (the diffusion coefficient, D, and the energy-barrier parameter, β), from the experimental short-time DST data. The new methodology has the following advantages over the traditional procedure used to analyze the experimental DST data: (a) it does not require using a model for the equilibrium surfactant adsorption behavior, and (b) it only requires using the experimental short-time DST data measured at two initial surfactant bulk solution concentrations. I applied the new methodology to analyze the experimental short-time DST data of the following alkyl poly(ethylene oxide), C_iE_j, nonionic surfactants: $C_{12}E_4$, $C_{12}E_6$, $C_{10}E_8$, and $C_{12}E_8$ measured using the pendant-bubble apparatus. I found that for $C_{12}E_4$ and $C_{12}E_6$, the effect of the energy barrier on the overall rate of surfactant adsorption can be neglected for surfactant bulk solution concentrations below their respective critical micelle concentrations (CMCs), and therefore, that the rate-limiting adsorption kinetics mechanism for $C_{12}E_4$ and $C_{12}E_6$ is diffusion-controlled at any of their premicellar surfactant bulk solution concentrations. On the other hand, for $C_{10}E_8$ and $C_{12}E_8$, I found that their respective CMC values are large enough to observe a significant effect of the energy barrier on the overall rate of surfactant adsorption. In other words, for $C_{10}E_8$ and $C_{12}E_8$, the rate-limiting adsorption kinetics mechanism shifts from diffusion-controlled to mixed diffusion-barrier controlled as their premicellar surfactant bulk solution concentrations increase. I tested the new methodology by predicting the short-time DST profiles at other initial surfactant bulk solution concentrations, and then comparing the predicted DST profiles with those measured experimentally. Very good agreement was obtained for the four C_iE_j nonionic surfactants considered. I also compared the

results of implementing the new methodology with those of implementing the existing procedure, and concluded that using a model for the equilibrium adsorption isotherm can lead not only to different values of D and β, but it can also lead to a completely different determination of the rate-limiting adsorption kinetics mechanism. Since the new methodology proposed in Chapter 3 does not require using a model for the equilibrium adsorption isotherm, I concluded that it should provide a more reliable determination of the rate-limiting adsorption kinetics mechanism, including the deduced kinetics parameters, D and β. Based on the β values deduced for the four $C_i E_j$ nonionic surfactants considered, I observed that the energy barrier may be related to the hydrophobic effect.

In Chapter 4, I demonstrated that the common assumption of diffusive-transport of surfactant molecules in the bulk solution may not be valid when conducting pendant-bubble experimental DST measurements. Specifically, I analyzed the experimental pendant-bubble DST data of $C_{12}E_4$ and $C_{12}E_6$ corresponding to the entire relaxation process, and demonstrated that both surfactants exhibit 'super-diffusive' adsorption behavior. I first predicted the DST behaviors of $C_{12}E_4$ and $C_{12}E_6$ at several C_b values corresponding to the diffusion-controlled adsorption model, which corresponds to the *fastest rate* of surfactant adsorption from a stagnant fluid, and then compared the predicted DST profiles with the experimental DST profiles. This comparison revealed the existence of *systematic deviations* for both $C_{12}E_4$ and $C_{12}E_6$, where the experimental DST profiles exhibit a higher rate of surfactant adsorption as compared to the rate predicted by the diffusion-controlled model whenever $t > \approx$ 100-200 s. I investigated possible causes for the observed 'super-diffusive' adsorption behavior, including inaccuracies in the specification of the diffusion-controlled model, and the breakdown of key assumptions underlying the diffusion-controlled model. The analysis pointed to the breakdown of the assumption of diffusive-transport of surfactant molecules in the bulk solution as a potential cause of the observed systematic deviations. I then hypothesized the onset of natural convection in the solution induced by the evaporative cooling of water at the pendant-bubble surface, and showed that this hypothesis can be used to rationalize the observed systematic deviations.

In Chapter 5, I explored a novel approach to predict equilibrium adsorption properties from experimental DST data and the known rate-limiting adsorption kinetics mechanism, an approach

which was never pursued in the DST literature. Specifically, I developed a new methodology to predict the Equilibrium Surface Tension versus surfactant bulk solution Concentration (ESTC) behavior of nonionic surfactants from experimental DST data when the adsorption kinetics rate-limiting mechanism is diffusion-controlled. The new methodology requires the following three inputs: (1) experimental DST data measured at a *single* surfactant bulk solution concentration, C_b, (2) the diffusion coefficient of the surfactant molecule, D, and (3) a *single* equilibrium surface tension data point, to predict the *entire ESTC curve* applicable over a wide range of surfactant bulk solution concentration values which are less than, or equal to, C_b. I demonstrated the applicability of the new methodology by predicting the ESTC curves of $C_{12}E_4$ and $C_{12}E_6$, and validated the results by comparing the predictions with: (a) equilibrium surface tension measurements, (b) surface-expansion measurements, and (c) dynamic surface tension measurements for $t <\approx$ 100 - 200 s (when the assumption of diffusive-transport of surfactant molecules in the bulk solution is valid). Very good agreement was obtained between the predictions and the measurements in (a), (b), and (c) for both $C_{12}E_4$ and $C_{12}E_6$. Based on these results, I concluded that the new methodology represents an efficient method to predict reliable ESTC curves for nonionic surfactants.

In Chapter 6, I proposed a novel theoretical framework to design nonionic surfactant formulations that result in a desired surfactant adsorption kinetics behavior specified in the form of a desired dynamic surface tension profile (referred to as the 'design problem'). The new theoretical framework circumvents the more widely used and time consuming experimental trial-and-error surfactant selection approach. Specifically, the proposed new theoretical framework involves using predictive DST models in conjunction with optimization techniques to identify the surfactant formulation that optimally meets a desired dynamic surface tension behavior. To demonstrate the feasibility of the proposed new theoretical framework, I implemented it using: (i) the molecularly-based Mulqueen-Stebe-Blankschtein (MSB) adsorption kinetics model, which is applicable to model the DST behavior of nonionic surfactant mixtures when the adsorption kinetics is diffusion-controlled, and (ii) the optimization package SNOPT (Sequential Nonlinear OPTimization). I formulated the design problem as an optimization problem using the MSB adsorption kinetics model, and developed a framework to find the solution of the formulated optimization problem using SNOPT. I demonstrated the effectiveness of the new theoretical framework by analyzing a representative

case study in which I identified the nonionic surfactant formulation that results in an unconventional 'linear' DST profile on the $\log(t)$ axis. Using this case study, I demonstrated and concluded that the new theoretical framework can be extremely effective in designing surfactant formulations that meet a required adsorption kinetics behavior in specific applications.

7.2 Future Research Directions - Expanding the Capabilities of the Methodologies Developed in this Thesis

Recall that, in this thesis, I examined the adsorption kinetics of *simple nonionic* surfactants at their *premicellar* surfactant concentrations. In addition, recall that the new methodology presented in Chapter 5 to predict equilibrium adsorption properties from experimental DST data, as well as the new theoretical framework presented in Chapter 6 to design optimal surfactant formulations, are both applicable solely for the *diffusion-controlled* (DC) adsorption kinetics model of nonionic surfactants. It is noteworthy, that the development of the new methodology in Chapter 5 was possible in the case of the DC model primarily because the DC model requires as input only a single kinetics parameter, D, the diffusion coefficient of the surfactant molecule, which can be estimated reliably using independent methods, including the use of empirical correlations like the Wilke-Chang correlation[1]. Moreover, note that the development of the new theoretical framework in Chapter 6 was possible because of the availability of the MSB adsorption kinetics model to describe the DST of nonionic surfactant mixtures. As can be seen, the prerequisites for the development of these methodologies include: (i) knowing the underlying rate-limiting adsorption kinetics mechanism, and (ii) knowing the values of the relevant kinetics parameters. Accordingly, extension of the methodologies developed in this thesis to model: (a) the mixed-controlled adsorption of nonionic surfactants, (b) the adsorption kinetics behavior of complex surfactants, (c) the adsorption kinetics behavior of ionic surfactants, and (d) the adsorption kinetics behavior when C_b is greater than the Critical Micelle Concentration (CMC), will require:

1. Reliable values of the energy barrier parameter, β, for nonionic surfactants.

2. A detailed model to describe the adsorption kinetics behavior of surfactant mixtures which contain surfactants that undergo surface phase transitions, including the relevant adsorption

kinetics parameter values.

3. A detailed model to describe the adsorption kinetics behavior of surfactant mixtures which contain ionic surfactants, including the relevant adsorption kinetics parameter values.

4. A detailed model to describe the adsorption kinetics behavior of surfactants at concentrations above the CMC, including the relevant adsorption kinetics parameter values.

An in-depth review of the adsorption kinetics literature reveals that items 1-4 above involve a number of long-standing challenges which need to be resolved before one can extend the methodologies developed in this thesis to address items (a)-(d) above. In the remainder of this section, I will elaborate on the existing challenges associated with items 1-4 above.

7.2.1 Reliable Values of the Energy Barrier Parameter, β, for Nonionic Surfactants

Recall that the existence of the energy barrier was hypothesized more than 50 years ago [2]. The original introduction of the energy barrier concept was motivated primarily by the inability of the diffusion-controlled model to explain the observed DST behavior of alcohols [2-4]. Although the energy barrier was identified to play a significant role in controlling the overall rate of adsorption of alcohols, the β values obtained for different alcohols did not reveal any clear pattern. Only about ten years ago, Lin and co-workers [5-8] demonstrated the high sensitivity of the chosen equilibrium adsorption model on the analysis of the experimental DST data of nonionic surfactants. In view of this important observation, there is a clear need to systematically re-analyze the experimental DST data of alcohols, and to obtain reliable β values. With this in mind, the experimental DST data of alcohols needs to be re-analyzed using the new methodology presented in Chapter 3, and reliable values of β need to be determined. In general, one needs to 'broaden' the list of nonionic surfactants that exhibit mixed-controlled adsorption kinetics, including determining the corresponding β values in order to better understand the importance of the energy barrier in affecting the adsorption kinetics behavior of nonionic surfactants. Such an investigation will also reveal any underlying trends in the values of β, which, in turn, will be useful: (a) to develop a fundamental understanding of the physical basis of the energy barrier, and (b) to validate any model developed to predict β molecularly for nonionic surfactants.

259

7.2.2 Modeling Surfactant Mixtures that Exhibit Surface Phase Transitions

Although the existence of surface phase transitions in the case of adsorbed surfactant molecules is well documented [9], understanding the effect of these phase transitions on the *kinetics of surfactant adsorption* has received very little experimental and theoretical attention [10–16]. To the best of my knowledge, the effect of surface phase transitions on DST has been studied solely for a few nonionic surfactants [10–16]. In fact, by studying the DST behavior of surfactants that exhibit surface phase transitions, current efforts are aimed at *detecting* these phase transitions by experimentally monitoring the DST behavior. Specifically, the existence of a surface phase transition is detected by observing a plateau and a subsequent cusp in the measured DST data, and has been further confirmed through the use of Brewster Angle Microscopy (BAM) images. As an illustration, in Figure 7-1, I show the experimental DST data of 1-dodecanol [15], where the plateau and the subsequent cusp in the DST profile can be clearly seen. In Figure 7-1, oval 1 indicates the plateau and the cusp associated with the Gas-Liquid Expanded (G-LE) surface phase transition, and oval 2 indicates the plateau and the cusp associated with the Liquid Expanded-Liquid Condensed (LE-LC) surface phase transition[15].
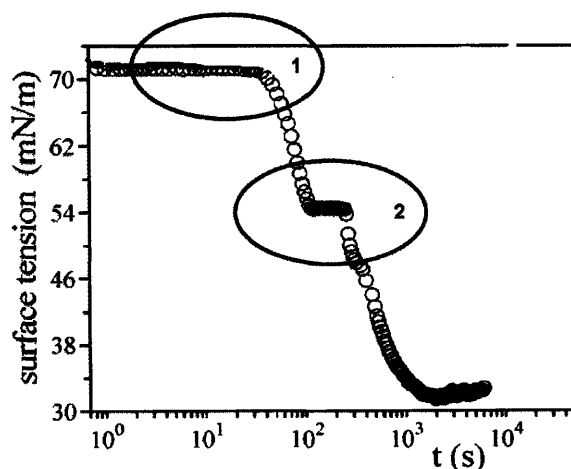
Figure 7-1: Experimental DST data of 1-dodecanol at $C_b = 10.6 \times 10^{-9}$ mol/cm^3 reported in Ref.[15] (see Figure 1 in Ref.[15]). Ovals 1 and 2 indicate the regions where a plateau and the subsequent cusp are observed (for more details, see the text).

Note that a *quantitative* analysis of the DST behavior when surfactants exhibit surface phase transitions was reported only in Refs. [16] and [10], where the classical diffusion-controlled model

and the mixed-controlled model were used to understand the observed DST behavior. Considering that the experimental study of the DST behavior of surfactants that exhibit surface phase transitions represents a relatively new research area, there is a clear need to: (i) determine the DST behavior of a broader class of surfactants that exhibit surface phase transitions, and (ii) analyze the observed DST behavior to identify the adsorption kinetics rate-limiting mechanism. A systematic analysis of the DST of surfactants that exhibit surface phase transitions will also help to better understand the kinetics associated with the surface phase transitions.

Note that the methodology presented in Chapter 3 to determine the adsorption kinetics rate-limiting mechanism from experimental short-time DST data was developed assuming that: (i) the nonionic surfactants do not exhibit surface phase transitions at the short-time DST values of interest, and (ii) the adsorption kinetics mechanism is mixed-controlled[2]. Accordingly, accounting for the existence of the surface phase transitions, and including the effect of the kinetics associated with surface phase transitions, will involve significant modifications to the methodology presented in Chapter 3. In such cases, the specific nature of the modification will depend on the specific form of the model used to describe the kinetics associated with the surface phase transition.

7.2.3 Modeling the Adsorption Kinetics Behavior of Ionic Surfactants

The kinetics associated with the adsorption of ionic surfactants is different from that of nonionic surfactants because, as the adsorption process takes place, the water/fluid (air or oil) interface acquires charge, and the resulting electric field slows down any additional adsorption of the ionic surfactant molecules[17]. Unlike the case of surfactants that exhibit surface phase transitions (see Section 7.2.2), the adsorption kinetics of ionic surfactants has been studied extensively. In this section, I will review key contributions in the area of adsorption kinetics of ionic surfactants and stress possible research directions that could be pursued.

In the case of ionic surfactants, adsorption of the charged surfactant molecules leads to a non-zero electric field near the surface, which, in turn, repels the charged surfactant ions and attracts the counterions. Due to the screening of the electric field by the counterions, the electrostatic repulsions are not felt over the entire region where diffusion takes place. The length scale over

---

[2]Recall that, in Chapter 3, I showed that diffusion-controlled adsorption is a special case of the mixed-controlled adsorption when $\beta \to \infty$.

which the charged interface affects diffusion (ℓ_e) is given by the *Debye-Hückel screening length* (κ^{-1}), as shown schematically in Figure 7-2.
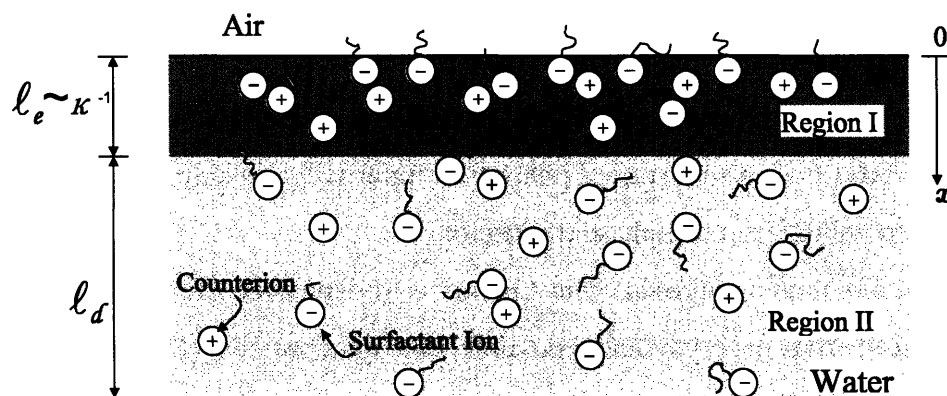

Figure 7-2: Schematic illustration of the electro-diffusion process.

Borwankar and Wasan [17] proposed a model for the DST of ionic surfactants, referred to as the quasi-equilibrium model, that assumes a diffusion-controlled adsorption and a negligible length scale associated with the electro-diffusion process ($\ell_e \sim \kappa^{-1}$) as compared to the length scale associated with the diffusion process (the diffusive length scale, ℓ_d, see Figure 7-2). MacLeod and Radke [18] proposed a rigorous numerical model that accounts for the effect of the electric field on the diffusion of the charged surfactant molecules (electro-diffusion), which makes use of the equilibrium Frumkin adsorption isotherm.

All the existing theoretical formulations [18–31] of the adsorption kinetics of ionic surfactants contain parameters, associated with the equilibrium adsorption isotherm, whose evaluation re-quires experimental fitting. Considering the extensive use of surfactant mixtures composed of ionic and nonionic surfactants in almost all practical applications involving interfacial effects, there is a clear need to develop a theoretical framework to *molecularly predict* the dynamic surface tension of ionic/nonionic surfactant mixtures which eliminates the need for experimental fitting.

It is fairly well established that the assumption of electro-diffusion limited adsorption is valid for commonly used ionic surfactants [32]. This implies that, given a suitable model to describe the equilibrium adsorption behavior of the ionic surfactants, and the diffusion coefficient of the ionic surfactant molecules, the DST behavior can be predicted. With this in mind, in order to develop a predictive model to describe the DST of surfactant mixtures containing ionic and non-

ionic surfactants, one can use the equilibrium adsorption formalism for ionic/nonionic surfactant mixtures developed by Mulqueen and Blankschtein [33]. According to this theoretical formalism, given the molecular structures of the ionic and the nonionic surfactants comprising the mixture, and the concentrations of the surfactants, the model is able to predict the resulting DST behavior. Once the model to predict the DST of surfactant mixtures containing ionic and nonionic surfactants is developed, it can be incorporated into the new theoretical framework to design optimal non-ionic surfactant formulations presented in Chapter 6 to expand its capabilities to design surfactant formulations containing mixtures of ionic and nonionic surfactants that meet specific surfactant adsorption kinetics requirements.

7.2.4 Modeling the Adsorption Kinetics Behavior Above the CMC

It is well known that when the total surfactant bulk solution concentration, C_b, is above the surfactant CMC, the surfactant molecules self-assemble to form aggregate structures called micelles[34]. In these cases, the concentration of the surfactant *monomers* remains approximately constant at a value equal to the CMC, and the *excess* surfactant molecules form micelles.

As surfactant adsorption takes place from an aqueous surfactant solution at a concentration $C_b >$ CMC, due to the adsorption of the surfactant monomers at the surface, the local surfactant monomer concentration decreases to a value below the CMC. As a result, micelles disassemble to increase the local surfactant monomer concentration to the CMC value [35]. In essence, micelles act like supply sources of surfactant monomers driven by the local surfactant monomer concentration. Accordingly, when modeling surfactant adsorption kinetics at C_b values above the CMC, it is essential to account for the kinetics of micelle disassembly in addition to accounting for surfactant diffusion in the bulk solution and for the possible role of the energy barrier [35]. An in-depth review of the literature [35–39] reveals that DST models that incorporate this new physical aspect have been developed and analyzed extensively. One of the key aspects associated with predicting the adsorption kinetics behavior of surfactants when C_b is above the CMC, is that reliable micellar kinetics models, including the values of the relevant micellar kinetics parameters, are not currently available. This, in turn, reflects the extremely short time scales associated with micellar kinetics ($\sim$ milliseconds), which makes it extremely difficult to probe this phenomenon experimentally. In fact,

typically, the experimental DST data corresponding to $C_b >$ CMC is actually used to obtain useful information about the kinetics of micellization [36].

Overall, the development of predictive models to describe the kinetics of surfactant adsorption above the CMC is severely hindered by the current unavailability of reliable micellar kinetics models, including the values of the micellar kinetics parameters.

7.3 Future Research Directions - New Research Projects in the Surfactant Adsorption Kinetics Area

The kinetics of surfactant adsorption onto surfaces has been investigated for over half a century. Significant progress has been made on: (i) the *theoretical understanding* of the adsorption kinetics, (ii) the *experimental methods* that are used to probe the adsorption kinetics, and (iii) the manner in which one can *utilize* the theoretical understanding gained in (i) above in practical applications. A number of original contributions made in this area have not only helped to develop a better understanding of the factors that affect the adsorption kinetics of surfactants, but also point to several fundamental issues that affect the kinetics of surfactant adsorption which require further investigation. In this section, I propose three new research projects that address several outstanding issues on the kinetics of surfactant adsorption, that if solved, could be practically very useful. Specifically, I propose: (i) a systematic approach to develop a fundamental physical understanding of the energy barrier (Section 7.3.1), (ii) a new experimental method to measure the DST of surfactants (Section 7.3.2), and (iii) a new practical application of DST (Section 7.3.3).

7.3.1 Molecular Dynamics Simulations Approach to Model the Energy Barrier

Note that, originally, the existence of the energy barrier was hypothesized in order to rationalize the observed DST behavior of alcohols [2–4]. An independent validation was not possible at that time because of the non-availability of experimental and computational methods to study the behavior of alcohols or surfactant molecules very close to the surface. However, recent developments in the area of Molecular Dynamics Simulations (MDS) provide a potentially very powerful tool to probe the behavior of surfactant molecules close to the surface, including probing the micro-structural

characteristics of the surfactant molecule. In addition, recent MDS packages like GROMACS [40] contain powerful analysis tools to compute relevant thermodynamic observables like the free energy, the enthalpy, and the entropy from the simulated micro-structural information. In essence, probing the nature of the energy barrier using molecular dynamics simulations represents a fertile scientific area in which one could make original contributions and significantly impact the area of the kinetics of surfactant adsorption. It is noteworthy, that there have been relatively few attempts to use MDS to study the behavior of solute molecules close the water/air surface [41–44]. All of these studies have investigated primarily the *equilibrium* behavior of surfactants close to the water/air surfaces, and they reveal the existence of an apparent energy barrier close to the water/air surface; however, the magnitude of the computed energy barrier is comparable to the computational accuracy of the simulations. Clearly, there is an urgent need for a systematic investigation of the fundamental physical basis underlying the energy barrier for adsorption.

Note that the energy barrier can, potentially, originate from: (i) interactions between the surfactant head and the solvent molecules close to the surface, or/and (ii) interactions between the surfactant tail and the solvent molecules close to the surface. Accordingly, in order to fully characterize the nature of the energy barrier, one needs to perform MDS with different types of solute molecules (hydrophobic, hydrophilic, and amphiphilic) using different types of fluid/fluid interfaces (water/air, water/oil, and oil/air). One may begin such an analysis by considering a perfectly spherical solute (to eliminate effects associated with the orientation of the solute molecule as it approaches the surface), and studying the energy barrier at varying degrees of hydrophobicity (which can be tuned by varying the nature of the interactions between the spherical solute and the solvent molecules). Based on the results of such an analysis, one may further study the effect of the orientation of the solute molecule on the energy barrier by considering *cylindrical* solutes. Following such an analysis, one could proceed to associate 'surfactant-like' attributes to the solute by changing the nature of the interaction between different portions of the solute and the solvent molecules. A systematic analysis of this type, in addition to providing fundamental physical insights into the nature of the energy barrier, will generate valuable information on the energy barrier that can be used to validate any new molecularly-based model of the energy barrier.

7.3.2 Microfabricated Chip to Measure Dynamic Surface Tensions

In Chapter 4, I demonstrated the apparent 'super-diffusive' adsorption behavior observed in experimental pendant-bubble DST measurements for $C_{12}E_4$ and $C_{12}E_6$, and rationalized this observation by hypothesizing the onset of natural convection in the pendant-bubble apparatus. This analysis clearly points to the need to develop new experimental methods in which one could achieve better control of the experimental conditions (for example, eliminate convection effects) in order to obtain more reproducible and reliable experimental DST values.

The emerging area of *microfabrication* is changing the way in which experiments are conducted in the laboratory to measure material properties [45]. The efficacy of the 'lab-on-a-chip' philosophy has already been demonstrated through the fabrication of a number of chemical 'unit operations' on a chip, including reactors, separators, mixers, with these being used in a variety of areas ranging from colloids to drug development. The key driving force for this change in paradigm has been the ability afforded by the new devices to *control* material properties when compared to the traditional methods. Interestingly, in a recently published paper [46], the authors successfully demonstrated how one can use a microfabricated chip to measure equilibrium surface tensions of liquids. Specifically, in Ref. [46], the authors: (i) designed a chip containing a set of micro-capillaries, (ii) introduced liquid samples in the capillaries, and (iii) measured the equilibrium surface tension by measuring the rise of the liquid in the capillaries. The authors reported very good agreement between the equilibrium surface tensions measured using the new microfabricated chip and the equilibrium surface tensions measured using traditional laboratory techniques.

Keeping in mind: (i) the limitations of the pendant-bubble technique used to measure the DST of surfactant solutions (see Chapter 4), and (ii) the recent successful demonstration of using microfabrication to measure surface tensions, it would be interesting to investigate if one could build microfabrication devices to measure dynamic surface tensions of surfactant solutions. The excellent control that could be achieved using microfabrication devices has great potential to generate reliable and highly reproducible surfactant solution DST data, which, in turn, could be analyzed to identify fundamental factors that affect the adsorption kinetics behavior of surfactants.

266

7.3.3 Measurement of Dynamic Surface Tensions of Surfactant Solutions to Determine Other Fundamental Properties of Surfactants

A review of the literature reveals that surfactant solution DST measurements are increasingly being used to determine other fundamental properties of surfactants. For example, recall that: (i) Refs.[10–16] report using experimental surfactant solution DST data to detect the existence of surface phase transitions of the adsorbed surfactant molecules, and (ii) Refs. [35–38] report using experimental surfactant solution DST data to determine rate constants associated with the kinetics of micellization. In fact, the new methodology presented in Chapter 5 uses the experimental surfactant solution DST data as a probe to determine equilibrium adsorption properties of surfactants. Moreover, experimental DST data has also been used as a *detection* tool in several applications. Specifically, in Refs. [47–49], the authors correlate the DST of biological liquids, like serum and cerebrospinal fluid, with the diagnosis of rheumatic, neurological, or oncological diseases. In Refs. [50–52], DST data has been used to detect ppm levels of various surfactants and surface-active proteins present in aqueous solutions. Specifically, the approach involves: (i) forming a drop of the solution containing surfactants, or the surface-active proteins, in a steel capillary nozzle, (ii) measuring the dynamic surface tension of the drop during the drop formation process, and (iii) calibrating the resulting DST behavior for specific surfactants/proteins and concentrations [50–52].

In my view, the optimization framework presented in Chapter 6 could contribute significantly in the area of DST-based detection. Specifically, the optimization framework can be used effectively as a detection tool, where, instead of a desired DST profile, the user inputs the experimentally measured DST data of a solution containing surfactant mixtures, and the optimization framework can be used to find the specific combination of surfactants, including their concentrations, that best satisfies the DST data input by the user. However, note that this approach requires knowledge of the various surfactants that are present in the solution of interest. Using the proposed approach, one could increase the accuracy of detection, for example, by: (i) adding a known amount of a specific surfactant to the original solution, (ii) measuring the DST of the new surfactant solution, and (iii) providing the new DST as an additional input along with the DST of the original solution. In this case, the optimization framework will need to find the surfactant concentrations of the original solution such that the DST behaviors of both the original and the modified surfactants can

be best reproduced. Below, I address a possible limitation of the proposed optimization framework that could limit its utility as an effective detection tool, and suggest an approach to overcome this limitation.

Comment on a Possible Limitation of the Optimization Framework-Based Detection

As discussed in Chapter 6, the optimization framework requires information about : (i) the equilibrium adsorption model of surfactant mixtures, and (ii) the adsorption kinetics model and associated parameter values. Recall that the current optimization framework is only applicable to nonionic surfactant mixtures where the adsorption kinetics model is diffusion-controlled. While the requirement of a diffusion-controlled model is widely applicable to many classes of surfactants, the equilibrium adsorption model used is specific to every surfactant. In addition, in the case of surfactant mixtures, one must also account for the interactions between different types of adsorbed surfactant molecules. Accordingly, needing a model for the equilibrium adsorption behavior of the surfactant mixture can severely limit the ability to use the proposed optimization framework as an effective detection tool.

A possible way to overcome this limitation is to use the methodology presented in Chapter 5 to determine the equilibrium adsorption properties of the surfactants comprising the mixture using their respective experimental DST data, in conjunction with the molecularly-based equilibrium adsorption model of Nikas *et al.* [53]. Once the list of surfactants that could possibly be present in the solution, and their respective equilibrium adsorption behavior is implemented in the database of the optimization framework, the optimization framework can be used to detect solutions containing these surfactants, including determining their individual concentrations. The proposed specific method will require:

1. Using experimental DST data measured at a *single* C_b value for each of the specific surfactants comprising the mixture, including each D value estimated using, say, the Wilke-Chang correlation, to fit the molecular parameters associated with the equilibrium adsorption behavior of surfactant[3] i, that is, $\Gamma_{\infty,i}$, B_{ii}, and $\Delta\mu_i^0$ [33]. Note that one may not need the additional single equilibrium surface tension data point as an input (see Chapter 5), because, the pro-

---

[3]Recall that $\Gamma_{\infty,i}$ is the maximum surfactant surface concentration of surfactant i, B_{ii} is the second virial coefficient associated with the van der Waals attractions between surfactant molecules of type i, and $\Delta\mu_{i,0}$ is the difference in the standard-state chemical potentials of surfactant i at the surface and in the bulk solution.

posed approach can use the equilibrium surface tension value, γ_b^e, corresponding to C_b as the required additional single equilibrium surface tension data point. In other words, given a combination of the parameter values, the functional form of the molecular equilibrium adsorption isotherm can be used to *extrapolate* for the value of the equilibrium surface tension value at C_b. Note that the proposed approach may also be used to analyze the experimental DST of ionic surfactants, since the only additional parameter required to describe the equilibrium adsorption behavior of an ionic surfactant is its charge, which can be determined from the charge characteristics of the surfactant head.

2. Determining the values of the interaction parameters, B_{ij}, between surfactant molecules of type i and j using a simple mixing rule involving B_{ii} and B_{jj} values (for example, $B_{ij} = \sqrt{B_{ii}B_{jj}}$).

Therefore, by performing a *single* experimental DST measurement for each surfactant type comprising the mixture, one can determine the relevant equilibrium adsorption behavior of the surfactant mixture, which, in turn, can be used along with the optimization framework for design and detection purposes.

7.4　Concluding Remarks

This thesis has focussed on developing novel methodologies to analyze the adsorption kinetics behavior of nonionic surfactants at premicellar surfactant concentrations. It is hoped that the methodologies developed, the quantitative predictions made, and the overall fundamental understanding gained as part of this thesis will not only expand our fundamental knowledge of the adsorption kinetics behavior of surfactants, but will also serve as a solid foundation for future theoretical and experimental research in the surfactant science area.

Bibliography

[1] C. R. Wilke and P. Chang. Correlation of diffusion coefficients in dilute solutions. *AIChE Journal*, 1:264–270, 1955.

[2] K. L. Sutherland. The kinetics of adsorption at liquid surfaces. *Australian Journal of Scientific Research*, A5:683–696, 1952.

[3] R. Defay and J. R. Hommelen. The importance of diffusion in the adsorption process of some alcohols and acids in dilute aqueous solutions. *Journal of Colloid Science*, 14:411–418, 1959.

[4] R. S. Hansen. Diffusion and the kinetics of adsorption of aliphatic acids and alcohols at the water-air interface. *Journal of Colloid Science*, 16:549–560, 1961.

[5] C-T. Hsu, C-H. Chang, and S-Y. Lin. Comments on the adsorption isotherm and determination of adsorption kinetics. *Langmuir*, 13:6204–6210, 1997.

[6] Y-C. Lee, S-Y. Lin, and H-S. Liu. Role of equation of state on studying surfactant adsorption kinetics. *Langmuir*, 17:6196–6202, 2001.

[7] C-T. Hsu, C-H. Chang, and S-Y. Lin. A study of surfactant adsorption kinetics: Effects of interfacial curvature and molecular interaction. *Langmuir*, 16:1211–1215, 2000.

[8] C-T. Hsu, C-H. Chang, and S-Y. Lin. A study of surfactant adsorption kinetics: Effect of intermolecular interaction between adsorbed molecules. *Langmuir*, 15:1952–1959, 1999.

[9] G. L. Gaines. *Insoluble monolayers at liquid-gas interface*. Interscience, 1966.

[10] J. K. Ferri and K. J. Stebe. Soluble surfactants undergoing surface phase transitions: A

Maxwell construction and the dynamic surface tension. *Journal of Colloid and Interface Science*, 209:1–9, 1999.

[11] Md. M. Hossain, T. Suzuki, and T. Kato. Phases and phase transition in Gibbs monolayers of an alkyl phosphate surfactant. *Journal of Colloid and Interface Science*, 288:342–349, 2005.

[12] Md. M. Hossain, T. Suzuki, and T. Kato. Phase diagram of n-tetradecyl phosphate in Gibbs monolayers. *Colloids and Surfaces A: Physicochemical and Engineering Aspects*, 284-285:234–238, 2006.

[13] M. L. Pollard, R. Pan, C. Steiner, and C. Maldarelli. Phase behavior of sparingly soluble polyethoxylate monolayers at the air-water surface and its effect on dynamic tension. *Langmuir*, 14:7222–7234, 1998.

[14] R. Subramanyam and C. Maldarelli. Fluorescence evidence that a phase transition causes the induction time in the reduction in dynamic tension during surfactant adsorption to a clean air/water interface and a kinetic-diffusive transport model for the phase-induced induction. *Journal of Colloid and Interface Science*, 253:377–392, 2002.

[15] R-Y. Tsay, T-F. Wu, and S-Y. Lin. Observation of G-LE and LE-LC phase transitions of adsorbed 1-dodecanol monolayer from dynamic surface tension profiles. *Journal of Physical Chemistry B*, 108:18623–18629, 2004.

[16] S-Y.Lin, K. McKeigue, and C. Maldarelli. Diffusion-limited interpretation of the induction period in the relaxation in surface tension due to the adsorption of straight chain, small polar group surfactants: Theory and experiment. *Langmuir*, 7:1055–1066, 1991.

[17] R. P. Borwankar and D.T. Wasan. The kinetics of adsorption of ionic surfactants at gas-liquid surfaces. *Chemical Engineering Science*, 41:199–201, 1986.

[18] C. A. MacLeod and C.J. Radke. Charge effects in the transient adsorption of ionic surfactants at fluid interfaces. *Langmuir*, 10:3555–3566, 1994.

[19] H.Diamant, G.Ariel, and D.Andelman. Kinetics of surfactant adsorption: The free-energy

approach. *Colloid and Surfaces A: Physicochemical and Engineering Aspects*, 183-185:259–276, 2001.

[20] G. Ariel, H. Diamant, and D. Andelman. Kinetics of surfactant adsorption at fluid-fluid interfaces: Surfactant mixtures. *Langmuir*, 15:3574–3581, 1999.

[21] H. Diamant and D. Andelman. Kinetics of surfactant adsorption at fluid-fluid interfaces. *Journal of Physical Chemistry*, 100:13732–13742, 1996.

[22] S. S. Dukhin, R. Miller, and G. Gretzschmar. On the theory of adsorption kinetics of ionic surfactants at fluid interfaces: 1. The effect of the electric double layer under quasi-equilibrium conditions on adsorption kinetics. *Colloid and Polymer Science*, 261:335–339, 1983.

[23] R. Miller, S. S. Dukhin, and G. Kretzschmar. On the theory of adsorption kinetics of ionic surfactants at fluid interfaces: 2. Numerical calculations of the influence of a quasiequilibrium electric double layer. *Colloid and Polymer Science*, 263:420–423, 1985.

[24] S. S. Dukhin and R. Miller. On the theory of adsorption kinetics of ionic surfactants at fluid interfaces: 3. Generalization of the model. *Colloid and Polymer Science*, 269:923–928, 1991.

[25] R. Miller, G. Kretzschmar, and S. S. Dukhin. On the theory of adsorption kinetics of ionic surfactants at fluid interfaces: 4. Deceleration of the adsorption rate due to non-equilibrium distribution of adsorbed ions in the diffuse layer. *Colloid and Polymer Science*, 272:548–553, 1994.

[26] L. K. Filippov. On the theory of dynamic surface tension of ionic surfactant solutions, I. *Journal of Colloid and Interface Science*, 182:330–347, 1996.

[27] I. U. Vakarelski and C. D. Dushkin. Effect of counterions on the surface properties of surfactant solutions: Kinetics of the surface tension and surface potential. *Colloid and Surfaces A: Physicochemical and Engineering Aspects*, 163:177–190, 2000.

[28] K. D. Danov, V. L. Kolev, P. A. Kralchevsky, G. Broze, and A. Mehreteab. Adsorption kinetics of ionic surfactants after a large initial peturbation. Effect of surface elasticity. *Langmuir*, 16:2942–2956, 2000.

[29] K. D. Danov, P. M. Vlahovska, P. A. Krachevsky, G. Broze, and A. Mehreteab. Adsorption kinetics of ionic surfactants with detailed account for the electrostatic interactions: Effect of the added electrolyte. *Colloid and Surfaces A: Physicochemical and Engineering Aspects*, 156:389–411, 1999.

[30] P.M.Vlahovska, K.D. Danov, A.Mehreteab, and G. Broze. Adsorption kinetics of ionic surfactants with detailed account for the electrostatic interactions-I: No added electrolyte. *Journal of Colloid and Interface Science*, 192:194–206, 1997.

[31] S. S.Datwani and K. J.Stebe. The dynamic adsorption of charged amphiphiles: The evolution of the surface concentration, surface potential, and surface tension. *Journal of Colloid and Interface Science*, 219:282–297, 1999.

[32] The typical value of the energy barrier due to electrostatic effects for the adsorption of ionic surfactant molecules ($10 - 200k_B t$) is very high as compared to the non-electrostatic energy barrier for adsorption($0.5 - 7k_B t$). Therefore, it is sufficient to consider only the energy barrier due to electrostatic effects when modeling the adsorption of ionic surfactant molecules.

[33] M. Mulqueen and D. Blankschtein. Prediction of equilibrium surface tension and surface adsorption of aqueous surfactant mixtures containing ionic surfactants. *Langmuir*, 15:8832–8848, 1999.

[34] K.S. Birdi, editor. *Handbook of Surface and Colloid Chemistry*. CRC Press, 1997.

[35] B. A. Noskov. Kinetics of adsorption from micellar solutions. *Advances in Colloid and Interface Science*, 95:237 – 293, 2002.

[36] R. Miller. Adsorption kinetics of surfactants from micellar solutions. *Colloid and Polymer Science*, 259:1124 – 1128, 1981.

[37] C. D. Dushkin, I. B. Ivanov, and P. A. Kralchevsky. The kinetics of the surface tension of micellar surfactant solutions. *Colloids and Surfaces*, 60:235 – 261, 1991.

[38] J. V. Mitrancheva, C. D. Dushkin, and P. Joos. Kinetics of the surface tension of micellar

solutions: Comparison of different experimental techniques. *Colloid and Polymer Science*, 274:356 – 367, 1996.

[39] L. K. Filippov and N. L. Filippova. Dynamic surface tension and adsorption kinetics from micellar solutions on planar surfaces. *Journal of Colloid and Interface Science*, 187:304 – 312, 1997.

[40] D. Van der Spoel, E. Lindahl, B. Hess, G. Groenhof, and A. E. Mark H.J. C. Berendsen. GRO-MACS: fast, flexible, and free. *Journal of Computational Chemistry*, 26:1701 – 1718, 2005.

[41] A. Pohorille and I. Benjamin. Molecular dynamics of phenol at the liquid-vapor interface of water. *Journal of Chemical Physics*, 94:5599 – 5605, 1991.

[42] A. Pohorille and I. Benjamin. Structure and energetics of model amphiphilic molecules at the water liquid-vapor interface. A molecular dynamics study. *Journal of Physical Chemistry*, 97:2664 – 2670, 1993.

[43] R. S. Taylor, D. Ray, and B. C. Garrett. Understanding the mechanism for the mass acco-modation of ethanol by a water droplet. *Journal of Physical Chemistry B*, 101:5473–5476, 1997.

[44] L. X. Dang. Computational study of ion binding to the liquid interface of water. *Journal of Physical Chemistry B*, 106:10388–10394, 2002.

[45] K. F. Jensen. Microreaction engineering - is small better? *Chemical Engineering Science*, 56:293–303, 2001.

[46] J. Liu, H. Li, and J-M. Lin. Measurements of surface tension of organic solvents using a simple microfabricated chip. *Analytical Chemistry*, 79:371 – 377, 2007.

[47] V. N. Kazakov, A. F. Vozianov, O. V. Sinyachenko, D. V. Trukhin, V. I. Kovalchuk, and U. Pison. Studies on the application of dynamic surface tensiometry of serum and cerebrospinal liquid for diagnostics and monitoring of treatment in patients who have rheumatic, neurological or oncological diseases. *Advances in Colloid and Interface Science*, 86:1–38, 2000.

[48] V. N. Kazakov, O. V. Sinyachenko, D. V. Trukhin, and U. Pison. Dynamic interfacial tensiometry of biologic liquids - does it have an impact on medicine. *Colloids and Surfaces A: Physicochemical and Engineering Aspects*, 143:441–459, 1998.

[49] D.V. Trukhin, O.V. Sinyachenko, V.N. Kazakov, S.V. Lylyk, A.M. Belokon, and U. Pison. Dynamic surface tension and surface rheology of biological liquids. *Colloids and Surfaces B: Biointerfaces*, 21:231–238, 2001.

[50] T. E. Young and R. E. Synovec. Enhanced surfactant determination by ion-pair formation using flow-injection analysis and dynamic surface tension. *Talanta*, 43:889 – 899, 1996.

[51] K. E. Miller, E. Bramanti, B. J. Prazen, M. Prezhdo, K. J. Skogerboe, and R. E. Synovec. Multidimensional analysis of poly(ethylene glycols) by size exclusion chromatography and dynamic surface tension detection. *Analytical Chemistry*, 72:4372 – 4380, 2000.

[52] W. W. C. Quigley, E. Bramanti, B. A. Staggemeier, K. E. Miller, A. Nabi, K. J. Skogerboe, and R. E. Synovec. Determination, by dynamic surface-tension analysis, of the molar mass of proteins denatured in guanidine thiocyanate. *Analytical and Bioanalytical Chemistry*, 378:134 – 143, 2004.

[53] Y. J. Nikas, S. Puvvada, and D. Blankschtein. Surface tensions of aqueous nonionic surfactant mixtures. *Langmuir*, 8:2680–2689, 1992.